Chemically tailored new sorbents for use into the 21st century.

Thesis

UNRESTRICTED

CHEMICALLY TAILORED NEW SORBENTS FOR USE INTO THE 21ST CENTURY

Submitted by

Claire Michelle Bambrough BSc(Hons)

as a thesis for the degree of

Doctor of Philosophy

in the Faculty of Science

October 1998

Date of submission: 12 October 1998
Date of award: 1 December 1998

ProQuest LLC.
789 East Eisenhower Parkway
P.O. Box 1346
Ann Arbor, MI 48106 – 1346

Dedicated to Roy Mitchell,

and to the memory of Grace Mitchell,

Bob and Phyllis Bambrough, my grandparents.

"The surface was invented by the devil."

- Wolfgang Pauli

ABSTRACT

A series of chemically-tailored mesoporous materials has been synthesized *via* a liquid-crystal templating mechanism and characterized using a variety of techniques. Materials include a series of MCM-41-type solids (including aluminosilicates, purely siliceous, and iron-containing materials) and a series of organically-modified mesoporous silicas (including phenyl-, vinyl-, aminopropyl- and mercaptopropyl-functionalized samples).

Two different synthesis compositions and three different sets of reaction conditions were tested for the synthesis of MCM-41. Characterization by XRD and N_2 sorption demonstrated that synthesis under pressure at 100 °C yielded materials with a uniform pore structure and narrow pore size distribution. Samples with pore widths in the mesoporous range and specific surface areas of between 500 - 950 $m^2\ g^{-1}$ were produced. The synthesis composition that used aluminium sulphate as the aluminium source was shown, by ^{27}Al MAS-NMR, to give a product, following calcination, containing tetrahedrally co-ordinated aluminium (necessary for acid catalysis).

N_2 adsorption on the organically-modified samples, demonstrated that the incorporation of organic functions reduced the pore diameter and yielded microporous materials. The use of auxiliary organics as pore-swelling agents was investigated and mesitylene was proved to be successful in the formation of a mesoporous phenyl-modified material.

The adsorption isotherms of water, benzene, *n*-butanol and *t*-butanol were measured for the phenyl-modified materials. N_2, benzene and *t*-butanol sorption on the unswollen sample yielded Type I isotherms, confirming the sample's microporosity.

Type IV isotherms were given by these adsorptives on the mesitylene-swollen sample, demonstrating the presence of mesopores.

n-butanol adsorption occurred *via* polar interactions with the surface hydroxyl groups of both samples and was sterically-hindered in the microporous sample. Water sorption (performed on the unswollen sample only) gave a Type V isotherm demonstrating the sample's hydrophobicity.

IINS studies of the phenyl-modified silica containing adsorbed benzene, detected the presence of the adsorbed species and differentiated between structural phenyls and adsorbed benzene.

CONTENTS

ACKNOWLEDGEMENTS

I would like to express my sincere gratitude to my two supervisors, Dr Ruth Williams and Professor Bob Slade, for their support, encouragement and guidance. Special thanks to Ruth for accompanying me to R.A.L. and helping with the TOSCA experiments.

Many thanks to Dr Kevin Young for his constant support, time and expertise (in so many areas!) and for drawing Figure 6.19. Thanks also to Dr Phil Evans for his help and guidance and to all other members of the Exeter Materials Chemistry Group for their support.

To Kate Charles, for your support and above all friendship, thank you so much.

I gratefully acknowledge:

- The Open University for funding, without which this work could not have been undertaken.
- Dr D.C. Apperley and co-workers at the University of Durham, EPSRC, Solid State NMR service for running spectra.
- Dr B.E. Gore and co-workers at the UMIST, EPSRC NMR of Sorbents and Catalysts Service for running spectra.
- Dr W. Kagunya and Dr J. Tomkinson at the Rutherford Appleton Laboratories for help with running the TOSCA experiments and for useful discussions.
- Ms Julia McManus at the Open University for running TEMs.
- The workshops and technical staff at the University of Exeter, especially Mr N. England for making the TOSCA sample cans and Mr M. Hart for constant repairs to the vacuum lines.
- Dr I. Stone at the University of Exeter, Earth Resources Centre, for running XRDs.

I am indebted to my family, especially my brother Graham (for computer support!), Mum and Dad - "You give your children two things; you give them roots and you give them wings." How true!

Finally, I would like to thank my husband, Graeme, for more than I could ever say.

GLOSSARY

AP-M.S. - aminopropyl-modified mesoporous material

APTES - aminopropyltriethoxysilane

A.S. - as-synthesized

CTMACl - cetyltrimethylammonium chloride

DTA - Differential Thermal Analysis

IINS - Incoherent Inelastic Neutron Scattering

IR - Infra-red

MAS-NMR - Magic-angle Spinning Nuclear Magnetic Resonance

MCM - Mobil Composite Material

MES - mesitylene (1,3,5-trimethyl benzene)

MP-M.S. - mercaptopropyl-modified mesoporous material

MPTMS - mercaptotrimethoxysilane

Ph-M.S. - phenyl-modified mesoporous material

S.E. - surfactant extracted

TEM - Transmission Electron Microscopy

TEOS - tetraethylorthosilicate

TET - tetradecane

TFXA - Time-Focused Crystal Analysis

TG - thermogravimetry

TMAOH - tetramethylammonium hydroxide

TMAS - tetramethylammonium silicate

TOSCA - IINS spectrometer (not an acronym)

V-M.S. - vinyl-modified mesoporous material

VTES - vinyltriethoxysiloane

XRD - X-ray Diffraction

CHAPTER 1

INTRODUCTION

1.1 General

While the title of this research is extremely broad, it is primarily concerned with mesoporous molecular sieves, species which can discriminate between molecules solely on the basis of size by virtue of a pore system of molecular dimensions. Specifically, it considers the synthesis and characterization of novel, mesoporous, silica-based materials which may be classified as belonging to the M41S group of materials[1-28] (see Section 1.2). This chapter aims to give a general introduction to porous materials with special attention being given to M41S-type solids. It discusses the original synthesis of the M41S materials and it will consider some alternative synthetic routes to these and to other porous solids. The use of porous solids as shape-selective catalysts will also be considered.

A valuable technique for determining the pore structure and surface area of such solids is gas adsorption and this technique, which plays a major part in this research, is discussed at length in Chapter 4. Introductions to general characterization techniques used in this research are given in Chapter 2 and a general introduction to Inelastic Neutron Scattering is given in Chapter 6.

1.2 Classification of Porous Solids

Porous inorganic solids, such as the zeolites, are used extensively in catalysis and as sorption media because of their large surface area and uniform pore structure.[29-32] IUPAC classify of porous solids according to their pore width and this classification system[33] is presented in Table 1.1, below.

Table 1.1 The IUPAC Classification of Porous Solids[33]

Pore Width / Å	Classification
< 20	microporous
20 - 500	mesoporous
> 500	macroporous

The classical aluminosilicate zeolites are examples of microporous solids (having pore diameter, d < 20 Å). Recent research in this field has concentrated on the synthesis of solids with pore structures in the mesoporous range; these include pillared layered solids and a family of mesoporous aluminosilicates designated M41S. A large amount of interest has recently been focused on this latter group of materials, which were discovered by the Mobil Research and Development Corporation in 1992.[1,2]

These materials combine the well-defined pore structure of the zeolites with the desirability of average pore diameters in the mesoporous range. It is possible to control precisely the pore diameter in these solids, thereby providing a potential route to the formation of highly shape-selective catalysts.

1.3 M41S Materials

The recent discovery of the mesoporous aluminosilicates designated M41S (by workers at Mobil) attracted a great deal of interest, and their potential as catalysts for the reactions of large organic molecules has guaranteed a continuous stream of papers investigating the rational synthesis of mesoporous solids, their characterization and their applications.[1-28]

The M41S materials are formed via a reaction which involves the use of aggregated organic surfactant molecules as templates or "structure-directing agents".

Zeolites are formed by the crystallization of silicate around a single molecule. In the case of M41S synthesis, micelles of cationic alkyltrimethylammonium surfactants serve as the template. The ability to control the template by increasing the carbon chain length of the surfactant provides a relatively simple method of tailoring the pore size and shape of the inorganic product. Characterization of these products has proved the existence of a lamellar, a cubic and a hexagonal M41S phase, the most well documented being the hexagonal phase MCM-41[1,8-13] and the cubic phase MCM-48.[20]

The factor that governs which of these phases is formed is the surfactant / silica molar ratio:

surfactant / silica < 1 gives MCM-41

surfactant / silica = 1 to 1.5 gives MCM-48

This research is concerned with materials having the MCM-41 structure.

1.3.1 MCM-41

MCM-41 has a hexagonal array of unidimensional pores that can be tailored with pore-diameters between 15 - 100 Å. It has been used as a model mesoporous solid in the field of adsorption, surface area and porosity measurements, and typical surface areas in excess of 650 $m^2 g^{-1}$ have been reported.

Speculation on the mechanistic pathway leading to the formation of MCM-41 initially resulted in two proposed routes. Beck *et al*[2] suggested that the surfactant molecules aggregate into micellar rods which in turn form a hexagonal array which acts as the template for the inorganic silica (Figure 1.1).

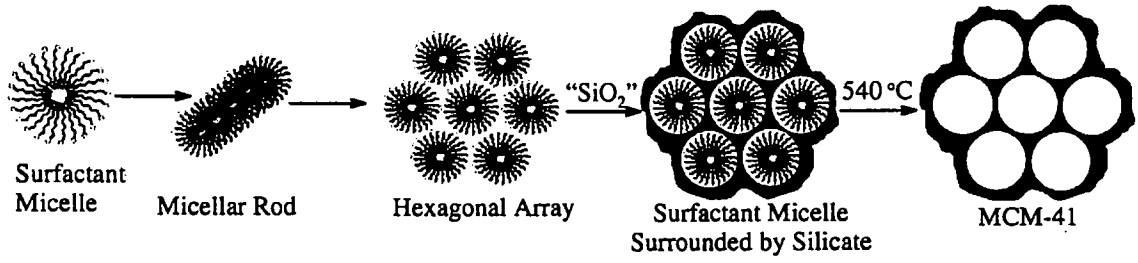

Figure 1.1 The Liquid-Crystal Templating Mechanism Suggested by Beck *et al.*

The second mechanism, suggested by Vartuli,[3] notes that spontaneous aggregation of the surfactant molecules into the liquid crystal hexagonal array is unlikely at the working concentration and that it is the addition of the silicate anions, by virtue of their charge balance with the cationic surfactants, that causes micelle formation. This more likely mechanistic pathway is shown in Figure 1.2 below.

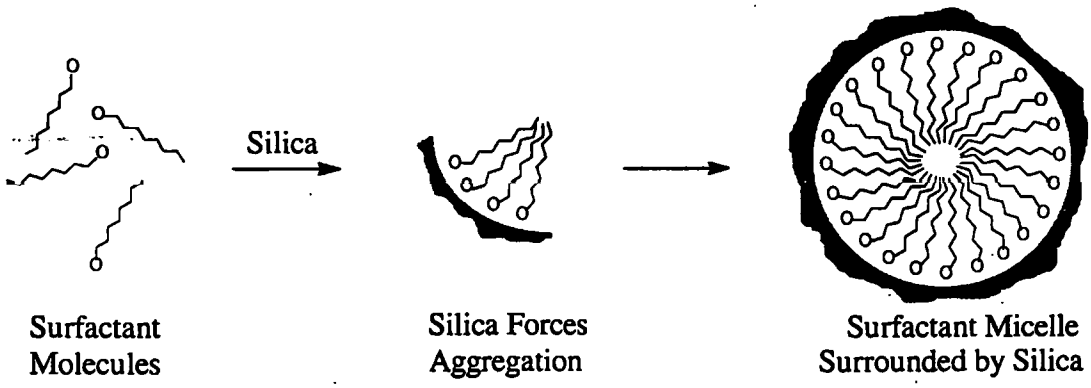

Figure 1.2 The Structure-Directing Mechanism Suggested by Vartuli *et al.*

It has recently been shown[3] that by progressively increasing the surfactant : silica ratio, each of the three M41S phases (lamellar, cubic and hexagonal) can be formed. This agrees with the second proposed mechanism in which the silicate anions trigger the liquid crystal state by serving as counter ions to the surfactants.

1.3.2 Alternative Synthetic Routes to MCM-41-Type Materials

(i) A Neutral Templating Route

An alternative to the synthetic route discussed above is the formation of mesoporous solids via a neutral templating route.[34-36] This method relies on hydrogen bonding interactions between neutral primary amine micelles and neutral inorganic precursors such as tetraethylorthosilicate (TEOS). The template may then be removed by neutral solvent extraction. These materials are reported to have thicker silica walls and improved textural mesoporosity.

(ii) Preforming the Liquid Crystal Mesophase

In the case of the original MCM-41 synthesis, the experimental concentration of the surfactant molecules is below that at which the liquid crystal mesophase will spontaneously form. An alternative synthetic procedure, first carried out by Attard *et al*,[37] involves preforming the liquid crystal mesophase before addition of the silica source. The pore structure of the final product is therefore accurately determined at the outset.

(iii) Surfactant Intercalation of Kanemite

As well as the synthetic route described above, attempts have been made to produce mesoporous materials by hydrothermal treatment of the layered silicate kanemite in the presence of alkyltrimethylammonium cations.[4] This route did produce a mesoporous silicate via surfactant intercalation of the kanemite layers and not via the micellar/silicate route observed in the M41S system. The properties of the kanemite-derived materials are different from those of the M41S group in that they have lower pore volumes, are more highly condensed and have thicker silica walls.

(iv) Gemini and Dual Alkyl Chain Surfactant Templating

Gemini surfactants contain two quaternary ammonium head groups separated by a variable length methylene chain. They have been used as templates for the synthesis of a mesoporous silicate designated SBA-2 that has hexagonal symmetry, regular supercages and a large inner surface area.[38] By altering the length of the inter-connecting methylene chain and surfactant tail it was possible to produce other phases including the cubic phase MCM-48. Dual chain dialkyldimethylammonium surfactants have also been

used successfully in the formation of M41S materials.[39] For the odd carbon numbers (n = 1, 3, 5, 7) MCM-41 was formed, while the even carbon numbers (n = 2, 4, 6, 8) and n > 9 surfactant produced a lamellar phase. The authors suggested that at $n > 7$ the surfactant behaves as a two-tailed molecule that favours the formation of a bilayer but were unable to explain the results obtained when $n < 7$.

1.3.3 The Use of Auxiliary-Organics as Pore-Swelling Agents

The pore size of M41S materials is easily tailored by altering the carbon chain length of the surfactant template. In one of the original Mobil papers, however, Beck *et al*[2] document the use of mesitylene as a pore-swelling agent to form even larger mesoporous solids. A recent paper by Ulagappan and Rao[40] investigates the use of straight chain alkanes as pore-swelling agents. The following schematic diagram (Figure 1.3) shows a micelle of surfactant molecules in (a) the absence and (b) the presence of a normal alkane. X-Ray diffraction patterns of mesoporous silica formed with a cationic surfactant in the presence of normal alkanes of increasing carbon chain lengths showed an increase in the observed d_{100} values that corresponded to the lengths of the alkane chain and surfactant tail being approximately additive in forming the micelle template.

In this study we document the use of mesitylene and tetradecane as pore-swelling agents in the synthesis of organically modified MCM-41 materials.

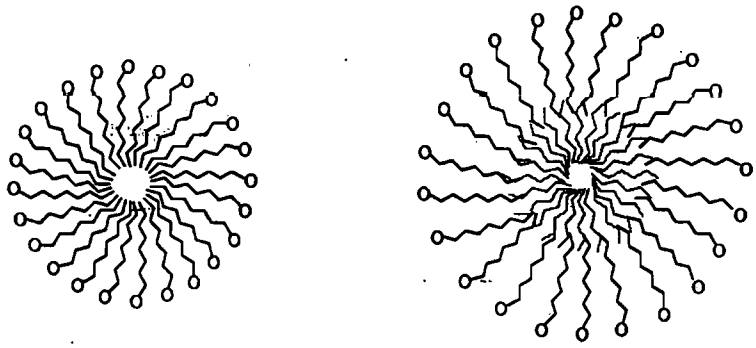

(a) (b)

Figure 1.3 Diagram showing (a) a liquid crystal micelle and (b) the use of straight chain alkanes as auxiliary organics.

1.3.4 Organically Modified MCM-41

As one of the major potential applications of MCM-41 is its use as a catalyst, it is desirable to incorporate catalytically active metals or organometallics into the MCM-41 framework. Early attempts to incorporate guest species in the channels of the mesoporous aluminosilicate MCM-41 resulted in low guest loadings, probably due to the absence of specific interactions between host and guest. The use of organically functionalized mesoporous materials may alleviate this problem and the synthesis of hybrid inorganic-organic mesoporous silicas have recently been reported.[41] A phenyl-modified MCM-41 type material was synthesised at room temperature by the hydrolysis and co-condensation of siloxane and organosiloxane in the presence of a surfactant. In this report, the analysis of this phenyl-modified MCM-41 by adsorption of benzene and water vapour is reported. Preliminary nitrogen sorption and powder XRD data suggested that the sample was microporous and for this reason the synthesis of a mesoporous

phenyl-modified MCM-41 has been performed and is reported here. The synthesis of several other organically-modified mesoporous silicas has also recently been reported[42-46] and, in this study, the synthesis and characterization of mesoporous silicas containing vinyl, aminopropyl and mercaptopropyl functions is also described.

1.3.5 Metal-containing MCM-41

The large surface area and tailorable pore structure of MCM-41 makes it a suitable support for catalytically-active metals. A large number of transition-metal substituted, hexagonal, mesoporous silicas have been prepared[47-51] including Ti-, V-, Cr-, Mo- and Mn-substituted materials.[52-58] The catalytic activity of these materials has been studied and some examples are given in Section 1.5.2, below.

In addition to these well-known catalytically-active metals, more unusual materials have been synthesized, such as an MCM-41 encapsulating a ruthenium porphyrin[59] (for alkene oxidation) and organolanthanide-containing MCM-41.[60]

In this study, the synthesis and partial characterization of an iron-containing MCM-41 is reported.

1.4 M41S-Type Materials in Context

In order to appreciate the relevance of M41S-type solids in the field of sorption and catalysis, it is useful to first consider some commonly used porous solids. The position of M41S-type materials, relative to various other types of porous solid in the IUPAC classification system, is given in Figure 1.3, below. As shown in the diagram,

M41S-type solids have pore diameters which fall in the range of 20 - 100 Å but most commonly, pore diameters of approximately 40 Å are observed.

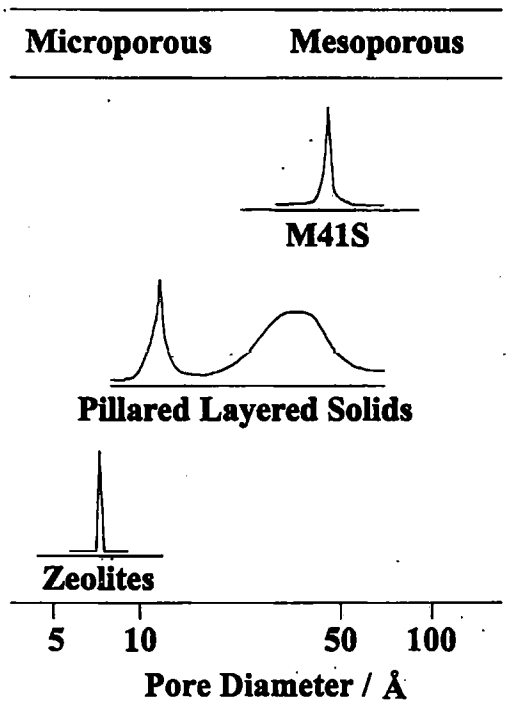

Figure 1.3 Pore-Size Classification of Various Types of Porous Solid[64]

As previously mentioned, zeolites are microporous, while pillared layered solids may display microporous and/or mesoporous characteristics. Basic descriptions of zeolites and commonly encountered pillared layered solids are given below.

1.4.1 Zeolites[61-63]

Zeolites are model microporous solids. The primary building blocks of all zeolites are SiO_4 and AlO_4 tetrahedra linked together by sharing corner oxygens to form ring systems. Four tetrahedra linked together form a so-called 4-ring, six tetrahedra form a 6-ring *etc* (Figure 1.4).

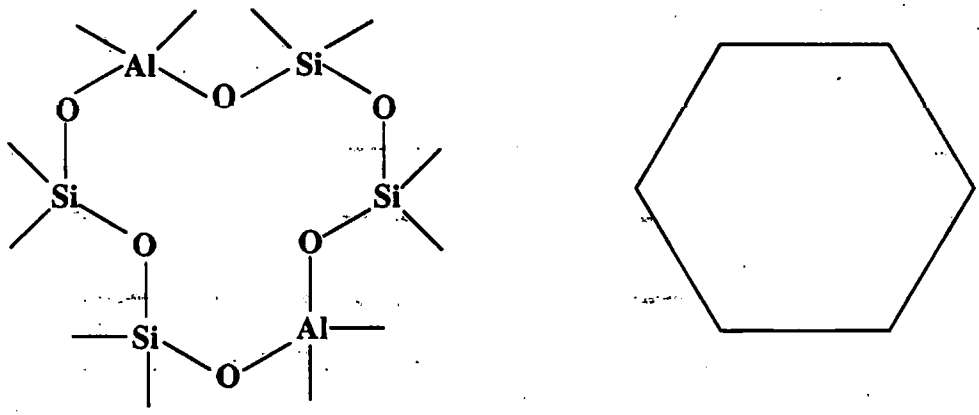

(a) (b)

Figure 1.4 (**a**) A Zeolite 6-ring and (**b**) The short-hand depiction of a 6-ring

A secondary building unit commonly observed in this family of materials is the sodalite unit which is a truncated octahedron composed of linked 4- and 6-rings. It is the packing of these sodalite units which yields large cavities in many zeolite structures in which sorption, diffusion and catalysis may take place.

1.4.2 Pillared Layered Solids

Pillared layered solids, which may contain micropores, mesopores or a mixture of both, are commonly used as catalysts and adsorbents. This section will briefly consider the three main types of layered solid used for pillaring.[64] These are smectite clays, layered double hydroxides (LDH), and phosphates and phosphonates of tetravalent metals.

(i) Smectite Clays

Smectite clays are naturally occurring three-layer sheet silicates containing two layers of tetrahedrally co-ordinated atoms surrounding a layer with octahedrally co-ordinated atoms. The net negative charge attributable to substitutions in either the tetrahedral or octahedral layer is compensated by interlayer cations. In naturally occurring smectite clays these cations are the alkali and alkaline earth metals. These clays swell easily in water and, after swelling, the interlayer cations may be exchanged for larger oligomeric cations such as the Keggin ion $[Al_{13}O_4(OH)_{24}(H_2O)_{12}]^{7+}$. Calcination of the exchanged product dehydrates the pillars and forms stable links between the layers resulting in a porous solid. Mesoporosity is achieved due to the clays delaminating on swelling and ion exchange to form small packages or single layers. When the clay is dried these packages are roughly arranged creating mesopores between them. The major disadvantage of this procedure, however, is that it is not controlled and the pore dimensions can, therefore, not be tailored.

(ii) Layered Double Hydroxides

Another important class of layered solids are the layered double hydroxides (LDHs). These structures are based on that of $Mg(OH)_2$, brucite in which magnesium ions occupy the octahedral sites between each second layer of a close-packing of hydroxide ions. By substituting the divalent Mg^{2+} by trivalent ions such as Al^{3+}, positively charged layers are formed. The interlayer gaps are filled by charge compensating anions and thus providing a means of pillaring these solids.

(iii) Phosphates and Phosphonates of Tetravalent Metals

Another type of pillared solid is based on the expansion of the interlayer space of phosphates by tetravalent metals such as Ti, Zr and Sn. The phosphate oxygens are co-ordinated to the metal atom and the phosphate proton projects into the interlayer region. Substances typically used for the intercalation of the acidic interlayer region are organic amines.

Pillared layered zirconium phosphonates similar to the metal phosphate, but with R groups protruding into the interlayer region keeping the layers apart, can also be prepared. By partially replacing the organic residue with a smaller R group, R', a porous solid should result. It is then the length of the organic residue, R, that controls the height of the pores and the ratio of R : R' that controls the pore width.

1.4.3 MCM-41 in Context

The major difference between MCM-41 and the materials discussed above is the degree of control which may be exerted over the formation of the pore systems. In the case of the pillared layered solids, the pore system that is produced often contains pores in the micro- and mesoporous range and these solids therefore have a large pore-size distribution. This is obviously a disadvantage when designing a shape-selective catalyst (see next section).

While the zeolites obviously have the advantage of being crystalline and of having a well-defined, narrow pore-size distribution, these materials are microporous and are therefore of limited use in the catalysis of the reactions of large organic molecules.

MCM-41 and related materials combine the advantage of having an easily-tailored, well-defined pore structure with pore-diameters in the mesoporous range. The major disadvantage of these materials is the fact that the pore walls are amorphous.

1.5 Porous Solids as Catalysts

1.5.1 Shape-selective Catalysis in Zeolites

Zeolites are the crystalline analogues of the amorphous silica-aluminas that have long been used as acid catalysts. As previously mentioned, the primary building block of all zeolites are SiO_4 and AlO_4 tetrahedra. These are linked at every corner oxygen to yield a three dimensional framework containing regular channels and cavities. It is this very fine pore structure that is responsible for the zeolites ability to select molecules of a certain size to penetrate into, or escape from, the interior of the crystal.

It is acid sites arising from the AlO_4^- tetrahedra in the structure that are responsible for the catalytic activity of the zeolites. These sites are located both within the pore structure and on the outside surface. Surface areas of zeolites fall typically between 200 to 800 $m^2 g^{-1}$.

Shape-selective catalysis may be divided into three categories, namely reactant selectivity, product selectivity and restricted-transition-state selectivity. These three categories are discussed separately below.

(i) Reactant Selectivity

Reactant selectivity arises when one or more reactant species is denied access to the zeolite's active sites as a result of its molecular sieving properties. An example of this is the dehydration of a mixture of *n*-butanol and *iso*-butanol to form an alkene over two different zeolites.[61] Faujasite NaX (window size ≈ 8.5 Å), resulted in similar conversion rates for both *n*-butanol and *iso*-butanol whereas another zeolite, CaA, (window size ~ 4.5 Å) resulted in negligible dehydration of the bulky *iso*-butanol.

(ii) Product Selectivity

Product selectivity arises when only those species with the appropriate dimensions can diffuse out of the zeolitic cavity and appear as observed products. This is exemplified by the alkylation of toluene with methanol over the zeolite ZSM-5.[61] The product contains the *ortho*-, *meta*- and *para*-isomers of xylene with the latter in excess. The disproportionately high percentage of *para*-xylene in the product mixture may be explained by the "stream-line" structure of the *para*-isomer, which fits easily within the channels of ZSM-5; in contrast, the movement of the *ortho*- and *meta*-isomers within the zeolite channels is restricted by their bulky structure.

(iii) Restricted-transition-state Selectivity

A third type of shape-selective catalysis is based on the fact that reaction of the organic species takes place inside the zeolite cavity. It follows, therefore that, if the cavity dimensions are restrictive to the formation of a certain bulky transition state, further constraints are made on the reaction pathway. This restricted-transition-state selectivity is demonstrated by a study of the relative rates of disproportionation and

isomerisation of *o*-xylene over a variety of zeolites.[61] The results show that the rate of disproportionation relative to isomerisation falls considerably as the cavity size is reduced. This can be explained by considering the nature of the two reactions. Disproportionation is a bimolecular process requiring the formation of a bulky transition state, while isomerisation is unimolecular involving intra-molecular methyl shifts and transition states with dimensions similar to those of the product.

1.5.2 M41S Materials as Shape-selective Catalysts

The large pore size of M41S type materials relative to zeolites has led to a great deal of interest in the possible use of these materials as catalysts and catalyst supports.[65-71] The use of mesoporous solids as acid catalysts is permitted by the incorporation of aluminium, as substitution of silicon with aluminium yields Bronsted and Lewis acid sites. Catalytically-active metals have also been incorporated into the inorganic framework. Recently, attention has been focused on the acid catalysis of larger organic molecules. An example of this is the study made of the alkylation of the bulky 2,4-di-*t*-butyl phenol with cinamyl alcohol using aluminosilicate MCM-41 as the catalyst.[72] It was shown that the primary alkylation product 6,8-di-*t*-2phenyl-2,3-dihydro[4H]benzopyran was formed with MCM-41, while the restricted environment of the zeolite HY did not permit alkylation to occur.

As mentioned in Section 1.3.5, various catalytically active metals such as vanadium[55] and titanium[54] have been incorporated into M41S type materials and the selective oxidation of large organic molecules investigated. Corma *et al*[54] have produced a titanium silicate isomorphous to MCM-41 that has an average pore diameter of 20 Å and a surface area of 936 m^2 g^{-1}. They have shown that this titanium silicate catalyses

the epoxidation of hex-1-ene by H_2O_2, and the epoxidation of norbornene with terbutylhydroperoxide (THP). The latter reaction is of interest as the bulky nature of the oxidant prevented the zeolite TS-1 from being used as a catalyst. Corma *et al*[67] have also developed a NiMo-MCM-41 which may be used as a catalyst in the hydrocracking of vacuum gasoil. It was found to be more effective at desulfurization and denitrogenation than zeolite analogues with the same metal loading. The authors attributed this to be due to a combination of large surface area, uniform pore size distribution and reduced diffusion problems, combined with the required mild acidity due to the presence of aluminium centres.

1.6 Objectives

The main aims of this study were the synthesis and characterization of novel, chemically tailored MCM-41 type sorbents *via* a liquid-crystal templating method. The application of different synthesis protocols to yield ordered mesoporous materials was under investigation.

The synthesis of a series of materials containing functions which could potentially be used for catalysis purposes was also an objective.

Gas adsorption studies of this class of materials can yield important information concerning pore structure and surface characteristics. The measurement of the adsorption isotherms of various adsorptives on these materials (using both automated volumetric and manual gravimetric techniques) was therefore an objective.

REFERENCES

1. Kresge, C.T.; Leonowicz, H.E.; Roth, W.J.; Vartuli, J.C.; Beck, J.S. *Nature*, **1992**, *359*, 710-712.
2. Beck, J.S.; Vartuli, J.C.; Roth, W.J.; Leonowicz, M.E.; Kresge, C.T.; Schmitt K.D.; Chu, C.T-W.; Olson, D.H.; Sheppard, E.W.; McCullen, S.B.; Higgens, J.B.; Schlenker, J.L. *J. Amer. Chem. Soc.* **1992**, *114*, 1083-1043.
3. Vartuli, J.C.; Schmitt, K.D.; Kresge, C.T.; Roth, W.J.; Leonowicz, M.E.; McCullen, S.B.; Hellring, S.D.; Beck, J.S.; Schlenker, J.L.; Olson, D.H.; Sheppard, E.W. *Chem. Mater.* **1994**, *6*, 2317-2326.
5. Vartuli, J.C.; Kresge, C.T.; Leonowicz, M.E.; Chu, A.S.; McCullen, S.B.; Johnson, I.D.; Sheppard, E.W. *Chem. Mater.*, **1994**, *6*, 2070-2077.
6. Coustel, N.; Di Renzo, F.; Fajula, F. *J. Chem. Soc., Chem. Commun.*, **1994**, 967-968.
7. Schmidt, R. *J. Chem. Soc., Chem. Commu.n*, **1994**, 1493-1494.
8. Edler, K.J.; White, J. W., *J. Chem. Soc., Chem. Commun.*, **1995**, 155 - 156
9. Edler, K.J.; Dougherty, J.; Durand, R.; Iton, L.; Kirton, G.; Lockhart, G.; Wang, Z.; Withers, R.; White, J.W., *Colloids and Surfaces, A: Physicochemical and Engineering Aspects*, **1995**, *102*, 213-230.
10. Alfredsson, V.; Keung, M.; Monnier, A.; Stucky, G.; Unger, K.; Schuth, F., *J. Chem. Soc., Chem. Commun.*, **1994**, 1921 - 1922.
11. Luan, Z.; Cheng, C-F.; Zhou, W.; Klinowski, J., *J. Phys. Chem.* **1995**, *99*, 1018-1024.
12. Luan, Z.; Heyong, H.; Cheng, C-F.; Zhou, W.; Klinowski, J., *J. Chem. Soc., Faraday Trans.*, **1995**, *91*(17), 2955-2959.

13. Borade, R.B.; Clearfield, A., *Catalysis Letters*, **1995**, 267-272.

14. Scmidt, R.; Junggreen, H.; Stocker, M., *J. Chem. Soc., Chem. Commun.*, **1996**, 875-876.

15. Alfredsson, V.; Anderson, M.W. *Chem. Mater.* **1996**, *8*, 1141-1146.

16. Wu, C. G.; Bein, T. *J. Chem. Soc., Chem. Commun.*, **1996**, 925-926.

17. Hamdon, H.; Endud, S.; He, H.; Muhid, M.; Kilnowski, J., *J. Chem. Soc., Faraday Trans.*, **1996**, *92*(12), 2311-2315.

18. Silva, H.P.; Pastore, H.O., *J. Chem. Soc., Chem. Commun.*, **1996**, 833-834.

19. Edler, K.J.; Reynolds, P.A.; White, J.W.; Cookson, D., *J. Chem. Soc., Faraday Trans.*, **1997**, *93*(1), 199-202.

20. Alfredsson, V.; Anderson, M.W.; Ohsuna, T.; Terasaki, O.; Jacob, M.; Bojrup, M., *Chem. Mater.*, **1997**, *9*, 2066-2070.

21. Corma, A.; Kan, Q.; Navarro, M.T.; Perez-Pariente, J.; Rey, F.; *Chem. Mater.*, **1997**, *9*, 2123-2126.

22. Gallis, K.W.; Landry, C.C., *Chem. Mater.*, **1997**, *9*, 2035-2038.

23. Ko, C.H.; Ryoo, R., *J. Chem. Soc., Chem. Commun.*, **1996**, 2467-2468.

24. Huo, Q.; Feng, J.; Schuth, F.; Stucky, G., *Chem. Mater.*, **1997**, *9*, 14-17.

25. Mann, S.; Burkett, S.L.; Davis, S.A.; Fowler, C.E.; Mendelson, N.H.; Sims, S.D.; Walsh, D.; Whilton, N.T., *Chem. Mater.*, **1997**, *9*, 2300-2310.

26. Raimondo, M.; Perez, G.; Sinibaldi, M.; De Stefanis, A.; Tomlinson, A.A.G., *J. Chem. Soc., Chem. Commun.*, **1997**, 1343-1344.

27. Kim, J.M.; Kim, S.K.; Ryoo, R., *J. Chem. Soc., Chem. Commun.*, **1998**, 259-260.

28. Wang, X.; Dou, T,; Xiao, Y., *J. Chem. Soc., Chem. Commun.*, **1996**, 1035-1036.

29. Casci, J.L., *Advanced Zeolite Science and Applications, Studies in Surface Science and Catalysis,* **1994**, 329-356.

30. Brinker, C.J., *Current Opinion in Solid State and Materials Science.*, **1996**, *1*, 798-805.

31. Antonellii, D.M.; Ying, J.Y., *Current Opinion in Colloid and Interface Science.*, **1996**, *1*, 523-529.

32. Corma, A., *Chem. Rev.*, **1997**, *97*, 2373-2419.

33. Sing, K.S.W.; Everett, D.H.; Haul, R.A.W.; Moscou, L.; Pierotti, R.A.; Rouquerol, J.; Siemiemiewska, T. *Pure and App. Chem.*, **1965**, *57*, 603.

34. Tanev, P.T.,; Pinnavaia, T.J., *Science*, **1995**, *267*, 865-867.

35. Bagshaw, S.A.; Prouzet, E.; Pinnavaia, T.J., *Science*, **1995**, *269*, 1242-1244.

36. Tuel, G.; Gontier, S., *Chem. Mater.*, **1996**, *8*, 114-122.

37. Attard, G.S.; Glyde, J.C.; Goltner, C.G., Nature, **1995**, *378*, 366-368.

38. Huo, Q.; Leon, R.; Petroff, P.M.; Stucky, G., *Science*, **1995**, *268*, 1324-1327.

39. Sayari, A.; Karra, V.R.; Sudhaker Reddy, *J. Symp. on Synthesis of Zeolites*. Layered Compounds and other Microporous Solids: Division of Petrol Chem. 209th National American Chemical Society Meeting: **1995**; Anaheim, California.

40. N. Ulagappan and C.N.R. Rao, *J. Chem. Soc., Chem. Commun.*, **1996**, 2759-2760.

41. Burkett, S.L.; Sims, S.D.; Mann, S., *J. Chem. Soc., Chem. Commun.*, **1996**, 1367-1368.

42. Fowler, C.E.; Burkett, S.L.; Mann, S., *J. Chem. Soc., Chem. Commun.*, **1997**, 1769-1770.

43. Clark, J.H.; MacQuarrie, D.J., *J. Chem. Soc., Chem. Commun.*, **1998**, 853-860.

44. Rhijn, W.; Vos, D.; Sels, B.; Bossaert, W.; Jacobs, P., *J. Chem. Soc., Chem. Commun.*, **1998**, 317-318.

45. Lim, M.H.; Blanford, C.F.; Stein, A., *J. Am. Chem. Soc.*, **1997**, *119*, 40490-4091.

46. Macquarrie, D.J., *J. Chem. Soc., Chem. Commun.*, **1996**, 1961-1962.

47. Abdel-Fattah, T.M.; Pinnavaia, T.J., *J. Chem. Soc., Chem. Commun.*, **1996**, 665-666.

48. Li, J.; Delmotte, L.; Kessler, H., *J. Chem. Soc., Chem. Commun.*, **1996**, 1023-1024.

49. Diaz, J.F.; Balkus, K.J.; Bedioui, F.; Kurshev, V.; Kevan, L., *Chem. Mater.*, **1997**, *9*, 61-67.

50. Yuan, Z.Y.; Liu, S.Q.; Chen, T.H.; Wang, J.Z.; Li, H.X., *J. Chem. Soc., Chem. Commun.*, **1995**, 973-974.

51. Jones, D.J; Jimenez-Jimenez, J.; Jimenez-Lopez, A.; Maireles-Torres, P.; Olivera-Pastor, P.; Rodriguez-Castellon, E.; Roziere, J., *J. Chem. Soc., Chem. Commun.*, **1997**, 431-432.

52. Tanev, P.T.; Chibwe, M.; Pinnavaia, T.J., *Nature*, **1994**, 368, 321-323.

53. Alba, M.D.; Becerro, A.I.; Klinowski, J., *J. Chem. Soc., Faraday Trans.*, **1996**, *92*(5), 849-854.

54. Corma; Navarro; Pariente, *J. Chem. Soc., Chem. Commun.*, **1994**, 147-148.

55. Park, D.H.; Cheng, C-F.; He, Heyong.; Klinowski, J., *J. Mater. Chem.*, **1997**, *7*(1), 159-162.

56. Zhang, W.; Wang, J.; Tanev, P.T.; Pinnavaia, T.J., *J. Chem. Soc., Chem. Commun.*, **1996**, 979-980.

57. Ulagappan N.; Rao, C.N.R., *J. Chem. Soc., Chem. Commun.*, **1996**, 1047-1048.

58. Burch, R.; Cruise, N.; Gleeson, D.; Tsang, S.C., *J. Chem. Soc., Chem. Commun.*, **1996,** 951-952.

59. Liu, C-J.; Li, S-G.; Pang, W-Q.; Che, C-M., *J. Chem. Soc., Chem. Commun.*, **1997,** 65-66.

60. Anwander, R.; Roesky, R., *J. Chem. Soc., Dalton Trans.*, **1997,** 137-138.

61. O.U. Science : A Third Level Course. S342 Physical Chemistry : Principles of Chemical Change. Topic 2, Petrol from Coal, O.U. Press, Milton Keynes, **1985.**

62. Kokotailo, G.T.; Chu, P.; Lawton, S.L.; Meier, W.M., *Nature*, **1978**, *275*, 119-120.

63. Kokotailo, G.T.; Lawton, Olson, D.H.; S.L.; Meier, W.M., *Nature,* **1978**, *272*, 437-438.

64. Behrens, P. *Adv. Mater.* **1993**, *5*, 127-132.

65. Corma, A., *Current Opinion in Solid State and Materials Science*, **1997**, 2, 63-75.

66. Moyako, R.; Jones, W., *J. Chem. Soc., Chem. Commun.*, **1996,** 981-982.

67. Corma, A.; Martinez-Soria, V.; Monton, J.B.; *Journal of Catalysis,* **1995,** *153,* 25-31.

68. Mokayo, R.; Jones, W.; Luan, Z.; Alba, M.D.; Klinowski, J., *Catalysis Letters*, **1996,** *37*, 113-120.

69. Moyako, R.; Jones, W., *J. Chem. Soc., Chem. Commun.*, **1996,** 983-984.

70. Kloetstra, K.R.; van Bekkum, H., *J. Chem. Res.*, **1995**, 26-27.

71. Kloetstra, K.R.; van Bekkum, H., *J. Chem. Soc., Chem. Commun.*, **1995,** 1005-1006.

72. Armengol, E.; Cano, M.L.; Corma, A.; Garcia, H.; Navarro, M.T.; *J. Chem. Soc., Chem. Commun.*, **1995**, 519-520.

CHAPTER 2

EXPERIMENTAL

This chapter is divided into two parts. Part I details the synthesis of materials while Part II considers the characterization techniques employed in this study.

PART I - SYNTHESES

Part I of this chapter is divided into two sections. The first concerns the synthesis of M41S materials containing no organic functions, while the second section discusses the synthesis of organically-functionalized mesoporous silicas.

2.1 M41S Materials

Materials

The flow diagram shown as Figure 2.1 describes the general synthesis of M41S solids. The base catalyst used in the synthesis was either tetramethylammonium hydroxide (TMAOH, Aldrich) or sodium hydroxide (Hopkin and Williams, AnalaR), and the silica source was either (a) tetraethylorthosilicate (TEOS, Aldrich) or (b) tetramethylammonium silicate (TMAS, see synthesis in Section 2.1.1) and precipitated silica (BDH). The template used in each case was an aqueous solution of cetyltrimethylammonium chloride (CTMACl, Aldrich). Sodium aluminate (Riedel-de Haën), or aluminium sulphate (Hopkin and Williams, AnalaR) were used as the aluminium source. Table 2.1, given at the end of

this section, summarizes the reaction conditions for each batch. The aluminosilicate materials were prepared using two methods devised by Schmidt *et al* with the aim to produce a material containing aluminium in a tetrahedral environment (required for acid catalysis). The preparation of a range of materials is now described.

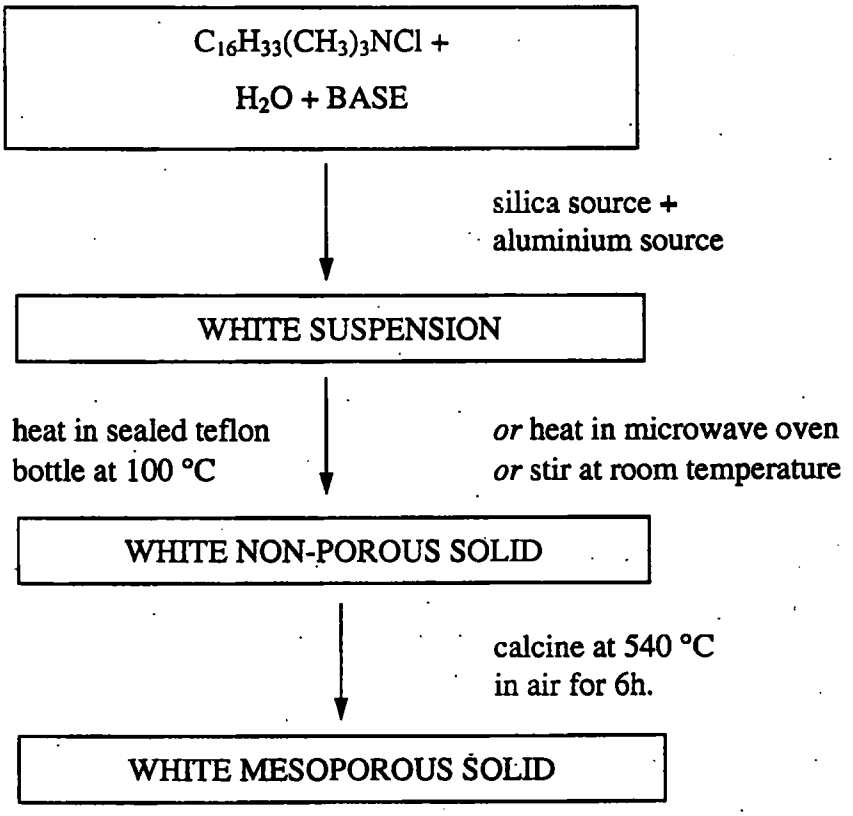

Figure 2.1 Flow diagram describing the general synthesis of M41S materials.

The microwave oven used in the following syntheses was a standard Hotpoint 850 W domestic microwave oven.

2.1.1 MCM-41 Preparation 1

(Preparation According to Schmidt.[1])

The synthesis of this MCM-41 sample differs from those of the other M41S materials described below in that it uses a tetramethylammonium silicate (TMAS) solution as a silica source. The preparation of this solution is now described: 30.48 g of 25% by mass aqueous tetramethylammonium hydroxide (0.084 mol, Aldrich) was combined with 16.82 g of 30% by mass aqueous colloidal silica (0.084 mol, Ludox, Du Pont) and 13 g (0.72 mol) of deionized water. Thus a 1:1 solution of TMAOH and SiO_2 (containing 10% SiO_2 by mass) was produced, which was then aged at room temperature for 96 h.

50 g of the above precursor solution was added to an aged solution containing 2.1 g (4.33 mmol) of sodium aluminate, 31 g (0.024 mol) of 25 % by mass aqueous cetyltrimethyl ammonium chloride (CTMACl) and 13 g (0.72 mol) of deionized water. To this white precipitate was added 12.5 g (0.2 mol) of precipitated silica and, after stirring, 10 g (0.105 mol) of 25% by mass tetramethylammonium hydroxide solution. The resulting gel was divided into two portions and treated as follows:

i) Sealed Teflon Bottle Synthesis - MCM-41(a)

One portion of the reaction mixture was loaded into a teflon bottle which was stoppered and heated in an oven at 100 °C for 23 h. The white solid was recovered by filtration, washed with copious deionized water and dried over $CaCl_2$. A portion of the product was calcined in air at 540 °C for 6 h.

ii) Microwave Synthesis - MCM-41(b)

The second portion of the reaction mixture was loaded into a conical flask, covered with a petri dish and heated in a 850 W domestic microwave at 10% power for 20 minutes, stirring the mixture every 2 minutes. The product was again recovered by filtration, washed with deionized water and was dried over $CaCl_2$. A portion was calcined at 540 °C in air for 6 h.

2.1.2 MCM-41 Preparation 2.

(Preparation According to Schmidt.[2])

21.3 g (0.102 mol) TEOS was added to a solution containing 2.48 g (0.062 mol) NaOH, 13.2 g (0.042 mol) of 25% by mass CTMACl and 180 g (10 mol) of deionized water. The solution was maintained at approximately 30 °C and stirred for 5 minutes to produce a white suspension (molar ratio *ca.* 100 H_2O : 1 TEOS : 0.4 CTMACl; surfactant/silica < 1, as required for MCM-41 formation, see chapter 1). 1.1 g (1.74 mmol) of aluminium sulphate was then added and the solution stirred at 30 °C for 1 h. Again the reaction mixture was divided into two portions and treated as follows:

i) Sealed Teflon Bottle Synthesis - MCM-41(c)

The first portion of reaction mixture was loaded into a teflon bottle which was stoppered and heated in an oven for 72 h at 100 °C. The solid was filtered, washed with deionized water and dried. A portion was calcined at 540 °C in air for 6 h.

ii) Microwave Synthesis - MCM-41(d)

The procedure used in the microwave synthesis of sample MCM-41(b) (section 2.1.1) was applied to the second portion of the reaction mixture.

2.1.3 Iron-containing MCM-41[3]

10.65 g (0.05 mol) of TEOS was added to a solution containing 1.3 g (0.03mol) of NaOH, 6.58 g (0.021 mol) of 25% by mass aqueous CTMACl and 90 g (5 mol) of deionized water (molar ratio *ca.* 100 H_2O : 1 TEOS : 0.4 CTMACl; surfactant/silica < 1, as required for MCM-41 formation). The resulting white suspension was stirred at room temperature for 5 min before the addition, with stirring, of 0.5 g (1.2 mmol) of $Fe(NO_3)_3.9H_20$ (BDH). A pale brown suspension was produced which was stirred at room temperature for 1 h before being loaded into a teflon bottle, which was sealed and heated in a conventional oven at 100 °C for 5 days. A slightly discoloured homogeneous product was recovered by filtration, washed with deionized water and dried at room temperature. The product was calcined in air at 540 °C for 6 h.

2.1.4 Purely siliceous MCM-41

To 56 g (3.1 mol) of H_2O was added 4.6 g (3.62 mmol) of 25% by mass CTMACl and 16 g of NaOH(aq) (1 mol dm^{-3}). To this was added 6.5 g (32 mmol) TEOS, and the resulting white suspension was stirred for 48 h at room temperature to produce sample SiMCM-41(a) (molar ratio *ca.* 100 H_2O : 1 TEOS : 0.1 CTMACl; surfactant/silica < 1, as required for MCM-41 formation). Half of the mixture was then loaded into a teflon bottle which was sealed and heated in an oven at 100 °C for 24 h. The white solid, sample

SiMCM-41(b), was recovered by filtration, washed with deionized water and dried under vacuum at 50°C. A portion was calcined in air at 540 °C for 6 h.

Table 2.1 Summary of the reaction conditions for M41S syntheses.

Sample	Template	Base	Silica Source	Metal Source	Heating Method
MCM-41 (a)	CTMACl	TMAOH	TMAS precipitated silica	sodium aluminate	Sealed vessel (100 °C)
MCM-41 (b)	CTMACl	TMAOH	TMAS precipitated silica	sodium aluminate	Microwave Oven
MCM-41 (c)	CTMACl	NaOH	TEOS	aluminium sulphate	Sealed vessel (100 °C)
MCM-41 (d)	CTMACl	NaOH	TEOS	aluminium sulphate	Microwave Oven
FeMCM-41	CTMACl	NaOH	TEOS	Iron nitrate	Sealed vessel (100 °C)
SiMCM-41 (a)	CTMACl	NaOH	TEOS	-	Stirred at ambient temperature
SiMCM-41 (b)	CTMACl	NaOH	TEOS	-	As SiMCM-41(a) + sealed vessel (100 °C)

CTMACl - Cetyltrimethylammonium chloride

TMAOH - Tetramethylammonium hydroxide

TMAS - Tetramethylammoniumsilicate

TEOS - Tetraethylorthosilicate

2.2 Organically-functionalized Mesoporous Silica

This section considers the synthesis of mesoporous silicas containing organic functional groups and the use of auxiliary organics as pore-swelling agents. A phenyl-modified sample, which was synthesized at the University of Bath by Burkett *et al*[4] and analyzed, at Exeter, by the author, is also described. Figure 2.2 describes the general synthesis of an organically modified mesoporous silica. In each case the amount of organosiloxane provided no more than 20 mol % of the total silicon. Again, cetyltrimethylammonium chloride (CTMACl) was used as the template in a solution of concentration less than that of the liquid crystal mesophase. Either tetradecane ($C_{14}H_{30}$) or mesitylene (1,3,5-trimethyl benzene) were used the as pore-swelling agent. A summary of synthesis conditions for each experiment is given in Table 2.2 at the end of this section.

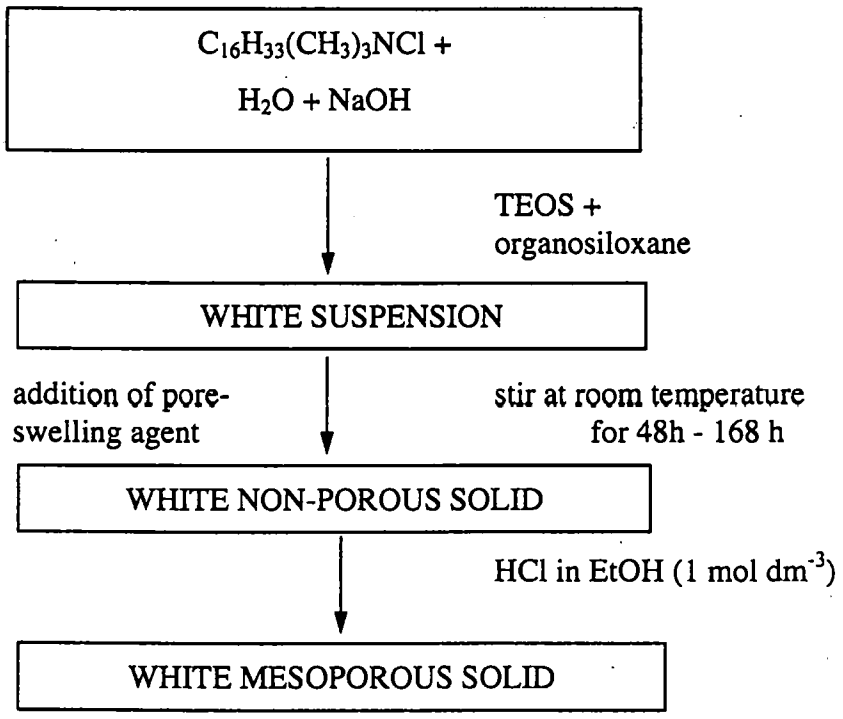

Figure 2.2 Flow diagram describing the synthesis of organically-functionalized mesoporous silicas.

It should be noted that the pore-swelling agent must be added after the silica source. Addition of the auxiliary organic before the silica source results in the formation of a non-porous solid. This could possibly be caused by the organic moiety preventing formation of the liquid crystal micelle.

(a) Analysis of PhMCM-41 Synthesized at the University of Bath

2.2.1 Characterization of PhMCM-41 (synthesized by Burkett et al[4])

The characterization of a phenyl-modified mesoporous silica, synthesized by Burkett *et al*[4] at the University of Bath, was carried out at Exeter. This involved X-ray powder diffraction, N_2 sorption at 77 K, water sorption at 303 K and benzene sorption at 293 K. Results of these studies are given in Sections 3.6 and Sections 5.4, 5.6 and 5.7 respectively. The synthesis of the material was carried out (at Bath) as follows:

The synthesis of a phenyl modified MCM-41 was realized by the hydrolysis and co-condensation of a siloxane and organosiloxane in the presence of a surfactant (molar composition = 0.12 CTMABr : 0.5 NaOH : 1.0 total siloxane : 130 H_2O). The organosiloxane used in the synthesis of PhMCM-41 was phenyltriethoxysilane (PTES) and this accounted for 20 mol % of the total siloxane used in the initial synthesis mixture. As calcination would result in the destruction of the organic function, the template molecules were removed using an acid extraction technique (stirred in HCl in EtOH (1 mol dm^{-3}) at 70°C for 24 h) to yield an ordered porous solid. A control sample containing no phenyl groups was synthesized using 100% TEOS as the silica source.

(b) Synthesis of Organically-Modified Mesoporous Silicas

The following syntheses were carried out by the author at the University of Exeter.

2.2.2 Phenyl-modified mesoporous silicas using auxiliary organics as pore swelling agents.

Mesoporous phenyl-modified silicas, containing 20 mol % PTES in the original synthesis composition, were prepared at ambient temperature at Exeter. An unmodified, (purely siliceous) sample (SiMCM-41(a)), prepared in the same conditions, was also synthesized and is described in section 2.1.4. The preparation of mesitylene-swollen, tetradecane-swollen and an unswollen phenyl-modified material is now reported.

Materials

Silica sources were tetraethoxysilane (TEOS, Aldrich) and phenyltriethoxysilane (PTES, Lancaster). The quaternary ammonium surfactant used as the templating agent was 25% by mass aqueous cetyltrimethylammonium chloride, $C_{16}H_{33}(CH_3)_3NCl$ (CTMACl, Aldrich). The auxiliary organics used as pore swelling agents[5,6] were mesitylene (MES, Lancaster) and tetradecane (TET, Aldrich). All chemicals were used as received.

(i) Unswollen phenyl-modified silica.

This sample uses the same preparative method as that used by Burkett *et al*[4] and was prepared as a control sample. 2.4 cm^3 (1.8 mmol) of 25 % by mass CTMACl was added to a solution of 8 g of NaOH(aq) (1.0 mol dm^{-3}) in 28 g of H_2O. 2.8 cm^3 (12.6

mmol) of TEOS and 0.8 cm^3 (3.3 mmol) of PTES were then added and the solution was then stirred at room temperature for 48 h. The white solid product was recovered by filtration, washed with deionized water and dried in an oven at 100 °C. Surfactant extraction was performed by stirring a suspension of the as-synthesized product in HCl in EtOH (1.0 mol dm^{-3}) at 70 °C for 24 h[4]. The extracted material was recovered by filtration, washed with ethanol and dried *in vacuo* (dynamic) at 100 °C.

(ii) Mesitylene-swollen phenyl-modified silica.

Procedure 2.2.2(i) was repeated, but with addition of 1.3 g (10.8 mmol) MES[5] to the reaction mixture following addition of the siloxane.

(iii) Tetradecane-swollen phenyl-modified silica.

Procedure 2.2.2(i) was repeated, but with addition of 0.36 g (1.81 mmol) TET to the reaction mixture following addition of the siloxane (TET / CTMACl molar ratio = 1)[6].

2.2.3 Mesitylene-swollen vinyl-functionalized mesoporous silica.

2.8cm^3 (12.6 mmol) of TEOS and 0.64 cm^3 (1.52 mmol) of vinyltriethoxysilane (VTES, Lancaster) were added to a solution of 2.4 cm^3 (1.8 mmol) of 25% by mass CTMACl and 8 g of 1 mol dm^{-3} NaOH(aq) solution in 28 g of H_2O. A white precipitate was produced to which was added 1.5 cm^3 (10.8 mmol) of MES. The suspension was stirred at room temperature for 36 h, filtered, washed with deionized water and dried in a vacuum oven at 50 °C overnight. The acid extraction technique described in 2.2.2(i) was employed to remove the template.

2.2.4 Mesitylene-swollen aminopropyl-functionalized mesoporous silica.

2.8cm^3 (12.6 mmol) of TEOS and 0.36 cm^3 (1.52 mmol) of 3-aminopropyl-triethoxysilane (APTES, Lancaster) were added to a solution of 2.4 cm^3 (1.8 mmol) 25% by mass CTMACl and 8 g of NaOH(aq) solution (1 mol dm^{-3}) in 28 g (1.56 mol) of deionized H_2O. A white precipitate was produced to which was added 1.5 cm^3 (10.8 mmol) of MES. The suspension was stirred at room temperature for 7 days, filtered, washed with deionized water and dried in air at room temperature. The acid extraction technique described in 2.2.2(i) was employed to remove the template.

2.2.5 Mesitylene-swollen mercaptopropyl-functionalized mesoporous silica.

5.4 cm^3 (25.0 mmol) of TEOS and 3.0 cm^3 (21.6 mmol) of MES were added to a solution of 5.0 cm^3 (3.6 mmol) 25% by mass CTMACl and 16 g of 1 mol dm^{-3} NaOH(aq) in 56 g (3.1 mol) deionized H_2O. A white precipitate was produced to which was added 1.25 cm^3 (6.6 mmol) of 3-mercaptopropyltrimethoxysilane (MPTMS, Lancaster) (carried out in a fume hood). In this case the organosiloxane was added at the end of the reaction due to the noxious nature of MPTMS. The suspension was stirred at room temperature for 7 days, filtered, washed with deionized water and dried in air at room temperature. The acid extraction technique described in 2.2.2(i) was employed to remove the template.

Table 2.2 Summary of the reaction conditions of each organically-modified synthesis.

Sample	Template	Organo-siloxane*	Reaction Time
PhMCM-41 (Burkett)	CTMABr	PTES (20 mol %)	24 h
Unswollen Ph-modified	CTMACl	PTES (20 mol %)	48 h
MES-swollen Ph-modified	CTMACl	PTES (20 mol %)	48 h
TET-swollen Ph-modified	CTMACl	PTES (20 mol %)	48 h
MES-swollen V-modified	CTMACl	VTES (10 mol %)	36 h
MES-swollen AP-modified	CTMACl	APTES (10 mol %)	1 week†
Mes-swollen MP-modified	CTMACl	MPTMS (20 mol %)	1 week†

* Figures in brackets are mole percentages of total siloxane.
PTES - phenyltriethoxysilane; VTES - vinyltriethoxysilane;
APTES - aminotriethoxysioxlane; MPTMS - mercaptotrimethoxysilane.

† A longer reaction time was employed in these cases in an attempt to improve the degree of siloxane condensation.

In each case:

Stirred at ambient temperature.

Silica source - TEOS; Base - NaOH; Surfactant extraction method - 1 mol dm^{-3} HCl/EtOH, 70 °C, 24 h.

PART II - CHARACTERIZATION TECHNIQUES

Characterization of the synthesized materials was achieved via X-ray powder diffraction, infra-red spectroscopy, thermogravimetry, transmission electron microscopy and magic-angle-spinning nuclear magnetic resonance (MAS-NMR) spectroscopy. These techniques are now described below. Table 2.3, given at the end of this section, details which characterization techniques were used for each sample. The background to gas adsorption and inelastic neutron scattering studies, which were also used to characterize these materials, are dealt with in detail in Chapters 4 and 6 respectively.

2.3 X-Ray Powder Diffraction (XRD)

2.3.1 Miller Indices[7,8]

When determining the structure of a solid-state material it is useful to be able to define the planes within a crystal structure and this is generally done by using Miller Indices. Close-packed structures such as ionic materials may, in certain orientations, be regarded as consisting of layers or planes of atoms in a three-dimensional arrangement. These lattice planes provide a reference structure to which the atoms in a crystal structure may be referred.

In amorphous, porous materials such as M41S type solids, lattice planes are still relevant when considering the periodicity of the pore system. The relationship between lattice planes and MCM-41 is discussed in the following section (2.3.2).

Lattice planes are identified by assigning three labels known as the Miller Indices: *hkl*. The values of these indices are calculated by considering the positions at which the planes intersect the axes of a unit cell. This is demonstrated in Figure 2.3.

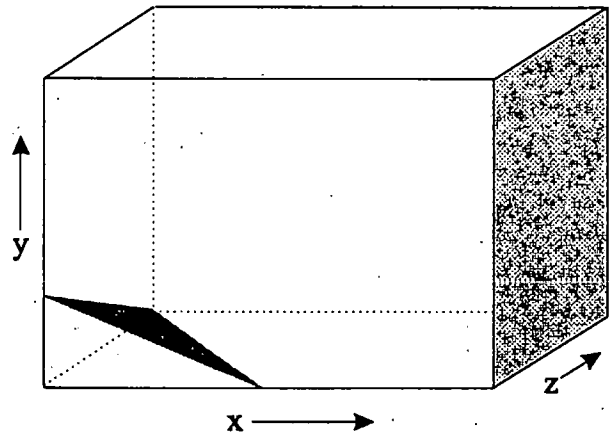

Figure 2.3 Two planes in a unit cell

If the axes are assumed to range from 0 to 1, the dark grey plane shown in Figure 2.3 intersects the x-axis at ½, the y-axis at ⅓ and the z-axis at 1. The fractional intersections are therefore, ½, ⅓, 1. By taking the reciprocals of these fractions, the Miller Indices of the plane are obtained; in this case *231*. The Miller Indices of the light grey plane are similarly calculated and found to be *100*.

The interplanar spacing (or perpendicular distance) between adjacent parallel planes is termed the d_{hkl}-spacing. This term is related to the Bragg angle θ by Bragg's law as described in Section 2.3.2 and d_{hkl} can therefore be determined by X-ray diffraction.

2.3.2 X-Ray Powder Diffraction Theory

X-ray Powder diffraction (XRD) is a useful tool in the characterization of inorganic solids and X-rays were first used as a means of structure determination by W.H. and W.L. Bragg in 1913. X-ray diffraction is based on the principle of a crystallite acting as a diffraction grating and, for X-ray diffraction to take place, the wavelength of the incident radiation must be roughly of the same order of magnitude as the spacings in the diffraction grating crystal.

In order that X-ray "reflections" are observed, it is necessary that constructive interference occurs. This means that for reflected X-rays to emerge as a single beam of reasonable intensity, they must be in phase with one another. From this "Bragg condition" it is possible to derive equation 2.1 known as the Bragg law:

$$\lambda = 2d_{hkl} \sin\theta \qquad 2.1$$

d is the spacing between the crystal planes, or in this case the solid's pores (see below) and λ is the wavelength of the emerging X-rays (the path difference of the emerging X-rays must be an integral number, n, of wavelengths). This is known as the Bragg equation and it is used to relate the Bragg angle, θ, to the d-spacing.

The pore walls of the materials under consideration here are amorphous, and so any diffraction that takes place will not be due to a regular crystal structure but will rather be due to the periodicity of the pore system. Thus the repeat distance, a, of the hexagonal MCM-41 structure represents the sample's pore diameter plus the thickness of the pore wall. This is shown schematically in Figure 2.4. The repeat distance, a, of MCM-41 is related to the d-spacing of the first XRD reflection (d_{100}) via equation 2.2:

$$a = 2d_{100} / \sqrt{3} \qquad 2.2$$

Thus, we have a means of roughly estimating the pore diameter of MCM-41. If the actual pore diameter has been calculated from gas adsorption (see section 4.2.2) it is also possible to determine the sample's pore wall thickness by subtracting the pore diameter from *a* (determined from XRD).

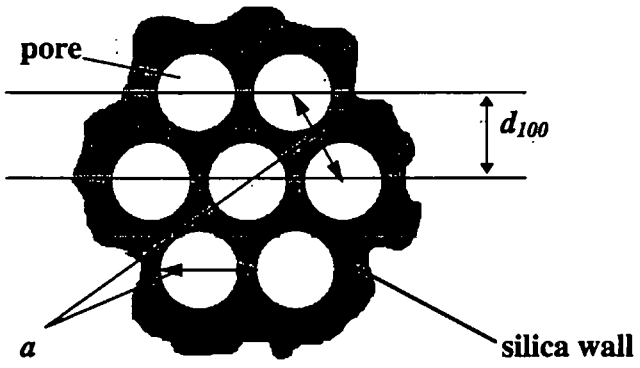

Figure 2.4 Schematic diagram (not to scale) showing relationship of d_{100} to pore structure of MCM-41. (The repeat distance, *a*, represented by the double headed arrows, represents the pore diameter plus the thickness of the pore wall and is related to the d_{100}-spacing via equation 2.4).

2.3.3 Experimental Details

Practical problems arise when analyzing materials with pore diameters in the mesoporous range. A d_{100}-spacing of 40 Å observed using CuKα radiation (λ = 1.54 Å) will occur at 2θ = 2.2° and may therefore be lost in the X-ray "through beam". For this reason it may be necessary to use a longer wavelength radiation. In this study CrKα (λ = 2.29 Å) radiation was used in addition to CuKα.

Powder XRD data of all samples, excluding the MCM-41 samples (a)-(d), were obtained on a computer-driven step-scanning diffractometer with a Philips PW 1050/25 goniometer and using CrKα radiation (λ = 2.29 Å). Data were collected at every 0.1° of 2θ (dwell time = 4s) and diffraction profiles were transferred to a personal computer for

further analysis. Analysis of the MCM-41 samples (a)-(d) were carried out, by the Earth Resources Centre at the University of Exeter, using a Philips step-scanning diffractometer with a Philips PW 1840 goniometer and using CuKα (λ = 1.54 Å) radiation; data were collected for 2 seconds at every 0.01° of 2θ. Diffraction profiles were produced following data transfer to a personal computer.

2.4 Infra-red Spectroscopy

2.4.1. General Background

Infra-red (IR) spectroscopy is a useful tool in the characterization of solids, especially those containing organic functions. When a functional group absorbs IR radiation, transitions between rotational and vibrational energy levels of the ground electronic energy state are observed. The theory of IR spectroscopy is based on the change in a dipole moment that arises from these "vibrations". Several classes of vibrational modes have been identified and may be classified as "stretching" or "deformation" vibrations. An IR spectrum records the position of these vibrational bands (quoted in units of wavenumber, cm^{-1}) and allows identification of functional groups contained in the sample. A wide range of texts are available on the theory and utility of vibrational spectroscopy and the reader is directed to references 9 - 11.

2.4.2 Experimental Details

IR spectra were obtained using a Nicolet Magna FTIR 550 Spectrometer. Samples were dispersed in KBr discs and spectra were collected over a range of 4000-400 cm^{-1}. In this study, IR spectroscopy is used to identify the incorporation of organic functions into MCM-41 and also to monitor template removal by loss of associated absorption bands from the spectra.

2.5 MAS-NMR Spectroscopy

2.5.1 General Considerations

NMR spectroscopy has been, for many years, a particularly useful tool in the determination of molecular structure. Problems arise, however, when applying this technique to materials in the solid-state. While NMR spectra obtained from liquid samples display sharp peaks of reasonable intensity, conventional NMR techniques performed on solid-state materials yield broad, featureless peaks from which little structural information can be obtained. This line-broadening is due to the close proximity of neighbouring atoms in the solid-state which results in dipolar and quadrupolar interactions and chemical shift anisotropy (CSA). Spinning a powder sample about an axis at an angle β to the applied magnetic field multiplies these interactions by $(3\cos^2\beta - 1)$. When $\cos\beta = (1/3)^{1/2}$ (i.e. β = 54° 44') this term becomes zero. Spinning the sample at an angle of 54° 44' to the direction of the magnetic field can therefore eliminate the sources of the line broadening and improve the resolution of the spectra. This technique is known as magic-angle-

spinning (MAS) NMR spectroscopy. The reader is directed to a number of excellent texts on this subject (references 12 - 14).

^{29}Si MAS-NMR

^{29}Si has a natural abundance of 4.7 % and a nuclear spin of I = ½ (thus no quadrupolar broadening will occur). Broadening due to CSA and dipolar coupling is still observed, however, which may be reduced by magic-angle-spinning.

The characterization of zeolites using ^{29}Si MAS-NMR was first carried out in the 1970's by Lippmaa *et al.* He discovered that the chemical shifts observed in a ^{29}Si MAS-NMR spectrum identified the nature of the SiO_4 tetrahedra in a silicate lattice i.e. it is possible to distinguish between isolated SiO_4 tetrahedra and SiO_4 tetrahedra joined through corner oxygen atoms, to either one, two, three or four other tetrahedra. This is also relevant to the characterization of M41S aluminosilicates. Each silicon atom (or SiO_4 tetrahedron) is usually assigned a 'Q value', ranging from zero to four, which represents the number of adjacent tetrahedra to which it is directly bonded. For each Q value, a characteristic range of chemical shifts is observed in the spectrum allowing the identification of the silicon environments present in the sample. Increased polymerisation results in a high field shift. The relative positions of these chemical shifts as a function of Q are shown in Figure 2.5 below.

Q^0	Q^1	Q^2	Q^3	Q^4
O- -O Si O- O-	O- -O Si O Si O-	O- Si O Si O Si O-	O- Si O Si O Si O Si	Si O Si O Si O Si O Si

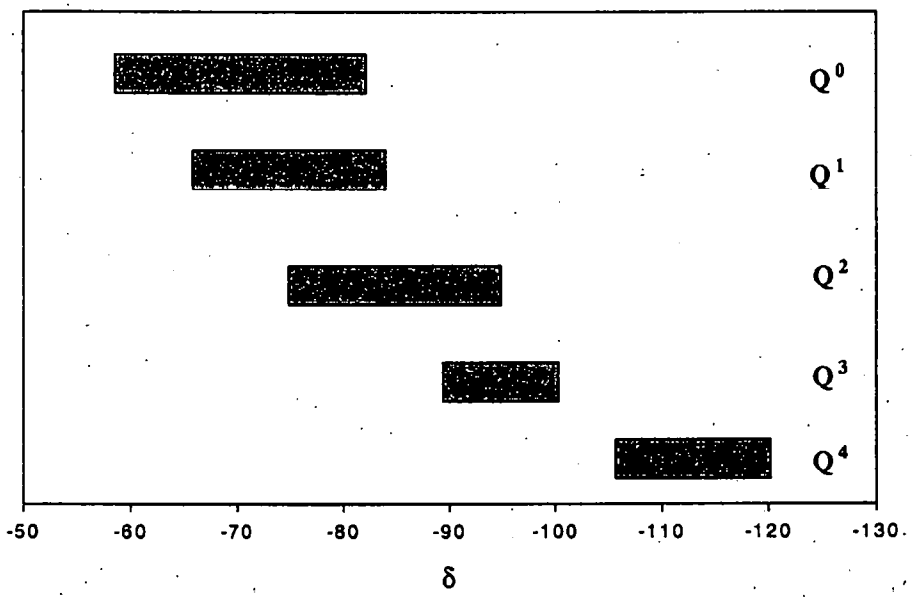

Figure 2.5 ^{29}Si chemical shifts as a function of Q

Silicon atoms in aluminosilicates such as zeolites are always in a Q^4 environment i.e. they are always surrounded by four other tetrahedral units. Chemical shifts, however, are influenced by the number of aluminium atoms attached to a given silicon unit. This is also observed in the M41S aluminosilicates. With increasing numbers of attached aluminium atoms, low field shifts are observed. The positions of these shifts and the nomenclature used to describe the silicon atoms are shown in Figure 2.6, below.

In the case of organically-modified silicas, such as those under investigation here, chemical shifts are also influenced by the organic function attached to the silicon atom. In

this case the silicons, attached to the organic function R, are described by "T-values" where $T^n = RSi(OSi)_nOH_{3-n}$ (n = 1-3). These T values also have a range of chemical shifts by which they can be recognized in a ^{29}Si spectrum, thus providing a means of determining functional-group incorporation.

Q^4(4 Al)	Q^4(3 Al)	Q^4(2 Al)	Q^4(1 Al)	Q^4(0 Al)
Al O Al O **Si** O Al O Al	Al O Al O **Si** O Si O Al	Al O Si O **Si** O Si O Al	Al O Si O **Si** O Si O Si	Si O Si O **Si** O Si O Si

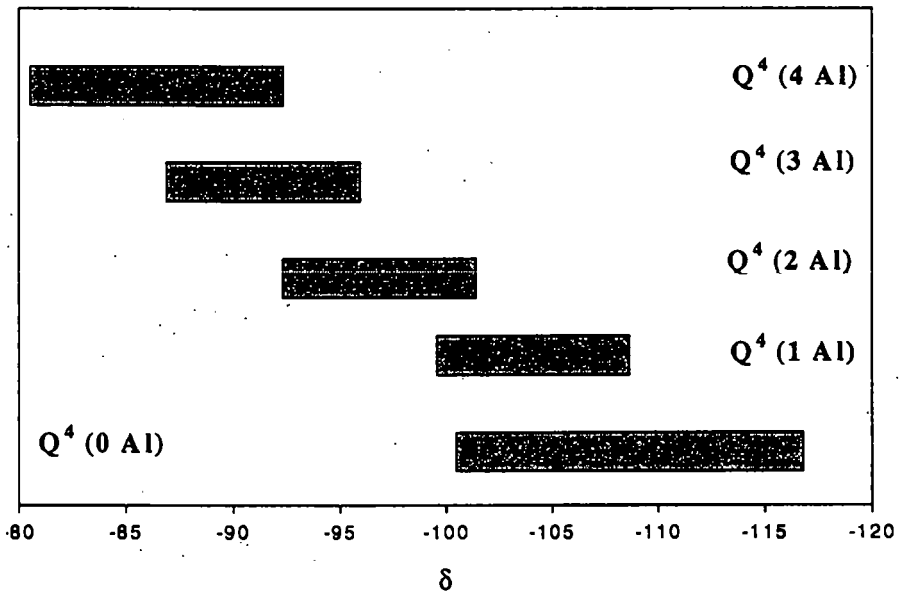

Figure 2.6 ^{29}Si chemical shifts with aluminium incorporation

^{27}Al MAS-NMR

^{27}Al has 100 % natural abundance (resulting in high NMR sensitivity) and a nuclear spin of I = 5/2 (resulting in broadening caused by quadrupolar interactions). When considering aluminosilicates, Loewenstein's rule[14] forbids the presence of Al-O-Al

linkages and so every tetrahedral aluminium environment will be $Al(OSi)_4$. ^{27}Al MAS-NMR is useful, however, when determining the co-ordination state of aluminium. Octahedrally co-ordinated aluminium, for example $[Al(H_2O)_6]^{3+}$, gives a peak at $\delta \approx 0$, while tetrahedrally co-ordinated aluminium, such as that present in an aluminosilicate framework, gives a peak in the range $\delta = 50 - 65$.

^{13}C MAS-NMR

^{13}C has a low natural abundance (1.108 %) and a nuclear spin quantum number I = ½. ^{13}C MAS-NMR has been used in these studies to investigate the incorporation of organic functions into mesoporous silica, and also to identify template molecules.

2.5.2 Experimental Details

MAS-NMR spectra were recorded at the EPSRC solid state NMR service at the University of Durham and the EPSRC NMR of Sorbents and Catalysts Facility at UMIST. The spectra were produced using a Varian UNITY 300 spectrometer fitted with a Doty MAS probe (Durham) or a Bruker MSL 400 instrument (UMIST).

^{29}Si MAS-NMR spectra were recorded, at Durham, at 59.58 MHz for sample MCM-41(a) before and after calcination using TMS as the external standard. An investigation was also carried out into the structural effects of water sorption by analyzing sample MCM-41(c) before and after exposure to water vapour. The organically-modified mesoporous silicas were analyzed at UMIST at 79.49 MHz before and after template removal, in order to determine the extent of functional group incorporation.

^{27}Al spectra were recorded at Durham at a frequency of 78.16 MHz using $AlCl_3(aq)$ (1 mol dm^{-3}) as the external standard. Samples MCM-41(a) and MCM-41(c) were analyzed before and after calcination to investigate the effect of template removal on the symmetries of aluminium sites.

^{13}C MAS-NMR spectra were recorded for the as-synthesized aluminosilicate samples MCM-41(a) and MCM-41(b) (to confirm the presence of the template) and for the phenyl-modified mesoporous silica, at Durham at a frequency of 75.43 MHz. ^{13}C MAS-NMR studies were carried out at UMIST at a frequency of 100.61 MHz, on the aminopropyl- and mercaptopropyl-modified samples to investigate functional-group incorporation.

2.6 Thermogravimetry

Thermogravimetry (TG) is a technique which measures the change of mass of a sample with change in temperature. An associated technique is differential temperature analysis (DTA) which measures the difference in temperature ΔT between the sample and a reference material (in this case calcined α-alumina) as a function of temperature. DTA thus determines whether a specific mass loss is due to an exothermic or endothermic process.

TG and DTA experiments were carried out simultaneously in flowing air using the Stanton and Redcroft STA-781 apparatus. The purely siliceous sample (SiMCM-41) and all of the organically-functionalized materials were analyzed following template removal. The "as-synthesized" SiMCM-41 sample was also analyzed.

2.7 Transmission Electron Microscopy

Transmission electron microscopy (TEM) was carried out on the aluminosilicate sample MCM-41(a) at the Open University, Walton Hall. A JEOL 2000fx microscope (accelerating voltage, V = 200kV) was used. The samples were dispersed on carbon film on a 3 mm, 200 mesh copper grid. Micrographs were taken using a standard, cut film TEM camera with no modifications.

Table 2.3 The characterization techniques used for each sample.

	XRD	IR	^{29}Si MAS NMR	^{27}Al MAS NMR	^{13}C MAS NMR	T.E.M	T.G.
MCM-41 (a)	✓	✓	✓	✓	✓	✓	
MCM-41 (b)	✓	✓			✓		
MCM-41 (c)	✓	✓	✓	✓			
MCM-41 (d)	✓	✓					
FeMCM-41	✓	✓					
SiMCM-41 (a)	✓	✓					✓
SiMCM-41 (b)	✓	✓					
PhMCM-41 (Burkett)	✓						
Unswollen Ph-modified	✓	✓					
MES-swollen Ph-modified	✓	✓	✓		✓		✓
TET-swollen Ph-modified	✓	✓					
MES-swollen V-modified	✓	✓					✓
MES-swollen AP-modified	✓	✓	✓		✓		✓
MES-swollen MP-modified	✓	✓	✓		✓		✓

Ph = phenyl, V = vinyl, AP = aminopropyl, MP = mercaptopropyl.

REFERENCES

1. Schmidt, R.; Akporiaye, D, Stocker, M.; Ellestad, O.H; *J. Chem. Soc., Chem. Commun.*, **1994,** 1493.
2. Schmidt, R. *J. Chem. Soc., Chem. Commun.*, **1996,** 875.
3. Zhong, Y.Y.; Shu, Q.L.; Tie, H.C.; Jing, Z.W.; He, X.L., *J. Chem. Soc., Chem. Commun.*, **1995,** 973.
4. Burkett, S.L.; Sims, S.D.; Mann, S., *J. Chem. Soc., Chem. Commun.*, **1996,** 1367.
5. Beck, J.S.; Vartuli, J.C.; Roth, W.J.; Leonowicz, M.E.; Kresge, C.T.; Schmitt K.D.; Chu, C.T-W.; Olson, D.H.; Sheppard, E.W.; McCullen, S.B.; Higgens, J.B.; Schlenker, J.L. *J. Amer. Chem. Soc.* **1992**, *114*, 1083-1043.
6. N. Ulagappan and C.N.R. Rao, *J. Chem. Soc., Chem. Commun.*, **1996**, 2759.
7. Smart, L.; Moore, E., "*Solid State Chemistry, An Introduction*", Chapman and Hall, London, **1995**, *24-25.*
8. West, A.R., "*Basic Solid State Chemistry*", John Wiley and Sons, Chichester, **1984**, *9-12.*
9. Nakamoto, K., "*Infra-Red and Raman Spectra of Inorganic and Co-ordination Compounds*", Fourth Edition, John Wiley and Sons, New York, **1986**.
10. Cross, A.D., *"Introducton to Practical Infrared Spectroscopy"*, Butterworths, **1960**.
11. Banwell, C.N., *"Fundamentals of Molecular Spectroscopy"*, McGraw-Hill, Maidenhead, **1972**.
12. Hore, P.J., "*Nuclear Magnetic Resonance*," Oxford University Press, Oxford, **1995**.
13. Kemp, W, "*NMR in Chemistry, A Multinuclear Introduction*," Macmillan Education Ltd., London, **1984**.

14. Englehardt, G.; Michel, D., "*High-Resolution Solid-State NMR of Silicates and Zeolites*", J. Wiley and Sons, London, 1987.

CHAPTER 3

CHARACTERIZATION

Definitive characterization of M41S-type materials is problematic due to their amorphous nature (lack of long range crystal structure). It is therefore very difficult to assign a chemical formula to these samples. As the most interesting feature of these materials is their uniform pore structure, gas adsorption studies yield the most interesting information. This characterization technique has therefore played a major part in this work and is considered, separately, in Chapter 5.

This chapter, which is divided into two parts, considers the basic characterization (by XRD, IR, TG, NMR and TEM) both of the M41S materials and of the organically-modified mesoporous silicas. The results of the vibrational analysis of these materials by inelastic neutron scattering are presented in Chapter 6.

PART I - M41S MATERIALS

3.1 X-ray Powder Diffraction

Results from powder XRD studies of the M41S samples, are given in Table 3.1 overleaf. As mentioned in Chapter 2, powder XRD profiles of amorphous M41S solids detect the periodicity of the pore structure and, if the peaks are indexed to a hexagonal structure, it is possible to determine a value of the lattice parameter, a ($a = 2d_{100} / \sqrt{3}$), representing the pore diameter plus the thickness of the pore wall. The values of a obtained for these materials (Table 3.1) fall in the range of 37 - 45 Å, typical of MCM-41

materials. It is evident from Table 3.1 that samples produced under pressure (in a sealed teflon bottle at 100 °C) have larger *a* values than those prepared in a microwave oven or at room temperature and pressure. The positions of the three peaks observed for samples MCM-41(a), FeMCM-41 (Figure 3.1, below) and SiMCM-41 (Figure 3.2, below) confirm that the samples have a hexagonal structure. XRD investigation of FeMCM-41 at $2\theta \leq 50$ °, detected no crystalline iron oxide in the sample.

Table 3.1 Powder XRD results for calcined M41S samples

Sample		Kα radiation †	d_{100} / Å	d_{110} / Å	d_{200} / Å	a / Å
MCM-41(a)	i	Cu (1.54 Å)	33.94	-	-	39
MCM-41(b)	ii	Cu	*	-	-	-
MCM-41(c)	i	Cu	39.05	22.92	19.62	45
MCM-41(d)	ii	Cr (2.29 Å)	34.53	-	-	40
FeMCM-41	i	Cr	37.49	21.52	18.50	43
SiMCM-41(a)	iii	Cr	31.62	-	-	37
SiMCM-41(b)	i	Cr	37.50	21.17	18.36	43

(i) prepared in sealed vessel in conventional oven, (ii) prepared in microwave oven, (iii) stirred at room temperature in an open vessel. *a* - unit cell dimension ($a = 2d_{100} / \sqrt{3}$). † Figures in brackets are wavelengths of Kα radiation. * Peak too broad to assign a d_{100} value.

In many publications concerning MCM-41 materials only one diffraction peak, representing the d_{100} reflection, can be observed, and this is the case for samples MCM-41(a), (b) and (d) (see Appendix A1). In the case of sample MCM-41(b) the diffraction peak obtained was so broad that it was not possible to obtain a value for the d_{100}-spacing.

It is evident that a more ordered material is produced if the sample is heated under pressure *i.e.* in a sealed vessel in an oven.

When a powder XRD analysis is performed on an M41S material before the template is removed, a profile very similar to that of the calcined material is obtained (see Figure 3.1). Often the intensity of the peaks is diminished (due to a reduction in the contrast between the pore and the pore-walls), and in every case the position of the peaks is shifted to lower 2θ *i.e.* larger d-spacings are observed in uncalcined materials. The decrease in *d*-spacing observed upon calcination is due to the pore contracting after template removal *e.g.* for FeMCM-41 a contraction of *ca.* 5 Å is observed.

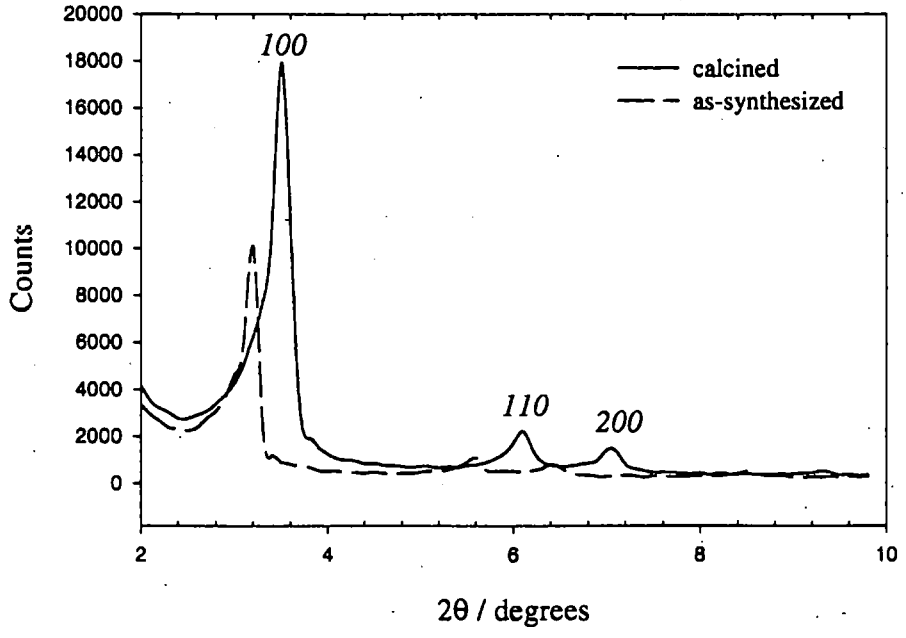

Figure 3.1 Powder XRD profile of as-synthesized and calcined FeMCM-41.

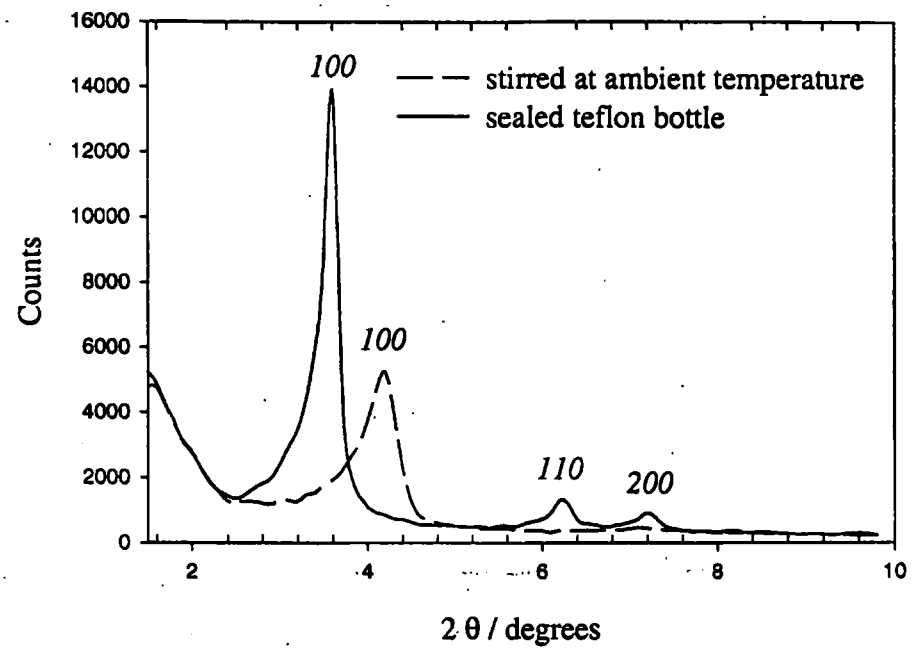

Figure 3.2 Powder XRD profile of calcined SiMCM-41.

All other XRD profiles are given in Appendix A1.

3.2 Infra-red Spectroscopy

Infra-red spectroscopy was performed on all the MCM-41 samples following template removal, and on the as-synthesized SiMCM-41(b) sample. The band assignments are given in Tables 3.2 - 3.3, and the spectra are presented in Figures 3.3 - 3.7.

Table 3.2 The Principle IR Band Assignments for the Calcined Aluminosilicate Samples

Band Position / cm^{-1}				
MCM-41(a)	**MCM-41(b)**	**MCM-41(c)**	**MCM-41(d)**	**Assignment**
461	466	476	471	Si-O-Si_{def}
797	802	802	807	T-O-T_{str}
1082	1072	1102	1098	Si-O-Si_{str}
1642	1637	1642, 1662	1653, 1665	O-H-O_{def}
3446	3445	3450	3445	O-H_{str}

T - tetrahedrally co-ordinated ion. *def* - deformation, *str* - stretch

Table 3.3 The Principle IR Band Assignments for the Siliceous and Iron-Containing Samples

Band Position / cm^{-1}				
SiMCM-41(a) S.E.	**SiMCM-41(b) A.S.**	**SiMCM-41(b) S.E.**	**FeMCM-41 S.E.**	**Assignment**
471	451	466	471	Si-O-Si_{def}
-	-	-	660 (weak)	Si-O-Fe
807	802	797	812	T-O-T_{str}
970	970	970	970 (weak)	Si-O-T
1087	1072	1098	1087	Si-O-Si_{str}
1250	1240	1245	-	Si-O-C_{str}
-	1474	-		C-H_{def}
1647	1642	1652	1657	O-H-O_{def}
-	2859, 2930	-	-	C-H_{str}
3475	3424	3465	3465	O-H_{str}

T - tetrahedrally co-ordinated atom. *def* - deformation, *str* - stretch
A.S. - As-synthesized, S.E. - After template removal.

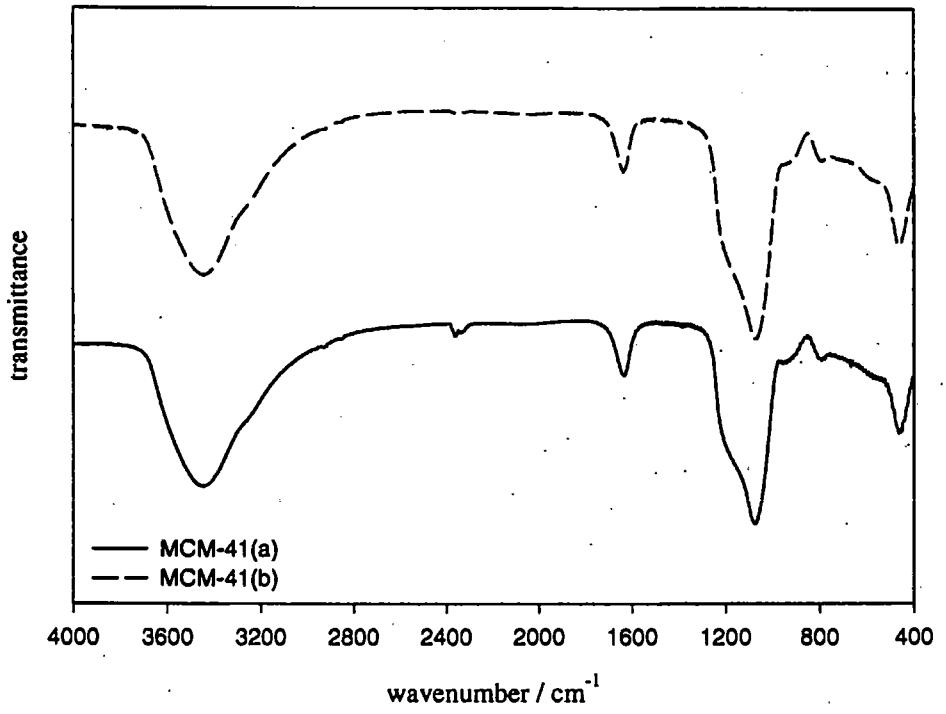

Figure 3.3 IR spectra of calcined MCM-41(a) and MCM-41(b).

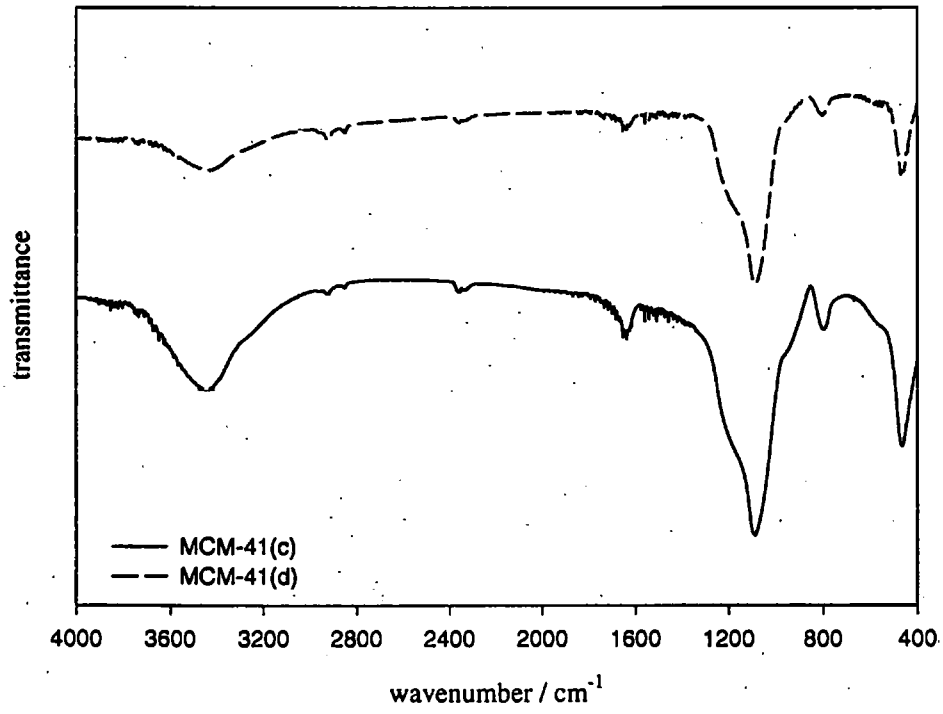

Figure 3.4 IR spectra of calcined MCM-41(c) and MCM-41(d).

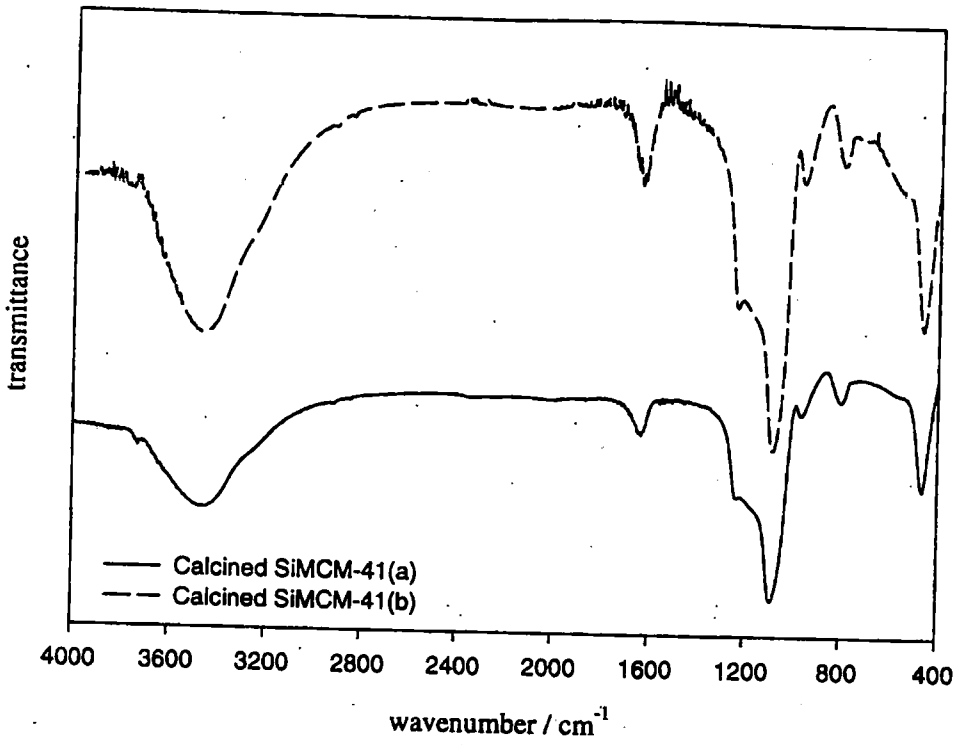

Figure 3.5 IR spectra of calcined SiMCM-41(a) and SiMCM-41(b).

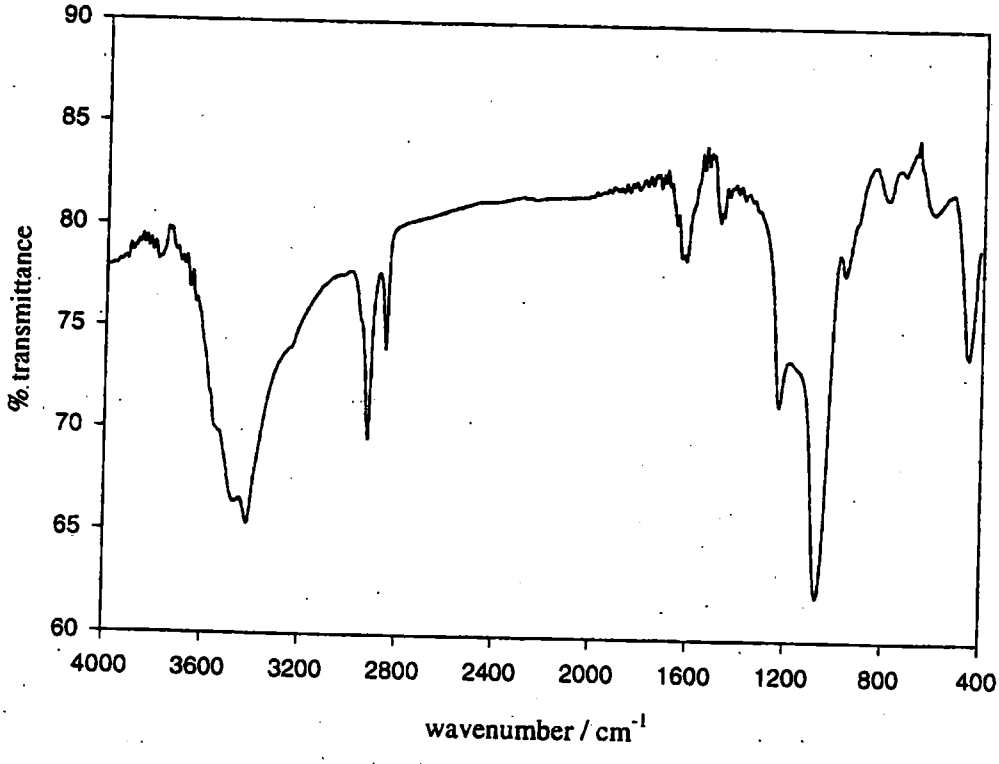

Figure 3.6 IR spectrum of as-synthesized SiMCM-41(b)

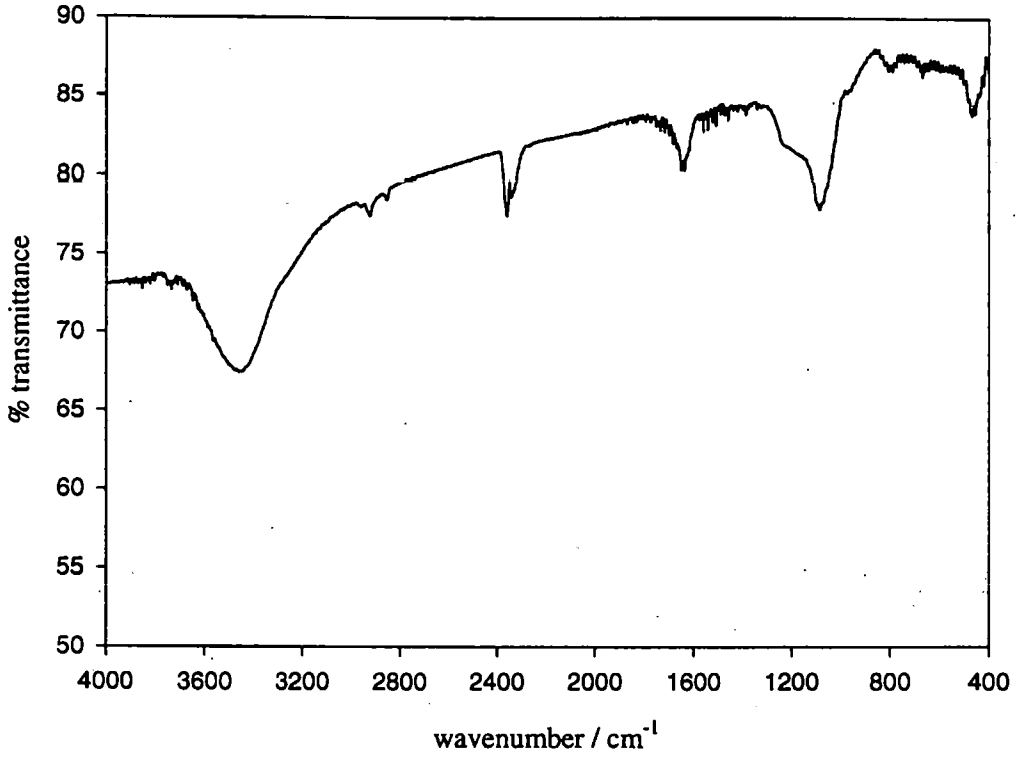

Figure 3.7 IR spectrum of calcined FeMCM-41

As can be seen from Tables 3.2 and 3.3 and from Figures 3.3 - 3.7, the main feature of the IR spectra of these materials is a large absorption band at *ca.* 1100 cm^{-1}, which is due to Si-O-Si asymmetric stretching vibrations. A peak is also visible in each spectrum at approximately 470 cm^{-1} due to Si-O-Si deformations. The small peak at approximately 800 cm^{-1} was assigned by Lazarev[1] and by Flanigen *et al*[2] as representing T-O-T symmetrical stretching, where T is a tetrahedral unit of either Si or Al.

In the case of the purely siliceous materials, an additional band is visible at *ca.* 1250 cm^{-1}. This is a very weak absorption in the case of the calcined materials, but is quite strong in the spectrum of the as-synthesized material. It is likely that this peak represents a Si-O-C stretching vibration and is due to the template (suggesting that residual template is present in the calcined material). Bands at 2859 cm^{-1}, 2930 cm^{-1} (C-

H_{str}) and 1474 cm^{-1} (C-H_{def}), also present in the spectrum of the as-synthesized material, confirm the presence of the template molecules.

A broad absorption band in the O-H_{str} region of the spectra (*ca.* 3400 cm^{-1}) identifies surface hydroxyl groups, while a series of bands in the region of 1400 - 1650 cm^{-1} represent the scissoring deformations of water.

An additional strong band is observed in the purely siliceous material at 970 cm^{-1}. This absorption, which was assigned by Zhong *et al*[3] as a framework Si-O-T vibration, is weak for Fe-MCM-41 and is absent from the aluminosilicate spectra. Zhong *et al*[3] and Szostak and Thomas[4] identified an absorption due to Si-O-Fe linkages at *ca.* 660 cm^{-1}, and this is observed as a small peak in the FeMCM-41 spectrum.

3.3 Thermogravimetry

Thermogravimetry (TG) was carried out on sample SiMCM-41(b), both before and after calcination. The results are presented in Figure 3.8 and 3.9 below. Due to the absence of ^{29}Si NMR data, TG analysis could not be related directly to a chemical formula in this case.

The as-synthesized product (Figure 3.8) undergoes three separate mass losses, corresponding to an overall mass loss of *ca.* 50 %. The first loss occurs up to approximately 200 °C, and corresponds to an 8 % loss which may be attributed to physisorbed surface water. The second mass loss is the exothermic and occurs over the temperature range of 220 - 360 °C. This corresponds to a mass loss of *ca.* 37 % and may

be attributed to loss of the organic template. Surface dehydroxylation is then observed as a gradual loss over the range 360 - 1200 °C; this corresponds to a mass loss of *ca.* 6%.

TG analysis of the calcined sample (Figure 3.9) indicated two major mass losses between 30 - 1200 °C (due to the minimal mass loss of this material, the DTA is not shown).The first, endothermic, loss corresponds to 8% of the sample mass and occurred over the range 30 - 150 °C; this likely to represent loss of surface water. The second mass loss is very gradual and occurs over the range of 150 - 1200 °C. This represents a further 3% mass loss, and can probably be attributed to surface dehydroxylation and structural collapse.

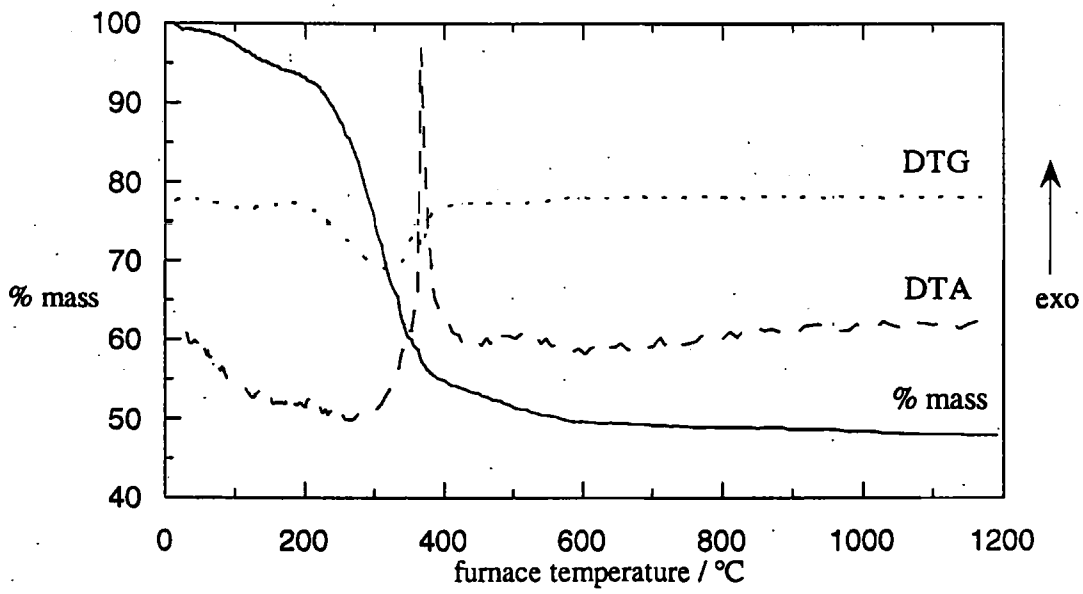

Figure 3.8 TG of as-synthesized SiMCM-41

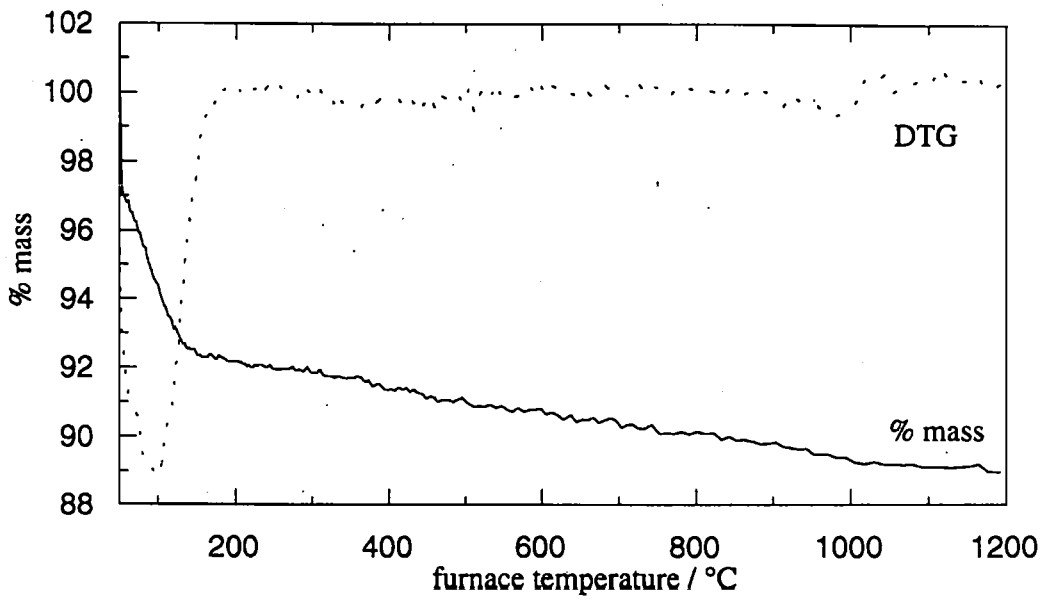

Figure 3.9 TG of calcined SiMCM-41

3.4 Transmission Electron Microscopy (T.E.M)

The T.E.M. micrograph of sample MCM-41(a), presented in Figure 3.10, shows large regions of disorder, in agreement with the X-ray powder diffraction pattern of this sample which displays only a small broad peak. Regions of order are apparent, however, and these are highlighted in Figure 3.11.

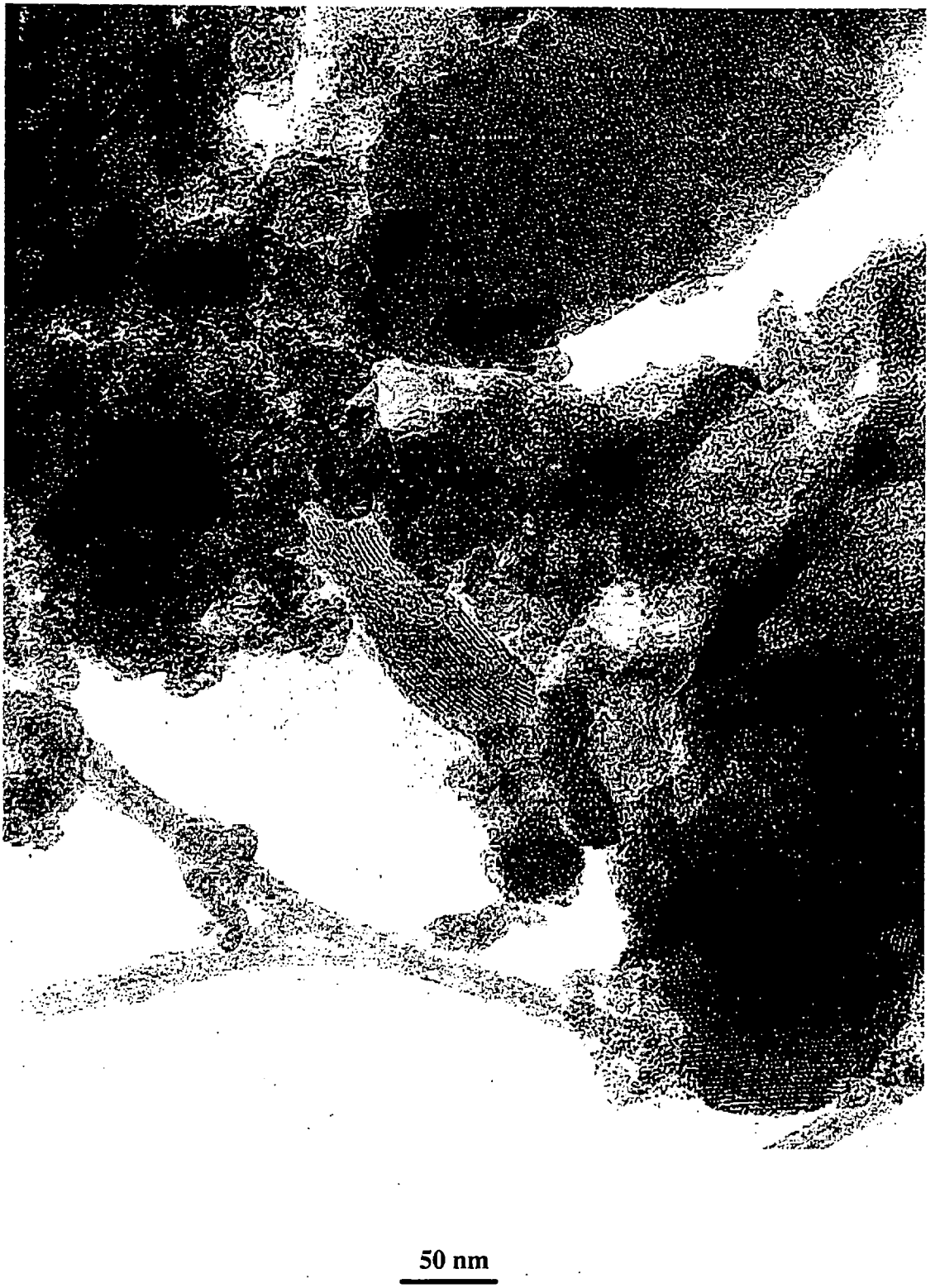

Figure 3.10 Transmission Electron Micrograph of sample MCM-41(a)

(i) (ii) (iii)

50 nm

Figure 3.11 Expansions of the T.E.M micrograph of sample MCM-41 (a)

Figure 3.11 (i) shows the pore-channels "end-on", and hexagonal symmetry is evident. Figures 3.11 (ii) and (iii) show a series of pore channels over 50 nm in length, again suggesting a degree of ordering.

3.5 MAS-NMR

^{29}Si, ^{27}Al and ^{13}C MAS-NMR spectroscopy was carried out on the aluminosilicate MCM-41 samples at the EPSRC solid-state NMR service at the University of Durham. The spectra obtained are given in Appendix A3.

3.5.1 ^{29}Si MAS-NMR

(i) MCM-41(a)

^{29}Si MAS-NMR allows identification of the immediate environment of the silicon atoms. Spectra were taken of MCM-41(a) before and after calcination. Three resonances, Q^2, Q^3 and Q^4 (where Q^n = $\underline{Si}(OSi)_n(OH)_{4-n}$), were detected by decomposition. The data are given in Table 3.4, below and the spectra, showing the decomposition, are presented in Figures 3.12 and 3.13, overleaf.

Table 3.4 ^{29}Si MAS-NMR features after data reduction for MCM-41(a).

		δ*		
Sample		**Q^2**	**Q^3**	**Q^4**
MCM-41(a)	A.S.	-89.9 (7.4 %)	-97.6 (35.1 %)	-105.4 (57.5 %)
	S.E.	-91.6 (8.7 %)	-99.3 (28.2 %)	-107.1 (63.1 %)

*TMS as external reference.
A.S. - as-synthesized, S.E. - after template removal.
Figures in brackets are percentage contributions of each peak after decomposition.

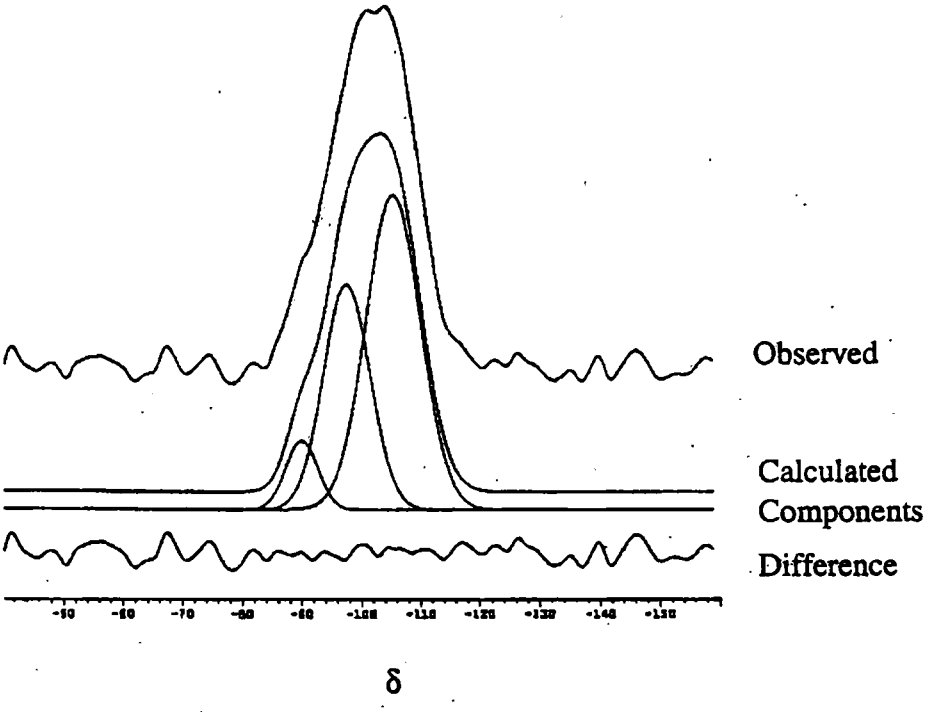

Figure 3.12 Decomposition of ^{29}Si MAS-NMR spectrum of as-synthesized MCM-41(a).

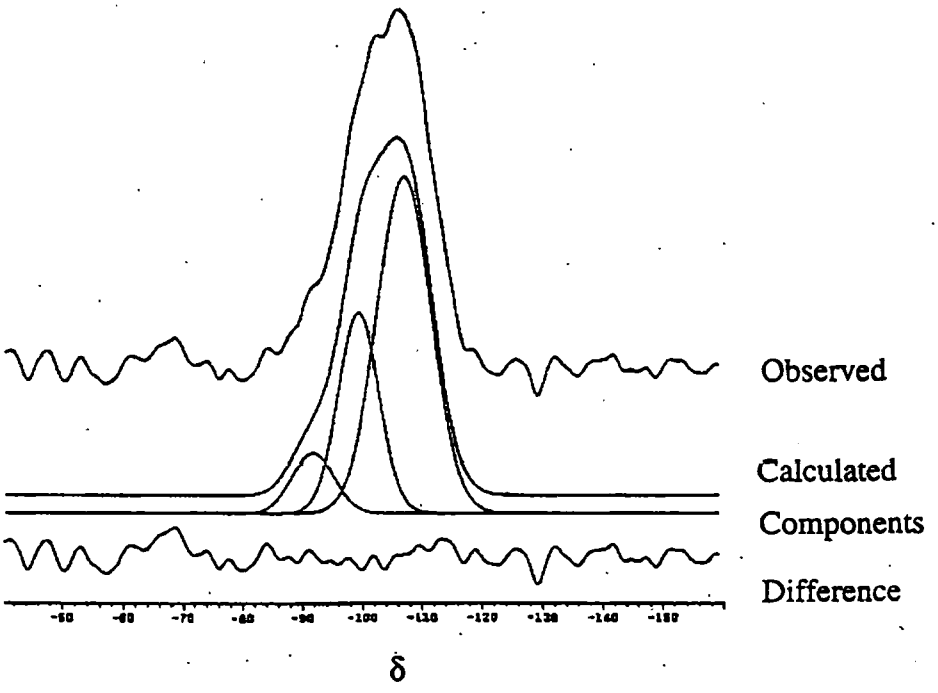

Figure 3.13 Decomposition of ^{29}Si MAS-NMR spectrum of calcined MCM-41(a).

(ii) MCM-41(c) Before and After Water Sorption

Water sorption on sample MCM-41 (c) yielded a Type V isotherm displaying low pressure hysteresis (see Section 5.3). The reason for this low pressure hysteresis and non-closure of the hysteresis loop is thought to be rehydroxylation of the silica surface[5-7] as shown in Figure 3.14.

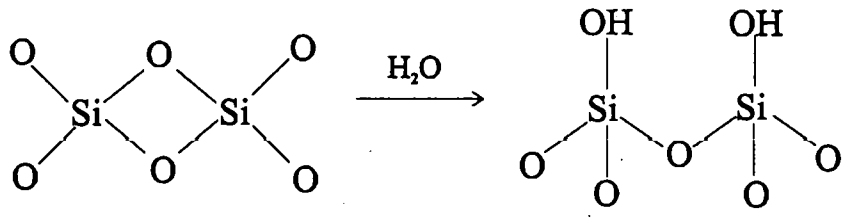

Figure 3.14 Rehydroxylation of a silica surface

If this is indeed the case, an increase in the number of surface hydroxyls should be evident in the sample following water sorption.

^{29}Si MAS-NMR was performed on the sample using a long relaxation delay (300 s) both before and after water sorption. Results of the decomposition are given in Table 3.5 and presented in Figures 3.15 and 3.16.

Table 3.5 Decomposition of ^{29}Si MAS-NMR spectra of MCM-41(c) before and after water sorption.

		δ	% Contribution
MCM-41(c), calcined	Q^2	-92	1.8
	Q^3	-100	25.6
	Q^4	-108	72.6
MCM-41(c), H_2O adsorbed	Q^2	-93	5.3
	Q^3	-102	32.1
	Q^4	-110	62.6

As shown in Table 3.5, the percentage of total silicon atoms in Q^2 [$\underline{Si}(OSi)_2(OH)_2$] and Q^3 [$\underline{Si}(OSi)_3OH$] environments is greater following water sorption. Concurrently, the percentage of Q^4 silicon atoms [$\underline{Si}(OSi)_4$] has diminished. This confirms that surface rehydroxylation occurs during water sorption.

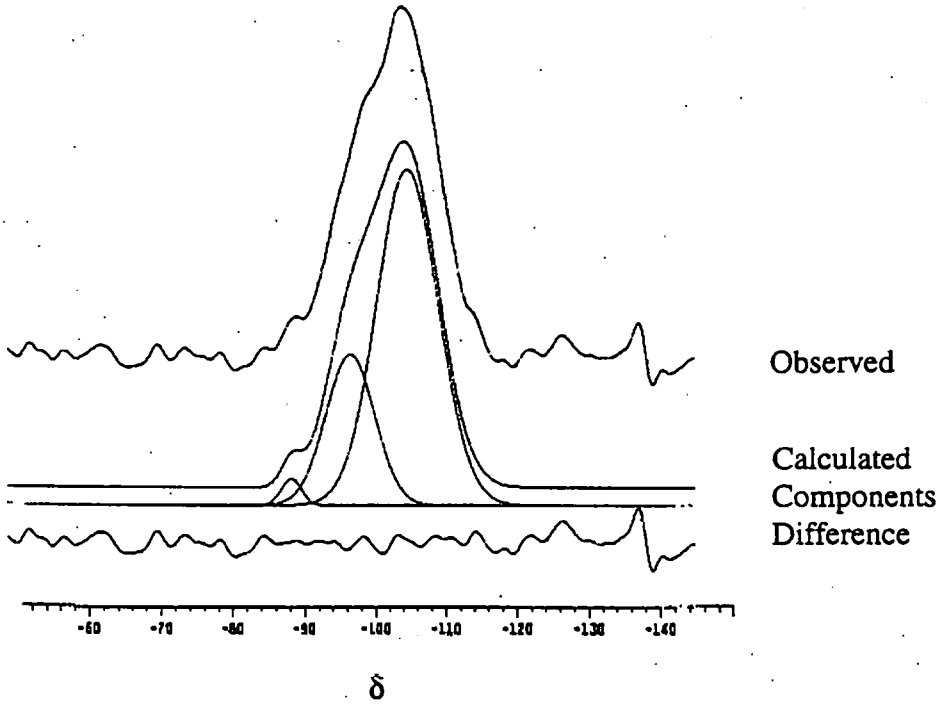

Figure 3.15 Decomposition of ^{29}Si MAS-NMR spectrum of sample MCM-41(c) following calcination.

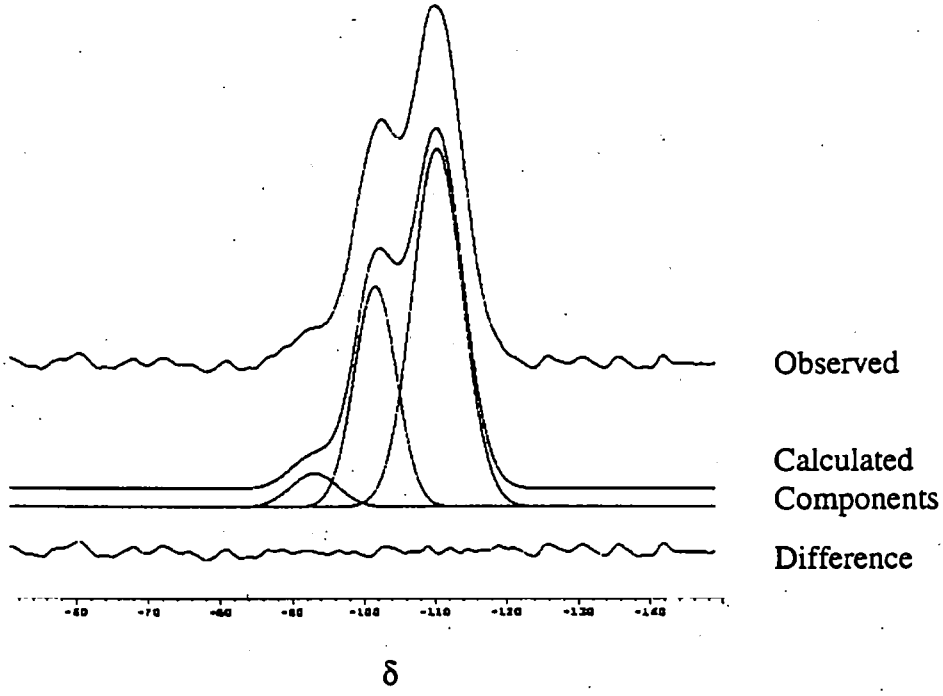

Figure 3.16 Decomposition of ^{29}Si MAS-NMR spectrum of sample MCM-41(c) following water sorption.

3.5.2 ^{27}Al MAS-NMR

^{27}Al MAS-NMR was used to compare the site symmetry for aluminium in samples MCM-41(a) and MCM-41(c), before and after calcination (this is of interest when the sample is to be used as an acid catalyst, as tetrahedrally co-ordinated aluminium is then required[8,9]). The spectra are given in Appendix A3 and the extracted data are given in Table 3.6, below.

Table 3.6 ^{27}Al MAS-NMR results for aluminosilicate MCM-41 samples

		δ*	
Sample		**Tetrahedral Al**	**Octahedral Al**
MCM-41(a)	A.S.	50.7	-
	S.E.	52.6 (weak)	-1.1
MCM-41(c)	A.S.	51.1	-
	S.E.	47.7	shoulder

* $Al(H_2O)_6^{3+}$ (aq) (1 mol dm^{-3}) as external standard.
A.S.-as-synthesized, S.E.-after template removal.

As-synthesized MCM-41(a) gave a single peak at $\delta \approx 52$ corresponding to tetrahedrally co-ordinated Al, but after calcination only a very weak signal was observed, suggesting that relatively few tetrahedral aluminium ions were present after calcination. Also, regular octahedrally co-ordinated aluminium, normally identified by a peak at $\delta \approx 0$, was not observed in significant amounts. In contrast, MCM-41(c) gave a strong signal at $\delta \approx 52$ both before and after calcination, indicating that tetrahedrally co-ordinated aluminium was present in both cases. This result suggests that for catalytic purposes in which catalytically active metals are required in the walls, MCM-41(c)-type

materials (synthesized using aluminium sulphate) could be of greater interest than MCM-41(a) type solids (synthesized using sodium aluminate).

3.5.3 ^{13}C MAS-NMR

^{13}C MAS-NMR results for the as-synthesized MCM-41(a) and MCM-41(b) samples are given in Table 3.7 below.

Table 3.7 ^{13}C MAS-NMR results for as-synthesized MCM-41(a) and MCM-41(b)

	δ*				
Sample	**C1**	**C2**	**C3-15**	**C16**	**C17**
MCM-41(a)	14.14	23.22	30.61	66.88	53.92 & 56.98
MCM-41(b)	14.30	23.26	30.65	67.07	54.05 & 56.58

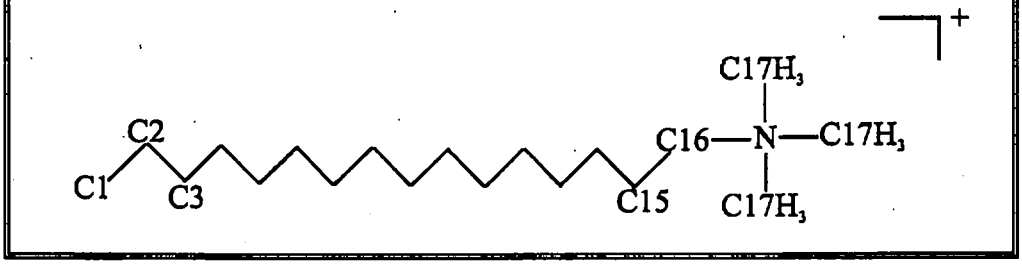

* TMS as external standard

As can be seen from Table 3.7, ^{13}C MAS-NMR studies of the as-synthesized MCM-41(a) and MCM-41(b) samples confirm the presence of the intact cetyltrimethylammonium ion.

3.6 Overview of M41S-Material Characterization

3.6.1 Aluminosilicate MCM-41

Four mesoporous, aluminosilicate MCM-41-type samples, synthesized using two reaction mixtures and two heating methods, have been characterized using XRD, IR, TEM and MAS-NMR techniques. XRD studies demonstrated that heating the reaction mixtures in a sealed teflon bottle yielded a material with a uniform hexagonally-ordered pore structure and narrow pore size distribution. Conversely, samples synthesized in a microwave oven gave poor XRD profiles as a consequence of having poorly-defined pore-structures. TEM performed on sample MCM-41(a) showed large regions of disorder, in agreement with the XRD profile, but some hexagonal structure was observed.

^{27}Al MAS-NMR, performed on sample MCM-41(a) and MCM-41(b), revealed that Al was present in a tetrahedral environment in both samples before calcination, but was only present, in significant amounts, in sample MCM-41(c) following calcination. As tetrahedral aluminium is required for acid catalysis purposes, this result suggests that samples of the MCM-41(c)-type are of greater interest. ^{29}Si MAS-NMR performed on sample MCM-41(c) (before and after water sorption) confirmed that surface modification takes place upon contact with water vapour (see Chapter 5).

3.6.2 Purely Siliceous MCM-41

Two purely siliceous mesoporous MCM-41-type samples were characterized using XRD, IR and TG techniques. XRD studies demonstrated that the sample prepared at high temperature and pressure had the more well-defined pore structure.

3.6.3 Iron-containing MCM-41

The iron-containing MCM-41 was characterized by XRD and IR spectroscopy. XRD studies demonstrated that the sample had a uniform pore-structure that could be indexed to a hexagonal lattice, and a peak in the IR spectrum (assigned to an Si-O-Fe vibration) confirmed that iron had been incorporated into the structure.

Further characterization (*e.g.* via Mossbauer spectroscopy studies) is required to determine how the iron is incorporated into the sample. X-ray powder diffraction studies at $2\theta \leq 40\ ^\circ$ have proved that crystalline iron oxide is not present.

PART II

ORGANICALLY-MODIFIED MESOPOROUS SILICAS

3.7 X-Ray Powder Diffraction

X-ray powder diffraction (XRD) results, obtained from profiles recorded using CrKα radiation (λ = 2.29 Å), are given in Table 3.8.

Table 3.8 Powder XRD results for organically-modified mesoporous silicas.

Sample	d_{100} / Å (A.S.)	d_{100} / Å (S.E.)
PhMCM-41 (Burkett)	36.1	31.4
Unswollen phenyl-modified mesoporous silica	37.5	36.0
MES-swollen phenyl-modified mesoporous silica	52.0	49.5
TET-swollen phenyl-modified mesoporous silica	37.5	32.0
Vinyl-modified mesoporous silica	40.2	39.8
Aminopropyl-modified mesoporous silica	48.6	*
Mercaptopropyl-modified mesoporous silica	36.5	34.5

A.S. - as-synthesized, S.E. - after template removal.
* No peak was observed, consequent on loss of ordering upon template removal.

Examples of typical XRD profiles are given in Figure 3.17 below (all other profiles can be found in Appendix A1).

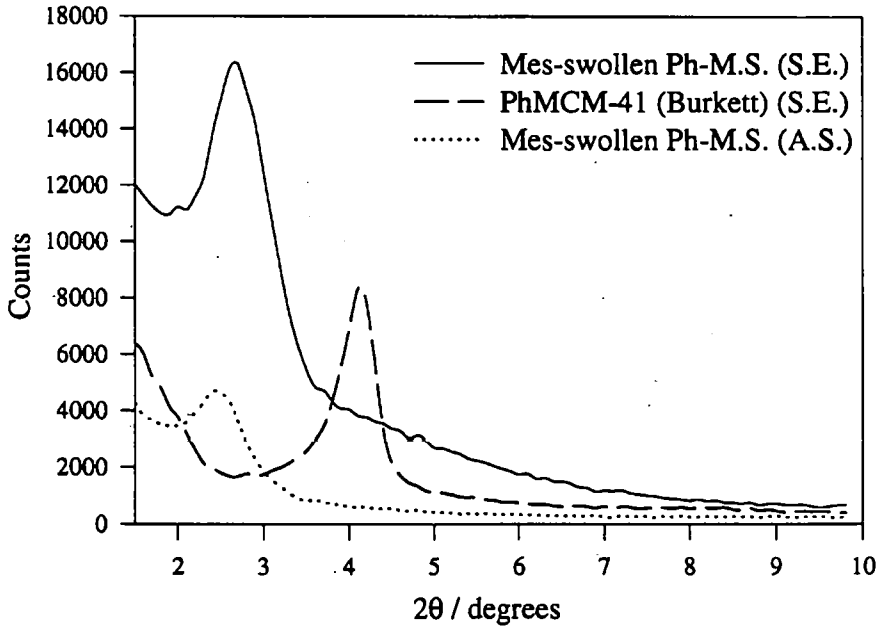

Figure 3.17 Powder XRD profiles of MES-swollen and unswollen phenyl-modified mesoporous silica (Ph-M.S.) and of PhMCM-41. (A.S. - as-synthesized, S.E. - after template removal)

The XRD profiles indicate that a single phase is formed for both the swollen and unswollen organically-modified samples. Following template removal, structural order is maintained (except in the case of the aminopropyl sample) and a small degree of contraction is observed. Only one peak is observed for each material in contrast to the M41S materials, which gave three peaks. For this reason it is impossible to definitively index the XRD profile to a hexagonal lattice and confirm that the samples are MCM-41-type materials.

It is evident from the XRD data that the addition of mesitylene to the phenyl-modified material increases d_{100}, which is directly related to pore diameter. In contrast, the addition of tetradecane does not result in an increase in d_{100}, indicating that

tetradecane is not a suitable pore-swelling agent for the formation of phenyl-modified mesostructured silica.

3.8 Infra-red spectroscopy

FTIR spectra were collected for the organically-modified samples before and after template removal. The results obtained for each sample are now discussed in turn.

3.8.1 Phenyl-Modified Mesoporous Silica

The spectra obtained for the MES-swollen phenyl-modified silica are shown below (Figure 3.18). Due to the similarity of the samples, the spectra obtained for the TET-swollen and unswollen phenyl-modified samples are given in Appendix A1 only, and are not discussed here.

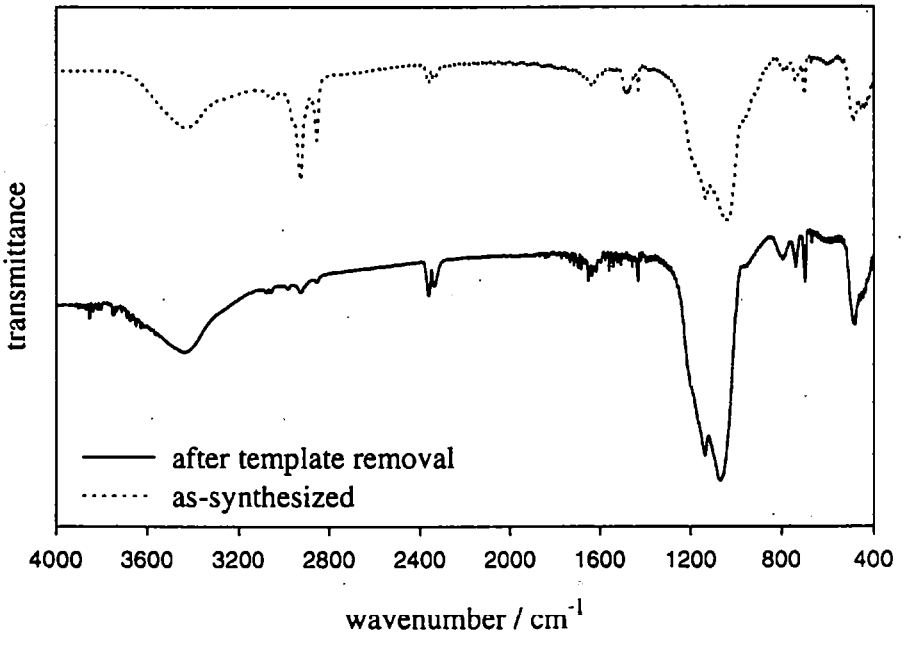

Figure 3.18 Infra-red spectra of MES-swollen phenyl-modified mesoporous silica before and after template removal.

Expansions of the as-synthesized spectrum are shown in Figures 3.19 and 3.20, below.

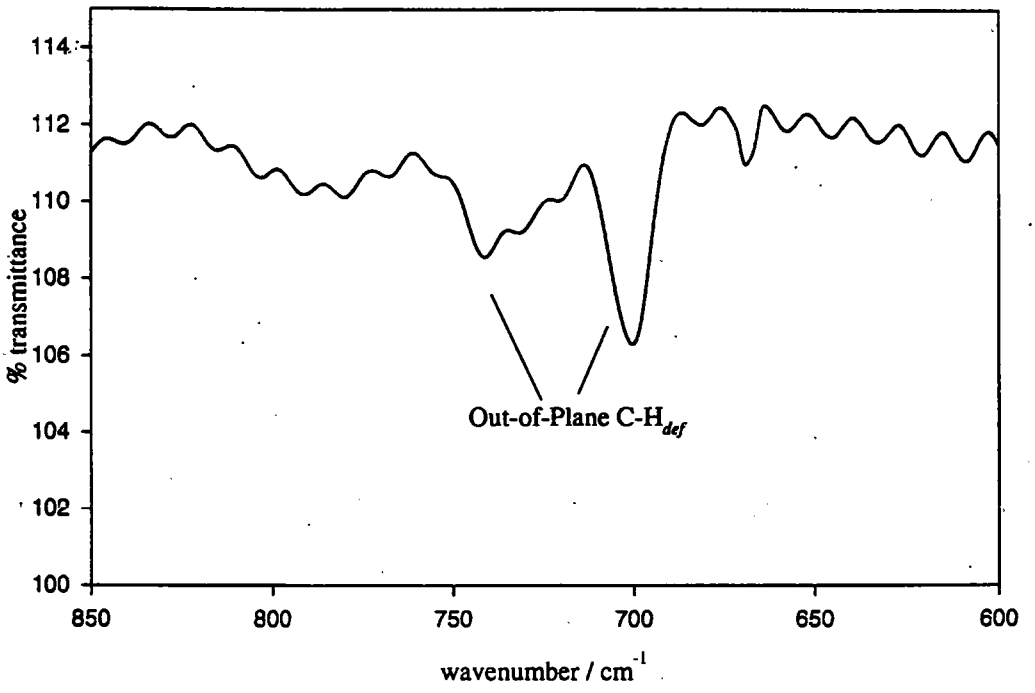

Figure 3.19 Expanded IR spectrum of MES-swollen phenyl-modified mesoporous silica: range 600 - 850 cm^{-1}.

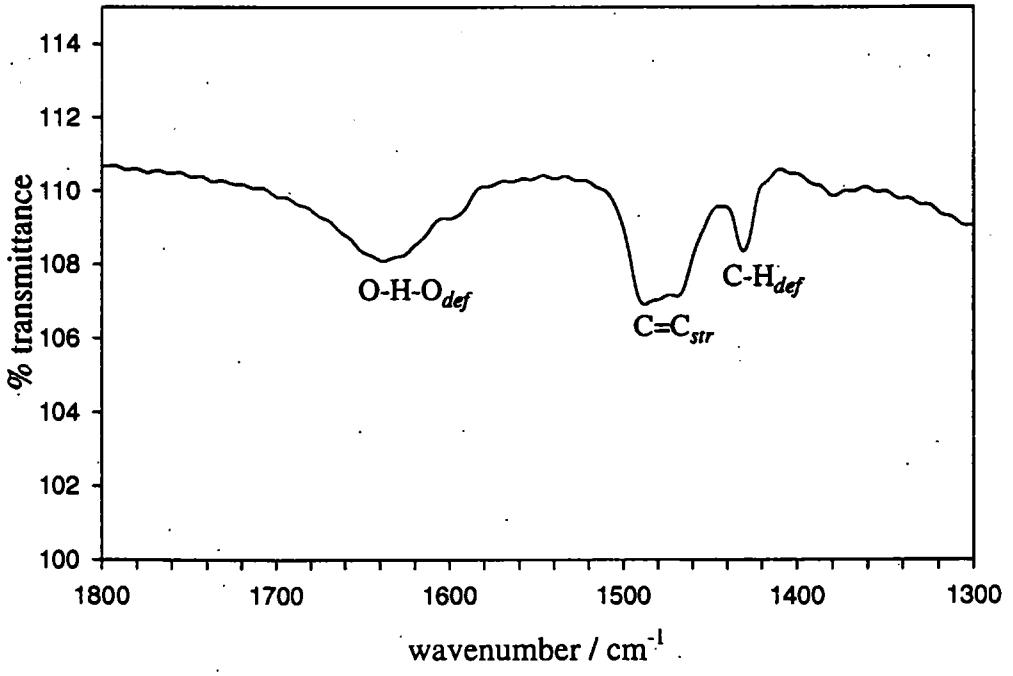

Figure 3.20 Expanded IR spectrum of MES-swollen phenyl-modified mesoporous silica: range 1300 - 1800 cm^{-1}.

The principal band assignments are given in Table 3.9, below. As the purely siliceous sample SiMCM-41 could be considered as a control sample, bands not observed in the SiMCM-41 spectra (see Table 3.3) are most likely due to the phenyl function and are shaded in Table 3.9.

Table 3.9 Principal IR bands for MES-swollen phenyl-modified mesoporous silica.

Band Position / cm^{-1}	Assignment
491	Si-O-Si_{def}
710, 746	Phenyl Out-of-Plane C-H_{def}
802	Si-CH_{3str}
1072	Si-O-Si_{str}
1143	Si-C_{str}
1433*	C-H_{def}
1480	Phenyl C=C_{str}
1662	O-H-O_{def}
2854, 2930*	C-H_{str}
3439	O-H_{str}

Shaded cells show additional bands not observed for control SiMCM-41.
* observed for "as-synthesized" product only. *str* - stretch, *def* - deformation.

As shown in Figure 3.18, a peak in the Si-O-Si region (1143 cm^{-1}) is indicative of an Si-C bond,[10] indicating the successful incorporation of organic functions. In addition, vibrations due to the phenyl group can be identified and these have been highlighted in the expanded spectra, presented as Figures 3.19 and 3.20. A comparison of the IR and inelastic neutron scattering spectra is made in Chapter 6.

IR spectroscopy is a useful tool in monitoring template removal in these materials, and in this case, C-H_{str} (2931 and 2854 cm^{-1}) and C-H_{def} (1433 cm^{-1})

absorptions due to the surfactant are observed in the as-synthesized sample, but are very weak in the spectrum following acid extraction of the template.

3.8.2 Vinyl- , Aminopropyl- and Mercaptopropyl-Modified Mesoporous Silica

Infra-red analysis of the remaining organically-modified materials yielded inconclusive results. The full spectra are given in Appendix A2. As can be seen from the expanded spectra presented here in Figures 3.21 - 3.23, there are many peaks which cannot be conclusively assigned. This may be due to inadequate background subtraction. The principal bands are assigned in Table 3.10, with the bands not observed in the SiMCM-41 control sample once again shaded in grey.

Table 3.10 Principal IR bands for MES-swollen organically-modified mesoporous silica.

Band Position / cm^{-1}			
V-M.S.	**AP-M.S.**	**MP-M.S.**	**Assignment**
466	461	466	Si-O-Si_{def}
-	-	690	Sulphonic acid C-S_{str} or S=O_{str}
797	802	802	Si-CH_{3str}
975	949	955	Si-O-T
1082	1087	1072	Si-O-Si_{str}
1214 (sh)	1260	1200(sh)	Si-C_{str}
-	1469, 1485	1460, 1500	C-H_{def}
-	1555	-	Amino N-H_{def}
1625	-	-	Vinyl C=C_{str}
-	1650	1662	O-H-O_{def}
2859, 2930	2854, 2930*	2930	C-H_{str}
3455	3460	3439	O-H_{str}

V-, AP-, MP-M.S.: vinyl-, aminopropyl-, mercaptopropyl-modified mesoporous silica. *str* - stretch, *def* - deformation, (sh) - shoulder.
* observed for as-synthesized material only.

(i) Vinyl-modified

C=C stretching vibrations from a vinyl function usually occur in the region 1610 - 1690 cm^{-1}; unfortunately this region is very noisy in the spectrum obtained for the vinyl-modified mesoporous sample. Likewise, $C=C_{def}$ vibrations usually occur at *ca.* 1400 cm^{-1}, a region that may not be easily resolved for these spectra. An expanded spectrum of the surfactant-extracted material is presented in Figure 3.21 showing a peak at *ca.* 1625 cm^{-1}. It is possible that the presence of this peak indicates that the vinyl function is present in this sample but, due to the large number of peaks in this area which can not easily be assigned, it cannot be taken as conclusive confirmation of this.

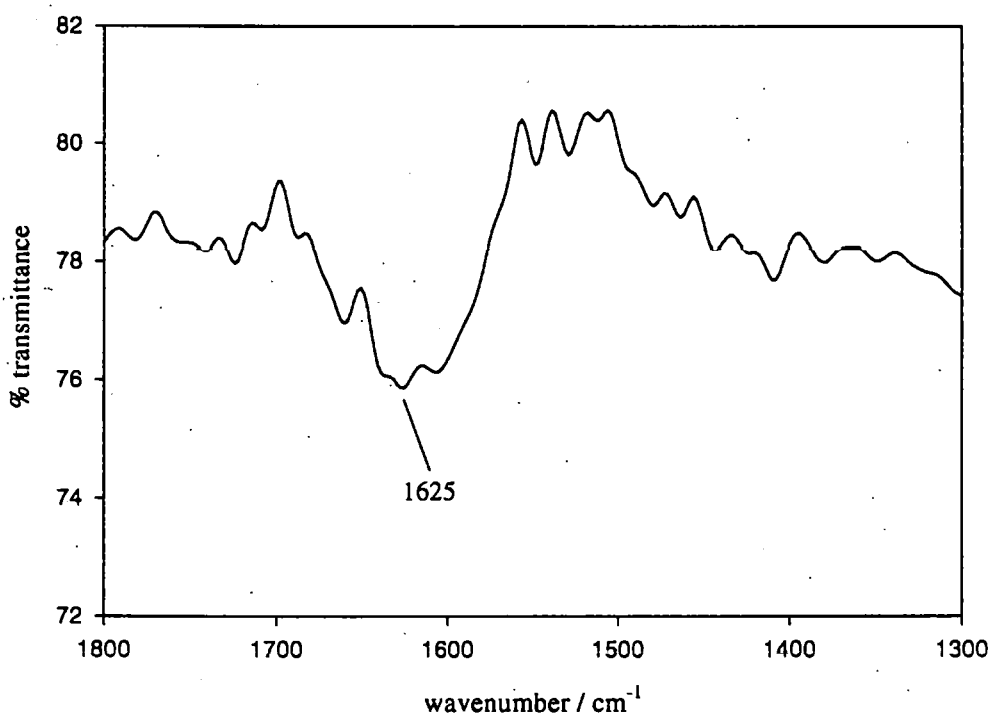

Figure 3.21 Expanded IR Spectrum of Vinyl-Modified Mesoporous Silica

(ii) Aminopropyl-modified

The N-H_{str} vibrations of a primary amine are normally located in the 3300 - 3500 cm^{-1} region, and are therefore impossible to locate for this sample due to swamping by the broad OH absorption at 3460 cm^{-1}. In contrast, N-H_{def} vibrations[11] are usually located between 1550 - 1650 cm^{-1}, and so an expanded spectrum of as-synthesized AP-M.S. is shown in Figure 3.22. Unfortunately, the spectrum is very noisy in this region, making band-assignment very difficult. The band at 1555 cm^{-1} has been tentatively assigned to the N-H_{def} vibration but, due to the plethora of peaks in this region, this result cannot definitively confirm that the aminopropyl function is present.

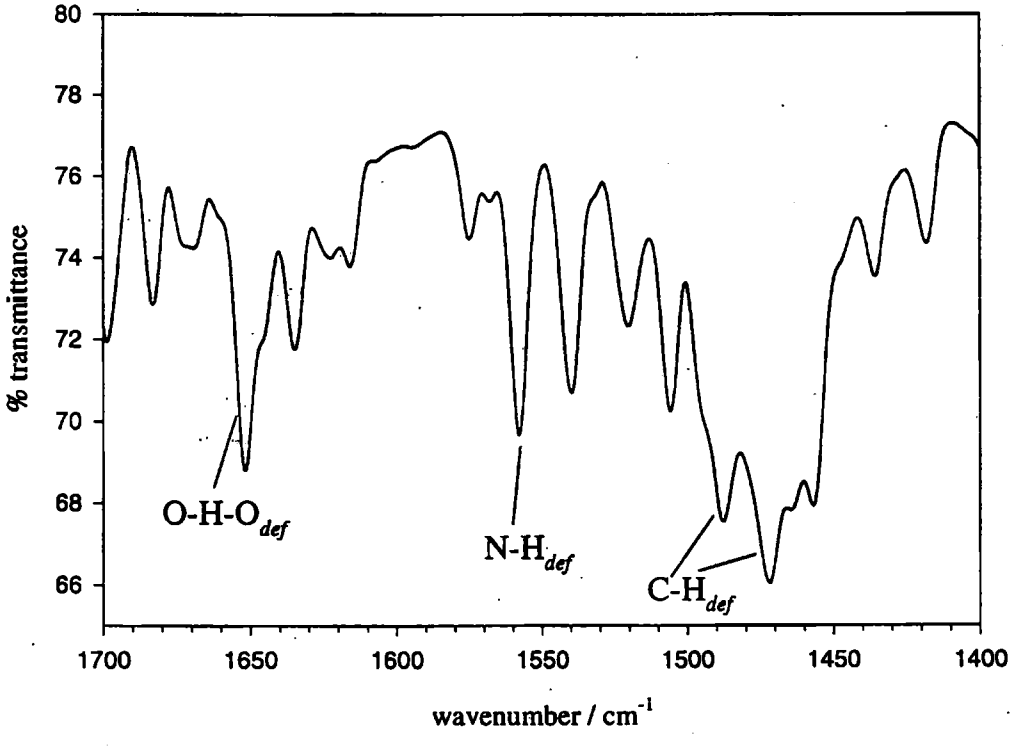

Figure 3.22 Expanded IR spectrum of MES-swollen AP-modified mesoporous silica: the range 1400 - 1700 cm^{-1}.

(iii) Mercaptopropyl-modified

The presence of intact thiol groups should be indicated by an S-H absorption[11,12] at *ca.* 2570 cm^{-1}. This is clearly not observed in this case which suggests that the thiol group has, in some way, been destroyed during the synthesis procedure (possibly *via* conversion to the sulphonic acid). The expanded spectrum presented in Figure 3.23, however, shows the presence of a broad absorption band at *ca.* 690 cm^{-1}, which could be due to either C-S_{str}[13] or S=O_{str}[13] (from RSO_3H) vibrations. Note that the sharp peak at *ca.* 675 cm^{-1} is also present in the spectrum of the aminopropyl-functionalized material, which suggests that this is not due to any S-H or S=O vibrations.

Additional peaks due to the sulphonic acid, if present, should be observed in the region *ca.* 1200 cm^{-1} which, unfortunately, is swamped by the Si-O-Si absorption. The very large absorption in the O-H_{str} region (3455 cm^{-1}) is observed, however, even following heating at 100 °C, which suggests that it could possibly be due to O-H_{str} of the SO_3H function.

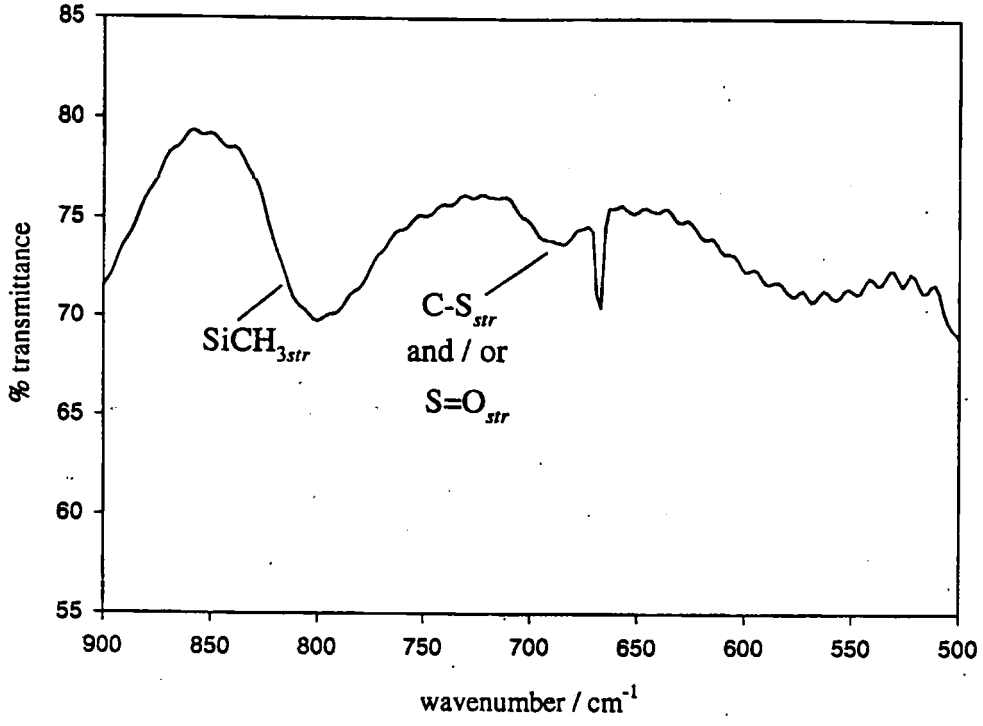

Figure 3.23 Expanded IR spectrum of MES-swollen MP-modified mesoporous silica in the range 500 - 900 cm^{-1}.

3.9 Thermogravimetry

Thermogravimetry (TG) was carried out for each of the organically-modified materials (after surfactant extraction) over the range 30 - 1200 °C. The results obtained for each sample are now discussed in turn.

3.9.1 Phenyl-modified Mesoporous Silica

The TG analysis of the surfactant-extracted, MES-swollen, phenyl-modified sample is presented in Figure 3.24 below.

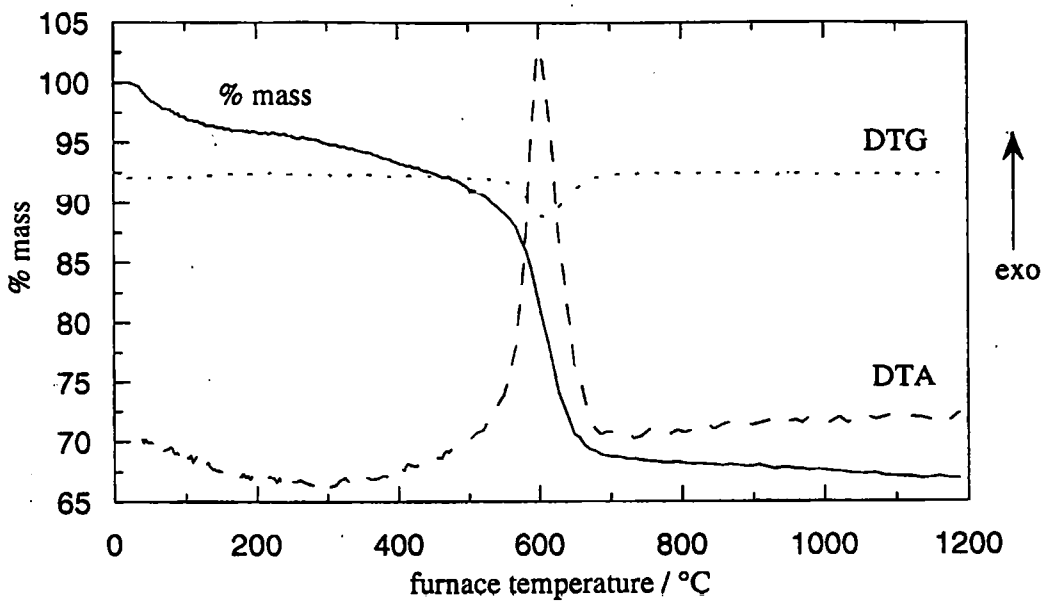

Figure 3.24 TG analysis of phenyl-modified mesoporous silica.

As is evident from Figure 3.24, TG analysis of the phenyl-modified sample results in a total mass loss of approximately 34 %. In the low temperature region a small mass loss, corresponding to *ca.* 3 %, is observed up to approximately 100 °C. This is likely to correspond to loss of physisorbed surface water, as observed for the purely siliceous material. An exothermic event then occurs up to 650 °C, which corresponds to approximately 28 % of the sample's total mass and represents loss (by oxidation) of the phenyl groups. Decomposition of the ^{29}Si MAS-NMR spectrum of this sample (see Section 3.10.1) yields an approximate molecular formula of $(SiO_2)_{0.4}(SiO_{1.5}OH)_{0.3}(PhSiO_{1.5})_{0.2}(PhSiO(OH))_{0.1}$ (disregarding the small amount of Q^2 and T^1 silicon atoms present) and calculation of the percentage mass of phenyl groups in the sample from this formula gives a value of 27.4 %, in reasonable agreement with the value obtained from the TG analysis. Calculation of the percentage mass of hydroxyls in the sample from the above formula yields a value of approximately 8 % which is not

observed by TG. A slight mass loss of *ca.* 3 % is observed over the range 650 - 1200 °C, however, which could correspond to dehydroxylation; it is possible that the formula obtained from NMR is inaccurate due to errors involved in decomposition.

The most likely "average" molecular formula for this material appears to be $(SiO_2)_{0.54}(SiO_{1.5}OH)_{0.15}(PhSiO_{1.5})_{0.31}\cdot 0.15H_2O$ which corresponds to a percentage mass of phenyl groups in the sample of 28.85 % and a percentage mass of hydroxyl groups in the sample of 2.99 %, in reasonable agreement with the TG results. This molecular formula is not entirely accurate, however, as it does not consider the relative amounts of Q^2, T^1 or T^2 silicon atoms that are present.

3.9.2 Vinyl-modified Mesoporous Silica

The TG analysis of the vinyl-modified material is presented in Figure 3.25.

This TG analysis reveals two major mass losses over the range 30 - 500 °C. The first, which occurs up to *ca.* 175 °C, is likely to be due to loss of physisorbed water. This corresponds to a mass loss of almost 20 %, much larger than that observed for the purely siliceous sample or the phenyl-modified sample. The IR spectrum of this material indicates that there is some template remaining in the sample following acid extraction, and this could contribute to some of the mass loss observed in this region.

The second mass loss is by an exothermic process and occurs over the range 180 - 500 °C. It corresponds to approximately 6.25 % of the sample's total mass and represents loss of the vinyl function by oxidation. Over the range 500 - 1200 °C a gradual mass loss of *ca.* 3.75 % is observed and this is likely to be due to surface dehydroxylation.

As the origin of the 20 % mass loss in the initial portion of the TG is ambiguous, it was not possible to assign a molecular formula for this material.

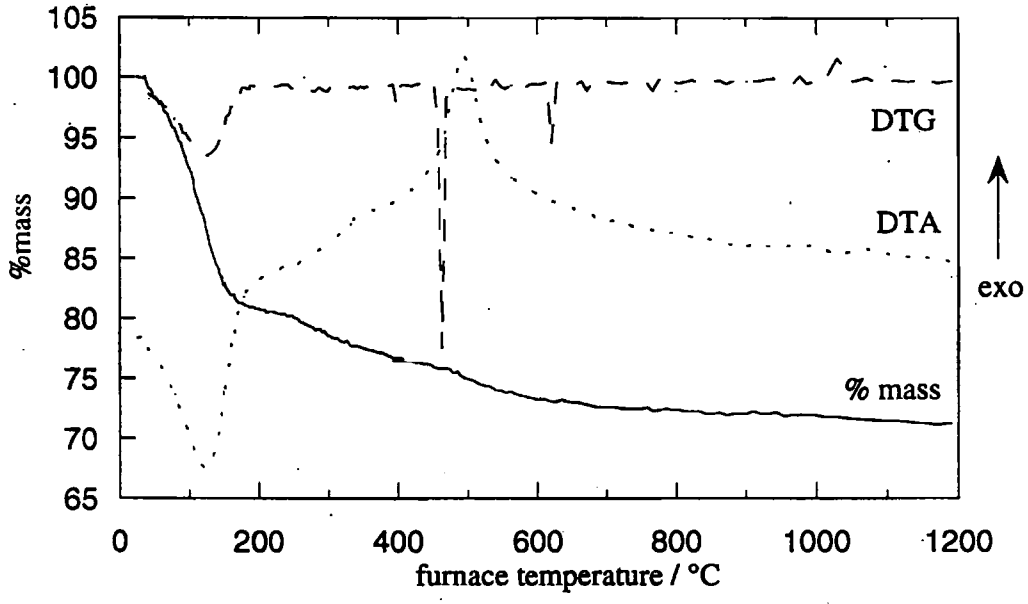

Figure 3.25 TG analysis for vinyl-modified mesoporous silica.

3.9.3 Aminopropyl-modified Mesoporous Silica

The TG analysis of the aminopropyl-modified sample is illustrated in Figure 3.26. The initial portion of the TG trace closely resembles that for the vinyl sample. A steep loss corresponding to almost 20 % of the total mass occurs up to *ca.* 175 °C, and this is likely to be due to loss of physisorbed surface water or trapped template molecules.

The second loss occurs, accompanied by an exotherm in DTA, over the range 175 - 380 °C, corresponding to a mass loss of approximately 10 % and representing loss of the aminopropyl groups. A third region of mass loss is very gradual and occurs between 400 - 1200 °C, corresponding to surface dehydroxylation.

Again, due to the ambiguity of the initial portion of the TG analysis, a molecular formula could not be assigned for this material.

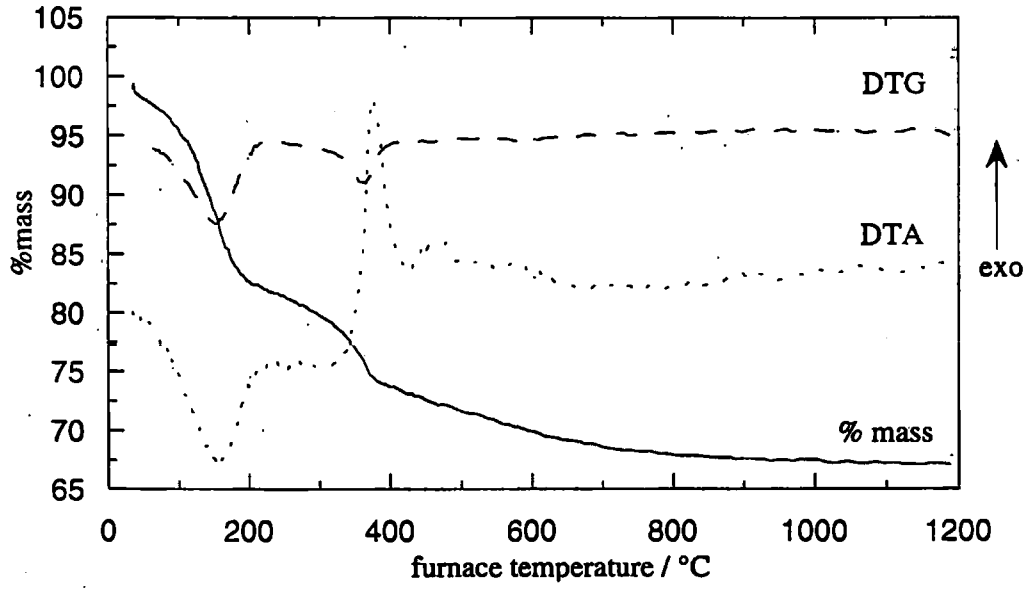

Figure 3.26 TG analysis of aminopropyl-modified silica

3.9.4 Mercaptopropyl-modified Mesoporous Silica

TG analysis of the mercaptopropyl-modified mesoporous silica is presented in Figure 3.27 showing two major mass losses over the range 30 - 1200 °C. The first, occurring from 30 - 125 °C, corresponds to approximately 8 % of the sample's total mass and could represent loss of physisorbed surface water. However, as the IR spectrum taken of this sample following template removal indicated the presence of residual template, it is possible that some of this mass loss corresponds to loss of template molecules.

The second mass loss (an exotherm in DTA) corresponds to approximately 28 % of the sample's total mass and occurs in two stages; the first stage occurs rapidly at *ca.* 360 °C, while the second stage occurs slowly over the range 360 - 600 °C. These two stages correspond to loss of the incorporated organic function (either propanthiol or propansulphonic acid). Above 600 °C a gradual mass loss corresponding to approximately 3 % of the total mass was observed, again being attributable to sample dehydroxylation.

A molecular formula could not be assigned for this material, again, due to the initial mass loss which could not be assigned to a particular moiety.

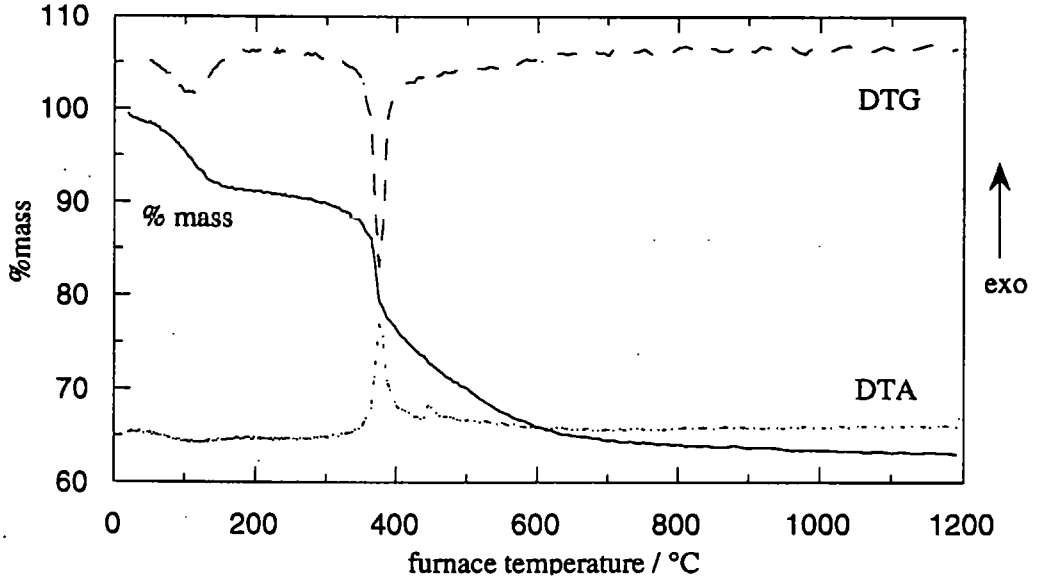

Figure 3.27 TG analysis of the mercaptopropyl-modified mesoporous silica.

3.10 MAS-NMR

3.10.1 ^{29}Si MAS-NMR

^{29}Si MAS-NMR spectroscopy was carried out on the MES-swollen phenyl-modified sample by the EPSRC solid-state NMR service at the University of Durham. Analysis of the MES-swollen aminopropyl- and mercaptopropyl-modified samples was carried out at the EPSRC sorbents and catalysts NMR service at UMIST. In each case, spectra were taken of each sample before and after template removal. The spectra obtained for the phenyl-modified sample are given in Figure 3.28, (below). Other spectra are given in Appendix A3.

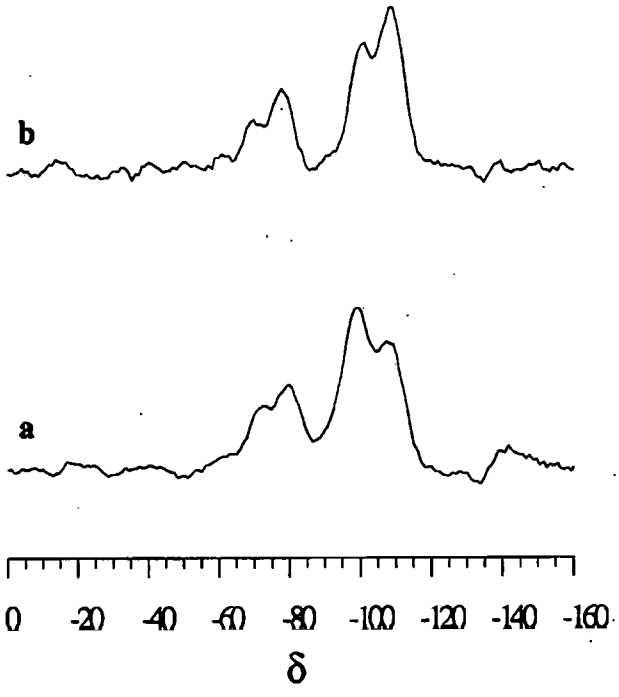

Figure 3.28 ^{29}Si MAS NMR spectra of MES-swollen phenyl-modified mesoporous silica: (a) as-synthesized, (b) after template removal.

In each of the samples after template removal, distinct resonances can be observed due to the siloxane [Q^n = $\underline{Si}(OSi)_n(OH)_{4-n}$, n = 2-4] and due to the

organosiloxane [T^m = $R\underline{Si}(OSi)_m(OH)_{3-m}$, m = 1-3] groups[10]. The chemical shifts of these resonances are given in Table 3.11.

Table 3.11 ^{29}Si MAS-NMR results for MES-swollen organically-modified mesoporous silicas.

		δ*					
Sample		**T^1**	**T^2**	**T^3**	**Q^2**	**Q^3**	**Q^4**
Phenyl-M.S.	A.S.	-	-70.6 (6.0%)	-79.7 (26.5%)	-	-98.8 (45.2%)	-108.9 (22.3%)
	S.E.	-61.6 (2.1%)	-69.8 (8.1%)	-78.2 (19.4%)	-92.0 (3.2%)	-100.3 (26.7%)	-109.0 (40.4%)
Aminopropyl-M.S.	A.S.	-	-	-	-	-100.3	-109.0
	S.E.	-55.0	-67.0	-	-92.0	-101.3	-110.4
Mercaptopropyl-M.S.	A.S.	-	-66.52	-	-	-100.1	-108.8
	S.E.	-	-67.17	-	-	-101.3	-109.1

*TMS as external reference, M.S. - mesoporous silica.
A.S. - as-synthesized, S.E. - after template removal.
Figures in brackets are peak ratios following decomposition.

In the case of the phenyl-modified material, after template removal, six distinct peaks were observed following spectral decomposition, indicating the presence of $Ph\underline{Si}(SiO)(OH)_2$, $Ph\underline{Si}(SiO)_2(OH)$ and $Ph\underline{Si}(SiO)_3$ moieties as well as the unmodified siloxanes. Four resonances were observed for the as-synthesized material. The decompositions are presented in Figures 3.29 and 3.30, and the peak ratios are given in brackets in Table 3.11.

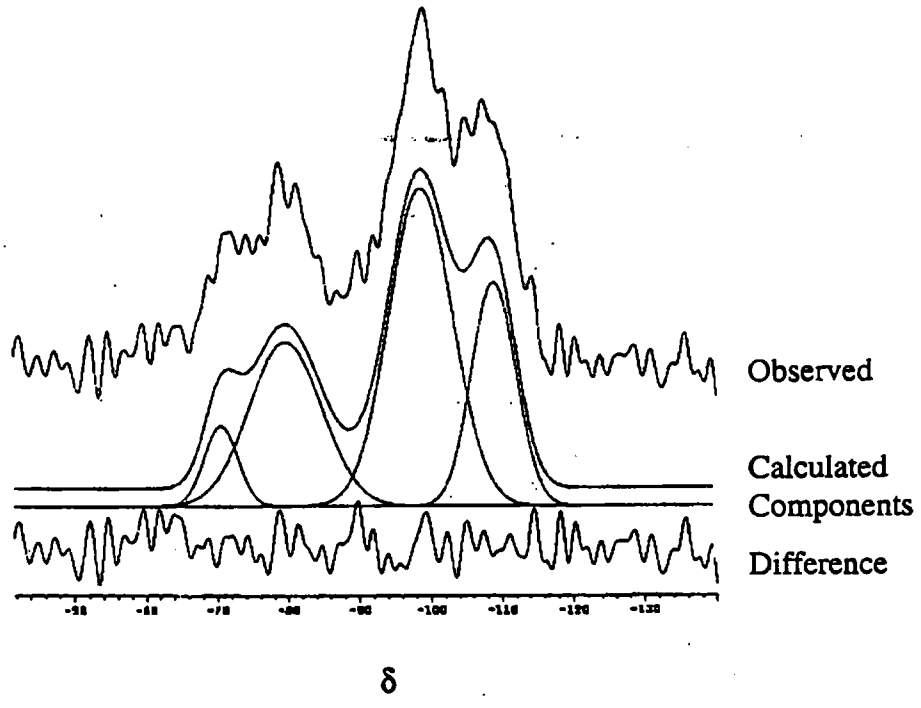

Figure 3.29 Decomposition of ^{29}Si MAS-NMR spectrum of as-synthesized MES-swollen phenyl-modified mesoporous silica.

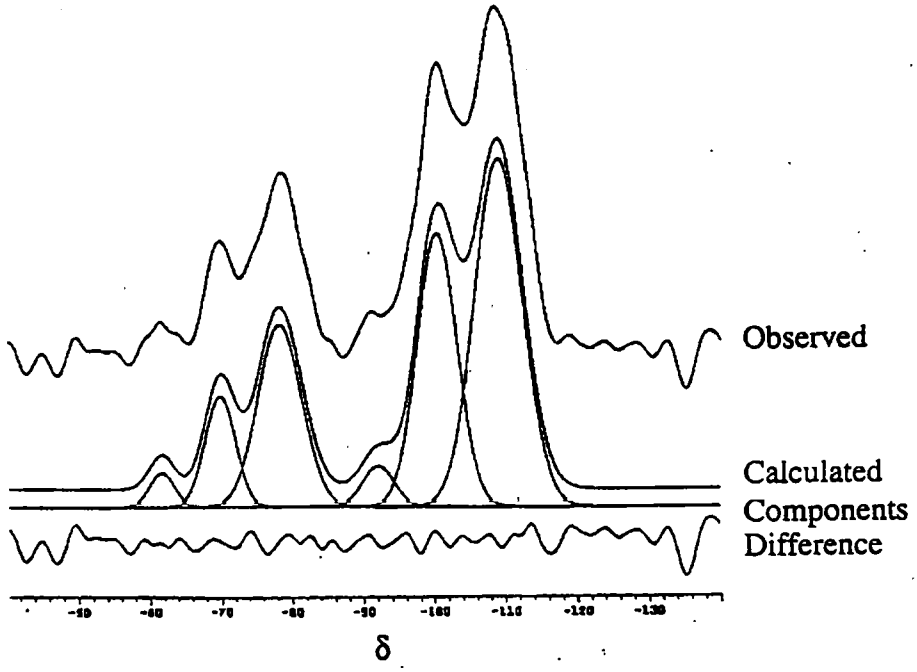

Figure 3.30 Decomposition of ^{29}Si MAS-NMR spectrum of MES-swollen phenyl-modified mesoporous silica following template removal.

Five peaks were detected for the extracted aminopropyl material, indicating that the aminopropyl function was incorporated in only two environments i.e. $H_3N(CH_2)_3\underline{Si}(SiO)(OH)_2$ and $H_3N(CH_2)_3\underline{Si}(SiO)_2(OH)$.

Only three peaks were detected for the extracted mercaptopropyl material, suggesting that the mercaptopropyl function was present as $HS(CH_2)_3\underline{Si}(SiO)_2(OH)$ only.

3.10.2 ^{13}C MAS-NMR

^{13}C MAS-NMR spectroscopy was carried out on the phenyl-modified mesoporous silica at the EPSRC solid-state NMR service at Durham. The aminopropyl- and mercaptopropyl-modified materials were analyzed at the EPSRC sorbents and catalysts NMR service at UMIST. NMR results are given in Tables 3.12 - 3.14 overleaf. The environments for carbon atoms identified from the spectra are shown in the respective ions / molecules presented in Figure 3.31. Spectra are given in Appendix A3.

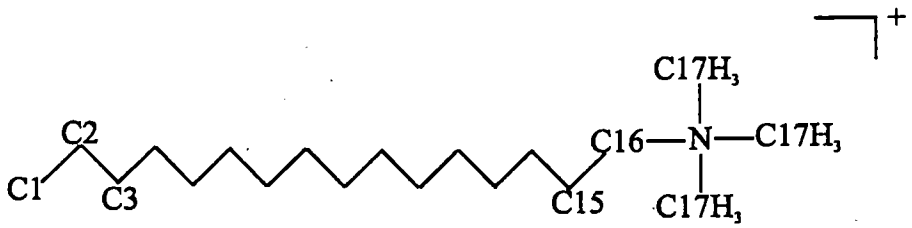

Cetyltrimethylammonium (CTMA) ion

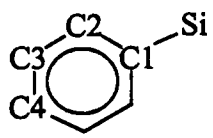

Phenyl function

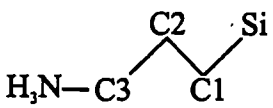

Aminopropyl function

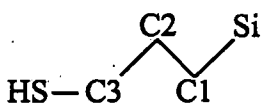

Mercaptopropyl function

Figure 3.31 Diagram showing the relative positions of the carbon atoms in the ions / groups under investigation.

Table 3.12 ^{13}C MAS NMR results for the phenyl-modified material

	δ* (CTMA)					δ* (Phenyl)		
Sample	**C1**	**C2**	**C3-15**	**C16**	**C17**	**C2**	**C3**	**C4**
A.S.	14.50	23.41	30.72	66.00	53.81	134.89	127.48	shoulder
S.E.	-	-	-	-	-	134.09	127.05	shoulder

*TMS as external reference. A.S. - as-synthesized, S.E. - after template removal.

Table 3.13 ^{13}C MAS NMR results for the aminopropyl-modified material

	δ* (CTMA)					δ* (Aminopropyl)		
Sample	**C1**	**C2**	**C3-15**	**C16**	**C17**	**C1**	**C2**	**C3**
S.E.	-	-	-	-	-	9.53	21.16	42.83

*TMS as external reference. S.E. - after template removal.

Table 3.14 ^{13}C MAS NMR results for the mercaptopropyl-modified material

	δ* (CTMA)					δ* (Mercaptopropyl)		
Sample	**C1**	**C2**	**C3-15**	**C16**	**C17**	**C2**	**C3**	**C4**
A.S.	14.50	23.36	30.59	67.31	53.98	-	27.41	
S.E.	-	23.19†	-	-	53.87†	11.47	27.54	

*TMS as external reference. A.S. - as-synthesized, S.E. - after template removal.
† See explanation in (iii), below.

(i) Phenyl-modified Mesoporous Silica

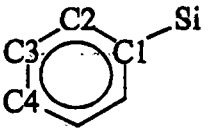

Phenyl function

In the case of the phenyl-modified sample, peaks for each of the template carbon atoms are observed for the as-synthesized sample, but are absent following template removal. In each case, two resolved peaks are observed corresponding to the C2 and C3 phenyl atoms. The C4 atom is observed as a shoulder only, while the C1 atom (attached directly to Si) cannot be observed.

(ii) Aminopropyl-modified

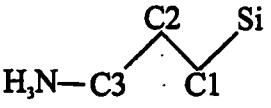

Aminopropyl function

^{13}C MAS-NMR was performed on this material only following template removal. Three peaks were observed, corresponding to the C1, C2 and C3 atoms of the aminopropyl function.

(iii) Mercaptopropyl-modified

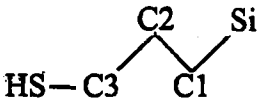

Mercaptopropyl function

The as-synthesized MP-modified sample displayed peaks assigned to the template molecule, as well as a peak at $\delta = 27.41$ assigned to the C2 and C3 atoms of the mercaptopropyl function. The extracted material also displayed a peak at $\delta \approx 27$ and an additional peak at $\delta = 11.47$, assigned to the C1 atom of the mercaptopropyl function. In addition, resonances were observed at $\delta = 23.19$ and $\delta = 53.87$. It is possible that these peaks are due to C-atoms of residual template molecules, but it is also possible that these resonances could signify the presence of other sulphur-containing functions. If, as was suggested earlier (Section 3.8.2), the thiol has been oxidised to a sulphonic acid, peaks would be expected at $\delta = 54$ (observed), 18 and 11(observed)[12]. Also, the presence of a propandisulphide function (the disulphide RS-SR, where R = $CH_2CH_2CH_3$ in this case, is easily produced by oxidation of the thiol) would be identified by a peak at $\delta = 23$[12] (observed). It is therefore possible that either, or both of these functions are present in this material.

3.11 Overview of the Characterization of the Organically-Modified Materials

3.11.1 Phenyl-modified Mesoporous Silica

X-ray powder diffraction studies of the phenyl-modified samples indicated that a single phase was formed and that structural order was maintained following template removal. Mesitylene was proved to be a successful pore-swelling agent by increasing the d_{100}-spacing of the final product. In contrast, the use of tetradecane as a pore-swelling agent was unsuccessful as an increase in d_{100} was not observed.

IR studies of the phenyl-modified materials showed a peak at 1143 cm^{-1} corresponding to an Si-C stretching vibration. Peaks due to phenyl C-H deformations and C=C stretching vibrations were also observed confirming the presence of phenyl groups in the sample.

TG analysis of the MES-swollen phenyl-modified sample (following surfactant extraction) yielded the molecular formula $(SiO_2)_{0.54}(SiO_{1.5}OH)_{0.15}(PhSiO_{1.5})_{0.31}\cdot 0.15H_2O$ as a very approximate formula for this material.

^{29}Si and ^{13}C MAS-NMR of the MES-swollen sample confirmed the presence of phenyl groups.

3.11.2 Vinyl-modified Mesoporous Silica

XRD studies of the vinyl-modified material showed that a single phase was formed and structural order was maintained following template removal. The obtained d_{100}-spacing suggested that a mesoporous material had been produced.

IR and TG studies were inconclusive and could not prove definitively that the vinyl function had been successfully incorporated into the material. A peak observed in the IR spectrum at 1625 cm^{-1}, however, probably corresponds to a vinyl C=C stretching vibration.

3.11.3 Aminopropyl-modified Silica

The XRD profile taken of the aminopropyl-modified material before template removal gave a single, broad peak corresponding to a d_{100}-spacing of 46.8 Å. Following template removal no XRD peaks were observed, suggesting that structural ordering had been lost. This loss of ordering could be due to incomplete condensation of the siloxanes during synthesis. As the reaction time for this synthesis was 1 week, however, (compared to 48 h for the phenyl-modified sample) this seems unlikely and it is possible that the reaction time was, in fact, too long in this case. A poster recently presented at the "First International Conference on Inorganic Materials" in Versailles,[14] demonstrated that MCM-41 materials synthesized with reaction times greater than eight days were non-porous following template removal.

Again IR studies proved to be inconclusive due to a large number of unassigned peaks in the region of interest in the IR spectrum. Results obtained from TG analysis were also inconclusive as the possible presence of surfactant molecules prevented the calculation of a molecular formula from the TG data.

^{29}Si MAS-NMR demonstrated the presence of an organosilicon moiety, and ^{13}C MAS-NMR confirmed that a propyl function was present.

3.11.4 Mercaptopropyl-modified Silica

XRD studies of the mercaptopropyl-modified sample demonstrated that structural order was maintained following template removal.

The S-H vibration was not detected in the IR spectra of this material. Bands that could be assigned to a sulphonic acid function were, however, observed. TG analysis did not permit the assigment of a molecular formula, however, due to residual surfactant molecules contributing to the sample's mass.

^{29}Si MAS-NMR confirmed the presence of an organosilicon moiety and ^{13}C MAS-NMR suggested the presence of more than one sulphur-containing function. A peak was observed which could correspond to the mercaptopropyl function ($\delta \approx 27$), while peaks at $\delta \approx 54$ and $\delta \approx 23$ could be due to the sulphonic acid or disulphide respectively.

ADDENDUM

3.12 Mesoporous Silica Spheres

When synthesizing batches of purely siliceous and aminopropyl-modified material using a particular magnetic stirrer, the product spontaneously formed into spheres of 5-10 mm in diameter (Figure 3.32). This was shown to be a function of the stirring rate (rather than the vessel) with only a "high" rate setting resulting in production of the spheres.

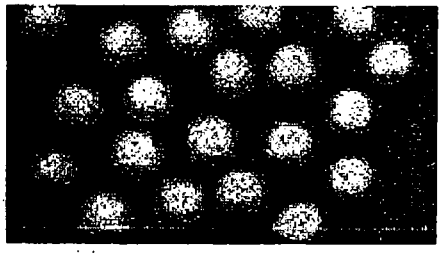

10 mm

Figure 3.32 Photograph of spheres of purely siliceous mesoporous silica.

XRD patterns consistent with a mesoporous structure were obtained. The spheres were very fragile and disintegrated when a scanning electron microscopy study was undertaken. Time did not permit further examination of these materials.

REFERENCES

1. Lazarev, A.N., *"Vibrational Spectroscopy and Structure of Silicates"*, Plenum Press, New York, **1972**.
2. Flanigen, E.M.; Khatami, H.; Szymanski, H.A., *Adv. Chem. Ser.*, **1971**, *101*, 201-229.
3. Zhong, Y.Y.; Liu, S.Q.; Chen, T.H.; Wang, J.Z.; Li, H.X., *J. Chem. Soc. Chem. Commun.*, **1995**, 973-974.
4. Szostak, R.; Nair, V.; Thomas, T.L., *J. Chem. Soc., Faraday Trans.*, **1987**, *1*, 487.
5. Bambrough, C.M.; Slade, R.C.T.; Williams, R.T.; Burkett, S.L.; Sims, S.D.; Mann, S., *J. Colloid and Interface Sci.*, **1998**, *201*, 220-222.
6. Ribeiro Carrott, M.M.L.; Carrott, M.M.L.; Candeias, A.J.E.; Unger, K.; Sing, K.S.W., Oral Presentation at the Sixth Fundamentals of Adsorption Conference, France, **1998**.
7. Chuang, I-S.; Maciel, G.E., *J. Phys. Chem. B*, **1997**, *101*, 3052-3064.
8. Moyako, R.; Jones, W., *J. Chem. Soc., Chem. Commun.*, **1996**, 981-982.
9. Mokayo, R.; Jones, W.; Luan, Z.; Alba, M.D.; Klinowski, J., *Catalysis Letters*, **1996**, *37*, 113-120.
10. Burkett, S.L.; Sims, S.D.; Mann, S., *J. Chem. Soc., Chem. Commun.*, **1996**, 1367-1368.
11. Kemp, W., *"Qualitative Organic Analysis, Spectrochemical Techniques", 2nd Edition*, McGraw-Hill, London, **1986**.
12. Rhijn, W.; Vos, D.; Sels, B.; Bossaert, W.; Jacobs, P., *J. Chem. Soc., Chem. Commun.*, **1998**, 317-318.
13. Cross, A.D., *"Introduction to Practical Infrared Spectroscopy"*, Butterworths, London, **1960**.
14. Blin, J.L.; Otjacques, C.; Herrier, G.; Su, B-L., *"Kinetic Study of MCM-41 Synthesis"*, Poster Presentation, First International Conference on Inorganic Materials, Versailles, **1998**.

CHAPTER 4

GAS ADSORPTION STUDIES

This chapter is divided into two parts. Part I considers the theoretical background to gas adsorption studies while Part II describes the experimental techniques employed.

PART I - THEORETICAL BACKGROUND

4.1 General[1]

It was first observed over 200 years ago that finely powdered solids have the ability to take up relatively large volumes of condensable gas. In 1881 Kayser[2] used the term *adsorption* to describe this condensation process. The term *adsorption* is now internationally employed to describe the enrichment of one or more components on a surface, while the term *desorption* describes the depletion of these components from the surface.

Adsorption is classified as being either physical (*physisorption*) or chemical (*chemisorption*). The former involves weak forces, such as van der Waals and hydrogen bonding, and occurs in most gas-solid systems. Physisorption can be multilayer and in some ways resembles condensation of a gas. Chemisorption (involving chemical bond formation) in contrast, only occurs in certain systems and is confined to a monolayer.

When a porous solid is exposed to a gas at a certain pressure in a closed space, the solid will adsorb the gas with a corresponding decrease in the pressure of the gas and

increase in the mass of the solid. The amount of gas (*the adsorptive*) taken up by a solid (*the adsorbent*) is dependent on the temperature of the experiment and the pressure of the gas, as well as on the nature of the solid and gas. Upon adsorption the adsorptive is termed *the adsorbate*.

For a specific solid and gas at a fixed temperature the general Equation 4.1 applies:

$$n = f(p)_{T,\,gas,\,solid} \qquad (4.1)$$

where n is the amount of gas adsorbed, normally expressed in moles per gram of adsorbent, and p is the adsorptive equilibrium pressure. This equation is an expression of the adsorption isotherm, which is the relationship at constant temperature between the amount of gas adsorbed by the solid and the pressure or relative pressure (p/p^0) of the adsorbate (p^0 is the saturation vapour pressure of the adsorptive at the experimental temperature). Most isotherms can be classed as belonging to one of the five common groups of isotherms as classified by Brunauer, Demming, Demming and Teller (BDDT)[3] and sometimes referred to as the Brunauer, Emmett and Teller (BET) classification.[4] Each of the five "ideal" types of isotherm and the very rare, stepped, sixth isotherm are characteristic of a certain type of solid and the six isotherms are shown in Figure 4.1.[5] As well as these six types of isotherm there are certain isotherms which may display characteristics of more than one type of "ideal" isotherm, and can therefore be described as borderline cases. There are also, of course, a number of isotherms which cannot easily be assigned to any class.

Samples may be classified according to the width of their pores (see Section 1.2). Table 4.1, given overleaf, describes the main pore characteristics of solids which give rise to isotherms of Types I to VI.

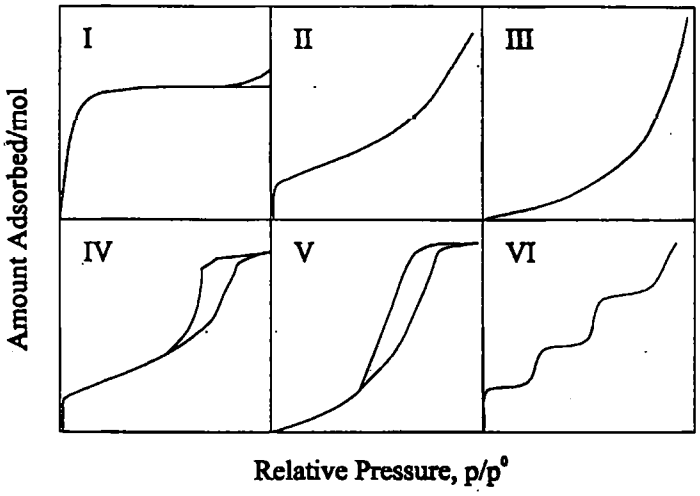

Figure 4.1[5] The five BDDT isotherm types (I - V) along with the rare, stepped isotherm (Type VI).

Table 4.1 The characteristics described by the BDDT isotherm classification.[3]

Isotherm Type	Main Pore Characteristics
I	microporous or non-porous chemisorbed monolayer
II	mainly non-porous or macroporous, but could still have some micropores
III	non-porous, weak adsorbent-adsorbate interactions
IV	mesoporous
V	shows porosity, but characteristic of weak adsorbent-adsorbate interactions
VI	very rare - shows stepwise multilayer adsorption on uniform surface

An adsorption isotherm can yield valuable information about the pore structure and specific surface area of a solid, of particular interest in the study of M41S-type materials. As these solids are mesoporous, one would expect gas adsorption to yield a Type IV isotherm. This isotherm is therefore of most interest here, and is discussed in greater detail in Section 4.2. However, as this study will also investigate solids with pores in the microporous range, the Type I isotherm is also relevant and its characteristics, along with those of the Type V isotherm, are also discussed in Sections 4.3 and 4.4 respectively.

4.2 The Type IV Isotherm

The Type IV isotherm initially displays a region of steep adsorption at low relative pressures, which then plateaus and often produces a sharp 'knee' (which represents monolayer coverage of the surface). A second steep region of the isotherm is then observed and is often accompanied by hysteresis. This region represents capillary condensation and is characteristic of mesoporous solids. Hysteresis is a result of the formation, upon adsorption, of a meniscus from which desorption will only occur at relative pressures below those at which it formed; in each hysteresis loop the amount adsorbed on the *adsorption* branch at a particular relative pressure is always less than the adsorbed amount on the *desorption* branch at the same relative pressure. An interesting feature of nitrogen isotherms determined for M41S-type materials at 77 K is the absence of hysteresis.[6] The reason for this is not completely understood, but it is thought to be due to the relative pressure value at which capillary condensation occurs ($p/p^0 \approx 0.4$) in these materials. This value of p/p^0 represents a region of instability in the

nitrogen meniscus and if M41S-type materials of different pore sizes were to be analyzed, or the temperature of the isotherm were altered, hysteresis would be observed.

The characteristic shape of the Type IV isotherm is therefore representative of the change between mono- and multilayer adsorption. The sharp 'knee' present in the Type IV isotherm (also present in the Type II isotherm) allows us to calculate the specific surface area, S_{sp} (m^2 g^{-1}), of the solid as described below in Section 4.2.1. It should be noted however that the presence of micropores in the solid may affect S_{sp} calculation as, in this case, the knee may be representative of micropore filling (see Section 4.3).

4.2.1 Determination of Specific Surface Area

A useful value that can be determined from gas adsorption studies is the specific surface area, S_{sp} of a solid. In studies where this is required, nitrogen is the adsorptive of choice for reasons discussed in Section 4.5. The S_{sp} (m^2 g^{-1}), of a solid may be calculated from equation 4.2:

$$S_{sp} = n_m L a_m \qquad (4.2)$$

where n_m is the monolayer capacity, L is the Avogadro number and a_m is the area occupied by an adsorbate molecule (usually nitrogen) in the completed monolayer.

In order to determine the specific surface area of a solid by gas adsorption it is therefore necessary to measure the monolayer capacity of the solid. The monolayer capacity, n_m (mol g^{-1}), is defined as the amount of gas that can be accommodated by a single molecular layer on the surface of 1 g of solid. There are two methods available for the calculation of n_m: the Point B method[7] and the BET model[8]. These methods and their applicability are discussed in the following Sections.

Calculation of a_m may be achieved by considering the density of the bulk liquid. This method, originally proposed by Emmett and Brunauer,[7] assumes that the molecules are arranged in the same manner when adsorbed on the surface as they would be if placed on a plane surface within the bulk liquid (i.e. in a close-packing arrangement). This leads to equation (4.3):

$$a_m = f(M / \rho L)^{2/3} \qquad (4.3)$$

where f is a packing factor (equal to 1.091 for 12 nearest neighbours in the bulk liquid and six on the plane surface)[7], M is the molar mass and ρ is the density of the adsorptive at the experimental temperature.

(The a_m values of the adsorptives used in this study are given in Table 4.2 in Part II of this chapter.)

i) The Point B Method of Surface Area Analysis

The sharp knee that is characteristic of Type II and Type IV isotherms was termed "Point B" by Brunauer and Emmett[7] and represents monolayer coverage of the surface (see Figure 4.2). It is therefore simply a matter of reading off the adsorbed amount from the y-axis (at the point at which the isotherm becomes linear after the knee) to obtain a value for the monolayer capacity of the solid. However, if the Point B region is somewhat ill-defined (i.e. the isotherm displays a rounded knee) the ease with which the monolayer capacity can be determined is diminished. In fact, in most cases the BET model[8] (see next Section) is a more accurate method of n_m determination, since it is effectively a mathematical method of determining Point B.

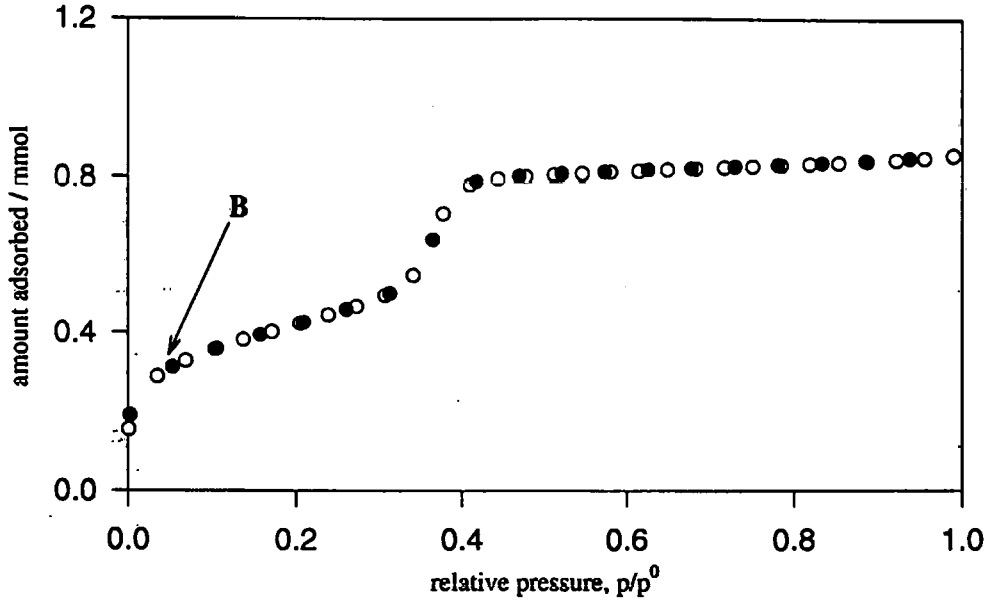

Figure 4.2 A nitrogen isotherm isotherm of MCM-41 showing the position of the 'Point B'.

ii) BET Analysis[8]

The equation most commonly used to describe multilayer physical adsorption is the BET equation, formulated from the Langmuir equation[9] (see Section 4.3) by Brunauer, Emmett and Teller.[8] The BET equation was derived kinetically for a state of dynamic equilibrium, where the rate at which molecules condense from the gas phase onto the surface is equal to the rate at which molecules evaporate from the occupied sites. The equation is shown below in its linear form:

$$\frac{p/p^0}{n(1-p/p^0)} = \frac{1}{n_m c} + \frac{c-1}{n_m c}\frac{p}{p^0} \qquad (4.4)$$

n is the amount adsorbed at equilibrium pressure p, p^0 is the saturation vapour pressure at the experimental temperature, n_m is the monolayer capacity and c is the BET parameter, which is related to the net heat of adsorption, (q_1 = heat of adsorption in first layer, q_L = heat of adsorption in subsequent layers) , as shown in equation 4.5.

$$c = e^{(q_1 - q_L)R/T} \qquad (4.5)$$

In this model, plotting $\frac{p/p^0}{n(1-p/p^0)}$ against $\frac{p}{p^0}$ will give a straight line with a slope $\frac{c-1}{n_m c}$ and an intercept $\frac{1}{n_m c}$, thus permitting the calculation of the monolayer capacity $\left(n_m = \frac{1}{\text{slope} + \text{intercept}}\right)$ and providing a means for calculating the specific surface area, S_{sp} of the solid. There are many limitations associated with applying the BET equation to calculating S_{sp} and these are discussed below.

The BET constant, c, gives a quantitative measure of the interaction between the surface and the adsorbed molecules in the monolayer, relative to those between the mono- and subsequent layers. In general, a value for c which lies between 50 and 250 will give a precise surface area value. Smaller constants are accompanied by a rounded 'knee' in the isotherm (and a correspondingly ill-defined Point B) and are due to insufficient differences in the adsorption strengths between the mono- and subsequent layers. Larger values for c may indicate the presence of micropores.

Limitations of the BET Model

While a BET model gives reasonable agreement in the low pressure region to Type II and Type IV isotherms (i.e. those isotherms with a sharp 'knee'), there are certain limitations of the BET model, namely one assumes that:

1) the surface is homogeneous, i.e. all adsorption sites are energetically identical
2) there are no lateral interactions between adsorbed particles
3) an infinite number of physically adsorbed layers can be formed

4) in all but the first layer, adsorption resembles the liquefaction of a gas.

The system being studied would not be expected to adhere to the above criteria. For example, a homogeneous surface is unlikely, and surface heterogeneity is the norm. It is also impossible to assume that lateral interactions between adsorbed molecules are negligible, especially when approaching layer completion. In addition, it is questionable how far all layers after the first should be treated as identical. Despite these assumptions, however, a BET model gives reasonable agreement in the range $0.05 \leq p/p^0 \leq 0.35$ and is a good working model for Type II and Type IV isotherms in that range. It should be noted that, even in the most favourable cases, an uncertainty in the calculation of specific surface area of ≥ 10 % is not unusual, and this may be attributed to the nature of the BET model and the assumptions it imposes.

4.2.2 Determination of Pore Width and Pore Volume

i) Pore Width

Type IV isotherms are characteristic of mesoporous solids and are usually easily recognised by their hysteresis loops. Although the exact shape of the hysteresis may vary with each sample, it is always the case that at any given relative pressure the amount adsorbed is greater in the desorption branch than in the adsorption branch (see Section 4.2). Zsigmondy[10] put forward a capillary condensation model to explain this. Thomson[11] (later Lord Kelvin) had stated (on thermodynamic grounds) that it is possible for a vapour to condense to a liquid in the pores of a solid even if the relative pressure is $p/p^0 < 1$. This is because the equilibrium vapour pressure, p^e, above a concave meniscus must be less than the saturation vapour pressure, p^0 at the same temperature. Zsigmondy's model assumed that along the initial part of the isotherm adsorption occurs only as a thin layer on the walls of the pore until, at the inception of the hysteresis loop,

capillary condensation occurs. With increasing pressures, condensation continues until even the widest pores are completely filled with condensate. It was assumed that the pores were cylindrical and ϕ, the angle of contact, was zero ($\cos\phi = 1$), thus giving a hemispherical meniscus. The mean radius of curvature of the meniscus is then equal to the radius of the pore minus the thickness of the adsorbed monolayer on the walls. The "Kelvin equation" is given below:

$$\ln\frac{p}{p^0} = \frac{-2\gamma V_L}{RTr_m}\cos\phi \qquad (4.6)$$

where p/p^0 is the relative pressure of the vapour in equilibrium with a meniscus of radius of curvature r_m at temperature T(K). γ is the surface tension of the liquid adsorptive, V_L is the molar volume of the adsorbate in liquid form and R is the gas constant.

It is therefore possible, by applying the Kelvin equation at the inception of the hysteresis loop, to calculate the minimum pore radius in which capillary condensation can occur. The usual pore diameter range between which capillary condensation occurs is 10 - 250 Å, and this is therefore the range over which the Kelvin equation may be applied.

As previously mentioned, the radius of curvature of the meniscus, r_m, is equal to the radius of the pore minus the thickness of the adsorbed film, t. The pore radius, r, is therefore obtained via equation (4.7):

$$r = r_m + t \qquad (4.7)$$

where t (Å) is calculated from equation (4.8):

$$t = (n / n_m) \sigma_t \qquad (4.8)$$

Here, n is the amount adsorbed at relative pressure p/p^0, n_m is the monolayer capacity and σ_t is the thickness of each layer.

ii) Pore Volume

The final plateau of the Type IV isotherm represents complete filling of all the pores with liquid adsorbate. It is therefore possible, by using the liquid density, to calculate the amount of liquid adsorbed onto the surface. The total pore volume (or Gurvitsch volume[12]) can then be calculated from equation (4.9):

$$\text{Total Pore Volume, } V_p = n_p M / \rho \qquad (4.9)$$

where n_p is the limiting adsorption value obtained from the plateau region of the isotherm, M is the molar mass of the adsorbate and ρ is the density of the liquid adsorbate. This volume should be the same for all adsorptives on a particular solid; this "Gurvitsch rule" is generally valid to within a few percent for those systems giving rise to a Type IV isotherm, but its accuracy is limited by the ease with which the plateau can be determined.

4.3 The Type I Isotherm

If a sample is microporous, the narrowness of the pores may cause enhanced adsorption as the potential fields from neighbouring walls interact to cause a distortion of the isotherm at low relative pressures. This, in the simplest case, will give rise to a Type I isotherm which displays a steep region at low relative pressures followed by a plateau at a limiting value. According to "classical" interpretation[9] this limit exists because pores are so narrow that they cannot accommodate more than a single molecular layer on their walls. This classical view assumes that the Type I isotherm conforms to the Langmuir equation[9] given below (equation 4.10).

$$\frac{n}{n_m} = \frac{Bp}{1+Bp} \qquad (4.10)$$

where

$$B = \frac{a_1 \kappa}{z_m \nu_1} e^{q_1/RT} \qquad (4.11)$$

a_1 is the condensation coefficient (i.e. the fraction of incident molecules which actually adsorb), z_m is the number of adsorption sites per unit area, ν_1 is the frequency of oscillation of the molecule in a direction normal to the surface, q_1 is the isosteric heat of adsorption and κ is a constant given by the kinetic theory of gases, $\left(\kappa = \frac{0.5L}{(MRT)^{1/2}}\right)$.

In practice, B is a constant which cannot be resolved experimentally via equation 4.11. However, if equation 4.10 is rewritten substituting relative pressure, p/p^0, for pressure, p, it then becomes:

$$\frac{n}{n_m} = \frac{c(p/p^0)}{1+c(p/p^0)} \qquad (4.12)$$

where c is the BET constant. When written in its linear form (equation 4.13), it becomes clear that a plot of $\frac{p/p^0}{n}$ against p/p^0 will yield a straight line with a slope of $1/n_m$.

$$\frac{p/p^0}{n} = \frac{1}{cn_m} + \frac{p/p^0}{n_m} \qquad (4.13)$$

It is therefore possible to calculate a value for the monolayer capacity, n_m, of the solid from a Type I isotherm and thus a value for the specific surface area, S_{sp} (see Section 4.2). In fact, if the plateau of the Type I isotherm is horizontal, when employing the classical interpretation, the monolayer capacity may be taken as identical to the total uptake, n_s, at saturation pressure.

A number of arguments[13,14] suggest that this classical interpretation is inapplicable however, not least that surface areas calculated from Type I isotherms are often improbably high[14]. Another fact which suggests that the limiting plateau of a Type I isotherm does not correspond to the monolayer capacity is that the Gurvitsch volume rule (see Section 4.2.2) is often obeyed for a variety of adsorbates by systems yielding this type of isotherm.[15,16,17] This conformity to the Gurvitsch rule suggests that the adsorbate is condensed in the pores in a form which has a density close to that of the liquid adsorptive. For this to occur, the pores must have a width in excess of two molecular diameters since the size and shape of different adsorbate molecules would influence the packing within the pore structure. In order for the adsorbate to simulate the bulk liquid, a pore width of several molecular diameters would therefore be required. Considering these arguments, it seems more likely that the uptake, n_s, at saturation is more likely to correspond to the pore volume of the adsorbent. This led Pierce, Wiley and Smith[14] and, independently, Dubinin[18] to postulate that the mechanism of adsorption in microporous solids is a pore filling process similar to capillary condensation, rather than a layer-by-layer build up of adsorbate on the pore walls. The Type I isotherm plateau therefore represents total pore filling and can be used to determine the micropore volume of the adsorbent if the isotherm has a sharp knee and a horizontal plateau. However, when determining the microporosity of a sample it is important to note that microporosity is often accompanied by a large external surface and / or mesopores, and care must therefore be taken when assigning a value to the micropore volume. More definitive methods of determining microporosity include preadsorption techniques,[19] *t*-plots[20] and α_s - plots[21].

4.4 The Type V Isotherm

The Type V isotherm is representative of weak adsorbate-adsorbent interactions and is often observed in water sorption on hydrophobic surfaces.[22] It is characterized by a region of low uptake at low relative pressures followed by a period of condensation accompanied by hysteresis. Water adsorbs preferentially on the silanol (SiOH) groups of a silica (rather than forming a uniform surface), and clustering of water molecules one on top of the other then follows, producing the upward sweep of the isotherm. The Point B, if observed, does not therefore correspond to the monolayer capacity of the solid, but refers to the density of the surface silanol groups. For this reason it is not possible to use water sorption by M41S materials to determine surface areas, but it can be a useful tool in monitoring other surface characteristics.

PART II - EXPERIMENTAL TECHNIQUES

4.5 The Adsorptives

Two methods of gas adsorption were used in these studies; automated volumetric adsorption and manual gravimetric adsorption. The adsorptives used in each technique are shown in Table 4.2, along with the experimental temperatures and the molecular areas, a_m, of the adsorptives.

Table 4.2 Adsorptives, their molecular areas and the adsorption temperatures used in each technique.

Adsorptive	Technique	Temperature / K	Molecular Area†, a_m / Å^2
N_2	*Volumetric*	77	16.2
O_2		77	14.1
H_2O	*Gravimetric*	303	10.5
C_6H_6		293	30.7*
n-BuOH		303	32.1
t-BuOH		303	33.1

† Molecular areas calculated from equation 4.3.
*While this value of $a_m(C_6H_6)$ = 30.7 Å was obtained using equation 4.3, the McClellan and Harnsberger "recommended" value of $a_m(C_6H_6)$ = 43 Å was used in S_{sp} calculations (see Section 5.7.1).

The sorption of organic and polar solvents can yield important information on the surface characteristics of a sample, but when determining the surface area, S_{sp}, nitrogen is the adsorptive of choice for the following reasons:

1) it is inert (will not chemisorb)
2) it has no dipole moment
3) the small N_2 molecules (assumed to be spherical) can easily penetrate most pores and are not sterically hindered
4) its saturation vapour pressure (1 atm) at the working temperature (77 K) is large enough to be measured accurately
5) it is easily and cheaply available

For these reasons, N_2 is the sorptive favoured for specific surface area determination, and all of the samples studied here were analyzed using nitrogen sorption.

The value quoted in Table 4.2 for the molecular area of benzene is obtained using equation 4.3. Problems arise, however, when assigning a molecular area for benzene[23], as this will differ greatly depending on whether the molecule is lying flat on the surface or is oriented perpendicular to it. Isirikyan and Kiselev[24] estimate a_m(flat) = 40 $Å^2$ and a_m(upright) = 25 $Å^2$, as appropriate molecular areas for benzene. In a review by McClellan and Harnsberger,[25] the recommended value of $a_m(C_6H_6)$ is given as 43 ± 3 $Å^2$, based on $a_m(N_2)$ = 16.2 $Å^2$ and as a result of examining benzene sorption on eleven adsorbents. In this study the McClellan and Harnsberger value (i.e. 43 ± 3 $Å^2$) is employed when determining specific surface areas from benzene sorption.

The a_m values quoted for *n*-BuOH and *t*-BuOH, calculated from equation 4.3, do not accurately reflect true molecular areas as these molecules are obviously not spherical. More accurate values may be calculated from isotherms of these species using

the specific surface area of the sorbent derived from nitrogen sorption. This is discussed further in Chapter 5 for benzene as well as for the alcohols.

4.6 Volumetric Adsorption

The sorption of nitrogen and oxygen at 77 K was performed on the fully automated and computer-controlled Micromeritics Gemini 2375 Surface Area and Porosimetry Analyzer. A two-stage rotary vacuum pump was connected to the apparatus and used to evacuate the system prior to adsorption and during desorption. The Gemini apparatus consists of identical balance and sample tubes, immersed in a dewar vessel of liquid nitrogen and exposed to identical experimental conditions. A flowing gas technique delivers the adsorptive to both tubes simultaneously. This duplicate operation means that any changes in the gas balance are due to adsorbance by the sample. The rate at which the adsorptive is supplied is determined by the rate at which the sample adsorbs. Results are displayed as an adsorption isotherm, and a BET multipoint surface area calculation is automatically performed. Typically, sample masses as low as 0.1 g can be successfully analyzed.

Before isotherm measurement commenced, the samples were outgassed for several hours to remove physisorbed vapours. The Micromeritics Flowprep 060 outgasser, in which the samples are heated under a flow of nitrogen without the use of a vacuum pump, was employed for this. All aluminosilicate and purely siliceous samples were outgassed at 150°C, while all organically functionalized materials were outgassed at 100°C (to prevent removal of the organic groups).

4.7 Gravimetric Adsorption

The gravimetric balance used for the sorption of vapours at 303 K and 293 K, was of the conventional McBain-Bakr[26] type, and was designed and built in-house by Branton.[27] The system, shown in Figure 4.2, was constructed from Pyrex tubing and vacuum-seated Pyrex stopcocks. The adsorption of organic solvents necessitated the use of Apiezon T as the stopcock lubricant. The balance mechanism consisted of two helical quartz springs (connected in series in order to increase the sensitivity) suspended from a hook and the sample, housed in a silica bucket, was suspended from the springs via a series of silica rods. One of these rods, the marker rod, contained two blue glass reference markers.

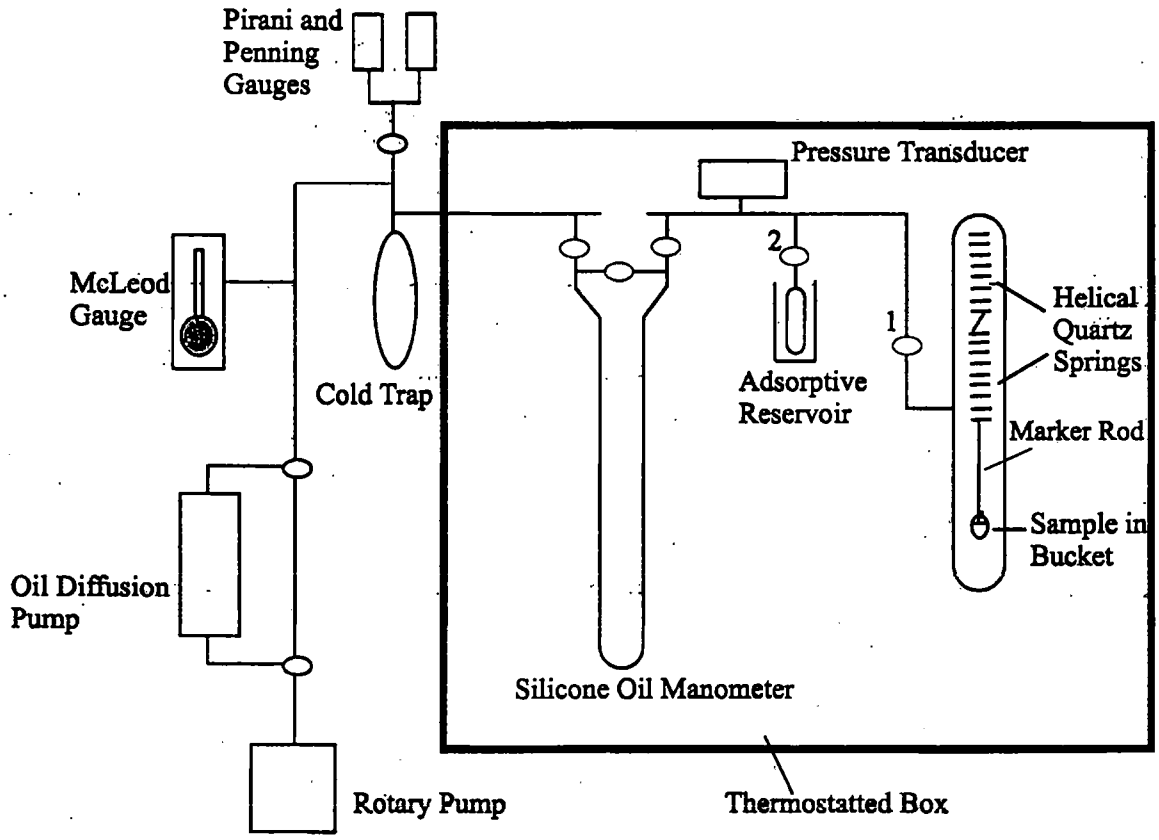

Figure 4.2 The Gravimetric Adsorption Balance

A rack-and-pinion-type microscope was focused on the tip of one of these blue markers to measure spring extension. The pumping apparatus consisted of a water-cooled oil diffusion pump and a two-stage rotary pump. Pirani and Penning gauges and a McLeod gauge attached to the line measured vacuum pressures of $< 1 \times 10^{-3}$ Pa. The sorptive pressures were measured using a silicone oil manometer and a pressure transducer.

The adsorptive was contained in a reservoir and its vapour pressure controlled by the water temperature in a surrounding dewar vessel. The whole vacuum line was then housed in a thermostatted box, the temperature of which was maintained at 303 K by two thermistor-controlled carbon filament bulbs and an air-circulating fan. For experiments carried out at 293 K, water from a thermostatted tank was circulated through a dewar vessel surrounding the sample. The springs were maintained at 303 K to maintain their calibration.

4.7.1 Spring Calibration

The gravimetric line was calibrated under vacuum at 303 K by suspending a silica bucket containing glass beads of known mass from the springs. As the mass was increased the extension of the spring was measured by means of the rack and pinion type microscope, fitted with a screw micrometer eyepiece focused on the tip of one of the blue glass reference markers. By plotting spring extension against mass, the spring response was shown to be linear and reversible; a sensitivity of 32.68 microscope units g^{-1} was determined.

4.7.2 Degassing of Liquid Adsorptives

The adsorptives (AnalaR grade) were distilled prior to loading in the reservoir soaked on a plug of glass wool (to prevent the glass reservoir from cracking upon liquid expansion). In order to remove dissolved gases, the adsorptives were exposed to three "freeze-pump-thaw" cycles. This process involved freezing the adsorptive by surrounding the reservoir with a dewar vessel containing liquid nitrogen. The adsorptive was then exposed to the pump and, when a stable vacuum of $< 1 \times 10^{-3}$ Pa was achieved, the tap was closed and the dewar vessel was removed to allow the adsorptive to return to room temperature. The procedure was then repeated.

4.7.3 Adsorbent Outgassing Procedure

Prior to adsorption it was necessary to remove any physisorbed vapour from the surface of the solid; this procedure is termed outgassing. The sample was heated in a tube furnace under vacuum to a constant pressure. Pressures of $< 1 \times 10^{-3}$ Pa were usually achieved. Typical outgassing times for M41S materials were 4-5 hours. It was important that the temperature chosen for this procedure did not cause any modification of the sample. Purely siliceous and aluminosilicate materials were outgassed at 150 °C, while organically-modified samples were outgassed at 100 °C to prevent the removal of incorporated organic functions.

4.7.4 Isotherm Measurement

Table 4.2 (above) shows the temperatures at which adsorption was carried out for each adsorptive. In each case, the thermostatted box was maintained at 303 K. Benzene sorption was carried out at 293 K due to the exceptionally high saturation vapour pressure (too high to read on the silicone oil manometer) of this solvent at

303 K. Also this made comparison with literature benzene isotherms, similarly carried out at 293 K, possible. To facilitate sorption at 293 K, water from a thermostatted tank was circulated through a dewar vessel surrounding the sample. The vapour pressure of the adsorptive was controlled by regulating the water temperature in a dewar vessel surrounding the reservoir.

Before adsorption commenced, the position of the blue reference marker, measured using the rack and pinion microscope was noted. Following degassing of the adsorbent and the adsorptive the line was evacuated to a pressure of $<1 \times 10^{-3}$ Pa. With tap 1 closed (Figure 4.2), tap 2 was opened and the vapour pressure of the adsorptive measured on the pressure transducer and silicone oil manometer. Tap 1 was then opened to expose the adsorbent to the vapour. Pressure readings and the position of the marker rod were noted at regular time intervals (10-15 min) until the system reached equilibrium; this was defined as the point at which no further decrease in pressure and no further spring extension were observed. Typically, equilibrium was reached in 0.5 - 3 h. Desorption points were obtained by exposing the sample to a reduced vapour pressure, obtained by opening the line to the pump.

Calculation of the amount adsorbed, n / mol, was achieved using equation 4.14:

$$n = \delta / \Delta M \qquad (4.14)$$

where δ is the spring extension, Δ is the sensitivity of the spring (32.68 mic. units g^{-1}) and M is the molar mass of the adsorptive.

Isotherms are presented as plots of relative pressure, p/p^0, against amount adsorbed (mol g^{-1}). The p^0 value for water was taken from the CRC Handbook of Chemistry and Physics[28], and p^0 values of all other adsorptives were measured using the pressure transducer and silicone oil manometer at the respective experimental temperatures. These are given in Table 4.3 below.

Table 4.3 The saturation vapour pressures of adsorptives at the experimental temperatures

Adsorptive	H_2O	C_6H_6	*n*-BuOH	*t*-BuOH
Temperature / K	303	293	303	303
Sat. Vapour Pressure, p^0 / kPa	4.24	10.21	1.68	7.73

REFERENCES

1. Gregg, S.J.; Sing K.S.W., *"Adsorption, Surface Area and Porosity"*, 2nd Edition, Academic Press, London, **1982.**
2. Kayser, H., *Wied. Ann.* **1881**, *14*, 451.
3. Brunauer, S.; Deming, L.S.; Deming, W.S.; Teller, E. *J. Amer. Chem. Soc.*, **1940**, *62*, 1723.
4. Brunauer, S.; Emmett, P.H.; Teller, E. *J. Amer. Chem. Soc.*, **1938**, *60*, 309.
5. Charles, K.E., *PhD 1st Year Report*, University of Exeter, **1995.**
6. Branton, P. J.; Hall, P.G.; Sing, K.S.W., *J. Chem. Soc., Chem. Commun.*, **1993**, 1257.
7. Emmett, P.H.; Brunauer, S., *J. Amer. Chem. Soc.*, **1937**, *59*, 1553.
8. Brunauer, S.; Emmett, P.H.; Teller, E. *J. Amer. Chem. Soc.*, **1938**, *60*, 309.
9. Langmuir, I., *J. Amer. Chem. Soc.*, **1916**, *39*, 2221.
10. Zsigmondy, A., *Z. Anorg. Chem.* **1911**, *71*, 356.
11. Thomson, W.T., *Phil. Mag.* **1871**, *42*, 448.
12. Gurvitsch, L., *J. Phys. Chem. Soc. Russ.*, **1915**, *47*, 805.
13. Culver, R.U.; Heath, N.S., *Trans. Faraday Soc.* **1955**, *51*, 1569.
14. Pierce, C.; Wiley, J.W.; Smith, R.N., *J. Phys. Chem.*, **1952**, *56*, 733.
15. Gregg, S.J.; Stock, R., *Trans. Faraday Soc.*, **1957**, *53*, 1355.
16. Broad, D.W.; Foster, A.G., *J. Chem. Soc.*, **1945**, 366.
17. Brown, M.A.; Foster, A.G., *J. Phys. Chem.*, **1952**, *56*, 733.
18. Dubinin, M.M.; Zaverina, E.D., *Zhur. Fiz. Khim.* **1949**, *23*, 1129. Dubinin, M.M., *Quart. Rev. Chem. Soc.* **1955**, *9*, 101.

19. Gregg, S.J.; Langford, J.F., *Trans. Faraday Soc.*, **1969**, *65*, 1394. Langford, J.F., PhD Thesis, Exeter University, **1967**.

20. Lippens, B.C.; De Boer, J.H., *J. Catalysis*, **1965**, *4*, 319.

21. Sing, K.S.W., in "*Surface Area Determination*", Proc. Int. Symp., 1969 (eds. Everett, D.H.; Ottewill, R.H.), p.25, Butterworths, London, **1970**.

22. Gregg, S.J.; Sing K.S.W., "*Adsorption, Surface Area and Porosity*", 2nd Edition, Ch. 5, Academic Press, London, **1982**.

23. Gregg, S.J.; Sing K.S.W., "*Adsorption, Surface Area and Porosity*", 2nd Edition, p.81, Academic Press, London, **1982**.

24. Isirikyan, A.A.; Kiselev, A.V., *J. Phys. Chem.*, **1961**, *65*, 601.

25. McClellan, A.L.; Harnsberger, H.F., *J. Colloid Interface Sci.*, **1967**, *23*, 577.

26. McBain J.W.; Bakr, A.M., *J. Am. Chem. Soc.* **1926**, *48*, 690.

27. Branton, P.J., *PhD Thesis*, University of Exeter, **1994**.

28. Linde, D.R. (ed. in chief), *CRC Handbook of Chemistry and Physics*, 73rd ed., CRC Press, **1992-1993**.

CHAPTER 5

GAS ADSORPTION RESULTS

The following chapter is divided into two parts. Part I considers the gas adsorption analysis of M41S-type materials, while Part II considers gas adsorption on organically-functionalized mesoporous silica. The BET plots used in the calculation of S_{sp} are given in Appendix A4.

PART I - M41S SOLIDS

5.1 Nitrogen Sorption

Nitrogen adsorption was carried out on all of the calcined samples using the Gemini apparatus. Sorption data are given in Table 5.1. (BET plots used in the calculation of S_{sp} are given in Appendix A4).

The isotherms, presented at the end of this section, were mostly Type IV[1] as expected, indicating mesoporosity. It is evident from Figures 5.1-5.7 that samples produced under pressure (i.e. in a sealed container) yield isotherms with a more well-defined capillary condensation step than those samples produced in open vessels. This suggests that the samples produced under pressure have a narrower pore size distribution (i.e. a more uniform pore structure) than those produced at atmospheric pressure.

Table 5.1 N_2 sorption data for M41S samples

Sample		BET surface area, S_{sp} / m^2 g^{-1}	Gurvitsch pore volume, V_p / cm^3 g^{-1}	Average pore diameter* / Å
MCM-41(a)	i	729	0.57	31.7 *(0.38)*
MCM-41(b)	ii	737	0.32	-
MCM-41(c)	i	794	0.59	31.2 *(0.37)*
MCM-41(d)	ii	511	0.26	24.3 *(0.25)*
FeMCM-41	i	833	0.44	26.6 *(0.29)*
SiMCM-41(a)	iii	936	0.45	24.0 *(0.24)*
SiMCM-41(b)	i	828	0.56	26.3 *(0.29)*

(i) prepared in sealed vessel in conventional oven, (ii) prepared in microwave oven, (iii) stirred at room temperature in an open vessel.
* Figures in brackets are the p/p^0 values at which the Kelvin equation was applied.

As mentioned in Chapter 4, a distinctive feature of M41S-type solids is the absence of hysteresis in the Type IV isotherms i.e. the isotherms are reversible.[2] The reason for this absence of hysteresis in M41S solids is not well understood, but it is thought to be due to the position of the capillary condensation step ($p/p^0 \approx 0.4$). Under the reaction conditions it seems that this is the lowest p/p^0 at which nitrogen can undergo the classical form of capillary condensation. This value of p/p^0 represents a region of instability in the nitrogen meniscus and if M41S materials of different pore sizes were to be analyzed, or the temperature of the isotherms altered, hysteresis would be observed.

The BET analysis was carried out on each isotherm in the range $0.04 \geq p/p^0 \geq 0.31$ (as pre-set by the Gemini apparatus). Specific surface areas of between approximately 500 and 1000 $m^2 g^{-1}$ were obtained, typical of MCM-41-type materials. Average pore diameters of between 24 and 32 Å (obtained by applying the Kelvin equation[3]) confirmed that the samples were indeed mesoporous. The Kelvin equation could not be applied to the isotherm obtained for sample MCM-41(b) as it did not show a well-defined capillary condensation step.

Gurvitsch pore volumes[4], V_p, were calculated from each isotherm. It can be noted from Table 5.1 that the pore volumes of samples prepared in a sealed vessel in a conventional oven are greater than those obtained for samples prepared in an open vessel. These results indicate that, in order to produce M41S-type materials with characteristics desirable for selective catalysis (e.g. uniform pore structure, high surface area, large pore volume) synthesis under pressure is the method of choice.

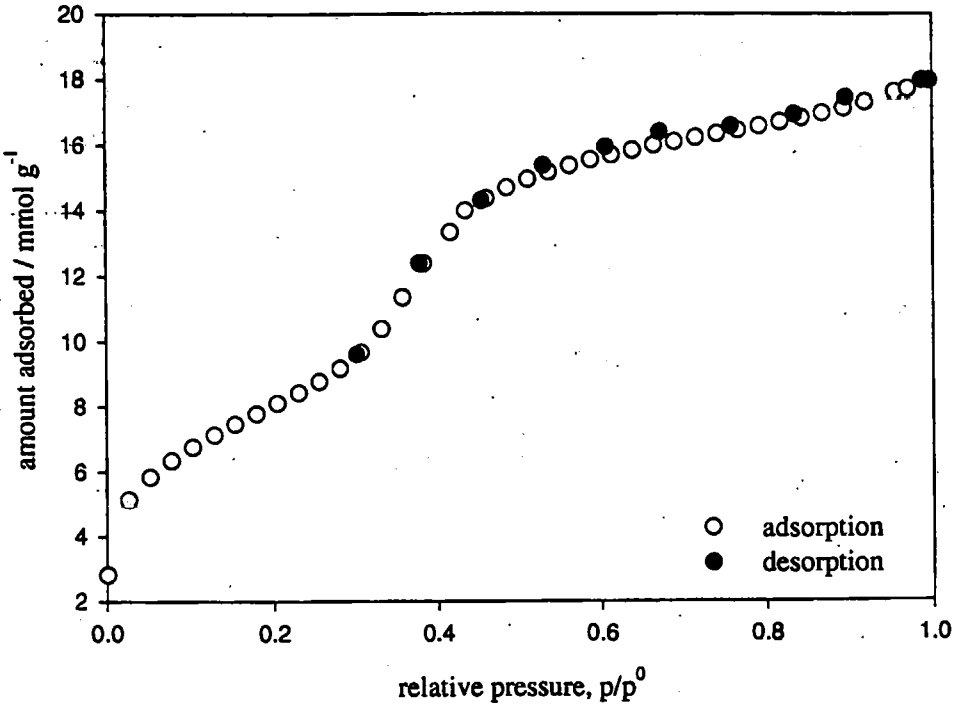

Figure 5.1 Nitrogen sorption at 77 K on calcined MCM-41(a).

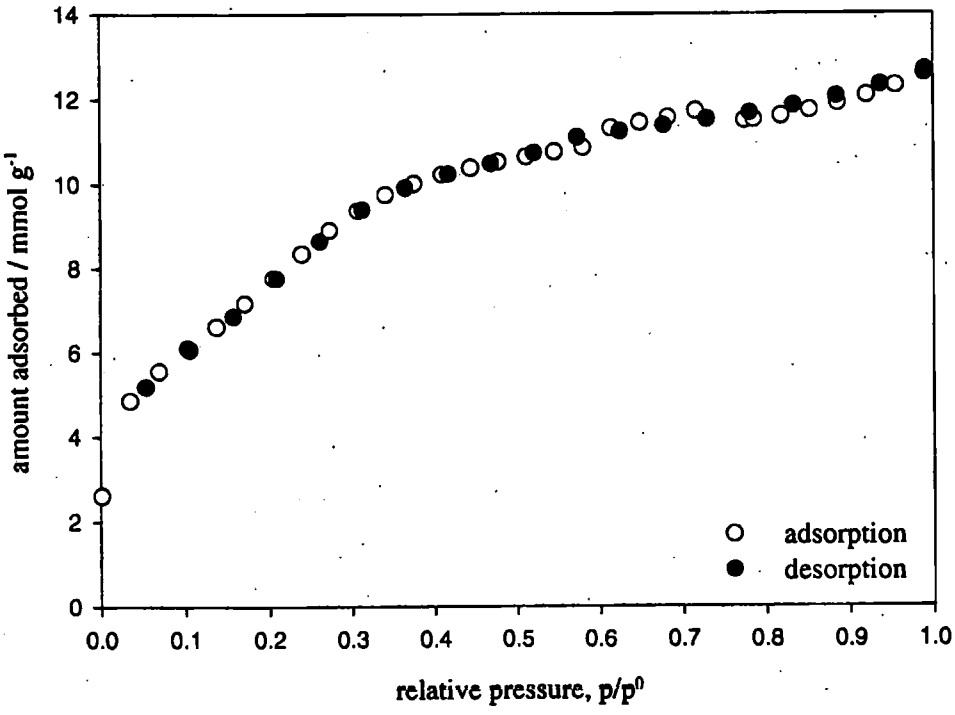

Figure 5.2 Nitrogen sorption at 77 K on calcined MCM-41(b)

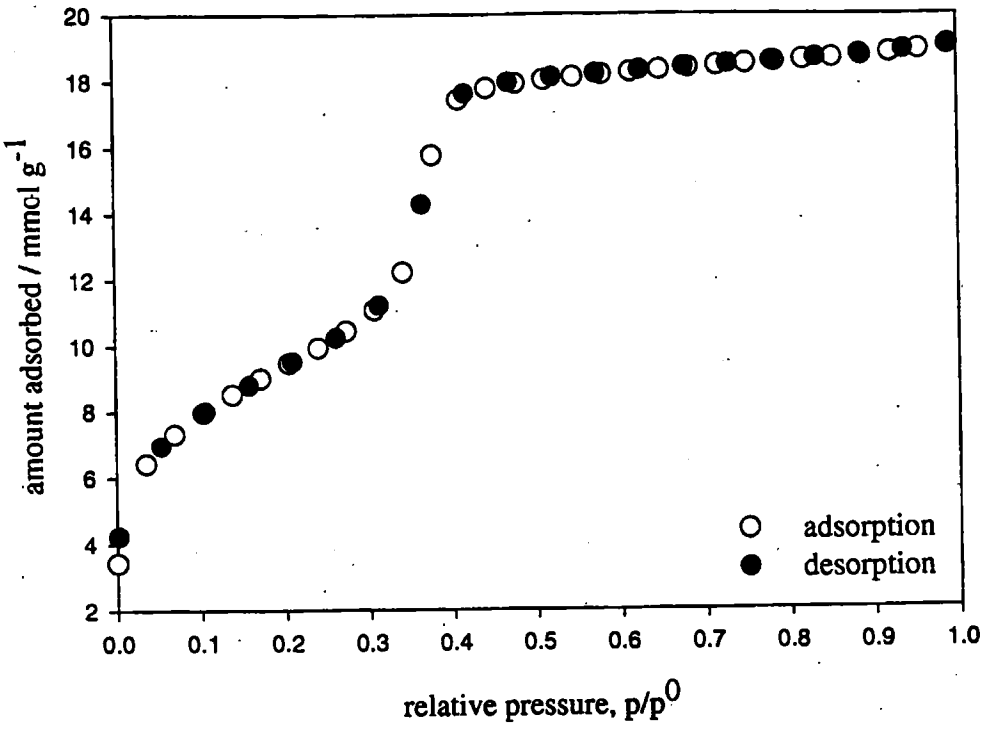

Figure 5.3 Nitrogen sorption at 77 K on calcined MCM-41(c).

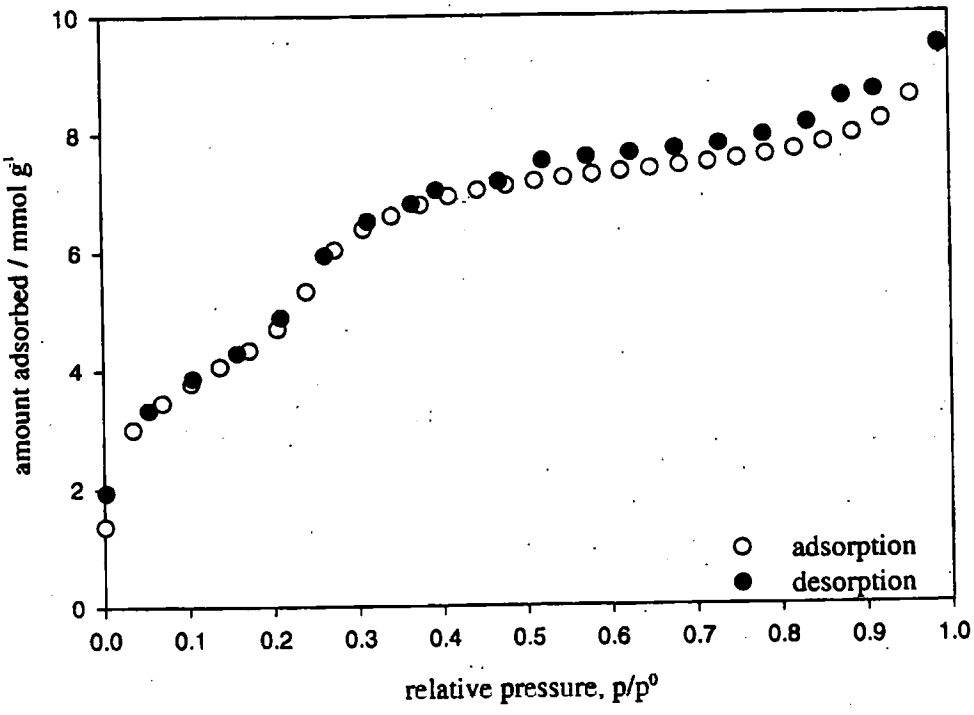

Figure 5.4 Nitrogen sorption at 77 K on calcined MCM-41(d).

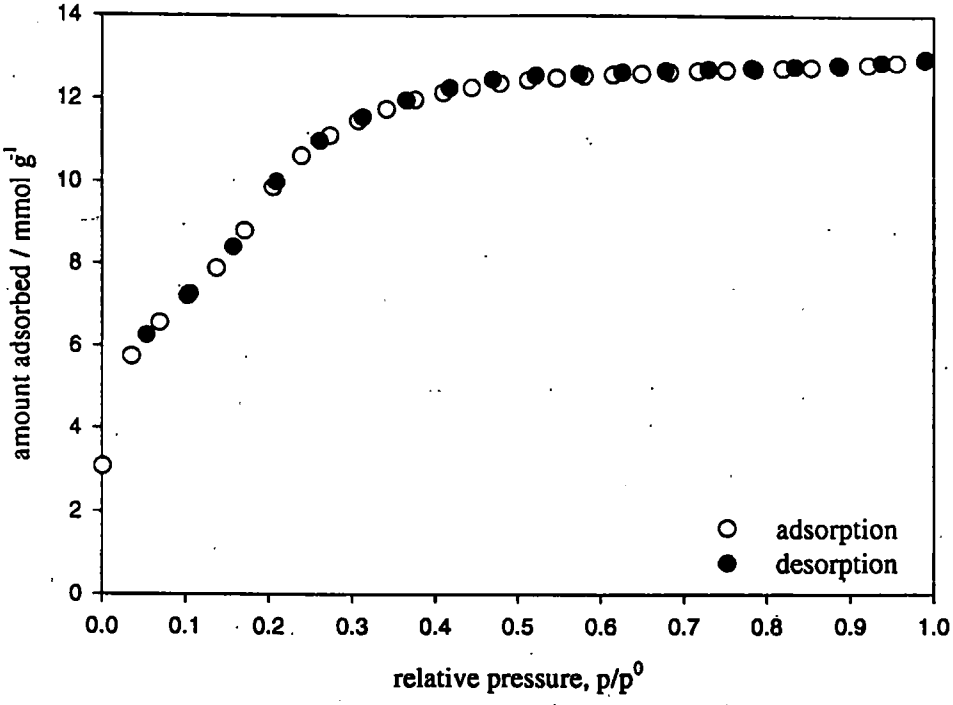

Figure 5.5 Nitrogen sorption at 77 K on calcined SiMCM-41(a).

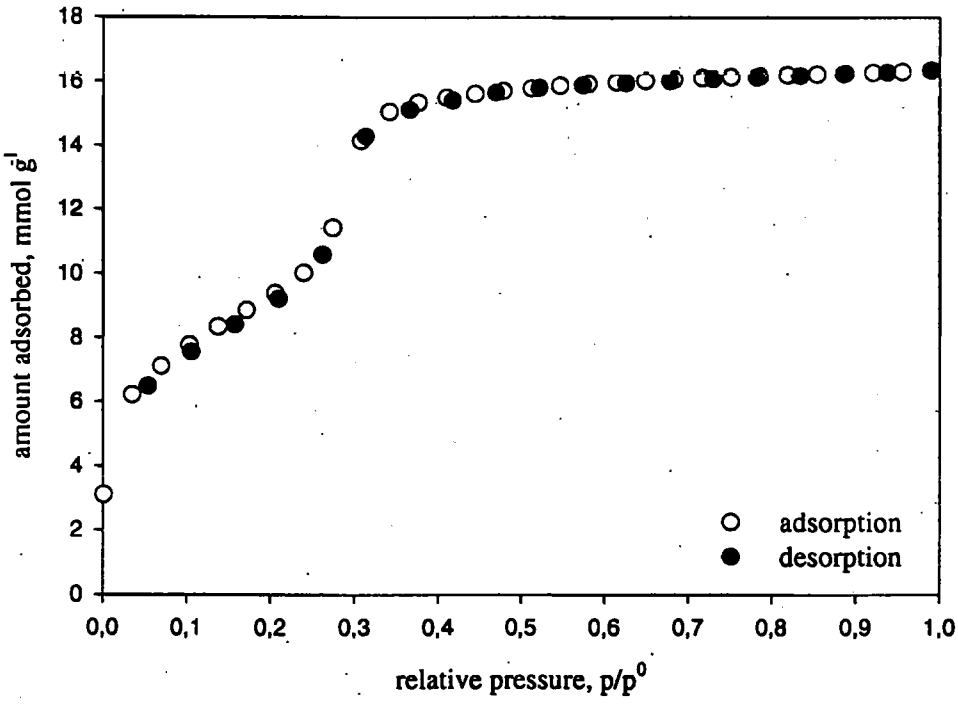

Figure 5.6 Nitrogen sorption at 77 K on calcined SiMCM-41(b).

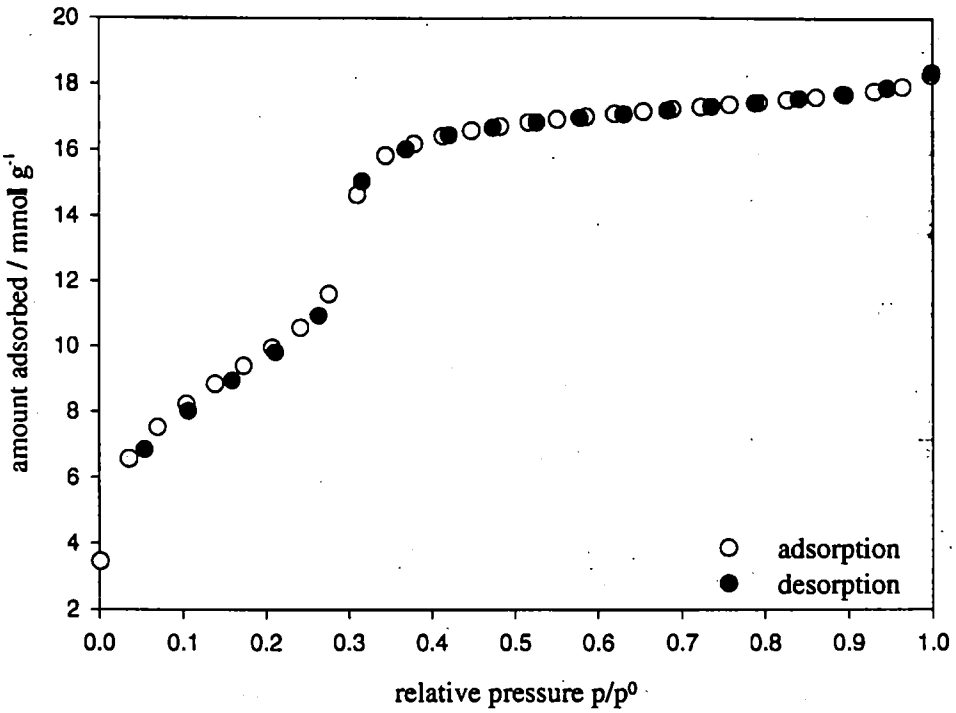

Figure 5.7 Nitrogen sorption at 77 K on calcined FeMCM-41.

5.1.1 Calculation of Pore Wall Thickness

It is possible to calculate the average pore wall thickness of a sample by subtracting the average pore diameter, obtained from the N_2 isotherm, from the unit cell dimension, *a*, obtained from XRD data. The results obtained for these samples are tabulated below (Table 5.2).

Table 5.2 Average pore wall thickness of M41S-type solids

Sample	Reaction Time & Temperature	Average Pore Diameter / Å	Unit cell, *a* / Å	Average Wall Thickness / Å
MCM-41(a)	100 °C, 23 h	31.7	39	7.3
MCM-41(b)	micro., 20 min	-	-	-
MCM-41(c)	100 °C, 72 h	31.2	45	13.8
MCM-41(d)	micro., 20 min	24.3	40	15.7
FeMCM-41	100 °C, 120 h	26.6	43	16.4
SiMCM-41(a)	ambient temperature, 1 h	24.0	37	13.0
SiMCM-41(b)	100 °C, 24 h	26.3	43	16.7

Table 5.2 highlights that samples synthesized *via* the hydrolysis and condensation of TEOS have thicker walls than those produced using TMAS and precipitated silica as the silica source. Also, the samples prepared at high temperature and under pressure have thicker walls than the sample prepared at room temperature and pressure.

5.2 Oxygen Sorption

Oxygen sorption was carried out at 77 K on sample SiMCM-41(b) (Figure 5.8).

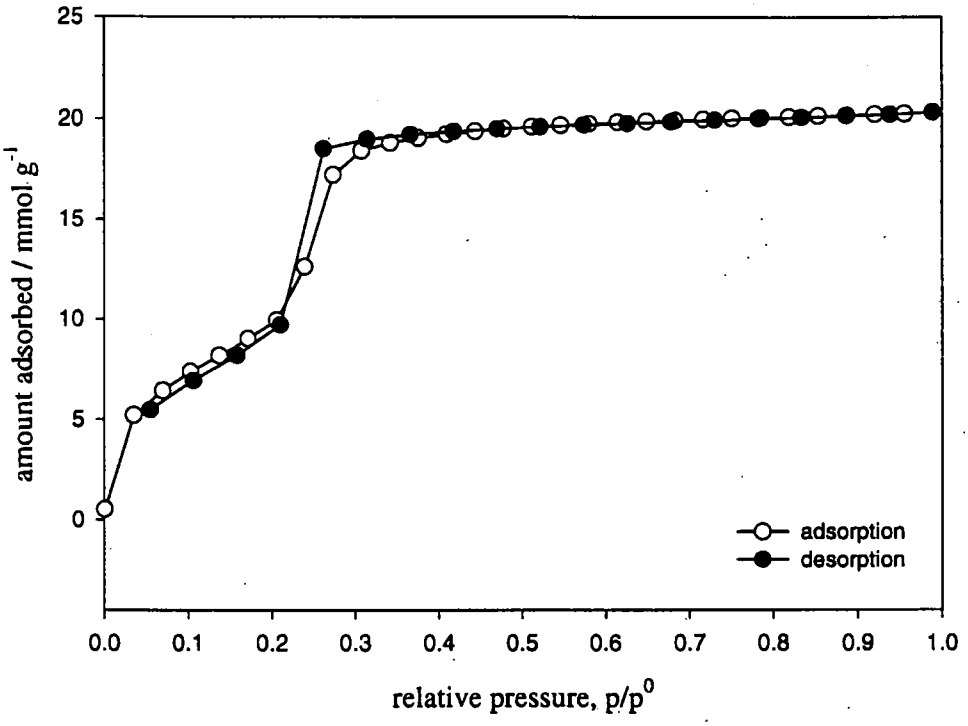

Figure 5.8 Oxygen sorption at 77 K on calcined SiMCM-41(b)

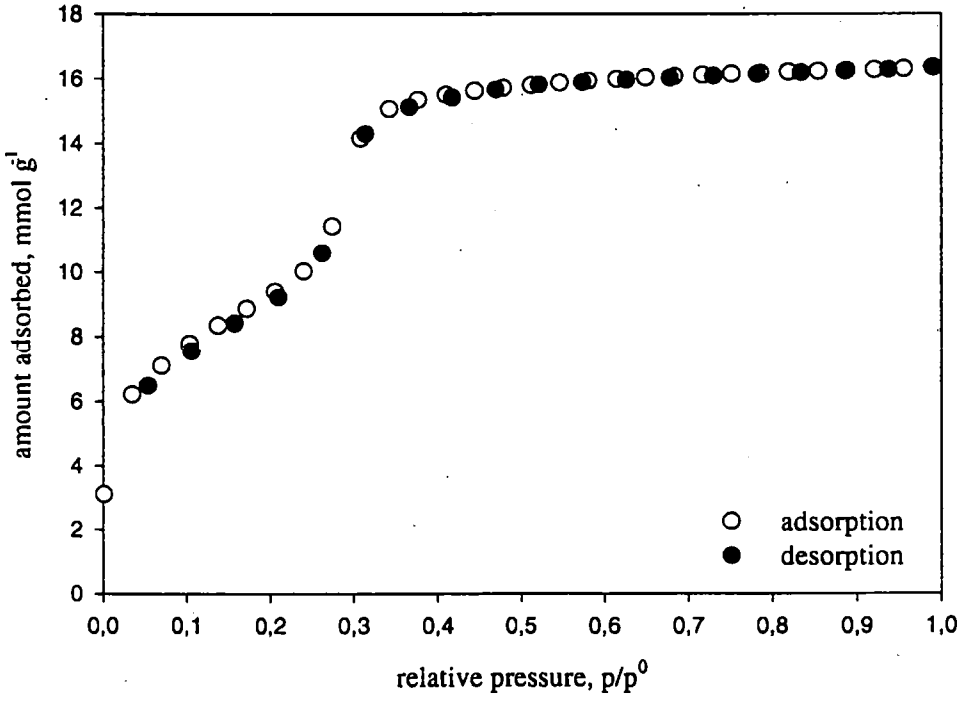

Figure 5.9 Nitrogen sorption at 77 K on calcined SiMCM-41(b).

The nitrogen sorption isotherm, carried out on the same sample at 77 K is shown for comparison purposes in Figure 5.9. Both isotherms are Type IV confirming that the sample is mesoporous. The major difference between the two isotherms that can be observed is the presence of a hysteresis loop in the oxygen isotherm. This is absent in the nitrogen isotherm as would be expected for an MCM-41-type material. This confirms that the absence of hysteresis in the nitrogen isotherm is a characteristic of the adsorbate rather than the adsorbent (see Section 5.1).

The pore volume, V_p, and BET specific surface area, S_{sp}, calculated from each isotherm, are compared in Table 5.3, below.

Table 5.3 Sorption data for O_2 and N_2 sorption on SiMCM-41(b).

	O_2 Sorption	**N_2 Sorption**
V_p / cm^3 g^{-1}	0.56 *	0.56
S_{sp} / m^2 g^{-1}	737	828

* Calculated using $\rho(O_2) = 1.184$ g cm^{-3}

As shown in Table 5.3, the pore volumes calculated from each isotherm are identical (V_p = 0.56 cm^3 g^{-1}) showing good agreement with the Gurvitsch rule. This proves that nitrogen and oxygen are adsorbed in a similar manner in this material. The specific surface areas obtained are slightly different, but this difference may be attributed to the assumptions made when applying a BET calculation (see Section 4.2.1). The BET plot used in the calculation of Ssp is given in Appendix A4.

5.3 Water sorption

Water sorption on calcined MCM-41(c) was studied using the gravimetric apparatus. A Type V isotherm was produced (Figure 5.10), indicating mesoporosity with weak adsorbate-adsorbent interactions. This is characteristic of a hydrophobic surface and suggests that there are few surface hydroxyl groups present. The initial low affinity of this sample for water vapour is highlighted by the long plateau at the start of the isotherm. Condensation occurs normally, however, around $p/p^0 = 0.6$. An interesting feature of this isotherm is that the desorption branch of the hysteresis loop does not close. This suggests rehydroxylation of the surface. Indeed, after heating under vacuum at 150°C for 4 h, water still remained on the surface and the isotherm could not be reproduced (condensation occurred upon readsorption). This is in contrast to the work carried out by Branton[5] on MCM-41 that showed the water isotherm to be reversible in the pre-hysteresis region thus suggesting that chemisorption did not occur.

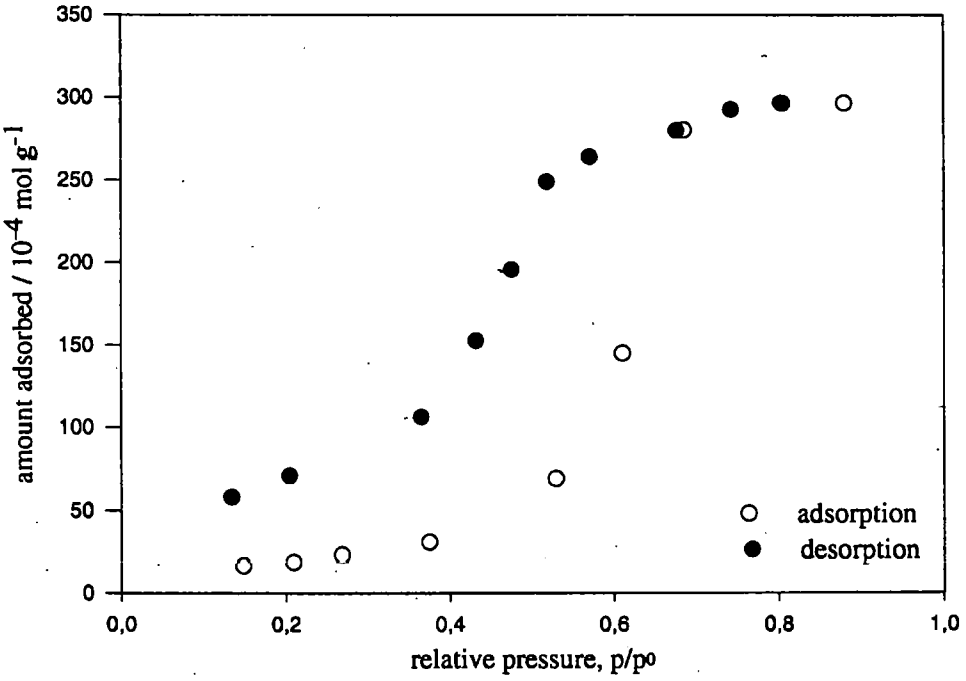

Figure 5.10 Water sorption at 303 K on calcined MCM-41(c).

This difference may be attributed to the differences in sample preparation. The Branton samples were prepared at high temperature in a static autoclave[6], while sample MCM-41(c) was prepared in a sealed teflon bottle at 100 °C in a conventional oven. It is possible that, in sample MCM-41(c), complete condensation of all of the siloxane groups has not occured producing a sample less stable than one prepared in an autoclave. The dehydroxylation of a silica surface is shown diagramatically in Figure 5.11. Chuang and Maciel[7] suggest that when two adjacent silanol groups condense at temperatures greater than 500 °C a strained 4-member Si-O ring is formed. This is highly reactive and therefore can easily undergo rehydroxylation when exposed to water vapour. If sample MCM-41(c) did not undergo complete siloxane condensation, then it is more likely that there will be adjacent SiOH and SiOEt groups present which, in turn, will make the sample more likely to undergo rehydroxylation upon water sorption.

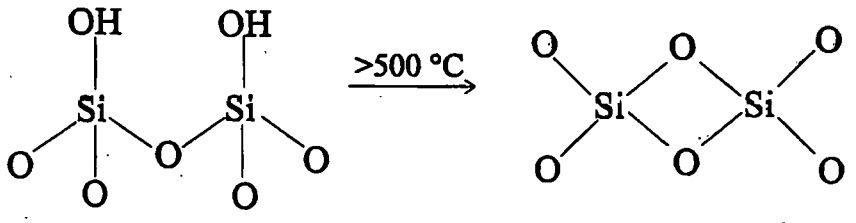

Figure 5.11 Diagram showing the formation of a strained 4-membered Si-O ring upon the dehydroxylation of a silica surface.

If rehydroxylation of a silica surface is the cause of low pressure hysteresis, an increase in the number of surface hydroxyl groups should be observed. Sample MCM-41(c) was therefore studied using ^{29}Si MAS-NMR both before and after water sorption. The results, given in Section 3.5.1, confirmed that rehydroxylation of the sample did occur upon water sorption at 303 K.

PART II - ORGANICALLY-FUNCTIONALIZED MESOPOROUS SILICA

The following Table (5.4) summarises the gas adsorption studies carried out on the organically-functionalized mesoporous silicas.

Table 5.4 The adsorptives used on each sample

Sample	N_2 (77 K)	H_2O (303 K)	C_6H_6 (293 K)	n-BuOH (303 K)	t-BuOH (303 K)
Phenyl (Burkett)	✓	✓	✓	✓	✓
Phenyl (Unswollen)	✓				
Phenyl (Mesitylene)	✓		✓	✓	✓
Phenyl (Tetradecane)	✓				
Vinyl	✓				
Amino-propyl	✓				
Mercapto-propyl	✓				

The sorption of each adsorptive is now discussed in turn.

5.4 Nitrogen Sorption

Nitrogen sorption data yield the values given in Table 5.5. The results obtained for each sample are discussed separately below.

Table 5.5 Nitrogen sorption data for organically-functionalized mesoporous silica

Sample	Isotherm Type	BET Surface Area, S_{sp} / m^2 g^{-1}	Langmuir Surface Area, S_L / m^2 g^{-1}	Gurvitsch Pore Volume, V_p / cm^3 g^{-1}
Phenyl (Burkett)	I	882	1258	0.45
Phenyl (Unswollen)	I	990	1424	0.50
Phenyl (Mesitylene)	IV	942	-	0.67
Phenyl (Tetradecane)	I	760	1138	0.42
Vinyl	I & IV	1339	-	0.76
Aminopropyl	I	299	415	0.15
Mercaptopropyl	I	522	761	0.27

Langmuir surface area calculations were performed for each sample that gave an isotherm displaying Type I characteristics. In each case, a relatively high surface area was obtained. For comparison purposes, the BET specific surface areas have been used

in this study and any reference to the specific surface area of a sample is referring to the value calculated using the BET model, unless otherwise stated.

5.4.1 Phenyl-Modified Samples

(i) PhMCM-41 (Burkett Sample)

Nitrogen sorption studies on the Burkett (unswollen)[8] material yielded an isotherm displaying mainly Type I characteristics confirming its microporosity (Figure 5.12). The pores are almost completely filled at a relative pressure $p/p^0 \approx 0.2$.

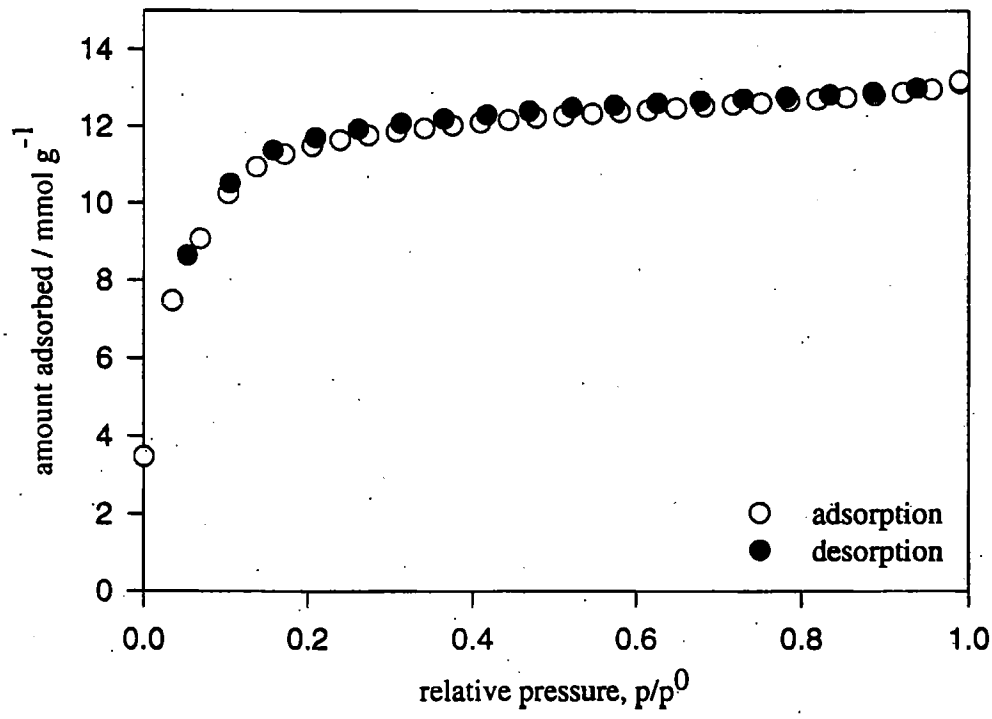

Figure 5.12 Nitrogen sorption at 77 K on PhMCM-41

As mentioned in Chapter 4 (Section 4.3), a number of arguments suggest that it is inappropriate to apply the Brunauer-Emmett-Teller (BET) equation to Type I isotherms as the "knee" observed is thought to represent pore filling rather than

monolayer coverage. However, if a BET calculation is performed on this isotherm over the range $p/p^0 = 0.04 - 0.31$, a surface area of 882 $m^2 g^{-1}$ is obtained, consistent with other large pore unmodified M41S-type solids. If we assume that the plateau of the isotherm represents complete pore filling, the isotherm yields a Gurvitsch pore volume, $V_p = 0.45$ $cm^3 g^{-1}$. If the sample is assumed to have 20 Å diameter cylindrical pores (from preliminary nitrogen sorption and XRD data) and the specific surface area of 882 $m^2 g^{-1}$ corresponds to the internal surface area of the pores, then a theoretical total pore volume of 0.44 $cm^3 g^{-1}$ is obtained, in good agreement with the experimental value. This confirms that the plateau of the isotherm does indeed correspond to complete filling of the pores. The fact that a reasonable BET surface area is obtained from the lower region of the isotherm may possibly be explained by the fact that the isotherm shape does not exactly mirror that of a Type I isotherm. The initial uptake at low relative pressures is not as steep as would be expected in a classical Type I case. Also, following the "knee" at $p/p^0 \approx 0.2$, the isotherm is not completely flat as would be expected if this represented total pore filling; it continues to slope gently upwards until saturation pressure. The reason for this deviation may be that the sample contains pores at the limit of the microporous range (i.e. pore diameter ≈ 20 Å).

(ii) Phenyl-Modified Mesoporous Silicas

Unswollen Phenyl-Modified Silica

The unswollen phenyl-modified mesoporous silica yields an isotherm (Fig. 5.13), displaying Type I characteristics, very similar to that given by the Burkett unswollen sample and a BET specific surface area $S_{sp} = 990$ $m^2 g^{-1}$ and a Gurvitsch pore volume,

V_p = 0.50 cm^3 g^{-1}. These values, particularly V_p, are very similar to those obtained for the Burkett sample (*cf.* 882 m^2 g^{-1} and 0.45 cm^3 g^{-1}) which is not surprising as the preparation methods of these two materials were identical. (This sample was prepared merely as a control sample for the synthesis of other mesoporous organically-modified samples).

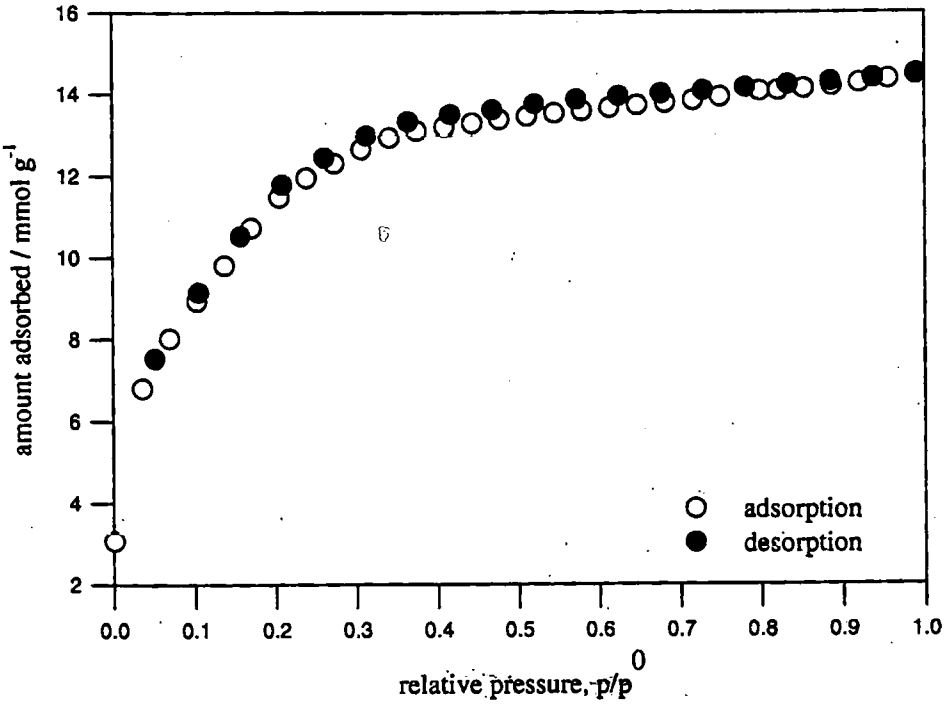

Figure 5.13 Nitrogen sorption at 77 K on unswollen phenyl-modified silica..

Mesitylene-Swollen Phenyl-Modified Silica

The Type IV isotherm (Figure 5.14) given by the mesitylene-swollen phenyl-modified sample displays a small degree of hysteresis and indicates that the sample is mesoporous. A BET specific surface, S_{sp} = 942 m^2 g^{-1} is consistent with M41S-type materials and the Gurvitsch pore volume, V_p = 0.67 cm^3 g^{-1} is larger than that obtained

for the unswollen material (0.50 cm^3 g^{-1}). This demonstrates that mesitylene is an effective pore-swelling agent in the synthesis of these materials.

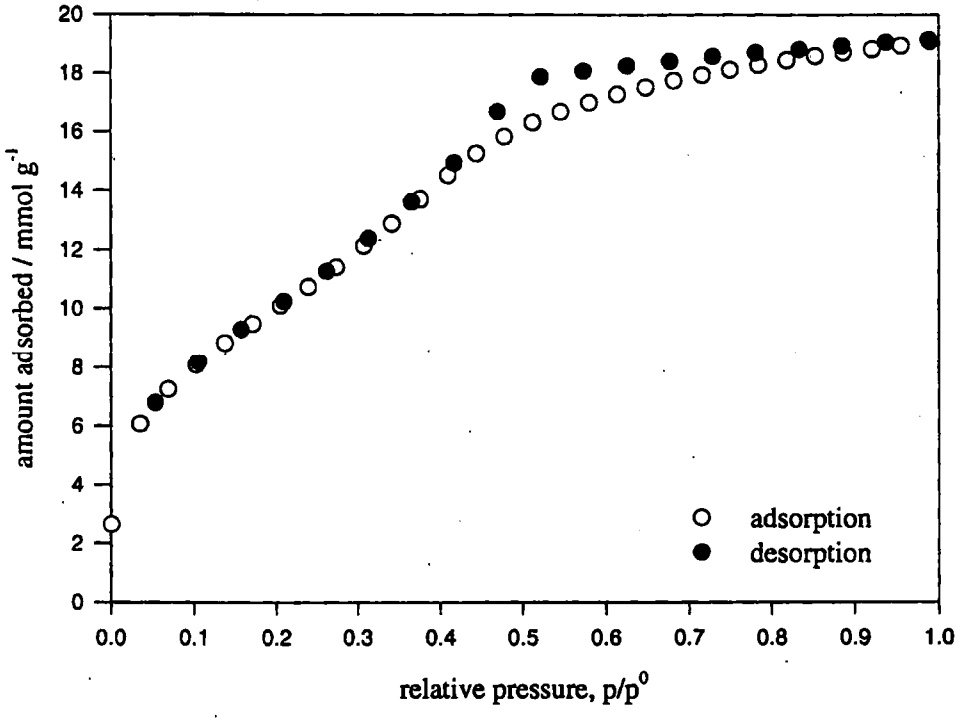

Figure 5.14 Nitrogen sorption at 77 K on MES-swollen phenyl-modified mesoporous silica.

Tetradecane-Swollen Phenyl-Modified Silica

The tetradecane-swollen phenyl-modified sample yields an isotherm similar to that obtained for the unswollen material, exhibiting Type I characteristics but displaying a small amount of hysteresis (Figure 5.15). This again indicates that the sample is microporous. The BET surface area, S_{sp} = 760 m^2 g^{-1} is consistent with M41S-type materials and the Gurvitsch pore volume, V_p = 0.42 cm^3 g^{-1} is similar to that of the unswollen material.

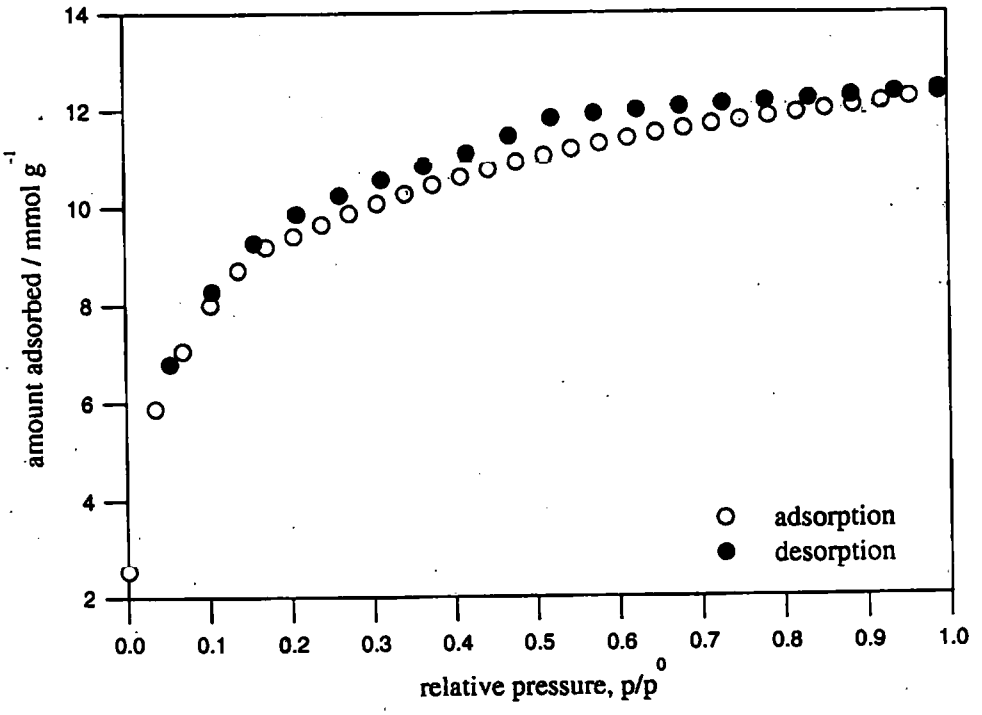

Figure 5.15 Nitrogen sorption at 77 K on TET-swollen phenyl-modified silica..

The Type I isotherm and lower Gurvitsch pore volume for the tetradecane-swollen material suggest that this alkane is not a suitable pore swelling agent for the synthesis of these materials. This could possibly be due to the fact that the tetradecane molecules overlap with the CTMACl molecules when the template is formed. It may be that the scenario shown in Figure 1.3, whereby n-alkane molecules position themselves at the end of the surfactant carbon chains,[9] cannot be supported when using an alkane molecule as large as tetradecane.

5.4.2 Vinyl-Modified Mesoporous Silica

Nitrogen sorption on MES-swollen vinyl-modified mesoporous silica yields an isotherm which, upon initial examination, exhibits both Type I and Type IV characteristics (Figure 5.16) .

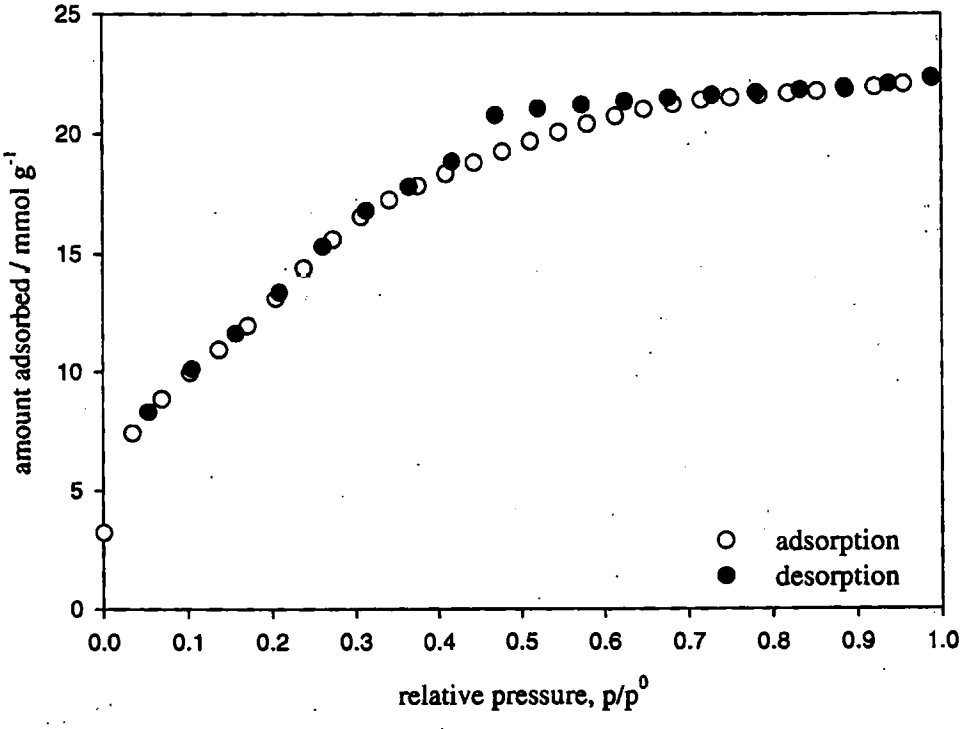

Figure 5.16 Nitrogen sorption at 77 K on MES-swollen vinyl-modified mesoporous silica

After an initial period of large uptake at low relative pressures, the isotherm slopes gently before reaching a plateau at $p/p^0 \approx 0.6$. A very large BET surface area (which suggests that the isotherm is more likely to be a Type I) and Gurvitsch pore volume ($S_{sp} = 1339\ m^2\ g^{-1}$, $V_p = 0.76\ cm^3\ g^{-1}$) are obtained, consistent with M41S-type materials. The shape of the isotherm and the high S_{sp} indicates that the sample contains a large volume of micropores; either the mesitylene did not successfully increase the pore diameter in this case or the vinyl function is arranged in such a manner as to reduce the pore diameter.

5.4.3 Aminopropyl-Modified Mesoporous Silica

A Type I isotherm (Figure 5.17) is given by nitrogen sorption on the aminopropyl-modified mesoporous silica.

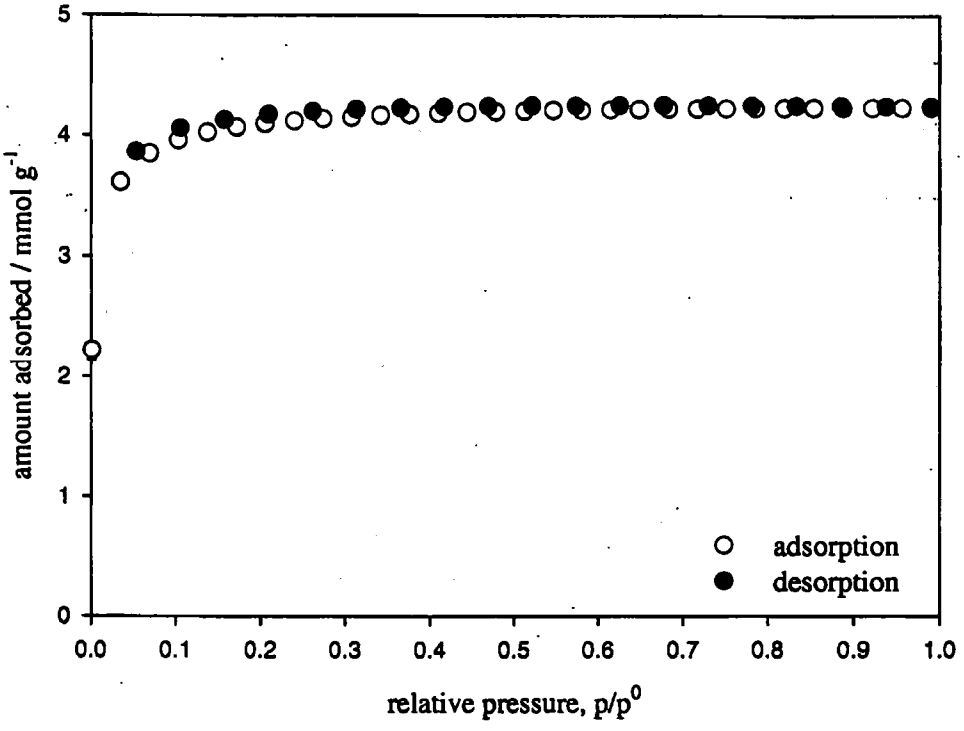

Figure 5.17 Nitrogen sorption at 77 K on aminopropyl-modified mesoporous silica.

The isotherm plateaus at a very low relative pressure ($p/p^0 \approx 0.1$) and the total uptake is relatively low for an M41S-type material (4.23mmol g^{-1}). The shape of the isotherm (e.g. the very steep initial portion) suggests that the total uptake at saturation pressure is likely to represent total pore filling. This translates to a Gurvitsch pore volume, V_p = 0.15 cm^3 g^{-1}, considerably lower than typical M41S-associated pore volumes. If, for reason of comparison, the BET equation is applied to this material, a specific surface area, S_{sp} = 299 m^2 g^{-1} is obtained. This value is, again, considerably lower than those commonly obtained for M41S-type materials and supports the XRD result which indicated that the sample's pores collapsed following template removal.

5.4.4 Mercaptopropyl-Modified Mesoporous Silica

The mercaptopropyl-modified sample also yields an isotherm (Figure 5.18) upon nitrogen sorption that resembles Type I. In this case, the isotherm plateaus at a higher relative pressure ($p/p^0 \approx 0.3$) and a higher total uptake (7.79 $cm^3\ g^{-1}$) than the aminopropyl-modified sample. However, the BET surface area and Gurvitsch pore volume (S_{sp} = 522 $m^2\ g^{-1}$, V_p = 0.27 $cm^3\ g^{-1}$) are still considerably less than those normally observed for M41S-type materials, again suggesting that the mesitylene was ineffective or that the organic function restricts access to the pores.

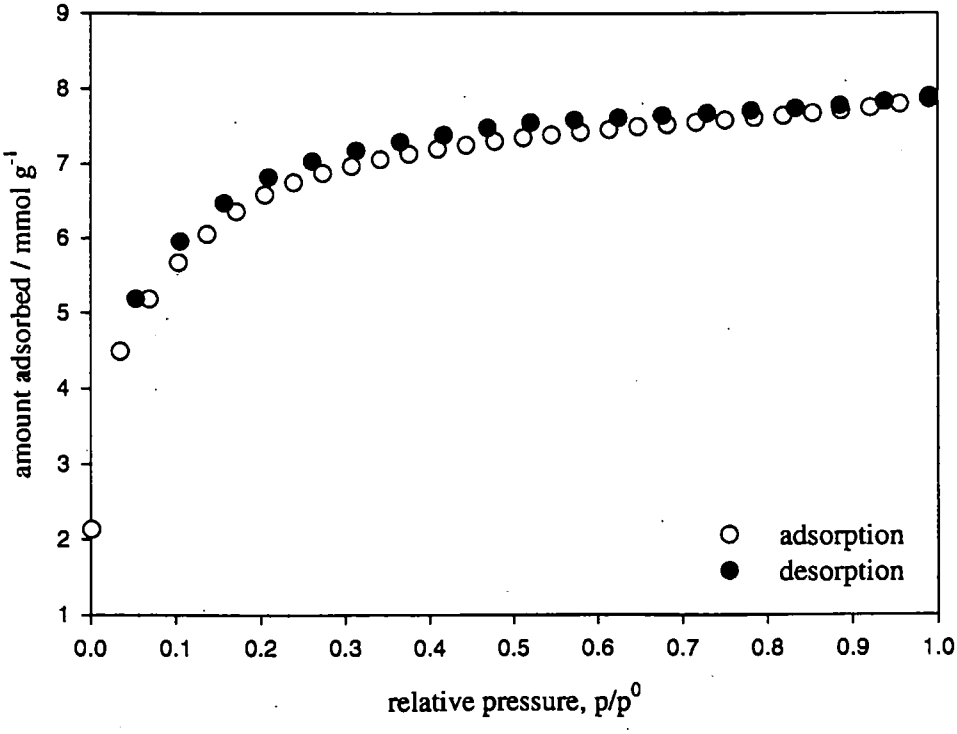

Figure 5.18 Nitrogen sorption at 77 K on mercaptopropyl-modified mesoporous silica.

5.5 Sorption of Water, Benzene and Butanol

The sorption (using the gravimetric apparatus) of water vapour, benzene, *n*-butanol and *t*-butanol was carried out on the Burkett PhMCM-41 sample (from Bath)[8] and the MES-swollen phenyl-modified mesoporous silica (Ph-M.S.). A summary of results is given in Table 5.6, below. Nitrogen sorption data are included for comparison purposes.

Table 5.6 Summary of water, benzene and butanol sorption data.

		PhMCM-41 (Burkett)*		MES-swollen Ph-M.S.	
H_2O	n_m / mmol g^{-1}	1.32		-	
	S_{sp} / m^2 g^{-1}	83		-	
	V_p / cm^3 g^{-1}	0.33		-	
	a_m / Å^2 a_c / Å^2	10.5	110	-	
C_6H_6	n_m / mmol g^{-1}	3.00 *(4.7)* †		4.06	
	S_{sp} / m^2 g^{-1}	750 ± 50 *(1217)*		1050 ± 50	
	V_p / cm^3 g^{-1}	0.31		0.76	
	a_m / Å^2 a_c / Å^2	43 ± 3	49 *(31)*	43 ± 3	39
n-BuOH	n_m / mmol g^{-1}	0.55		1.98	
	S_{sp} / m^2 g^{-1}	103		461	
	V_p / cm^3 g^{-1}	0.23		0.62	
	a_m / Å^2 a_c / Å^2	31	284	31	79
t-BuOH	n_m / mmol g^{-1}	2.12 *(3.70)* †		2.47	
	S_{sp} / m^2 g^{-1}	644 *(742)*		497	
	V_p / cm^3 g^{-1}	0.33		0.61	
	a_m / Å^2 a_c / Å^2	33	45 *(39)*	33	63
N_2	n_m / mmol g^{-1}	9.04		9.66	
	S_{sp} / m^2 g^{-1}	882		942	
	V_p / cm^3 g^{-1}	0.45		0.67	
	a_m / Å^2	16.2		16.2	

* Figures in brackets are calculated using the Langmuir equation.

† These values are calculated from Type I isotherms and are therefore more likely to be the micropore volume rather than the monolayer capacity.

a_m - molecular area of adsorbate used to calculate surface area; a_c - molecular area of adsorbate calculated from isotherm and $a_m(N_2)$ = 16.2 Å^2.

5.6 Water Sorption on Sample PhMCM-41 (Burkett)

Water sorption yielded a Type V isotherm (Figure 5.19) which is indicative of weak adsorbate-adsorbent interactions.[1]

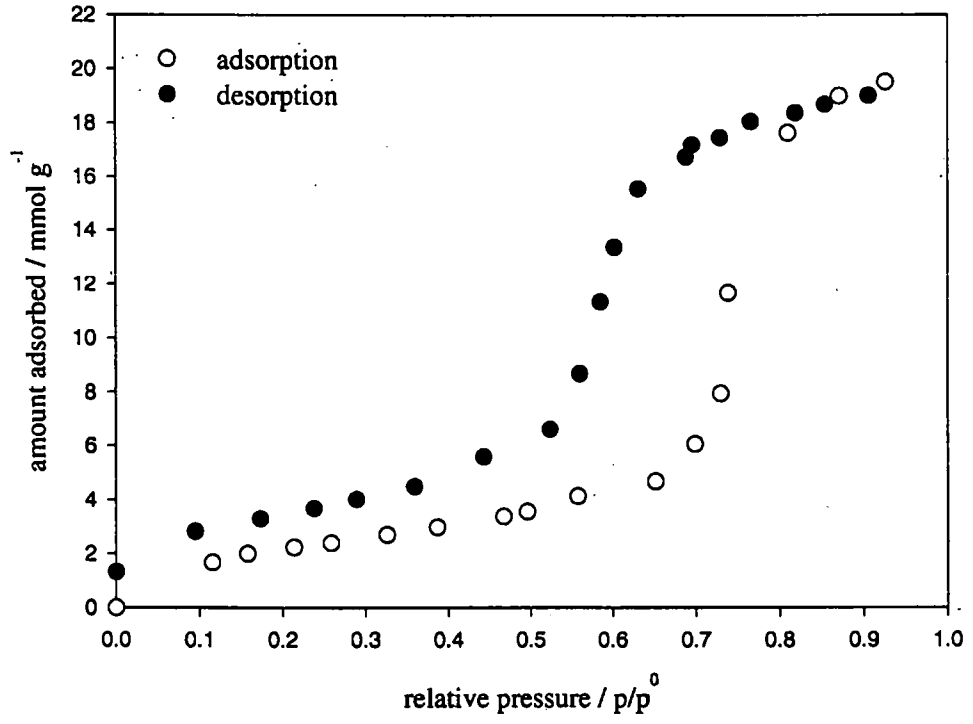

Figure 5.19 Water sorption at 303 K on PhMCM-41

The low uptake of water in the low pressure section of the isotherm is indicative of the hydrophobicity of this material at low relative pressures and suggests that there are few surface hydroxyl groups present. A region of slight curvature is observed at relative pressures of less than 0.1 and, if this is assumed to represent the point at which each surface hydroxyl group is occupied by a single water molecule, it is possible to obtain a value for the number of hydroxyl groups present per nm^2 of surface. If the amount of water adsorbed at this point is taken from the water isotherm, to be 1.32 mmol g^{-1} and the specific surface area of the sample is known, from N_2 sorption, to be

$882 m^2 g^{-1}$ then a value of 0.9 OH groups per nm^2 is obtained (using $a_m(H_2O)$ = 10.5 $Å^2$). This value is lower than that calculated from the water isotherm obtained by Llewellyn *et al*[10] on an unmodified MCM-41 (1.3 nm^{-2}), and can be attributed to the fact that phenyl groups occupy surface positions in this sample that would ordinarily be occupied by hydroxyl groups. The second region of the isotherm commences at $p/p^0 \approx$ 0.7 and represents condensation. At the top of this condensation step an uptake volume of 0.33 $cm^2 g^{-1}$ is observed. This value is lower than that obtained from the nitrogen isotherm (0.45 $cm^3 g^{-1}$), but is very close to that obtained from the benzene isotherm (0.31 $cm^3 g^{-1}$, see section 5.5). This may be a result of either water condensation occurring within the pores without complete pore filling or it may be due to the structure of the adsorbed water. Failure of water to obey the Gurvitsch rule is not uncommon, and Gregg and Sing suggest that adsorbed water may exist within pores in a form substantially less dense than ordinary water as a result of differences in hydrogen-bonding arrangements.[11]

Hysteresis extending to the low pressure region was observed in the water isotherm. This is caused by rehydroxylation of the silica surface during the course of isotherm determination. Prolonged exposure to pressures of $<1x10^{-2}$ Pa at experimental temperature did not result in loop closure. As mentioned in Section 5.2 this is probably due to incomplete condensation of siloxane groups during the short, room-temperature synthesis resulting in a sample prone to rehydroxylation upon contact with water vapour.

5.7 Benzene Sorption

5.7.1 PhMCM-41 (Burkett Sample)

Benzene sorption on the Burkett sample yielded an isotherm displaying Type I characteristics (Figure 5.20) exhibiting a very small degree of hysteresis.

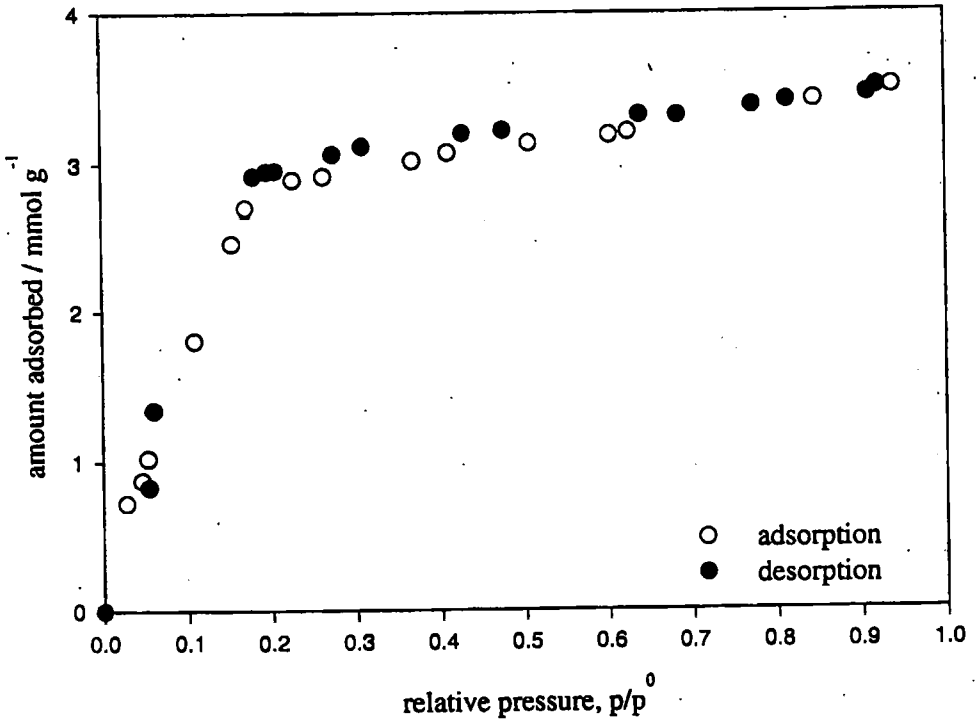

Figure 5.20 Benzene sorption at 293 K on PhMCM-41

A BET specific surface area S_{sp} = 750 m^2 g^{-1} ± 50 m^2 g^{-1}‡ was obtained. Problems arise in the calculation of surface areas when using benzene (as described in Section 4.5) because of the difficulty involved in assigning an accurate value to the cross-sectional area, a_m, of the benzene molecule.[12] In this study, the McClellan and Harnsberger[13] "recommended value" of $a_m(C_6H_6)$ = 43 $Å^2$ has been employed (this

‡ Uncertainty arises from the error margin of ± 3 $Å^2$ assigned to the molecular area of benzene by McClellan and Harnsberger.[13]

average value was obtained by McClellan and Harnsberger following the examination of fifteen papers covering the adsorption of benzene on eleven adsorbents).

It is possible to calculate the cross-sectional area, a_m, of an adsorbate molecule by using the nitrogen specific surface area obtained for the sample and applying equation 4.2 ($S_{sp} = n_m L a_m$). In this case, if the surface area is taken to be 882 $m^2 g^{-1}$ (from N_2 sorption) and the monolayer capacity to be 2.8 mmol g^{-1} (from the benzene isotherm), then an estimated benzene molecular area of 52 $Å^2$ is obtained. This is consistent with the benzene molecule lying flat on the surface of the solid.

Application of the Gurvitsch rule to the benzene isotherm gave a total pore volume, V_p = 0.31 $cm^3 g^{-1}$, less than the Vp = 0.45 $cm^3 g^{-1}$ obtained from the nitrogen isotherm. The difference between the observed values of the total pore volume obtained from the nitrogen and benzene isotherms is thus not insignificant; this discrepancy may be due to the size difference of the two types of adsorbate molecule and the structure of the adsorbed layer. If the surface phenyl groups are assumed to be arranged perpendicular to the surface, then it is possible that the adsorption of the large benzene molecules could be sterically hindered. Also, because of the presence of π-electrons in the benzene molecule, induced interactions with polar surface hydroxyl groups may affect the structure of the benzene monolayer.

5.7.2 Mesitylene-Swollen Phenyl-Modified Mesoporous Silica

Benzene sorption carried out on the mesitylene-swollen sample yielded a Type IV isotherm (Figure 5.21) exhibiting hysteresis, confirming the sample's mesoporosity.

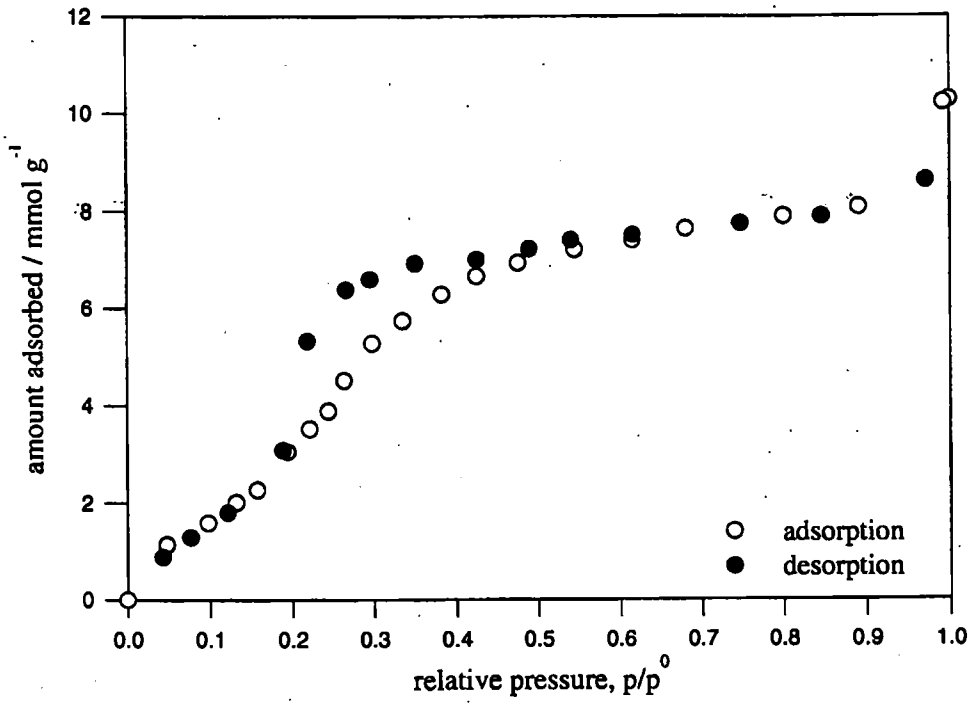

Figure 5.21 Benzene sorption at 293 K on MES-swollen phenyl-modified silica.

A BET specific surface area of 1051 $m^2\ g^{-1} \pm 50\ m^2\ g^{-1}$ was obtained using the "recommended" value of 43 $Å^2$ for the cross-sectional area of benzene. If, as in Section (*i*), we use the nitrogen specific surface area to calculate the actual value of $a_m(C_6H_6)$ we obtain a value of 38 $Å^2$ which also suggests that the molecule is oriented flat on the surface.

Application of the Gurvitsch rule to the benzene isotherm gave a total pore volume of 0.76 $cm^3\ g^{-1}$, significantly larger than that obtained from benzene sorption on the original (microporous) Burkett material (0.31 $cm^3\ g^{-1}$), reconfirming that MES is a suitable pore-swelling agent. The discrepancy in the values of the total pore volumes

obtained from the nitrogen (V_p = 0.67 cm^3 g^{-1}) and benzene (V_p = 0.76 cm^3 g^{-1}) isotherms is, again, probably due to the structure of the adsorbed benzene.

If the Kelvin equation is applied to the benzene isotherm at the inception of hysteresis (p/p^0 = 0.2), a Kelvin pore diameter, $2r_K$, of 26 Å is obtained. It should be noted that this is not a true pore diameter, d, as a value for the thickness of the adsorbed benzene monolayer, t, is not available [$d = 2(r_K + t)$] (see Figure 5.22). In reality, the pore diameter of this material is likely to fall in the range of 30-40 Å, well within the mesoporous regime.

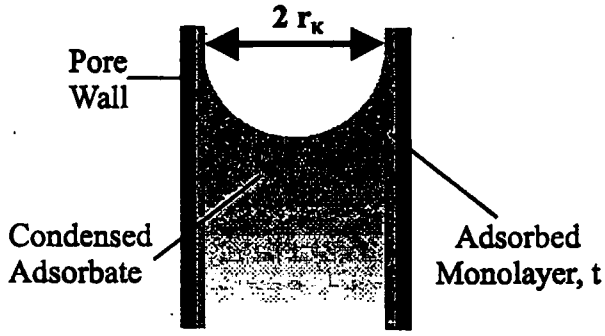

Figure 5.22 Diagram showing the Kelvin pore diameter, 2 r_K, and the adsorbed monolayer thickness, t, in a cylindrical pore.

5.8 Butanol Sorption

Sorption of *n*-butanol and *t*-butanol was carried out on the Burkett PhMCM-41 sample (from Bath)[8] and the MES-swollen phenyl-modified mesoporous silica. The sorption runs were carried out using the gravimetric apparatus at 303 K. Sorption data are given in Table 5.4.

5.8.1 PhMCM-41 (Burkett)

(i) n-Butanol

n-Butanol adsorption on the Burkett PhMCM-41 sample (from Bath) yielded an isotherm which appears, upon preliminary examination, to display Type IV characteristics (Figure 5.23). (The desorption run could not be completed due to problems with the apparatus.)

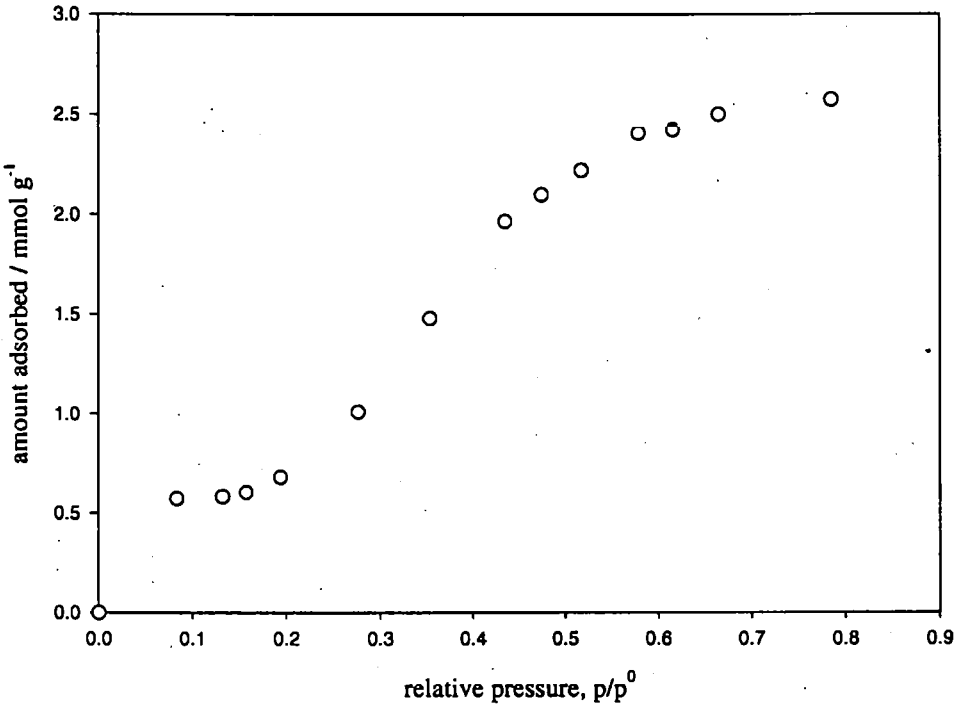

Figure 5.23 *n*-BuOH Sorption at 303 K on PhMCM-41 (Burkett).

A sharp knee is evident at $p/p^0 \approx 0.05$ which corresponds to a BET monolayer capacity, $n_m = 0.55$ mmol g^{-1}, much lower than those given by any other adsorbate for this sample (see Table 5.4). Using this n_m value, a specific surface area, $S_{sp} = 103$ m^2 g^{-1} is obtained, again much lower than the specific surface areas obtained for this material using other adsorbates ($S_{sp}(N_2) = 882$ m^2 g^{-1}). It is important to note in this instance that calculation of the specific surface area was performed using a value for the molecular

area, a_m = 31 Å^2, obtained via equation 4.3 ($a_m = 1.091\ (M / \rho\ L)^{2/3}$).[14] This equation assumes spherical molecules and hexagonal-packing which is inaccurate in the case of *n*-butanol (a straight-chain alcohol). For this reason, it is the monolayer capacity which is of real interest here.

If it assumed that *n*-butanol adsorbs on the surface of this material via polar interactions with surface hydroxyls, and if it is also assumed that one *n*-butanol molecule will adsorb on one surface hydroxyl, then it is possible to calculate the number of surface hydroxyl groups per unit area. Using the monolayer capacity, n_m = 0.55 mmol g^{-1} and the nitrogen specific surface area, $S_{sp}(N_2)$ = 882 m^2 g^{-1}, a value of 0.38 OH groups per nm^2 is obtained. This is considerably lower than that calculated from the water isotherm (0.9 nm^{-2}) which suggests that widespread localized bonding is occurring during *n*-butanol sorption (i.e. a monolayer is not being formed). If the sample is assumed (from water sorption) to have 0.9 OH groups per nm^2, then it appears that *n*-butanol is occupying just over a third of the available bonding sites. This could occur if adsorbed *n*-butanol molecules blocked the entrance to a pore channel or blocked access to adsorption sites by lying across them thus preventing further adsorption.

If the monolayer capacity and nitrogen specific surface area are used to calculate a value for the cross-sectional area of the *n*-butanol molecule, a highly unlikely value of a_c = 284 Å^2 is obtained. This is also evidence that a monolayer is not being formed during *n*-butanol sorption and suggests that polar interaction is the mechanism of adsorption in this case.

The total pore volume, V_p = 0.23 cm^3 g^{-1}, calculated for this isotherm is also considerably lower than those given by other adsorbates for this material (see Table 5.6) including *t*-butanol (V_p(*t*-BuOH) = 0.33 cm^3 g^{-1}, see next section). This also suggests

that complete surface coverage has not occurred during *n*-butanol adsorption and also that steric effects have influenced the structure of the adsorbed layer.

(ii) t-Butanol

t-Butanol sorption at 303 K on the Burkett PhMCM-41 sample yielded an isotherm displaying mainly Type I characteristics (Figure 5.24).

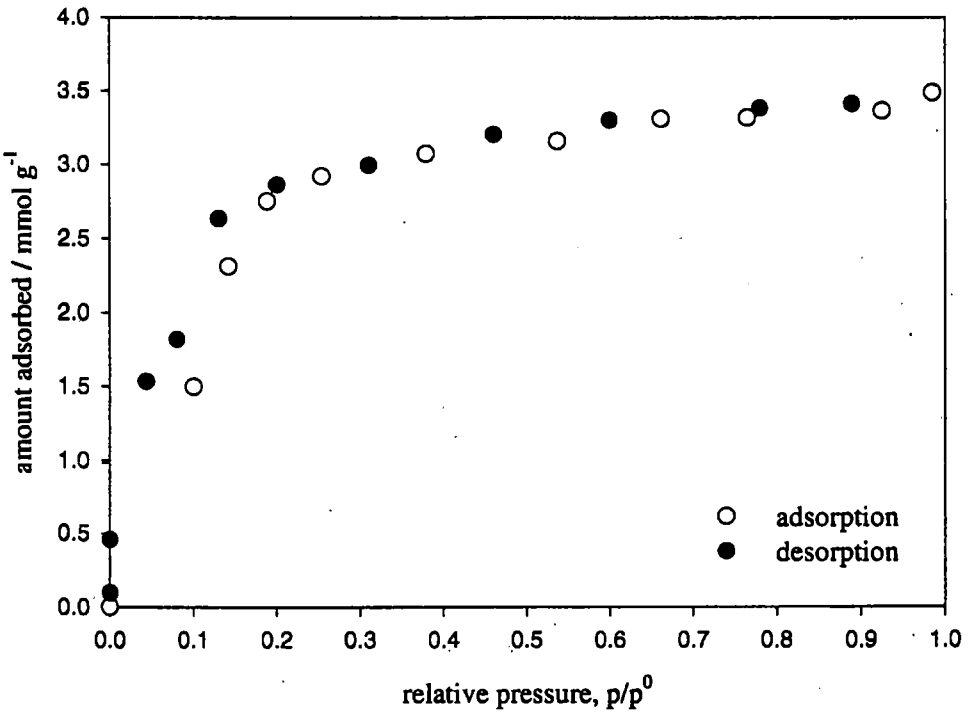

Figure 5.24 *t*-Butanol sorption at 303 K on PhMCM-41 (Burkett).

At low relative pressures there is a large uptake of adsorbate before the isotherm levels off at $p/p^0 \approx 0.2$. BET analysis yields a monolayer capacity of 2.12 mmol g^{-1}, considerably larger than that obtained by *n*-butanol sorption (n_m = 0.55 mmol g^{-1}). Figure 5.25 highlights the differences between the two isotherms by presenting them on the same axes.

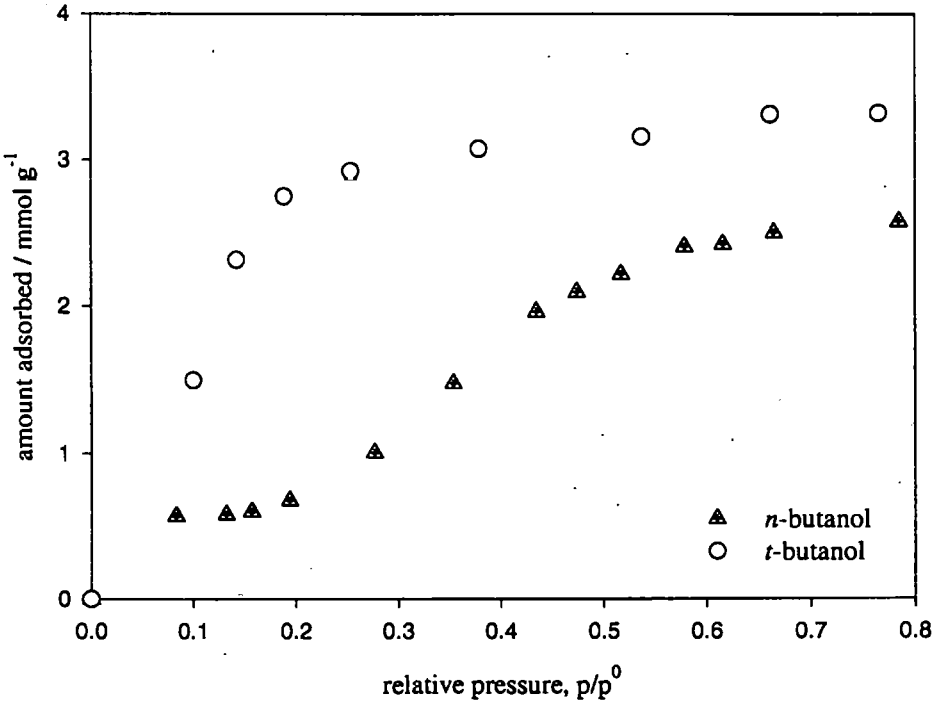

Figure 5.25 A Comparison of *n*- and *t*-butanol adsorption at 303 K on PhMCM-41

The obtained n_m value gives a specific surface area, S_{sp} = 664 m^2 g^{-1} which is slightly lower than would be expected for this material (S_{sp} (N_2) = 882 m^2 g^{-1}). As the isotherm resembles a Type I, Langmuir analysis was also performed and this yielded a monolayer layer capacity of 3.70 mmol g^{-1}, corresponding to a specific surface area, S_{sp} = 742 m^2 g^{-1} very similar to that given by benzene sorption (750 m^2 g^{-1}). Values of the cross-sectional area, a_c = 45 $Å^2$ (obtained using the BET monolayer capacity and the N_2 specific surface area) and a_c = 38 $Å^2$ (calculated using the Langmuir n_m value) are considerably lower than that obtained for *n*-BuOH on this material (a_c = 284 $Å^2$) suggesting that localized adsorption is not occurring in this case.

As mentioned in Section 4.3, there is some uncertainty when interpreting Type I isotherms as to whether the "knee" represents the monolayer capacity or the pore volume. The value obtained for the total pore volume (taken from the plateau of this

isotherm), V_p = 0.33 cm^3 g^{-1}, is identical to that given by the water isotherm and very similar to that given by the benzene isotherm (0.31 cm^3 g^{-1}). It is, however, considerably larger than that obtained from *n*-butanol sorption (0.23 cm^3 g^{-1}) which suggests that *t*-butanol (spherical) actually packs more efficiently than *n*-butanol (linear) in the pore channels. The fact that $V_p(N_2)$ = 0.45 cm^3 g^{-1}, suggests that *t*-butanol is somehow packed in a less-dense state than its liquid form. This may be due to localized bonding on surface hydroxyls (although the bulky nature of *t*-butanol may preclude polar interactions between the alcohol function and surface hydroxyls) but is more likely to be due to steric hindrance of some kind. Low pressure hysteresis is observed in the desorption branch of the isotherm which does suggest that some degree of rehydroxylation is occurring.

Further comparison with benzene sorption on this sample yields striking results if the two isotherms are plotted on the same axis as shown in Figure 5.26, below.

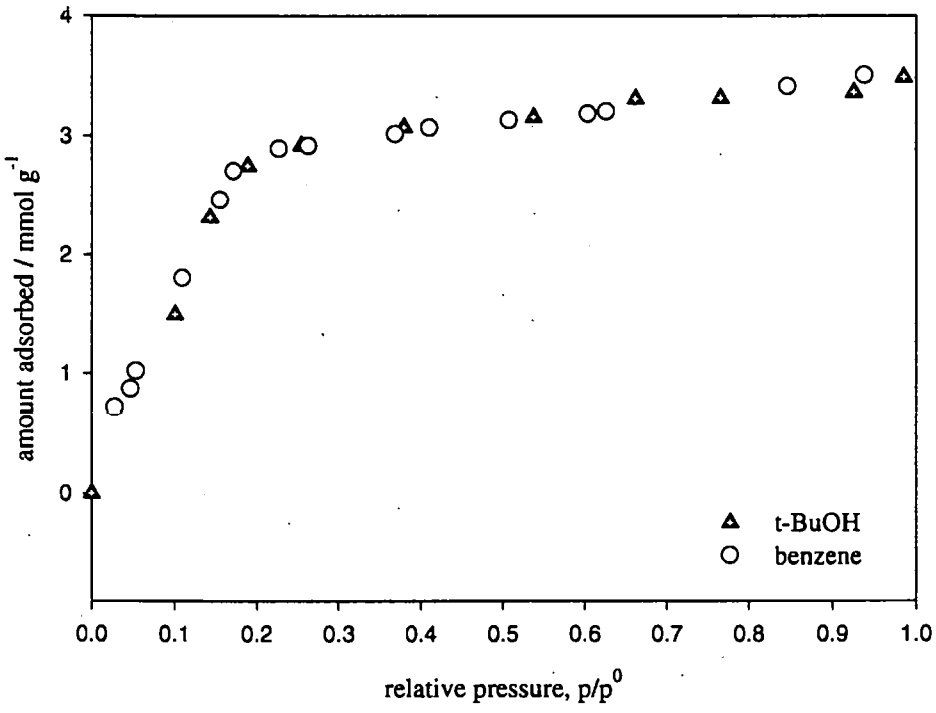

Figure 5.26 *t*-BuOH sorption at 303 K and benzene sorption at 293 K on PhMCM-41.

The fact that these two isotherms may be completely superimposed suggests that the mechanism of *t*-BuOH sorption is similar to that observed in benzene sorption. This indicates that the sorption mechanism of *t*-BuOH on this material is more influenced by organic interactions with the surface phenyl groups than by polar interaction with surface hydroxyls. (It should be noted, however that a small amount of rehydroxylation is indicated by the low pressure hysteresis.)

The preclusion of hydrogen-bonding in *t*-BuOH sorption is supported by the difference in the boiling points of *n*-BuOH (b.p. = 118 °C) and *t*-BuOH (b.p. = 83 °C). The lower boiling point of *t*-BuOH indicates that there is less hydrogen-bonding occurring than in *n*-BuOH.

Further evidence that H-bonding to surface hydroxyls is not the sorption mechanism in this case is highlighted when a value for the number of surface hydroxyls (1.45 nm^{-2}) is calculated from the monolayer capacity. This is much greater than that obtained from either the *n*-BuOH isotherm (0.38 nm^{-2}) or the water isotherm (0.9 nm^{-2}). If the value calculated from the water isotherm is taken to be the most accurate (due to the small, unhindered dimensions of the water molecules) it becomes evident that the *t*-BuOH molecules are not undergoing localized adsorption.

5.8.2 MES-Swollen Phenyl-Modified Mesoporous Silica

(i) n-Butanol

n-Butanol sorption at 303 K on the MES-swollen phenyl-modified mesoporous silica yielded a Type IV isotherm exhibiting a large degree of hysteresis (Figure 5.27).

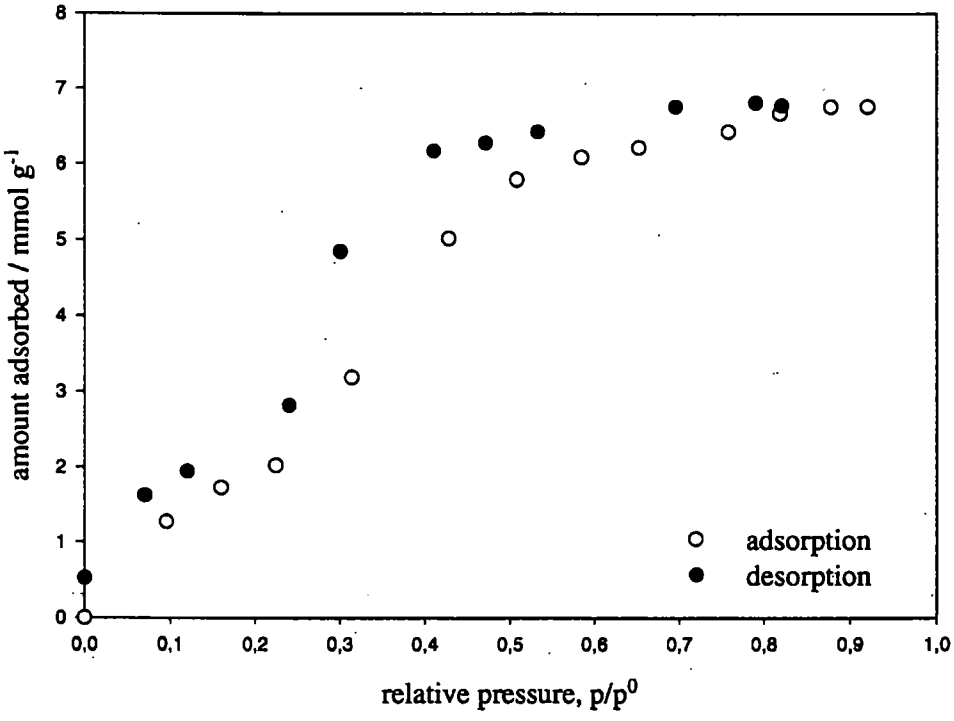

Figure 5.27 *n*-Butanol sorption at 303 K on MES-swollen phenyl-modified mesoporous silica

As in the water isotherm, low pressure hysteresis is evident, again suggesting a degree of chemisorption (surface rehydroxylation, see Section 5.2). Following application of the BET equation, a specific surface area, S_{sp} = 461 m^2 g^{-1} (n_m = 1.98 mmol g^{-1}) was obtained. This is lower than would be expected for this type of sample ($S_{sp}(N_2)$ = 942 m^2 g^{-1}) which indicates that localized adsorption (due to polar interactions between the alcohol and the surface hydroxyls) may have occurred. However, as mentioned in Section 5.7.1, the value of a_m = 31 $Å^2$ used to calculate S_{sp} is not entirely accurate due to the assumptions made in equation 4.3. This is therefore a

source of uncertainty in the calculation of S_{sp} and for this reason, the monolayer capacity is of greater interest.

Calculation of the cross-sectional area, a_c, from the monolayer capacity and N_2 specific surface area yields $a_c = 79$ Å^2, which is larger than expected and again indicates localized adsorption. This value is considerably lower than that calculated for *n*-BuOH on the microporous PhMCM-41 ($a_c = 284$ Å^2) however, which suggests that *n*-BuOH sorption is less localized or, as is more likely, less sterically hindered in the mesoporous MES-swollen sample.

A Gurvitsch pore volume, $V_p = 0.62$ cm^3 g^{-1} was obtained, very similar to that observed for the nitrogen isotherm (0.67 cm^3 g^{-1}) suggesting that *n*-butanol sorption was not sterically hindered in this larger pore MES-swollen sample.

Calculation of the number of surface hydroxyls present from this isotherm (n_m = 1.98 mmol g^{-1}) yields a value of 1.26 nm^{-2}.

(ii) t-butanol

The sorption of *t*-butanol on the MES-swollen sample also yielded a Type IV isotherm (Figure 5.28); hysteresis was not observed in this case. A monolayer capacity $n_m = 2.47$ mmol g^{-1} and a BET surface area, $S_{sp} = 497$ m^2 g^{-1} were calculated. These values are lower than would be expected for this material suggesting that localized adsorption has occurred. A calculated value of $a_c = 63$ Å^2 was obtained for the cross-sectional area of the *t*-BuOH molecule.

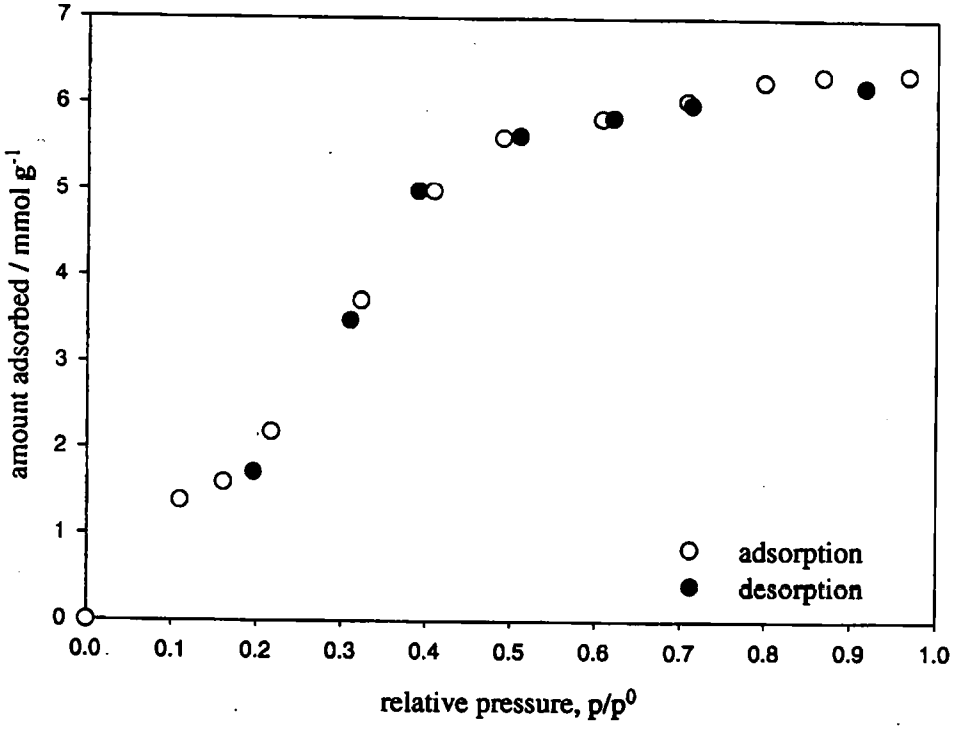

Figure 5.28 *t*-Butanol sorption at 303 K on MES-swollen phenyl-modified silica

It should be noted that this sorption run was performed on the same sample as the *n*-butanol sorption (following sample outgassing at 100 °C). It is possible that if chemisorption or rehydroxylation of the surface occurred during the first run (as indicated by the low pressure hysteresis) then the surface would be less reactive (i.e. have fewer four-membered Si-O rings) during the second sorption run making chemisorption, and the resulting hysteresis, less likely in this case.

A Gurvitsch pore volume of 0.61 $cm^3\ g^{-1}$ was observed, almost identical to that given by the *n*-butanol isotherm (V_p = 0.62 $cm^3\ g^{-1}$). This is highlighted by Figure 5.29 which presents both adsorption isotherms on the same axis. The similarity of the two adsorption isotherms in shape and total amount adsorbed indicates that the large pores of this MES-swollen sample do not restrict adsorption of either of these alcohols.

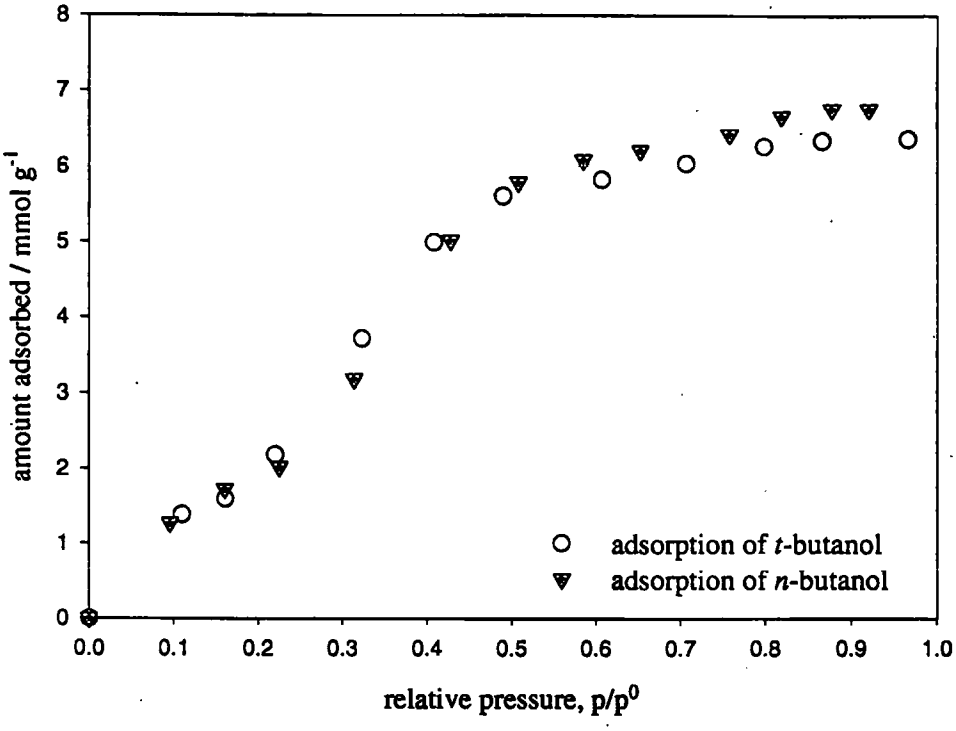

Figure 5.29 *n*-Butanol and *t*-butanol sorption at 303 K on MES-swollen Phenyl-modified silica.

Calculation of the number of surface hydroxyl groups present, from the *t*-BuOH isotherm, yields a value of 1.58 nm^{-2}. This is greater than that calculated from the *n*-BuOH isotherm (1.26 nm^{-2}), a fact which could be explained in the same manner as the lack of a hysteresis loop, i.e. rehydroxylation of the surface during *n*-BuOH sorption has increased the number of surface hydroxyls. An alternative explanation is that the adsorption mechanism in this case is not *via* H-bonding with Si-OH groups, but is due to organic interactions with the surface phenyls as observed in the microporous Burkett sample.

A comparison between the benzene and *t*-BuOH isotherms given by this sample is presented below in Figure 5.30.

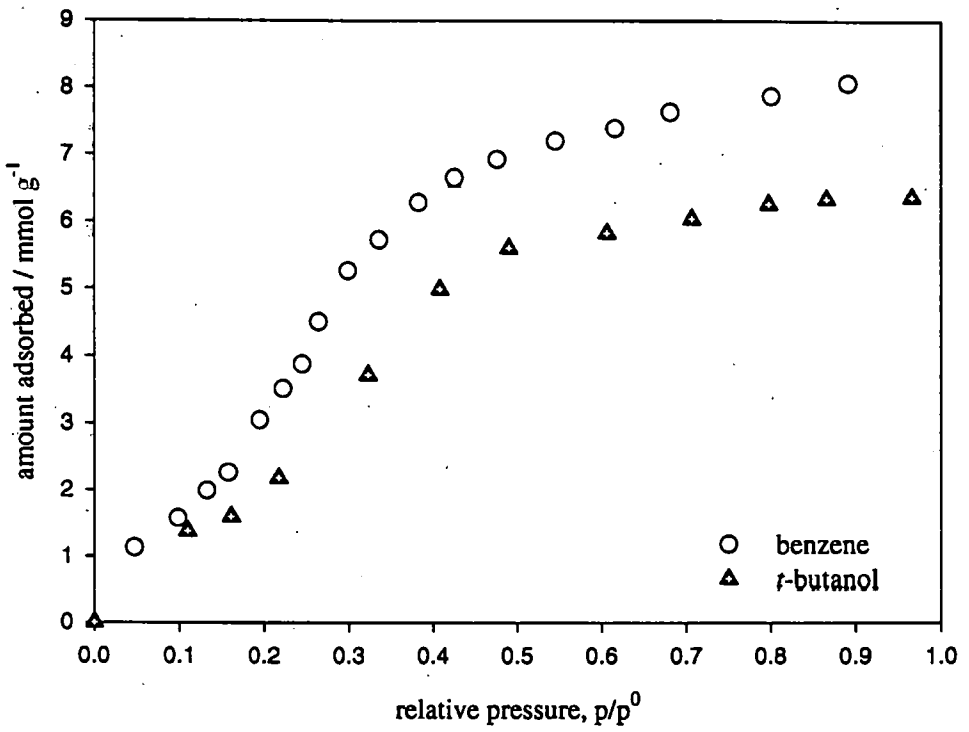

Figure 5.30 A Comparison of benzene and *t*-butanol adsorption on MES-swollen Ph-M.S.

The similarity in the shapes of these two isotherms also suggests that the sorption mechanism of *t*-BuOH is via organic rather than polar interactions.

5.8.3 Comparison of *n*- and *t*-Butanol Sorption on PhMCM-41 and MES Swollen Phenyl-Modified Mesoporous Silica

A comparison of *n*- and *t*-butanol sorption on the two samples is presented in Table 5.7.

Table 5.7 Comparison of BuOH Sorption on a Microporous and Mesoporous Phenyl-Modified Silica

		PhMCM-41 (Burkett)	MES-Swollen Ph-M.S.
***n*-BuOH**	**Isotherm Type**	IV	IV
	Hysteresis?	-	Yes
	n_m / mmol g^{-1}	0.55	1.98
	V_p / cm^3 g^{-1}	0.23	0.62
***t*-BuOH**	**Isotherm Type**	I	IV
	Hysteresis?	Yes	No
	n_m / mmol g^{-1}	2.12 *(3.70)*	2.47
	V_p / cm^3 g^{-1}	0.33	0.61

(i) n-Butanol

The major differences in the results obtained for *n*-BuOH sorption on the two samples is given by the monolayer capacities and total pore volumes. Much lower values are obtained for the microporous material, as would be expected, indicating that *n*-BuOH sorption is hindered by the narrowness of the pores. The two isotherms are presented on the same axes, for comparison purposes, in Figure 5.31.

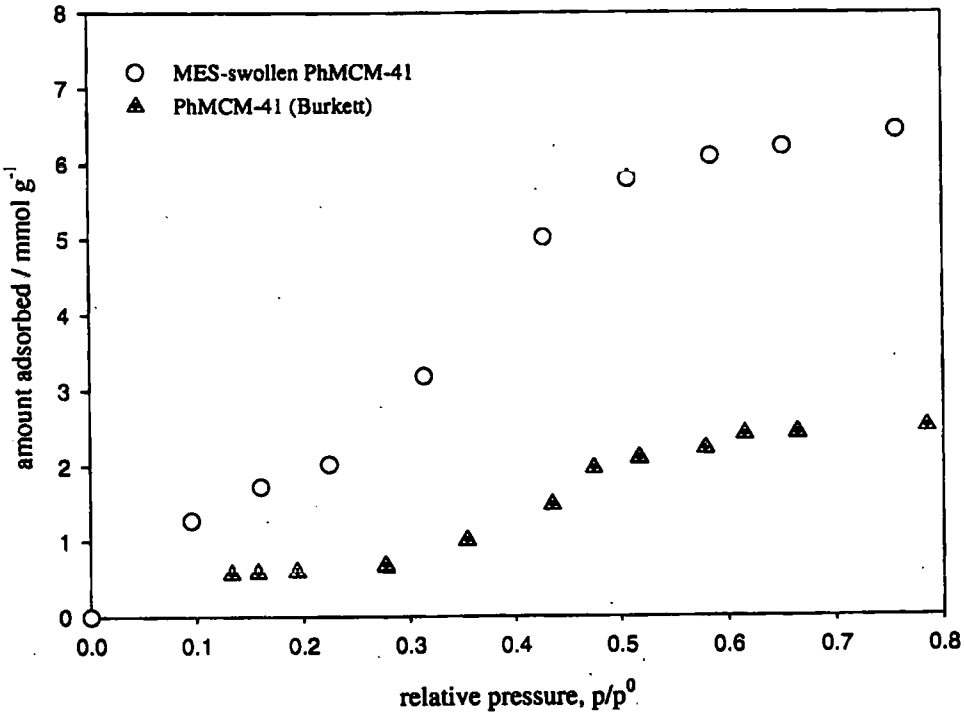

Figure 5.31 *n*-BuOH sorption at 303 K on PhMCM-41 and MES-swollen Ph-M.S.

(ii) t-Butanol

In the case of *t*-BuOH sorption, the major difference observed between the two samples is the shape of the respective isotherms (see Figure 5.32). The microporous PhMCM-41 sample yields a Type I isotherm (which may be totally superimposed with the benzene isotherm of this sample) while the mesoporous MES-swollen Ph-M.S. gives a Type IV. Similar monolayer capacities (if the value obtained from the Type I isotherm is taken to be a monolayer capacity) are observed for each sample. This indicates that *t*-BuOH sorption is not hindered by the narrowness of the PhMCM-41 pore-channels. The difference in the observed total pore volumes is almost of the same order as that observed between the nitrogen total pore volumes calculated for these materials, again suggesting that *t*-BuOH is not sterically hindered in the microporous sample.

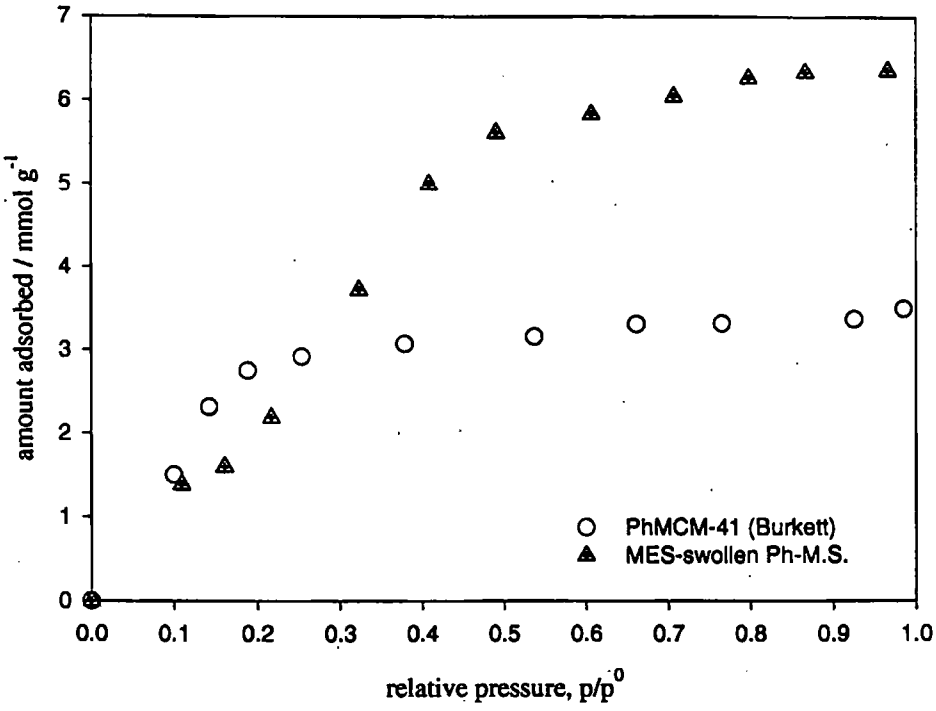

Figure 5.32 *t*-BuOH sorption at 303 K on PhMCM-41 and MES-swollen Ph-M.S.

(iii) Conclusions

In conclusion, it appears that *n*-BuOH sorption is more sterically-hindered than *t*-BuOH sorption. This is due to the difference in the shapes of the two molecules (see Figure 5.33). The "spherical" *t*-BuOH molecule is able to easily penetrate into the micropores of the Burkett PhMCM-41 sample without blocking the pore-entrance while the straight-chain *n*-BuOH molecule may block the pores upon adsorption.

In the case of *t*-BuOH sorption on the microporous Burkett sample, it appears that adsorption is *via* organic interactions with surface phenyls rather than hydrogen-bonding with surface hydroxyls. It is difficult to say whether this is the case with *t*-BuOH sorption on the MES-swollen sample as the isotherm is virtually identical to that given by *n*-BuOH. This could be due to the fact that, in the larger-pore material, the

surface hydroxyl groups are more accessible to the sterically-crowded -OH groups of *t*-BuOH resulting in polar interactions.

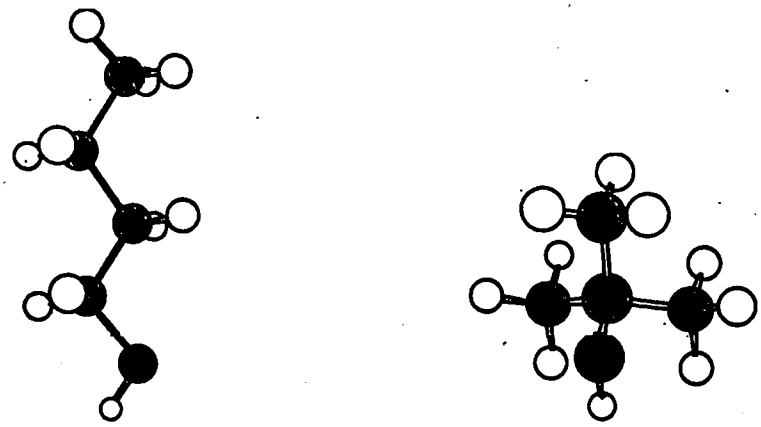

(a) (b)

Figure 5.33 (a) *n*-Butanol, (b) *t*-Butanol

REFERENCES

1. Sing, K.S.W.; Everett, D.H.; Haul, R.A.W.; Moscou, L.; Pierotti, R.A.; Rouquerol, J.; Siemiemiewska, T. *Pure and App. Chem.*, **1965**, *57*, 603.
2. Branton, P. J.; Hall, P.G.; Sing, K.S.W., *J. Chem. Soc., Chem. Commun.*, **1993**, 1257.
3. Thomson, W.T., *Phil. Mag.* **1871**, *42*, 448.
4. Gurvitsch, L., *J. Phys. Chem. Soc. Russ.*, **1915**, *47*, 805.
5. Branton, P. J.; Hall, P.G.; Treguer, M.; Sing, K.S.W., *J. Chem. Soc., Faraday Trans.*, **1995**, *91*(13), 2041-2043.
6. Branton, P.J., *PhD Thesis*, University of Exeter, **1994**.
7. Chuang, I-S.; Maciel, G.E., *J. Phys. Chem. B*, **1997**, *101*, 3052-3064.
8. Burkett, S.L.; Sims, S.D.; Mann, S., *J. Chem. Soc., Chem. Commun.*, **1996**, 1367-1368.
9. N. Ulagappan and C.N.R. Rao, *J. Chem. Soc., Chem. Commun.*, **1996**, 2759.
10. Llewellyn, P.L.; Schuth, F.; Grillet, Y.; Rouquerol, F.; Rouquerol, J.; Unger, K.K., *Langmuir*, **1995**, *11*, 574.
11. Gregg, S.J.; Sing K.S.W., "*Adsorption, Surface Area and Porosity*", 2nd Edition, *Chapter 5*, Academic Press, London, **1982**.
12. Gregg, S.J.; Sing K.S.W., "*Adsorption, Surface Area and Porosity*", 2nd Edition, *p.80*, Academic Press, London, **1982**.
13. McClellan, A.L.; Harnsberger, H.F., *J. Colloid Interface Sci.*, **1967**, *23*, 577.
14. Emmett, P.H.; Brunauer, S., *J. Amer. Chem. Soc.*, **1937**, *59*, 1553.

CHAPTER 6

INCOHERENT INELASTIC NEUTRON SCATTERING

This chapter is divided into two parts. Part I considers the elementary theory of incoherent inelastic neutron scattering and describes the experimental technique employed in this study. Part II presents the results obtained.

PART I - THEORETICAL AND EXPERIMENTAL CONSIDERATIONS

6.1 General

Incoherent Inelastic Neutron Scattering (IINS) studies were carried out at the Rutherford Appleton Laboratories' ISIS spallation neutron source. TOSCA, the new spectrometer commissioned in 1998 to replace TFXA, was used in these studies.

Vibrational spectroscopy techniques such as infra-red (IR) and Raman spectroscopy are commonly used in the characterization of solid-state materials. Inelastic neutron scattering is a form of vibrational spectroscopy which employs neutrons rather than photons. Wavelengths of neutrons ($\lambda \approx 10^{-10}$ m) are similar to interatomic distances, and can therefore be used to yield structural information.

The production of neutrons is costly and involves either shattering nuclei with a high energy proton beam (spallation - used at ISIS) or fission in a nuclear reactor (used at ILL, Grenoble). The advantages of neutron spectroscopy over conventional photon

techniques must therefore outweigh the great expense of producing a neutron beam. The major advantages afforded by employing neutrons are listed below:

1) The selection rules which govern IR (a vibration must cause an overall change in electrical dipole) and Raman (a vibration must cause a change in polarizability) spectroscopies do not apply to IINS. For this reason those peaks which are "lost" in spectra obtained using the two optical spectroscopies are observed in IINS spectra.
2) The absence of charge and the small absorption cross-sections for neutrons increase their penetrating power.[1] This is also aided by the fact that the neutron mass (1.675×10^{-27} kg) is much greater than that of an electron (9.109×10^{-31} kg).
3) Energy losses (relative to incident energy) on scattering are much greater than in photon techniques and are therefore easily detected.
4) The intensities of scattered neutrons are relevant and can yield valuable structural information.
5) The large incoherent cross-sectional of ^{1}H (see next section) means that intensities due to vibrational modes involving ^{1}H are selectively enhanced.

6.2 Theoretical Considerations

Neutron scattering theory is an extensive field and, as only the basic theory required to understand the TOSCA experiment is considered here, readers requiring a more in-depth treatment are directed to references 3 and 4.

As mentioned in the previous section, IINS is used particularly to investigate vibrations of hydrogenous samples. TOSCA is a "time-of-flight" IINS spectrometer

which is based on the same methodology as TFXA.[5,6,7] The quantities determined in a TOSCA experiment are the energy changes observed upon neutron scattering from the sample and the neutron intensities at those energies.

De Broglie's equation (6.1) relates the velocity, v, of a neutron with mass, m, to its wavelength, λ:

$$\lambda = \frac{h}{mv} \qquad (6.1)$$

where h is the Planck constant. The energy loss or gain upon scattering from the nucleus is usually expressed in terms of the angular frequency, ω[1]:

$$\eta\omega = \tfrac{1}{2}\ m\ (v_0^2 - v_1^2) \qquad (6.2)$$

where ηω is the energy transferred. $\omega = 2\pi\nu$ (where ν is the oscillation frequency of neutron wave), $\eta = h/2\pi$, m is the neutron mass and v_0 and v_1 are its initial and final speed, ($v_i = |\underline{v}_i|$ where $\underline{v}_i$ is the velocity).

As mentioned earlier, TOSCA is based on a time-of-flight technique, and this is made simple because a pulsed neutron source is employed at ISIS.

The various stages of the time-of-flight experiment are listed below:

1) Microsecond pulses of "white" neutron radiation are released from the source and arrive at the sample at different times.
2) Neutrons are elastically and/or inelastically scattered by the sample.
3) Pyrolytic graphite analyzers act as monochromators for the scattered neutrons directing only those of energy $3.0 \leq \eta\omega / \text{meV} \leq 4.8$ to the detectors.
4) Beryllium filters eliminate high order scattering (i.e. that which obeys Bragg's law for $n \neq 1$).

5) Since the instrument geometry give flight times between the sample and the detector which are identical for each scattered neutron, energy changes observed upon scattering from the sample may be calculated by considering neutron arrival times at the detector.

Thus, TOSCA is a time-of-flight spectrometer in which monochromation occurs after scattering (a spectrometer configured in this way is known as an inverted geometry spectrometer).

The Scattering Cross-Section

Spectra are presented as plots of energy transfer against neutron intensity. The neutron intensity is a function of the scattering cross-section, σ, of the nucleus (i.e. the amount of the incident beam scattered by the nucleus) and the solid-angle Ω into which the neutrons are scattered. (In a scattering experiment, a detector placed at an angle of 2θ to the incident beam measures the intensity of the scattered wave which passes through the solid angle Ω). The dependence of the cross-section, σ, on the energy of the neutrons is represented by the double differential cross-section defined as the change in the scattering cross-section with respect to both Ω and the energy, E:

$$\frac{\partial^2\sigma}{\partial\Omega\partial E} = \frac{k_s}{k_0}\langle b^2\rangle S(Q,\omega) \qquad (6.3)$$

k_0 and k_s are wavevectors of incident and scattered neutrons, $\langle b^2\rangle$ is the mean square of the neutron scattering lengths and $S(Q,\omega)$ is the scattering law. This latter term is a property of the system in question. The double partial differential cross-section describes the probability per neutron that incident neutrons are scattered through an angle of 2θ into a solid angle element $\delta\Omega$ with an energy in the range of E to $(E+\delta E)$.

The intensities of the scattered neutrons are directly proportional to the mean square displacement of the atoms during a vibration, and inversely proportional to the magnitude of the scattering vector, Q (where $\underline{Q} = \underline{k_0} + \underline{k_s}$). Q is large at high energy transfers and therefore intensities are small when high energy changes occur.

The scattering cross-sections of the nuclei in the sample under investigation are, therefore, of great importance. As mentioned in the previous section, ^1H has a particularly large incoherent scattering cross-section (79.7 barns; 1 barn = 10^{-28} m^2). This is many times greater than that observed for most other nuclei and isotopes, and therefore any incoherent neutron scattering observed for hydrogenous systems will be almost exclusively due to ^1H vibrations.

Coherent and Incoherent Scattering

The scattering of neutrons from a nucleus may be described as coherent (in phase with the incident wave) or incoherent. If a sample consists of one isotope having a nuclear spin I = 0, only coherent scattering is observed. However, when nuclei from several different elements or isotopes are present, or if the nuclei have non-zero spin, the scattering cross-section is given by the sum of the coherent and incoherent contributions (Equation 6.4). These incoherent contributions are termed "isotope incoherence" and "spin incoherence" respectively.

$$\sigma = \sigma_{coh} + \sigma_{inc} \qquad (6.4)$$

The incoherent scattering cross-section of hydrogen is over forty times greater than the coherent scattering cross-section as shown in Table 6.1, below.

Table 6.1 Values of the Scattering Cross-Sections of Hydrogen

Scattering Cross-Section Contribution	Value / barns (1 barn = 10^{-28} m^2)
Incoherent	79.8
Coherent	1.8
Total	81.6

As mentioned in the previous section, the scattering cross-section, σ, is related to the scattering length, b. The coherent term in equation 6.4 is related to b *via* equation 6.5:

$$\sigma_{coh} = 4\pi \langle b \rangle^2 \qquad (6.5)$$

while σ_{inc} is related to b *via* equation 6.6:

$$\sigma_{inc} = 4\pi\{ \langle b^2 \rangle - \langle b \rangle^2 \} \quad (6.6)$$

The total cross-section, σ, is therefore given by equation 6.7:

$$\sigma = 4\pi\langle b^2 \rangle \qquad (6.7)$$

6.3 Experimental Details

6.3.1 The Spectrometer

The IINS spectrometer, TOSCA, was commissioned in early 1998 to replace TFXA and installed on the N8 thermal beam line 12 m from the ISIS neutron source after a water moderator. It is an inverse geometry spectrometer with an energy range, 15 meV < E < 1000 meV.[8]

The analyzer/detector arrangement is similar to that used on the TFXA spectrometer. In TOSCA 10 modules are used instead of two (as in TFXA), resulting in a five-fold increase in sensitivity. Each detector module has a graphite monochromator, which selects neutrons of ≈ 32 cm^{-1} (≈ 4 meV), a Be filter to suppress higher order reflections, and 16 ^3He detector tubes. At the time of this study, eight detector modules were "on-line".

6.3.2 Aims of the TOSCA Experiments

As mentioned in Section 4.5, problems are encountered when calculating a specific surface area from a benzene isotherm due to the uncertainties; the problems include definition of the orientation of the benzene molecule on the surface of the sample.[9] In the case of the MES-swollen phenyl-modified mesoporous silica, the benzene monolayer capacity and the nitrogen specific surface area suggest that the molecule is lying flat on the surface ($a_c(C_6H_6)$ = 38 $Å^2$). The aim of this INS study was, therefore, to investigate benzene sorbed on the surface of the mesoporous phenyl-modified silica in an attempt to determine more conclusively the orientation of the benzene molecule. The samples that were prepared for analysis on TOSCA are given in Table 6.2, below. Due to some severe problems with the newly commissioned apparatus, not all of these runs were completed and so the samples that were analyzed successfully are marked in Table 6.2.

As well as studying the structure of the adsorbed layer, the effect that the layer had on the surface phenyls was also investigated. This was carried out by analyzing a sample containing a monolayer of d_6-benzene. (Because the scattering cross-section of

D is so much smaller than that of H, any results obtained would be dominated by modes involving the protons of the structural phenyl groups).

Table 6.2 Samples Prepared for Analysis on TOSCA

Sample	Spectra Recorded?
Benzene	✓
Outgassed MES-swollen phenyl-modified silica (Ph-M.S.)	✓
Ph-M.S. + C_6H_6 monolayer *	✓
Ph-M.S. saturated with benzene	✓
Ph-M.S. + C_6D_6 monolayer	✓
Ph-M.S. saturated with C_6D_6	x
Outgassed purely siliceous mesoporous silica	x

* Due to problems with the apparatus, approximately ⅓ of this sample was in the neutron beam.

6.3.3 Sample Preparation

A large batch of MES-swollen phenyl-modified mesoporous silica was produced for the TOSCA experiment by scale-up of synthesis 2.2.2(ii) (forty times the original quantities were used). The reaction mixture was stirred overnight at ambient temperature in a 2 dm^3 conical flask with a teflon overhead stirrer. The reaction mixture was then heated in a 850 W domestic microwave oven for 90 min at 20 % power (teflon bottle synthesis was not attempted due to the large batch size). The white solid was filtered, washed with deionized water and dried at ambient temperature overnight. X-ray powder diffraction of the as-synthesized sample yielded a broad peak at $2\theta = 2.7°$, corresponding to a d-spacing of 48.6 Å.

Due to the large quantities of sample involved, acid extraction was performed in three stages at room temperature. The sample was divided into two portions and loaded into two 1 dm^3 round bottom flasks. 500 cm^3 of HCl in ethanol (1 mol dm^{-3}) were then added to each flask and the suspensions were stirred overnight at ambient temperature. This procedure was repeated twice, using fresh HCl/EtOH solution and stirring the suspensions for several hours in each case. Infra-red spectroscopy showed both batches to be free of template.

The Sample Environment

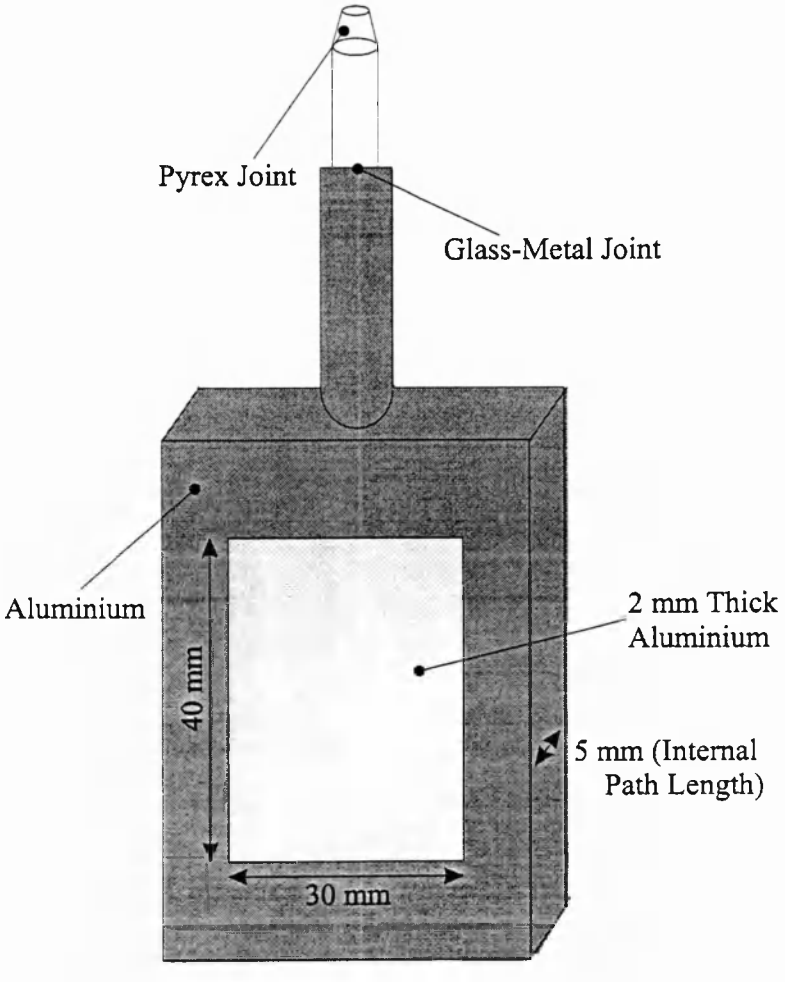

Figure 6.1 Sample can tailored for use in TOSCA

In order to analyze powder samples containing a known amount of adsorbed benzene, it was necessary to design and build sample cans that could be fitted to a vacuum line and having the dimensions and characteristics appropriate for use in TOSCA. A series of aluminium sample cans (aluminium is almost transparent to neutrons) similar to that shown in Figure 6.1, were built by the mechanical workshops at the University of Exeter. The cans were filled with the powder sample, which was then outgassed at 100 °C, under nitrogen, for several hours or overnight. The cans were attached to the gravimetric vacuum line (shown in Figure 4.2) via a Pyrex joint and evacuated to pressures of $< 1 \times 10^{-3}$ Pa.

Benzene and d_6-Benzene Sorption

Benzene and d_6-benzene sorption was achieved at 293 K by submerging the sample cans, attached to the vacuum-line, in a reservoir containing water at that temperature. The adsorptives were exposed to three "freeze-pump-thaw" cycles in order to remove dissolved gases.

When adsorbing a monolayer onto the sample, the adsorptive pressure was maintained at a value corresponding to the Point B observed in the benzene isotherm of this sample, $p/p^0 \approx 0.5$ (see Figure 5.19). The sample was exposed to the adsorptive for several hours to ensure that equilibrium had been reached. Following adsorption, the sample was frozen in liquid nitrogen and the glass tube connecting the can to the vacuum-line was sealed *in situ*. The sample was then allowed to return to room temperature and a hollow aluminium tube, having an M8 thread at one end, was attached to the can by fixing it into place over the glass-metal joint (Figure 6.2). This

connecting tube was the means of attaching the can to the cryostat centre-stick for TOSCA via the M8 screw thread.

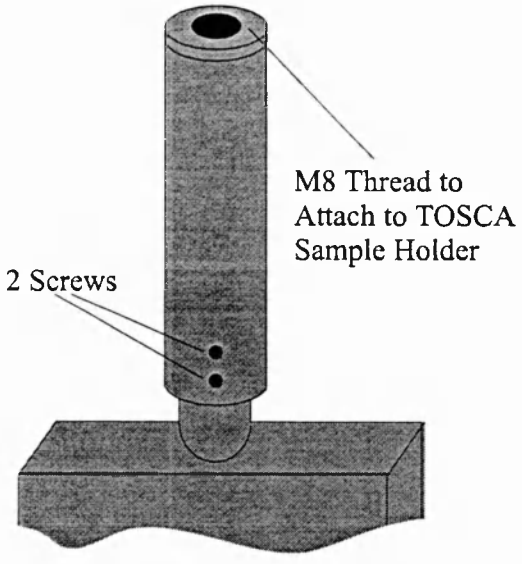

Figure 6.2 Detail of TOSCA Sample Can Showing Connecting Rod

The saturated sample was prepared on site at RAL by exposing a prefilled sample can to an atmosphere saturated with benzene (in a previously evacuated desiccator). The glass tube was then sealed with a rubber bung and a connector tube attached, as described above.

The "blank" sample (i.e. outgassed phenyl-modified mesoporous silica) was loaded into a sample can which was evacuated on the gravimetric vacuum line and sealed as previously described.

Benzene was analyzed in the same type of sample can as the solid samples, sealed with a rubber bung and PTFE tape.

Obtaining a Spectrum

Following attachment of the sample can to the TOSCA cryostat centre-stick *via* the connecting rod, a sheath of cadmium metal was wrapped around the can, leaving a window exposed on one side for the neutron beam. Cadmium has a very large neutron absorption cross-section and is therefore used to absorb "stray" neutrons.

The sample can on the centre-stick was lowered into the cryostat, which was evacuated and cooled with liquid helium to a temperature of approximately 10 K. Data were collected from 0 - 4000 cm^{-1}. Typical data acquisition times were in the order of six hours.

PART II - TOSCA RESULTS

As mentioned in Section 6.3.2, the aim of this experiment was to investigate the structure of benzene adsorbed on a phenyl-modified mesoporous silica. The effect that the adsorbed species had on the structural phenyls was also under investigation.

Due to the fact that TOSCA was newly commissioned when this study was undertaken, some problems were encountered with the sample housing and the detector modules (see below).

Each sample was analyzed in the range 0 - 4000 cm^{-1} and the entire spectrum of each sample, along with certain expanded regions, are given below. The principal band assignments are presented in Tables 6.3 and 6.4 and a discussion of the results is given, sample-by-sample, in Section 6.10.

6.4 The Background Spectrum

A spectrum was taken of a blank aluminium sample can in order to provide a "background" spectrum upon which to base the analysis of the other spectra. This is shown in Figure 6.3, below.

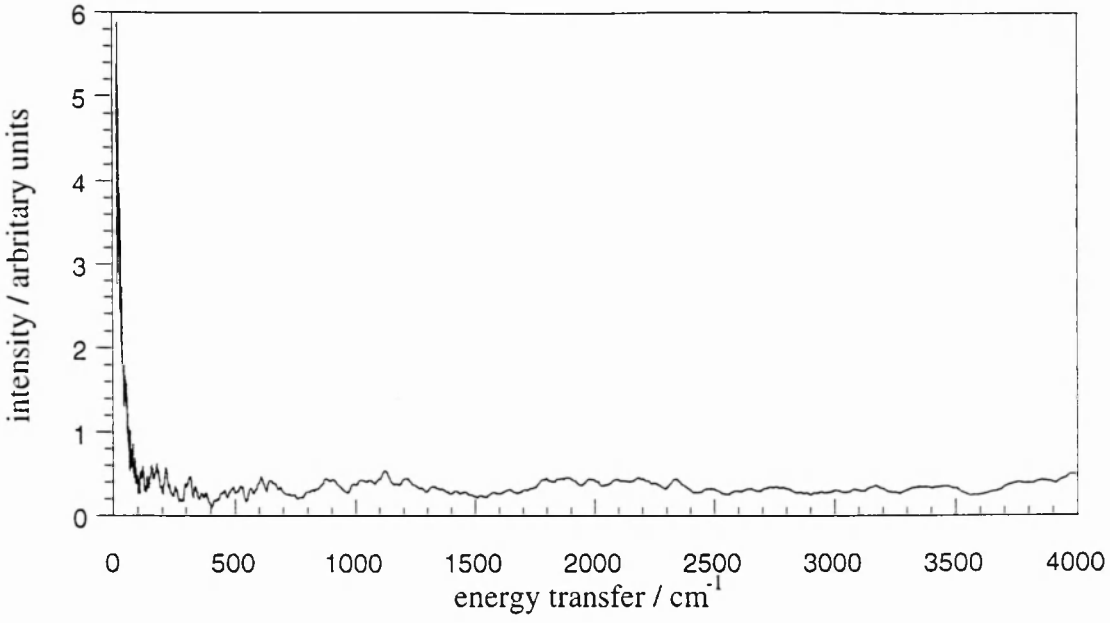

Figure 6.3 TOSCA spectrum of empty sample can (used as background and subtracted from all following TOSCA spectra).

All of the following spectra have had this background spectrum subtracted from them.

6.5 Outgassed MES-Swollen Phenyl-Modified Mesoporous Silica

A spectrum of the MES-swollen phenyl-modified sample was taken following sample outgassing at 100 °C. It is presented in the range 0 - 4000 cm^{-1} in Figure 6.4, below, in the range 0 - 2000 cm^{-1} in Figure 6.5 and in the range 2000 - 4000 cm^{-1} in Figure 6.6.

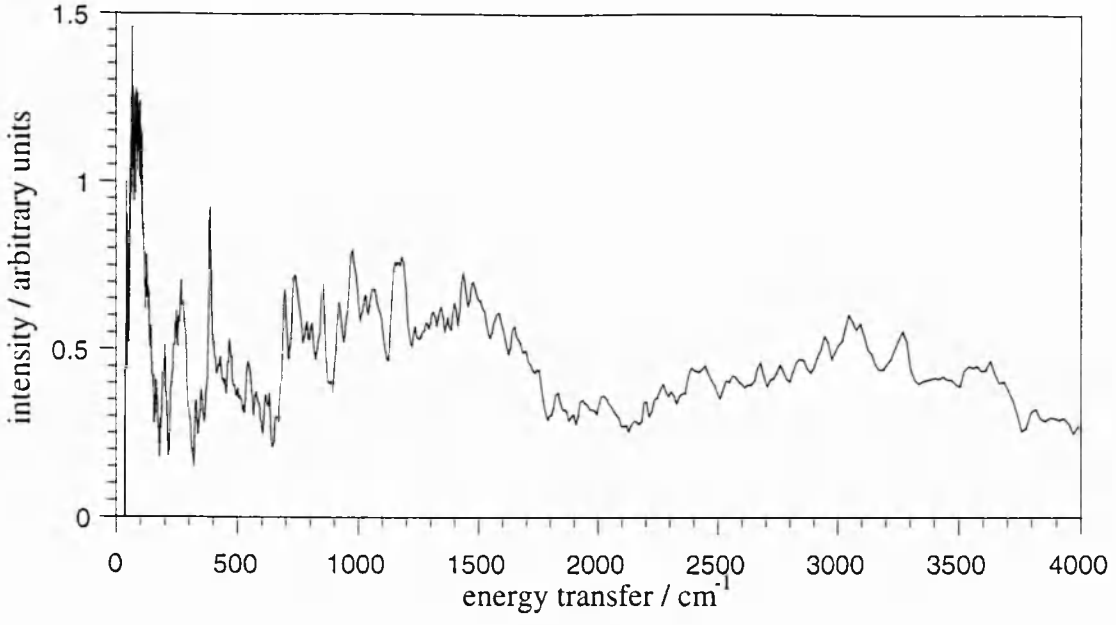

Figure 6.4 Entire TOSCA spectrum of outgassed MES-swollen phenyl-modified mesoporous silica.

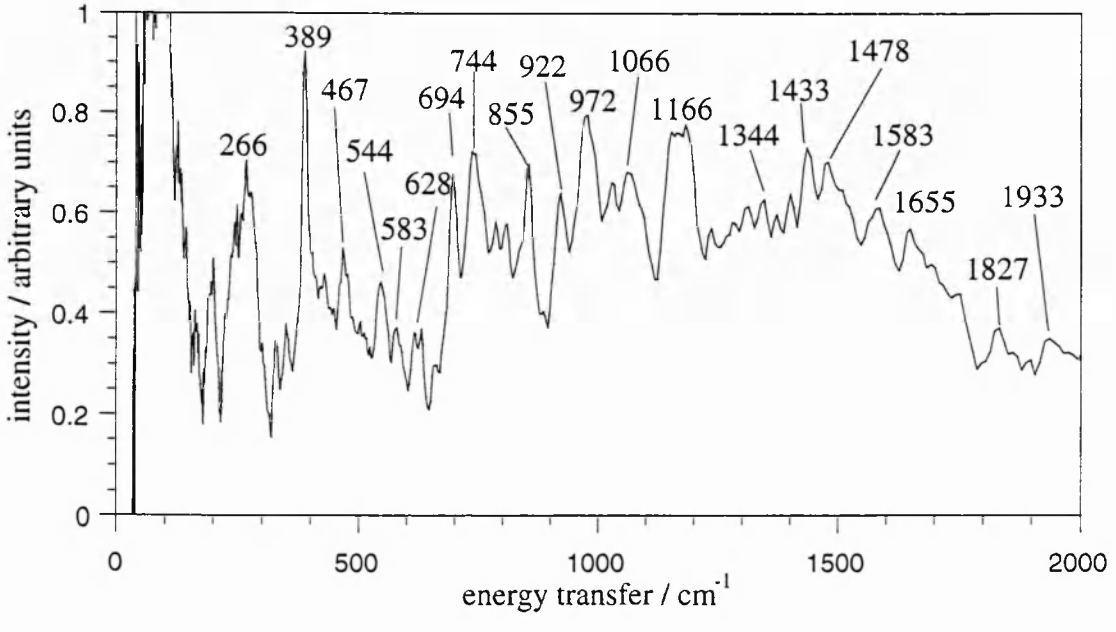

Figure 6.5 TOSCA spectrum of outgassed MES-swollen phenyl-modified mesoporous silica in the range 0 - 2000 cm^{-1}.

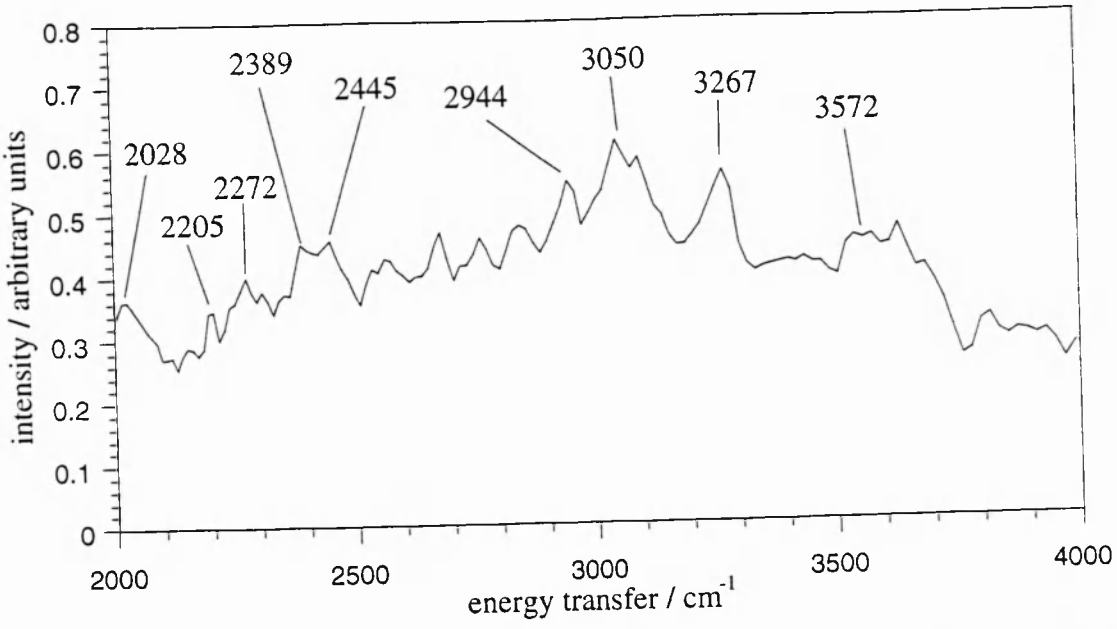

Figure 6.6 TOSCA spectrum of outgassed MES-swollen phenyl-modified mesoporous silica in the range 2000 - 4000 cm^{-1}.

A discussion of the results is given in Section 6.10.

6.6 Benzene

A sample of benzene was analyzed using the same type of sample can as used in the analysis of the powder samples. A volume of 6 cm^3 of benzene was therefore analyzed. The entire benzene spectrum is presented in Figure 6.7, the range 0 - 2000 cm^{-1} is presented in Figure 6.8 and the range 2000 - 4000 cm^{-1} is presented in Figure 6.9.

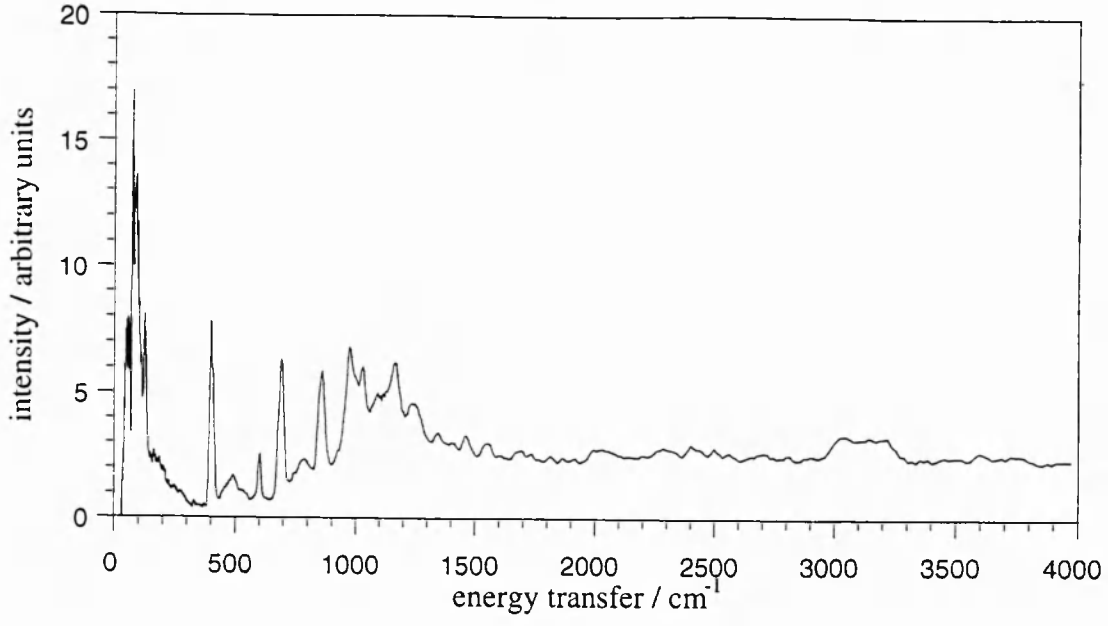

Figure 6.7 The entire TOSCA spectrum of Benzene.

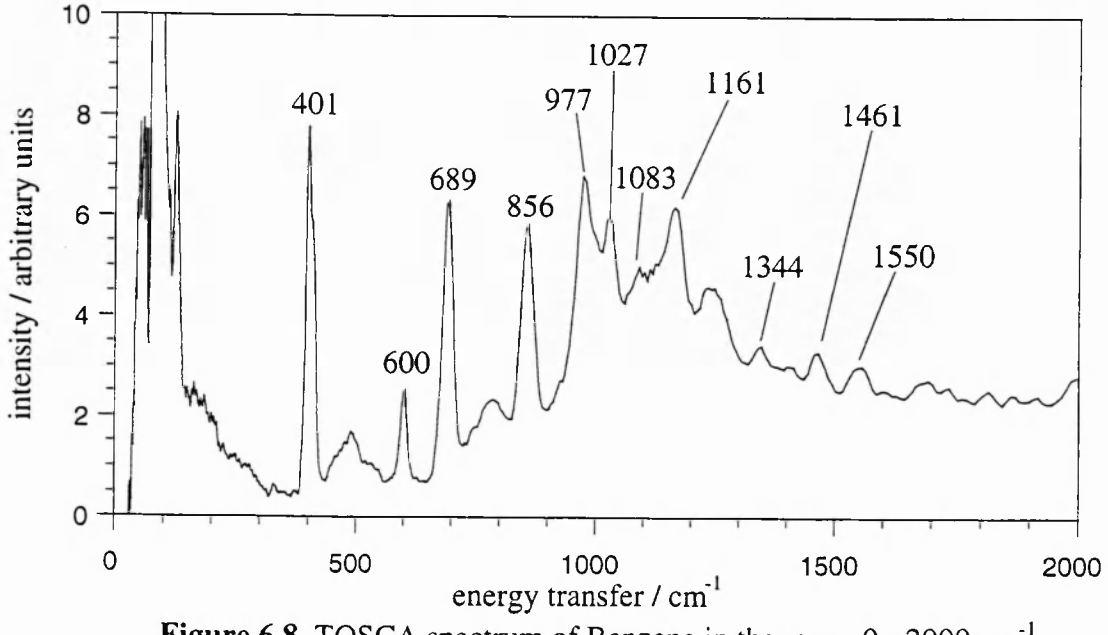

Figure 6.8 TOSCA spectrum of Benzene in the range 0 - 2000 cm^{-1}.

Discussion of the results is given below in Section 6.10.

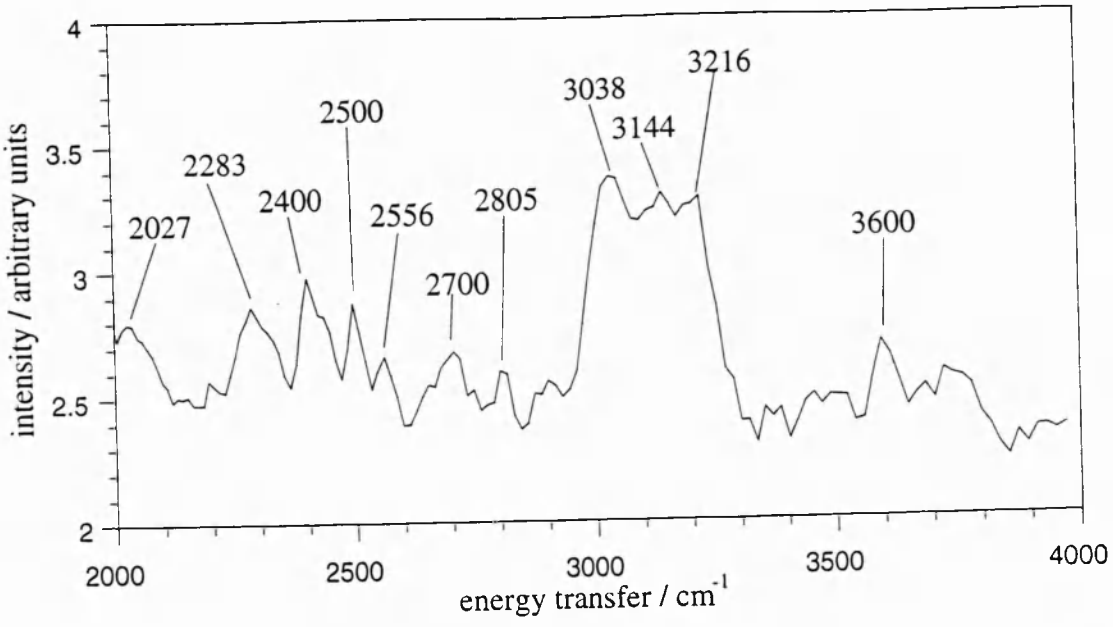

Figure 6.9 TOSCA spectrum of Benzene in the range 2000 - 4000 cm^{-1}.

6.7 Phenyl-Modified Mesoporous Silica with Adsorbed Benzene Monolayer

Due to the fact that TOSCA had only recently been commissioned when this study was undertaken, problems with the sample housing resulted in only approximately one third of this sample lying directly in the neutron beam. This accounts for the low intensity observed in the spectrum presented in Figure 6.10 below.

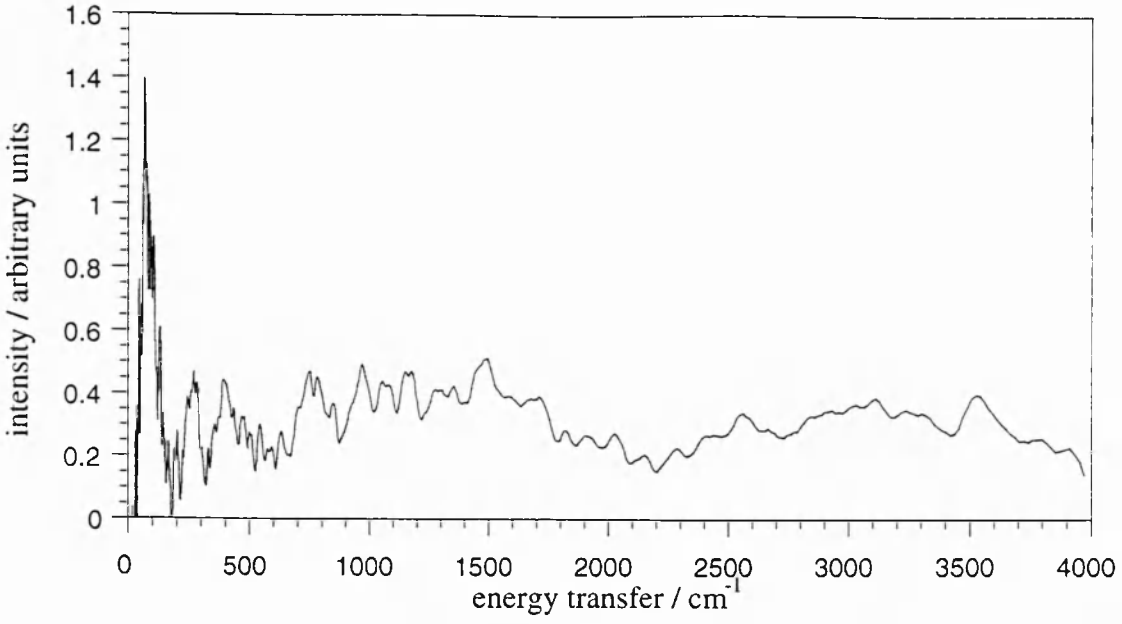

Figure 6.10 TOSCA spectrum of MES-swollen phenyl-modified mesoporous silica containing a C_6H_6 monolayer.

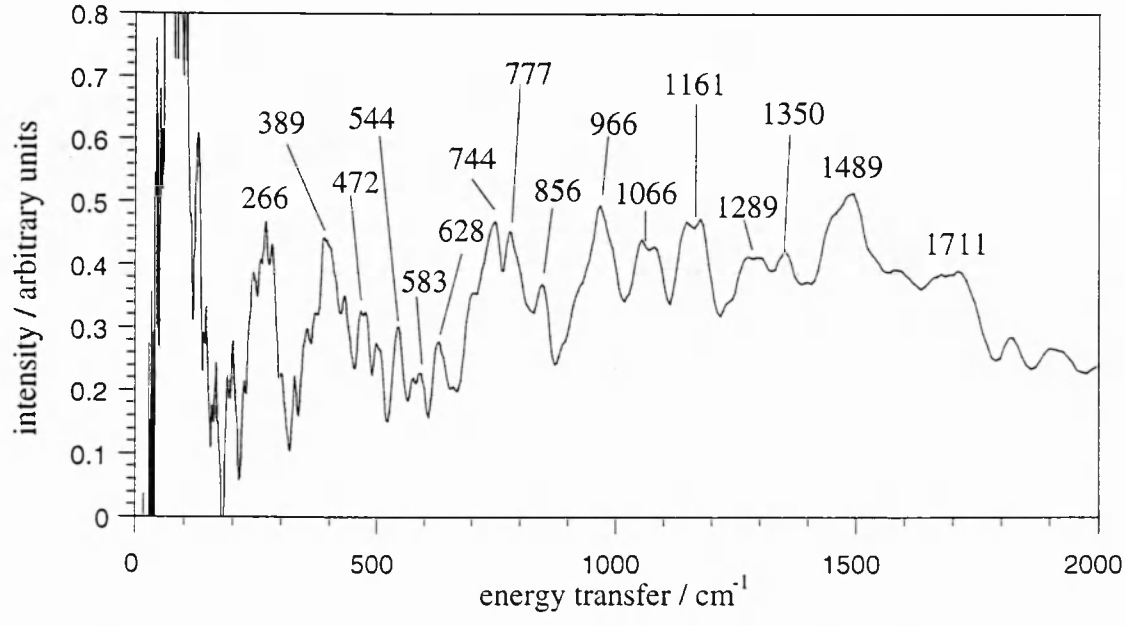

Figure 6.11 TOSCA spectrum of MES-swollen phenyl-modified mesoporous silica containing a C_6H_6 monolayer in the range 0 - 2000 cm^{-1}.

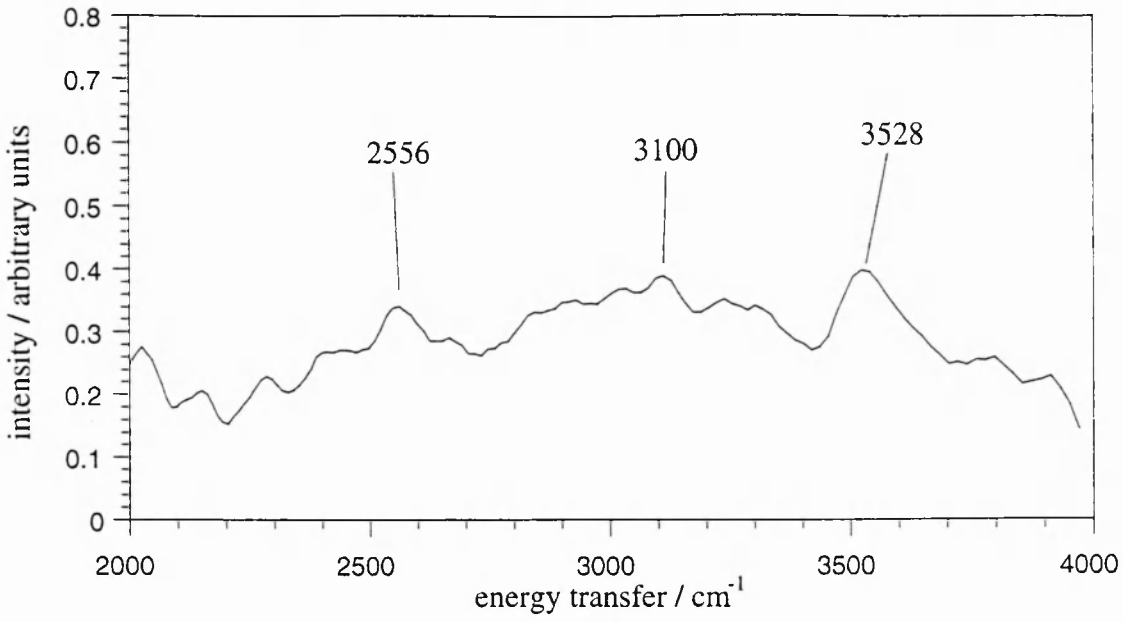

Figure 6.12 TOSCA spectrum of MES-swollen phenyl-modified mesoporous silica containing a C_6H_6 monolayer in the range 2000 - 4000 cm^{-1}.

The very low intensities of these peaks suggests that they may not be "real" features.

6.8 Phenyl-modified Mesoporous Silica with Adsorbed C_6D_6 Monolayer

An analysis was made of the phenyl-modified sample containing a C_6D_6 monolayer. The entire spectrum is presented in Figure 6.13 and expanded spectra are presented in Figures 6.14 and 6.15 respectively.

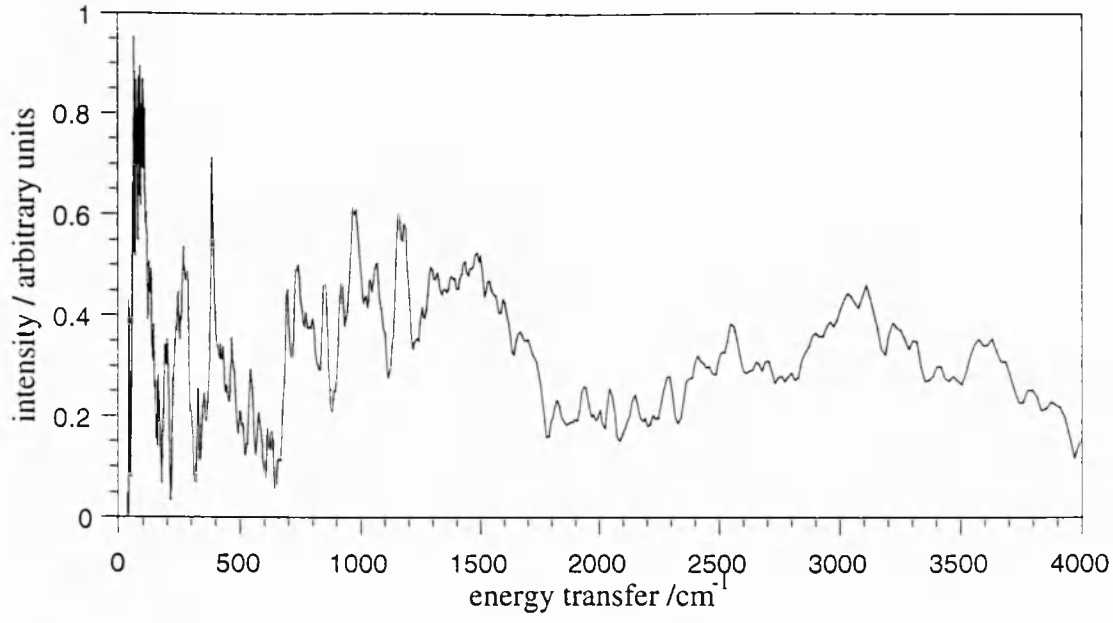

Figure 6.13 TOSCA spectrum of MES-swollen phenyl-modified mesoporous silica containing a C_6D_6 monolayer.

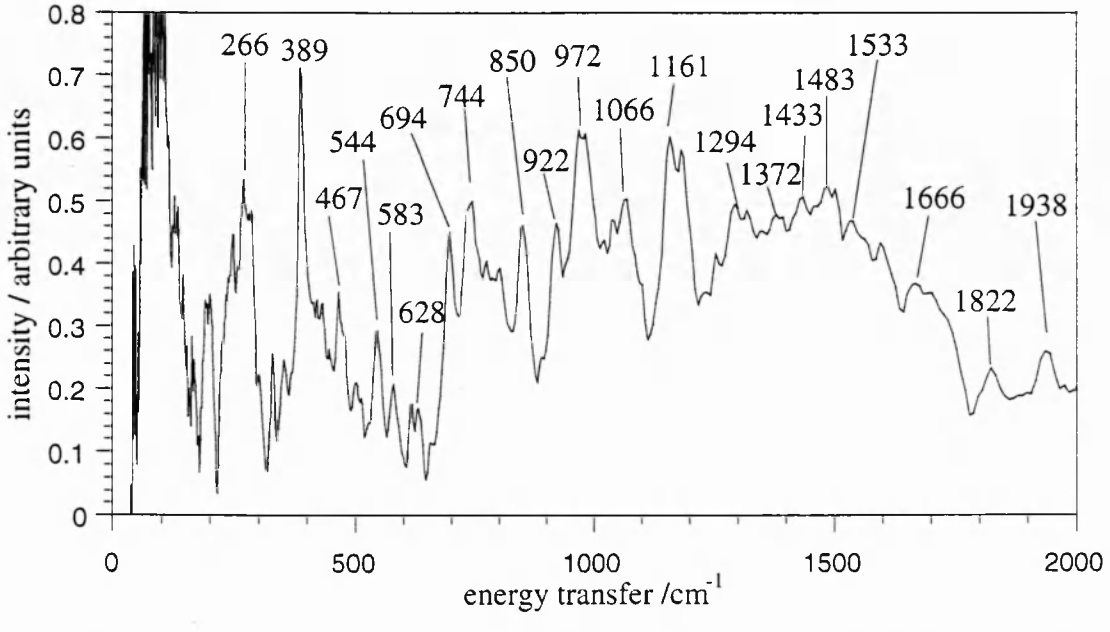

Figure 6.14 TOSCA spectrum of MES-swollen phenyl-modified mesoporous silica containing a C_6D_6 monolayer in the range 0 - 2000 cm^{-1}.

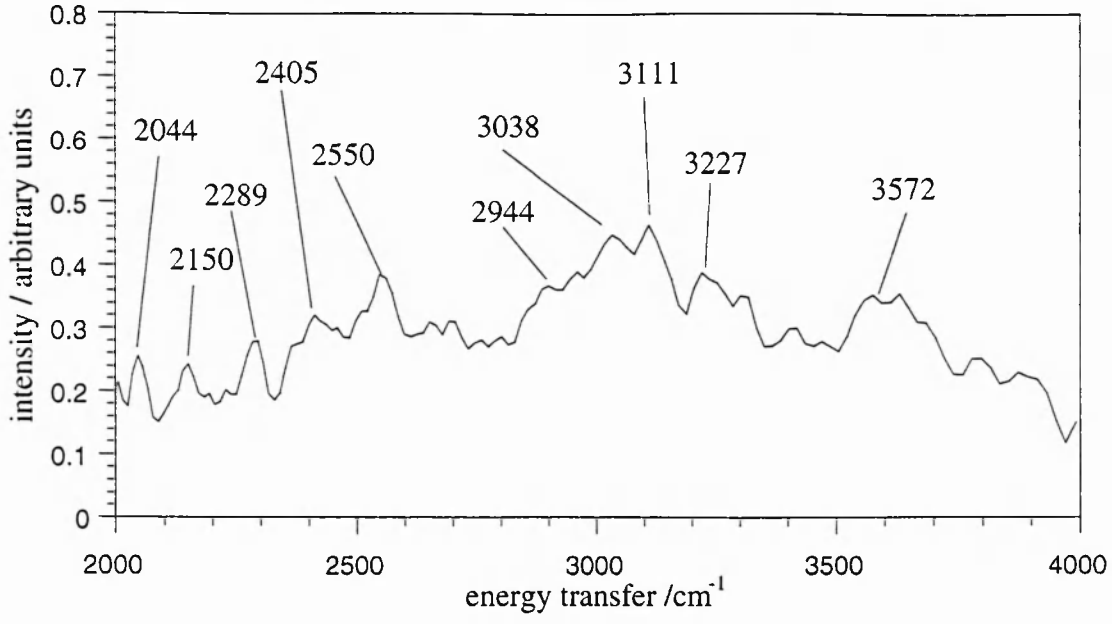

Figure 6.15 TOSCA spectrum of MES-swollen phenyl-modified mesoporous silica containing a C_6D_6 monolayer in the range 2000 - 4000 cm^{-1}.

6.9 Benzene Saturated Phenyl-modified Mesoporous Silica

The entire spectrum given by the benzene saturated material is presented in Figure 6.16, below. Expanded spectra are given in Figures 6.17 and 6.18.

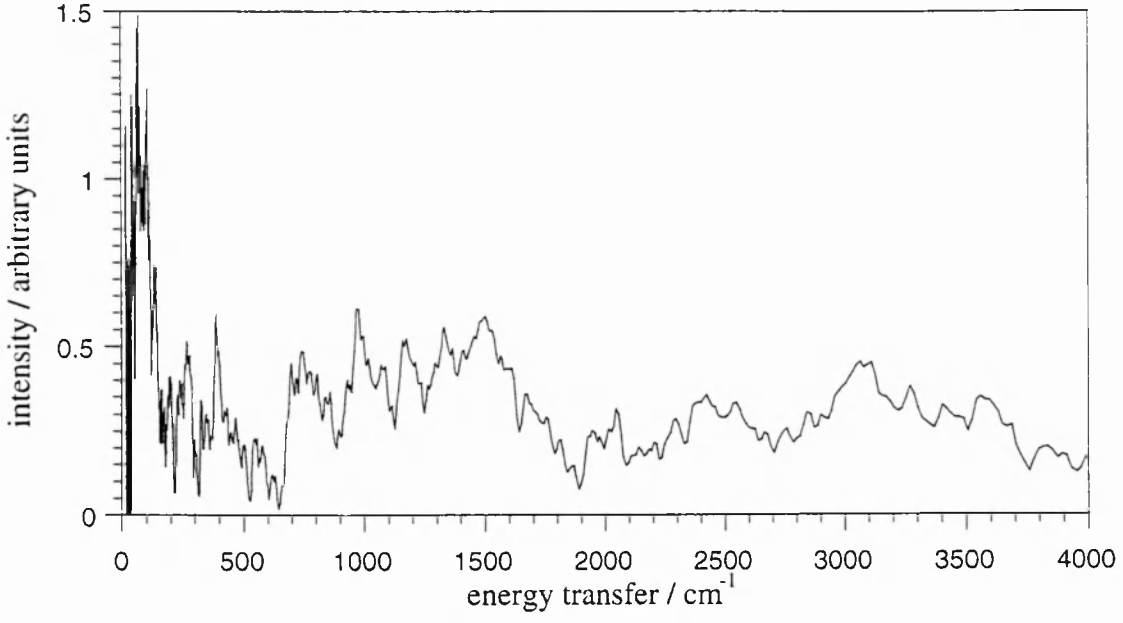

Figure 6.16 TOSCA spectrum of MES-swollen phenyl-modified mesoporous silica saturated with benzene.

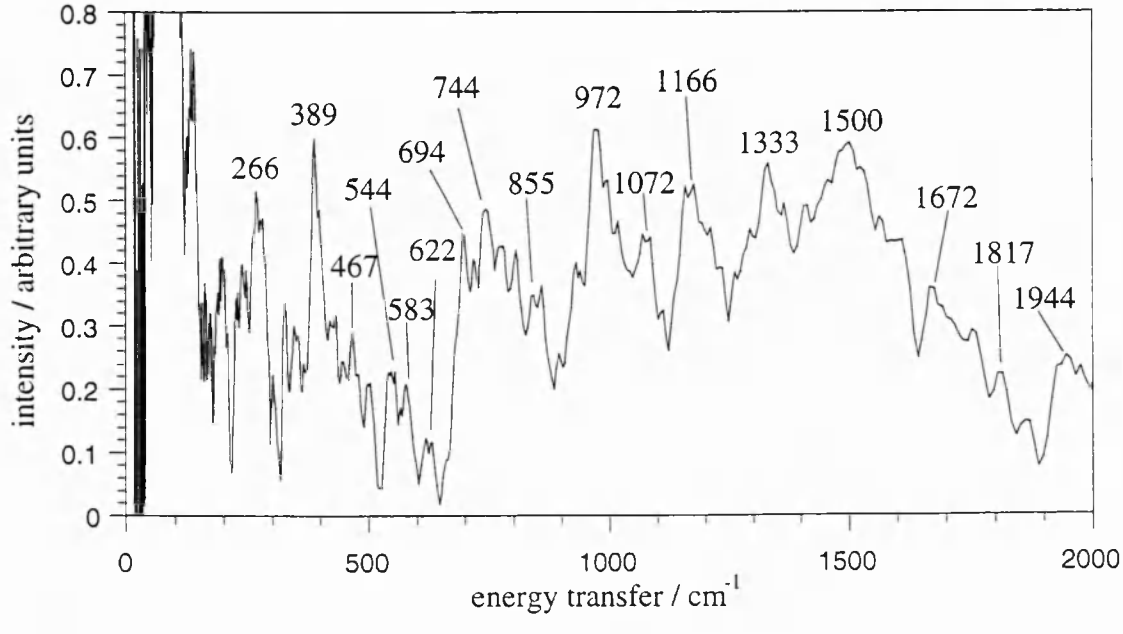

Figure 6.17 TOSCA spectrum, in the range 0 - 2000 cm^{-1}, of MES-swollen phenyl-modified mesoporous silica saturated with benzene.

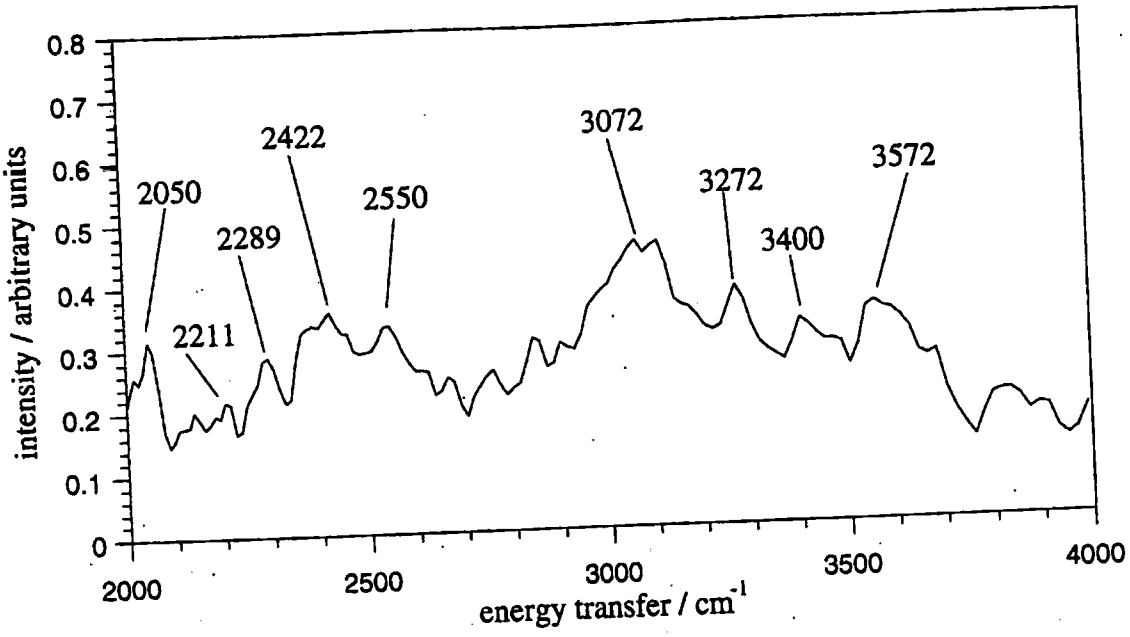

Figure 6.18 TOSCA spectrum, in the range 2000 - 4000 cm^{-1}, of MES-swollen phenyl-modified mesoporous silica saturated with benzene.

6.10 Discussion of TOSCA Results

6.10.1 Vibrational Spectroscopy of Benzene and Phenyl-containing Compounds

The benzene ring displays significant absorptions in five areas of a vibrational spectrum:

1) ring substitution bands occur up to approximately 1000 cm^{-1}

2) C-H deformation vibrations occur between 1000 - 1250 cm^{-1}.

3) C=C stretch vibrations are observed in the region of 1300 - 1665 cm^{-1}

4) Overtones and combination bands are observed between 1665 - 2000 cm^{-1}

5) C-H stretching vibrations are observed in the region of 3000 cm^{-1}

A well-known notation for the classification of compounds containing monosubstituted-phenyl groups is the Whiffen Classification.[10] This classification has been used in this study to assign the spectral bands given by the phenyl-modified silica. It is illustrated in Figure 6.19 below.

The fundamental modes of benzene were assigned by Jobic *et al*[11] in an IINS study of benzene and benzene adsorbed in Na-Y zeolite, carried out using the IN1B spectrometer at the I.L.L in Grenoble. These band assignments for benzene are used in this study and are given in Table 6.3.

The principal band assignments of benzene and of the powder samples, in the range 0 - 2000 cm^{-1}, are given in Table 6.3, below. A sample-by-sample discussion of the results is then given.

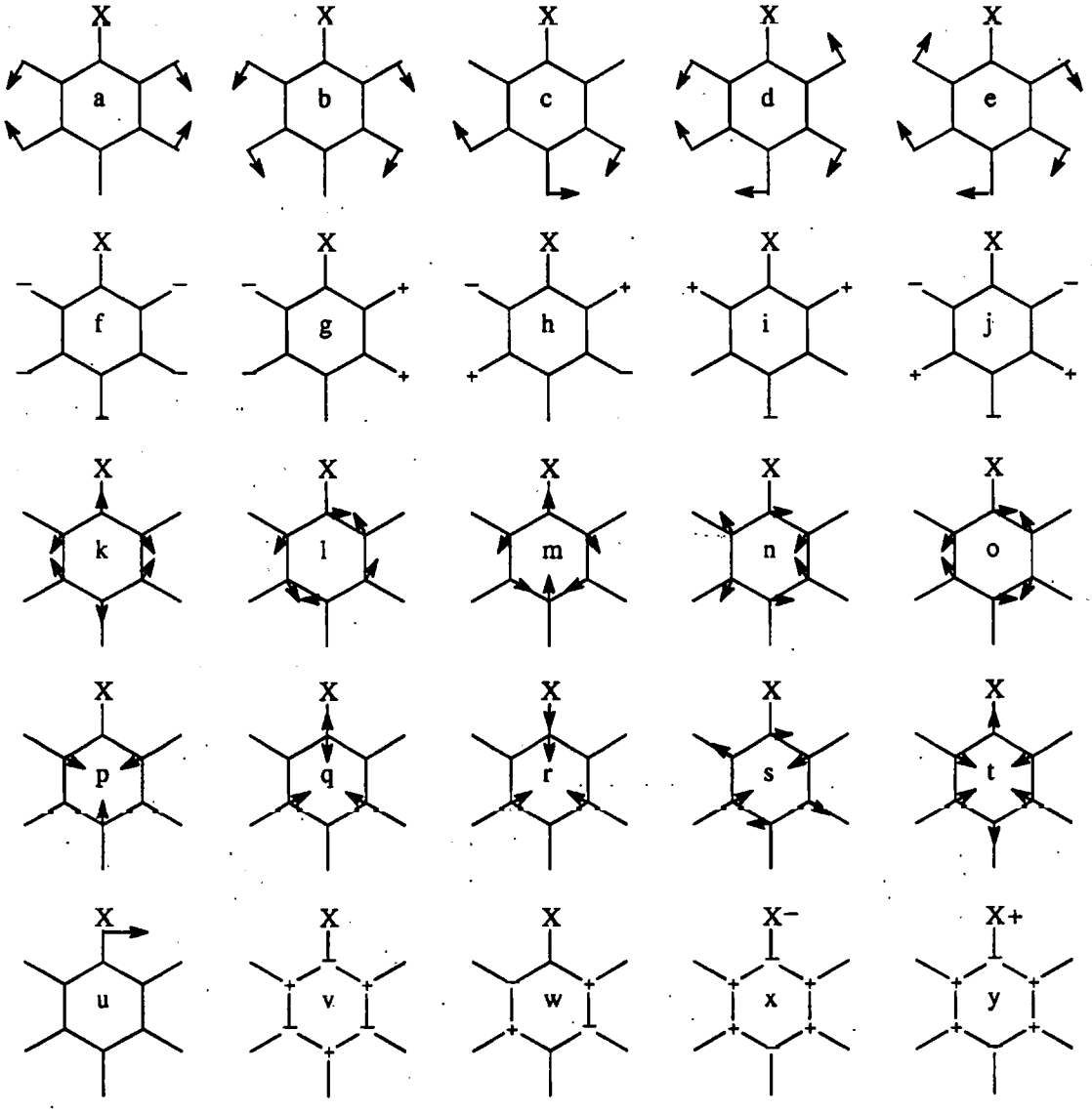

Figure 6.19 The Whiffen Classification of Fundamental Modes of Monosubstituted Phenyls[10]

Table 6.3 TOSCA Principal Band Assignment for Benzene and Ph-M.S.

Energy Transfer / cm^{-1}							
C_6H_6	Ph-M.S.	C_6H_6 Mono.	C_6D_6 Mono.	C_6H_6 Satd.	Assign-ment	Whiffen Notation	Benzene Mode[11]
	266	266	266	266	Si-C rot.		
	389	389	389	389	γ-ring	w	
401					γ-ring		ν_{16}
	467	472	467	467	γ-ring	y	
	544	544	544	544	split peak representing shifted ν_6?		
	583	583	583	583			
600					C-C str		ν_6
	628	628	628	622	δ-ring	s	
689	694	shoulder	694	694 split	γ-ring	v	ν_{11}
	744*	744 split	744	744	γ-(C-H)	f	
856	855	855	850	844 split	γ-(C-H)	g	ν_{10}
	922		922	927	γ-(C-H)	i	
977	972	966	972	972	γ-(C-H)	h	ν_{12}
1027					δ-(C-H)		ν_5
1083	1066	1066	1066	1072	δ-(C-H)	d	ν_{15}
1161	1166	1161	1161	1166	δ-(C-H)	c	ν_9
		1289	1294		δ-(C-H)	e	
1344	1344	1350	1372	1333	δ-(C-C)	o	ν_3
	1433*		1433		δ-(C-C)	n	
1461	1478*	1489	1483		δ-(C-C)	m	ν_{19}
1550			1533	1500	δ-(C-C)	l	ν_8
	1583				δ-(C-C)	k	
	1655		1666	1672	This region represents overtones and combination bands.		
		1711					
	1827		1822	1817			
	1933		1938	1944			

* observed in IR; γ - out-of-plane, δ - in-plane; split - peak splitting observed.

Table 6.4 Principal TOSCA Vibrations in the range 2000 - 4000 cm^{-1}.

Energy Transfer / cm^{-1}				
Benzene	**Ph-M.S.**	**C_6H_6 Monolayer**	**C_6D_6 Monolayer**	**C_6H_6 Saturated**
2027	2028		2044	2050
			2150	
	2205			2211
2283	2272		2289	2289
2400	2389		2405	
2500	2445			2422
2556		2556	2550	2556
2700				
2805				
	2944*		2944 (sh)	
3038	3050	3100	3038	3072
3144				
3216	3267		3227	3272
3600	3572	3572	3572	3572

* observed in IR; sh - shoulder.

6.10.2 Benzene

When considering the TOSCA spectrum of benzene, the most well-defined region is in the range 300 - 1500 cm^{-1}. This region represents in-plane and out-of-plane C-H deformation vibrations as well as C=C stretching vibrations. The spectrum obtained is very similar to that obtained for benzene by Jobic *et al*[11], and the principal band assignments, as classified in that work, are given in Table 6.3. The positions of the

principal C-H stretching vibrations are given in Table 6.4. For a description of the individual vibrational modes of benzene the reader is directed to references 10, 11 and 12.

6.10.3 Phenyl-modified Mesoporous Silica

The principal band assignments for the phenyl-modified samples in the range 0 - 2000 cm^{-1} are given in Table 6.3. The positions of vibrations observed in the region 2000 - 4000 cm^{-1} are shown in Table 6.4 (these vibrations are unassigned and may be due to C-H stretching vibrations they could, however, represent combination bands and overtones). Due to problems with TOSCA's sample-housing and the accompanying uncertainty as to how much of the sample was actually in the beam, the spectra have not been normalized for the mass of the sample.

The peak obtained for the outgassed phenyl-modified silica at 266 cm^{-1} is attributable to the rotation of the phenyl group about its axis through the Si-C bond.[5] The main peak of interest here and in all of the powder samples, however, occurs at an energy transfer of 389 cm^{-1}. According to the Whiffen Classification,[10] this is assigned to the benzene fundamental mode, **w**, which may be envisaged as a "butterfly mode" (Figure 6.19). This mode is usually observed for benzene at 401 cm^{-1} [5] and it appears that this is shifted to a lower energy transfer when the phenyl group is attached directly to a silica surface.

Another interesting feature of all the powder samples is the occurrence of peaks at 544 cm^{-1} and 583 cm^{-1} in each case, as a peak in this position does not occur in the Whiffen classification. It is possible that these peaks are actually a split peak and as the band assigned as ν_6 in the benzene spectrum (600 cm^{-1}) is absent from all of the Ph-

M.S. spectra, it is possible that the corresponding phenyl vibration is shifted to a lower energy transfer for a phenyl group attached directly to a silicon atom. If this vibration corresponds to a surface phenyl (as is suggested by its occurrence in the spectrum of the C_6D_6 monolayer sample), the peak splitting suggests that the surface phenyls are oriented in two different positions.

The peak observed at 694 cm^{-1} could be attributed to a Si-C symmetrical stretch,[5] but Jobic *et al*[11], however, attribute this peak to the phenyl internal mode ν_{11}, denoted **v** in the Whiffen Classification (Figure 6.19). The peak at 744 cm^{-1} is due to the phenyl out-of-plane deformation, **f,** and is also observed in the IR spectrum (see Section 3.7.1). Peaks were also observed in the IR spectrum in the region of 1450 cm^{-1} (corresponding to phenyl C=C stretching vibrations) and a peak, corresponding to vibration **n** can be identified in the TOSCA spectrum at 1443 cm^{-1}. The peak at 2944 cm^{-1}, corresponding to C-H stretching vibrations, is observed in the IR spectrum at 2930 cm^{-1}. The remaining identifiable peaks in the TOSCA spectrum at up to 1600 cm^{-1} can be attributed to the internal modes of phenyl as illustrated in Figure 6.19 and presented in Table 6.3.

6.10.4 Phenyl-modified Mesoporous Silica Containing Adsorbed Benzene

Table 6.3 shows the band assignments of the phenyl-groups in the range 0 - 2000 cm^{-1} for each sample analyzed and the positions of the C-H stretching vibrations are given in Table 6.4.

The "butterfly mode", assigned **w** in the Whiffen classification, is observed at 389 cm^{-1} for each of the samples containing adsorbed benzene. It is a sharp, intense peak in each case apart from in the spectrum given by the sample containing the benzene

monolayer. The spectrum from the latter sample displays a broad, moderately intense peak at 389 cm^{-1}. It is difficult to derive significance from this however, due to the fact that only approximately one-third of this sample was directly in the neutron beam.

There is very little difference between the positions of the peaks in the benzene spectrum and in the outgassed Ph-M.S. spectrum. The similarity in the positions of the peaks in these two spectra make it impossible to determine which peaks are due to benzene and which are due to structural phenyl groups when considering the adsorbed samples. The high loading of phenyl groups means that the peaks observed in the spectra of the adsorbed samples are probably exclusively due to the phenyl groups rather than the adsorbed benzene (the peaks due to benzene are probably present but are overlayed by the peaks due to the phenyl groups). This is highlighted particularly well by comparing the sample containing the C_6D_6 monolayer with the sample saturated with benzene. The peaks are in almost identical positions and as the "C_6D_6 spectrum" is dominated by peaks due to the surface phenyls only (due to the small scattering cross-section of D compared to H) it is evident that most of the peaks in the "saturated" spectrum must also be due to surface phenyls.

There is a notable difference, however, in the presence of a splitting of 23 cm^{-1} of the peak at 694 cm^{-1} for the benzene-saturated sample. This peak is assigned to the out-of-plane deformation vibration v in the Whiffen Classification. As the resolution of the spectrometer is 2 %,[13] these peaks may be regarded as two separate entities. Jobic *et al*[11] identified this splitting in their investigation of benzene adsorbed on Na-Y zeolite. It has also been observed in IR studies[14] of the same system and has been attributed to benzene occupying two different environments on the zeolite surface.

It is possible that in this case the splitting is caused by benzene being oriented both parallel and perpendicular to the surface but, as the sample is saturated with benzene, it is more likely that it corresponds to the different vibrations of structural phenyls and adsorbed benzene. A splitting is also observed, in the saturated sample, of the peak at 844 cm^{-1}. As that splitting is only 17 cm^{-1} in magnitude, it is at the limit of the spectrometer's resolution and it is therefore difficult to resolve these peaks.

A definite splitting is observed in the spectrum given by the sample containing a monolayer of benzene. The peak at 744 cm^{-1} is split by a magnitude of 33 cm^{-1}, well within the spectrometer's resolution, and corresponds to the out-of-plane C-H deformation **f**, in the Whiffen Classification; the splitting is evidence that benzene is adsorbed on the surface. The large difference in the values of these two peaks may reflect the structural phenyl groups and adsorbed benzene being present in two different orientations. If the structural phenyls are assumed to be oriented perpendicular to the surface, then it seems that the adsorbed benzene is lying flat on the surface, as suggested by benzene sorption studies.

Further evidence that adsorbed benzene is present in both of the monolayer samples (C_6H_6 and C_6D_6) is the presence of a peak at approximately 1290 cm^{-1} in each case. Peaks are also observed at 2150 cm^{-1} in the C_6H_6 monolayer sample and at *ca.* 2550 cm^{-1} in all of the adsorbed samples. As previously mentioned, vibrations in the C_6D_6 monolayer spectrum are due exclusively to the structural phenyls and not the adsorbed benzene. The fact that peaks are observed for the C_6D_6 monolayer sample and not for the outgassed "blank" sample, suggests that it is interaction between the structural phenyls and the adsorbed molecules that is permitting the resolution of these vibrations.

6.10.4 Conclusions

Due to the large loading of phenyl groups in the sample under investigation, it was very difficult to differentiate between structural phenyl groups and adsorbed benzene. The IINS analysis of a purely siliceous control sample, which would have alleviated this problem, was not possible due to problems with the newly commissioned apparatus.

Peak-splitting in the sample containing a C_6H_6 monolayer, and in the C_6H_6-saturated sample, identified the presence of adsorbed benzene and possibly indicated molecular orientation parallel to the surface. Vibrations at *ca.* 1290 cm^{-1} in the C_6H_6- and C_6D_6- monolayer-containing samples, and also at 2150 cm^{-1} and *ca.* 2550 cm^{-1}, which are absent in the spectrum given by the outgassed sample, indicated interaction between the structural phenyl and adsorbed benzene.

REFERENCES

1. Windsor, C.G., *"Pulsed Neutron Scattering"*, Taylor and Francis Ltd., London, **1981**.
2. Howard, J.; Bowland, B.C.; Tomkinson, J., *Chem. Phys.*, **1983**, *77*, 145.
3. Bacon, G.E., *"Neutron Diffraction"*, Clarendon Press, Oxford, **1955**.
4. Bacon, G.E., *"Neutron Scattering in Chemistry"*, Butterworths, Sevenoaks, **1977**.
5. Maynard, S.C.P., PhD Thesis, University of Exeter, **1991**.
6. Young, K.E., PhD Thesis, University of Exeter, **1991**.
7. Mangel, A., PhD Thesis, University of Exeter, **1994**.
8. Parker, S.F.; Carlile, C.J.; Pike, T.; Tomkinson, J.; Newport, R.J.; Andreani, C.; Ricci, F.P.; Sacchetti, F.; Zoppi, M., *Physica B*, **1998**, (*241-243*), 154-156.
9. Gregg, S.J.; Sing K.S.W., *"Adsorption, Surface Area and Porosity"*, 2nd Edition, *p.80*, Academic Press, London, **1982**.
10. Whiffen, D.H.; *J. Chem. Soc.*, **1956**, 1350.
11. Jobic, H.; Renouprez, A.; Fitch, A.N.; Lauter, H.J., *J. Chem. Soc., Faraday Trans.*, **1987**, *83*(10), 3199-3205.
12. Nakamoto, K., *"Infra-Red and Raman Spectra of Inorganic and Co-ordination Compounds"*, Fourth Edition, John Wiley and Sons, New York, **1986**.
13. S.Parker, TOSCA Instrument Scientist, Private Communication.
14. Primet, M.; Garbowski, E.; Mathieu, M.; Imelik, B., *J. Chem. Soc., Faraday Trans.*, **1980**, *76*, 1942.

CHAPTER 7

OVERVIEW AND CONCLUSIONS

7.1 M41S Solids

A series of MCM-41-type samples (S_{sp} = 500 m^2 g^{-1} - 950 m^2 g^{-1}) has been synthesized *via* a liquid crystal templating mechanism. Nitrogen sorption was carried out at 77 K on each sample and gave Type IV isotherms in each case, indicating that the materials were mesoporous. The nitrogen isotherms and XRD studies demonstrated that heating the reaction mixture in a sealed teflon bottle yielded a material with a uniform hexagonally-ordered pore structure and narrow pore size distribution. Conversely, samples synthesized in a microwave oven, or by stirring at ambient temperature and pressure, gave poor XRD profiles and ill-defined nitrogen-sorption isotherms.

Water sorption at 303 K on sample MCM-41(c) gave a Type V isotherm, indicating that the sample was hydrophobic. A large degree of hysteresis was observed, continuing to the low-pressure region, suggesting that rehydroxylation of the surface had occurred. This was confirmed by ^{29}Si MAS-NMR performed on the sample before and after water sorption. This result demonstrates that, although the sample is hydrophobic at low p/p^0 values, once it is exposed to a high vapour pressure of water it undergoes surface modification / chemisorption. This is in contrast to the MCM-41 samples analyzed by Branton *et al*[1] which were stable to water vapour. The difference may be due to the Branton samples being synthesized at high pressure and temperature, and

therefore undergoing more complete condensation in synthesis than the samples described here.

^{27}Al MAS-NMR, performed on sample MCM-41(a) and MCM-41(c), revealed that Al was present in a tetrahedral environment in both samples before calcination but was only present, in significant amounts, in sample MCM-41(c) following calcination. As tetrahedral aluminium is required for acid catalysis purposes, this result suggests that samples of the MCM-41(c)-type (synthesized using aluminium sulphate as the aluminium source) will be of greater interest.

7.2 Organically-modified Mesoporous Silica.

A range of organically-modified mesoporous silicas ($S_{sp} \approx 300\ m^2\ g^{-1}$ - 1350 $m^2\ g^{-1}$) has been synthesized. Nitrogen sorption isotherms, measured on these materials at 77 K, demonstrated that the incorporation of organic functions reduced the pore diameter and yielded microporous materials. The use of auxiliary organics as pore-swelling agents was investigated and mesitylene was proved to be successful in the formation of mesoporous phenyl-modified material. In contrast, tetradecane did not successfully swell the pores of a phenyl-modified sample and led to a microporous product.

^{29}Si MAS-NMR studies, carried out on the phenyl-, aminopropyl- and mercaptopropyl-modified materials confirmed the presence of organosilicon groups and ^{13}C MAS-NMR studies confirmed the presence of the phenyl and aminopropyl function. The ^{13}C MAS-NMR spectrum of the mercaptopropyl-modified material indicated the

presence of more than one sulphur-containing function (possibly propanthiol and propansulphonic acid).

The adsorption isotherms of water, benzene, *n*-butanol and *t*-butanol were measured for the phenyl-modified materials. N_2, benzene and *t*-butanol sorption on the unswollen sample yielded Type I isotherms, confirming the sample's microporosity. Type IV isotherms were given by these adsorptives on the mesitylene-swollen sample, demonstrating the presence of mesopores.

Comparison of *n*-butanol and *t*-butanol sorption on the unswollen and MES-swollen phenyl-modified samples demonstrated differences in the sorption mechanism of these adsorbates on these solids. *n*-BuOH sorption was sterically hindered in the microporous sample and a large degree of localized adsorption was demonstrated from the calculated number of surface hydroxyl groups. *t*-BuOH sorption on the unswollen sample gave an isotherm which could be completely superimposed on the benzene isotherm of this sample demonstrating that the mechanism of *t*-BuOH sorption is likely to involve organic interactions with the surface phenyls. Neither *n*- nor *t*-BuOH sorption was sterically hindered on the MES-swollen sample. Virtually identical isotherms were obtained making it impossible to determine the mechanisms of adsorption.

Water sorption (performed on the unswollen sample only) gave a Type V isotherm demonstrating the sample's hydrophobicity.

IINS studies of the phenyl-modified silica containing adsorbed benzene, detected the presence of the adsorbed species and differentiated between structural phenyls and adsorbed benzene.

7.3 Suggestions for Future Work

Future investigations of this work could include:

1. Mössbauer studies of the iron-containing MCM-41, in order to determine how the iron is incorporated into the framework.
2. A study of the acid sites in the aluminosilicate materials, *via* IR studies of adsorbed probe molecules such as pyridine
3. Development of the organically-modified materials for use as catalysts
4. Catalytic testing of the materials
5. Characterization of the silica spheres (Section 3.12)

REFERENCES

1. Branton, P. J.; Hall, P.G.; Treguer, M.; Sing, K.S.W., *J. Chem. Soc., Faraday Trans.*, **1995**, *91*(13), 2041-2043.

APPENDICES

APPENDIX A1 - XRD PROFILES

A1.1 M41S Materials

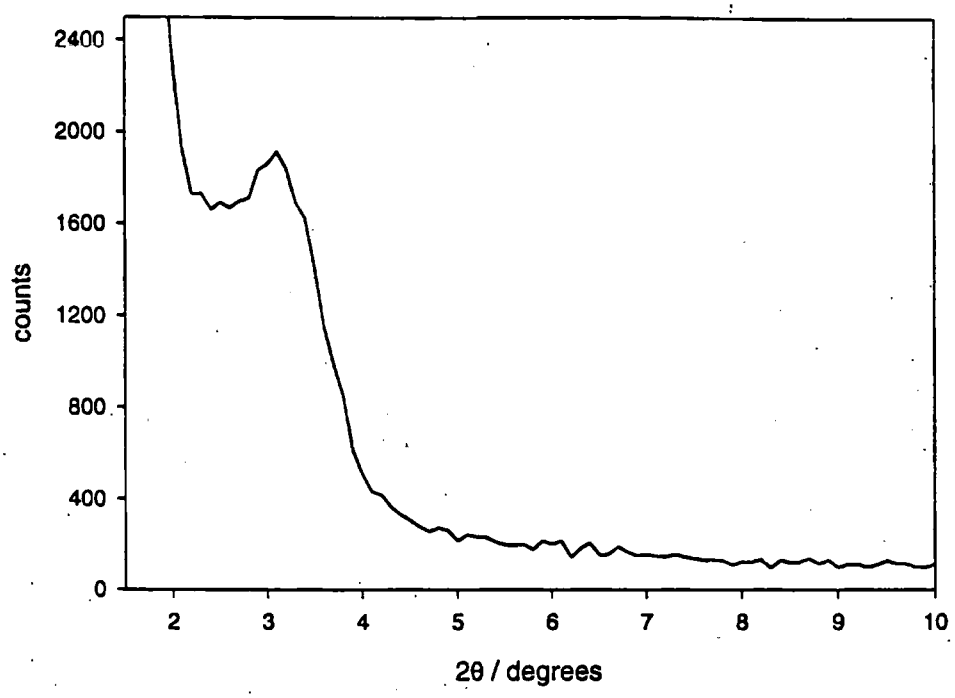

Figure A.1 XRD Profile of Calcined MCM-41(a)

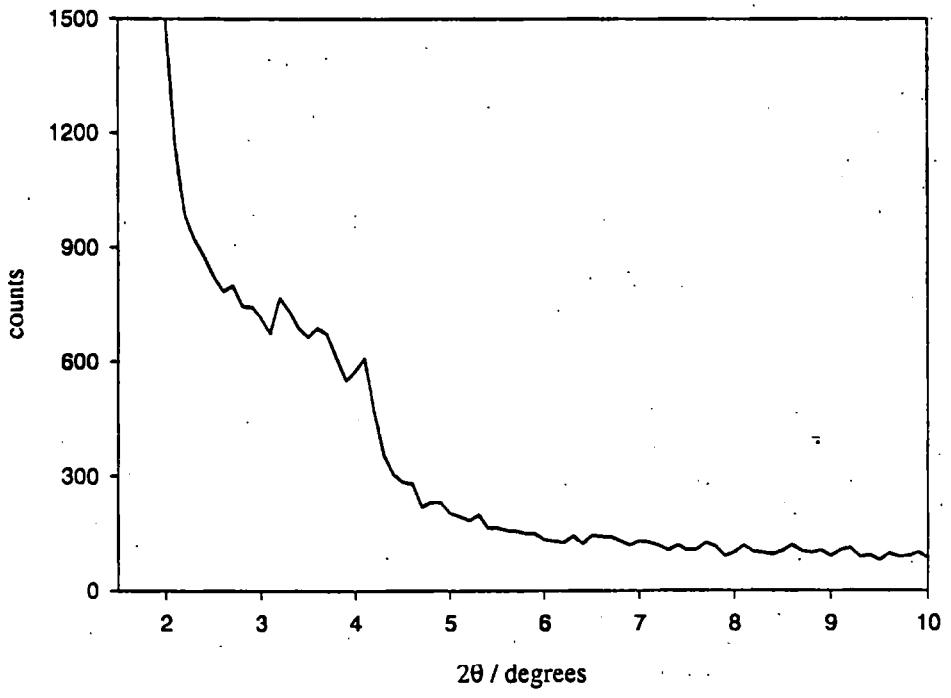

Figure A.2 XRD Profile of Calcined MCM-41(b)

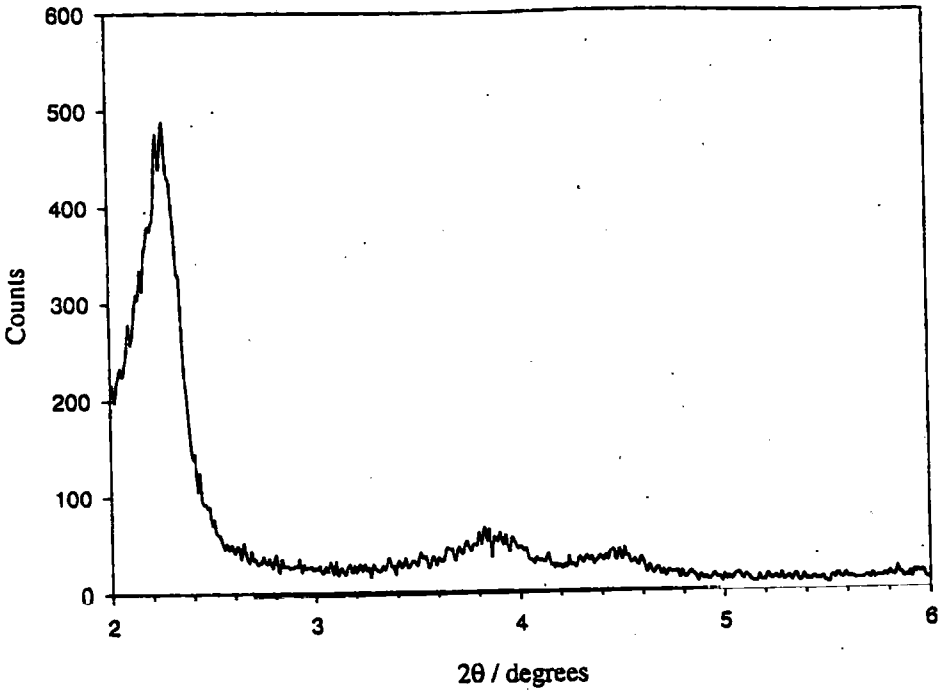

Figure A.3 XRD Profile of Calcined MCM-41(c)

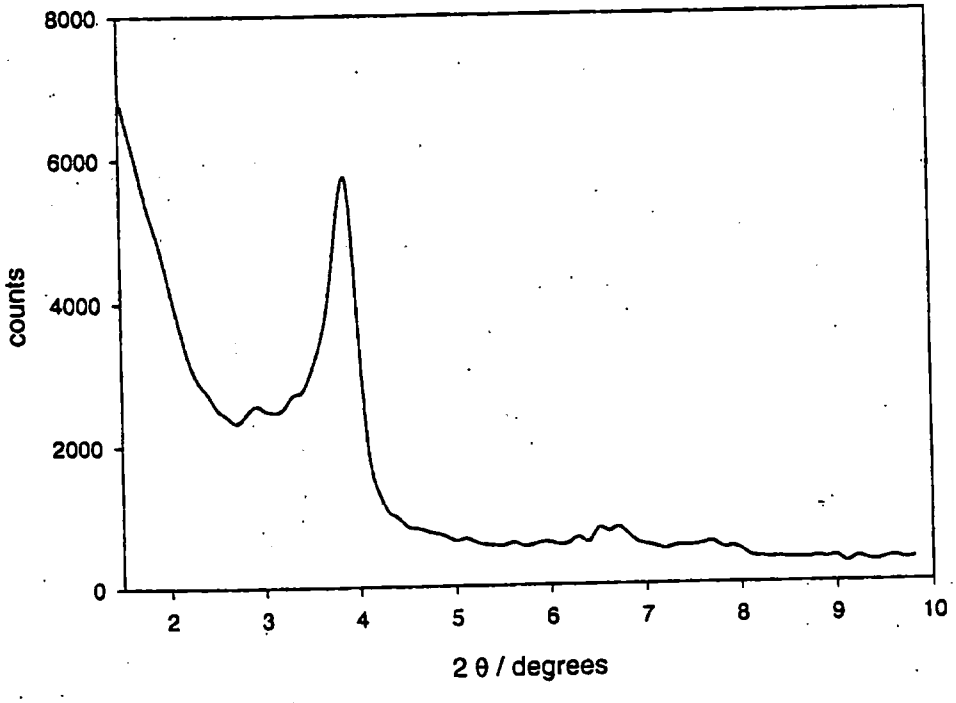

Figure A.4 XRD Profile of MCM-41(d) (Cr Kα radiation)

A1.2 Organically-Modified Mesoporous Silica

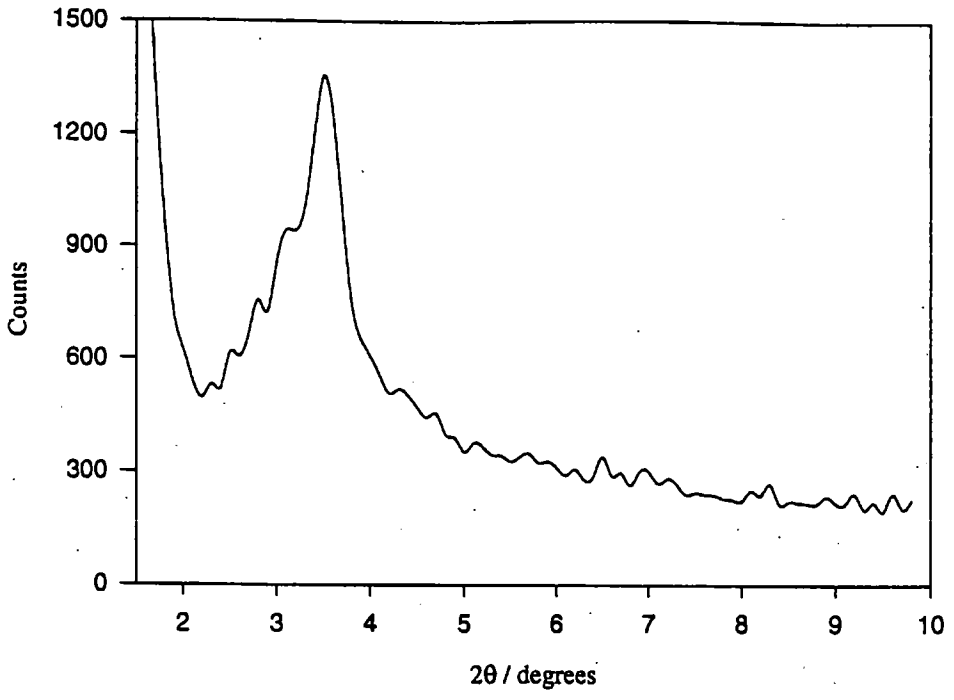

Figure A.5 Unswollen As-Synthesized Phenyl-Modified Mesoporous Silica

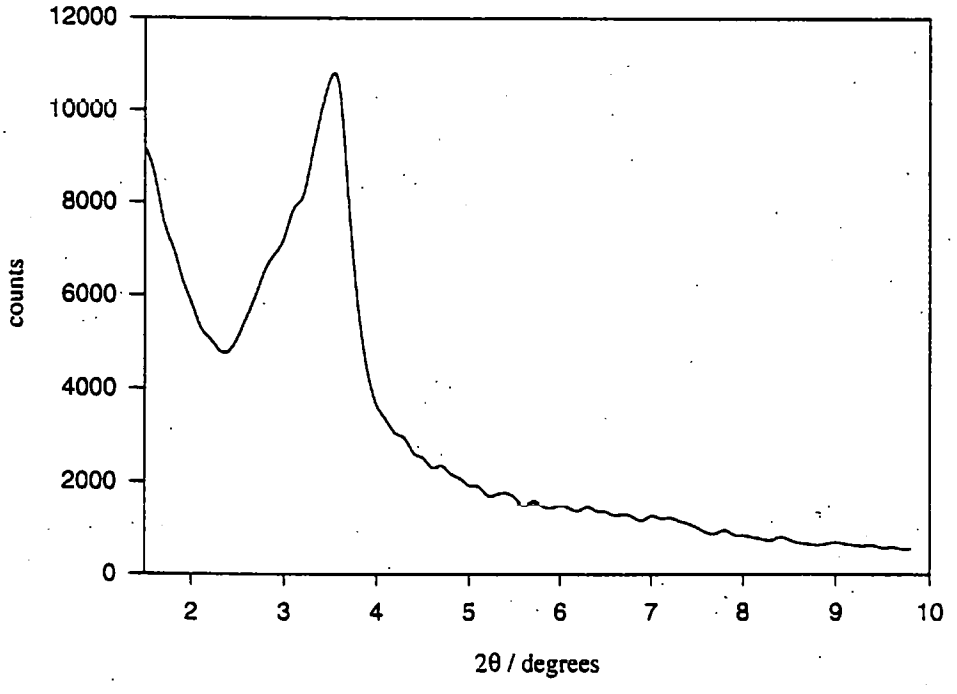

Figure A.6 Unswollen Phenyl-Modified Mesoporous Silica Following Surfactant Extraction

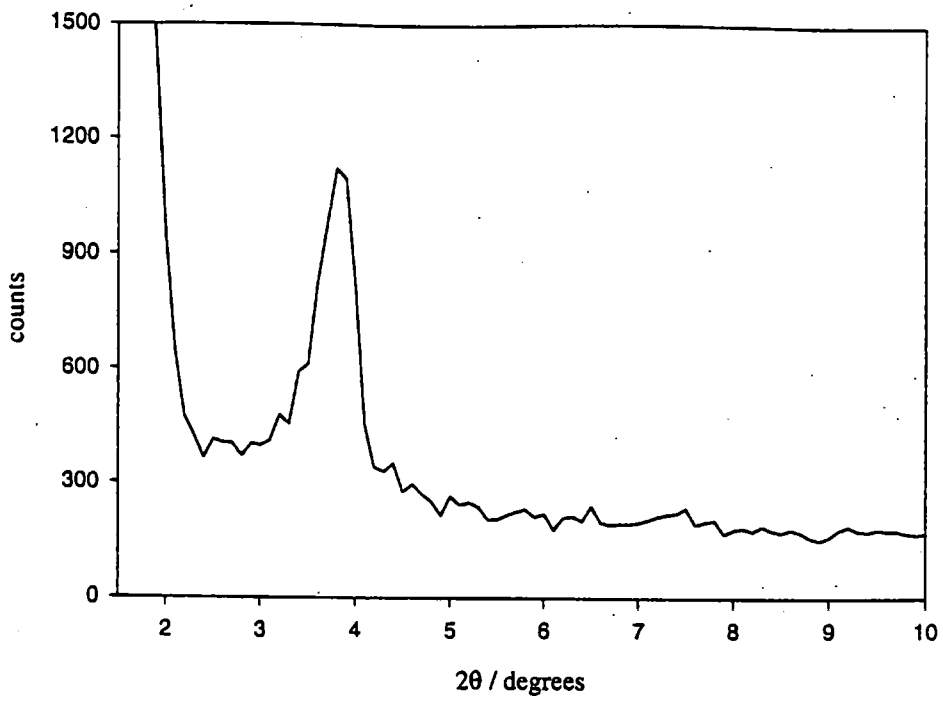

Figure A.7 As-Synthesized TET-Swollen Phenyl-Modified Mesoporous Silica

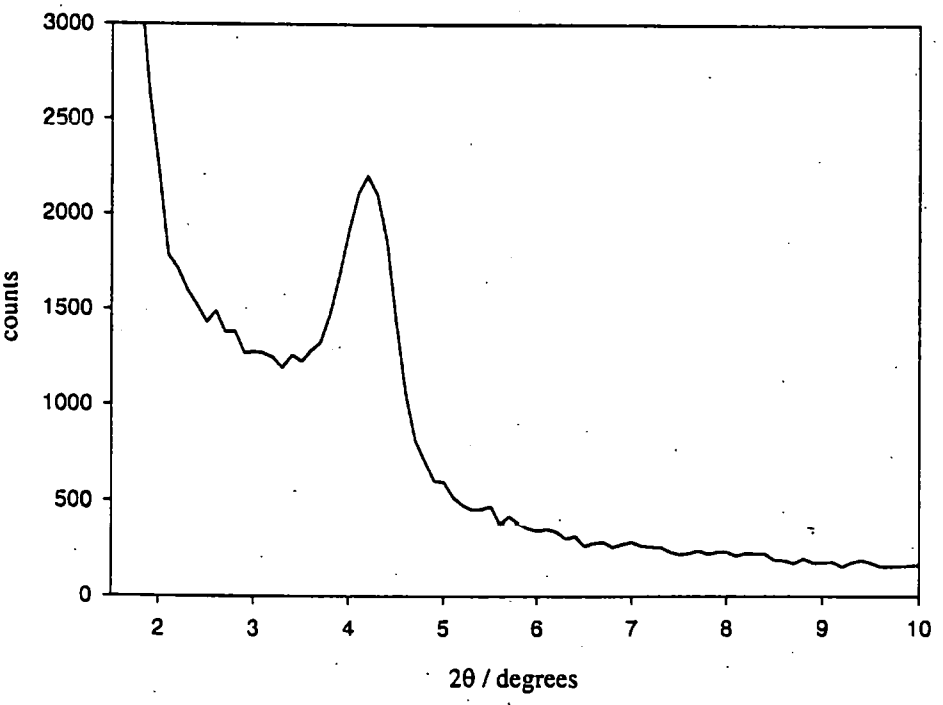

Figure A.8 TET-Swollen Phenyl-Modified Mesoporous Silica Following Template Removal

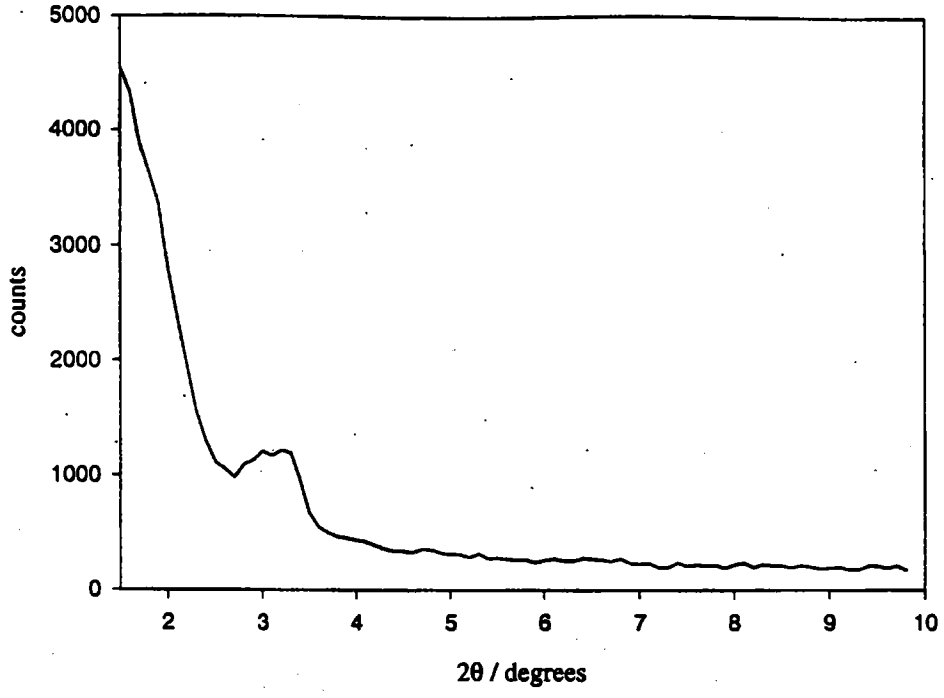

Figure A.9 As-Synthesized Vinyl-Modified Mesoporous Silica

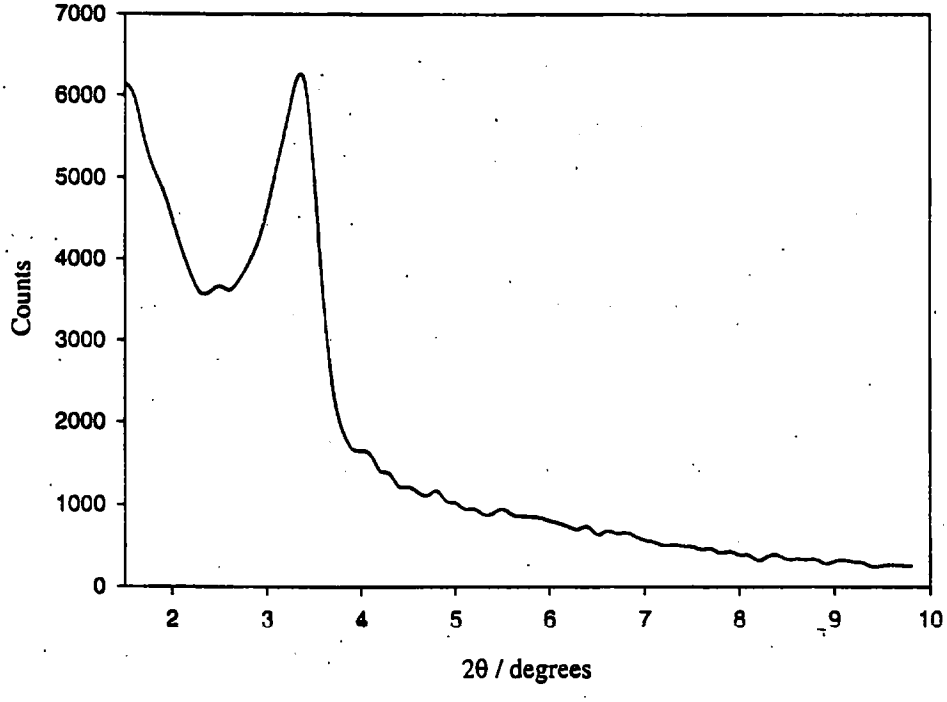

Figure A.10 Vinyl-Modified Mesoporous Silica Following Template Removal

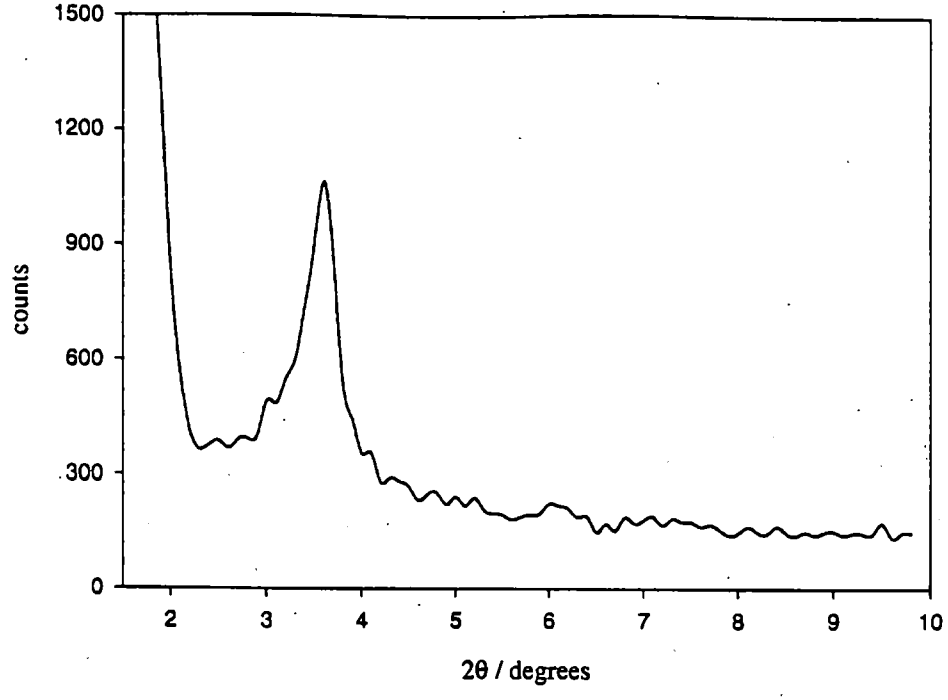

Figure A.11 As-Synthesized Mercaptopropyl-Modified Mesoporous Silica

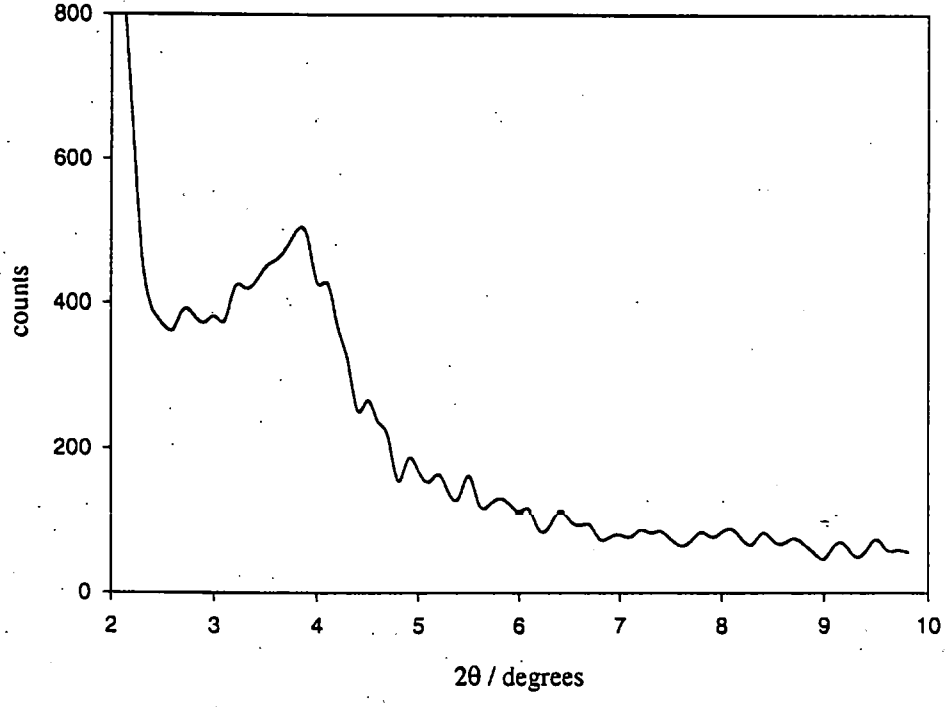

Figure A.12 Mercaptopropyl-Modified Mesoporous Silica Following Template Removal

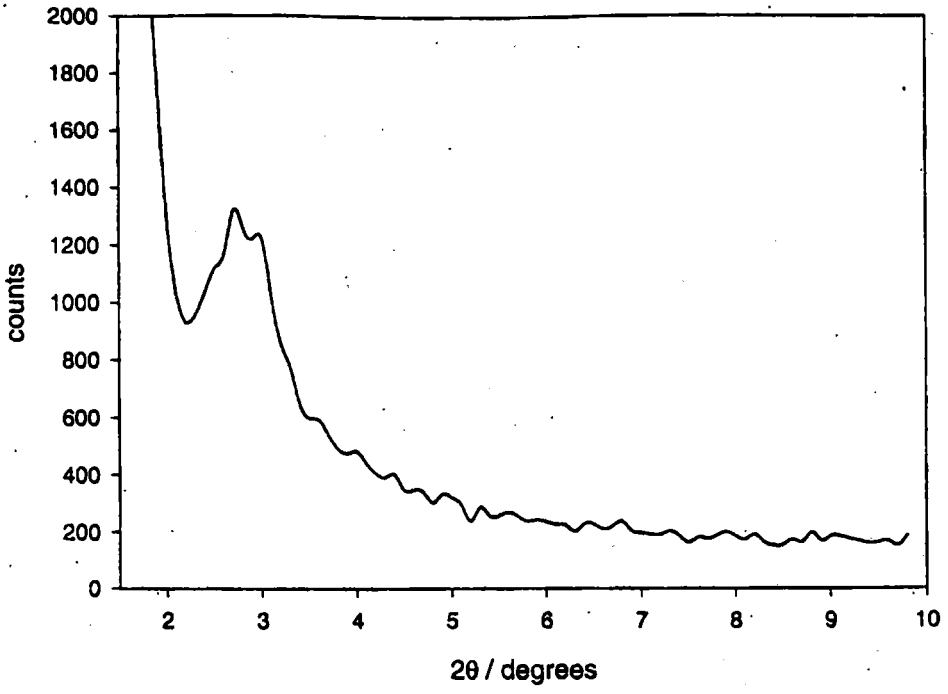

Figure A.13 As-Synthesized Aminopropyl-Modified Mesoporous Silica

APPENDIX A2 - IR SPECTRA

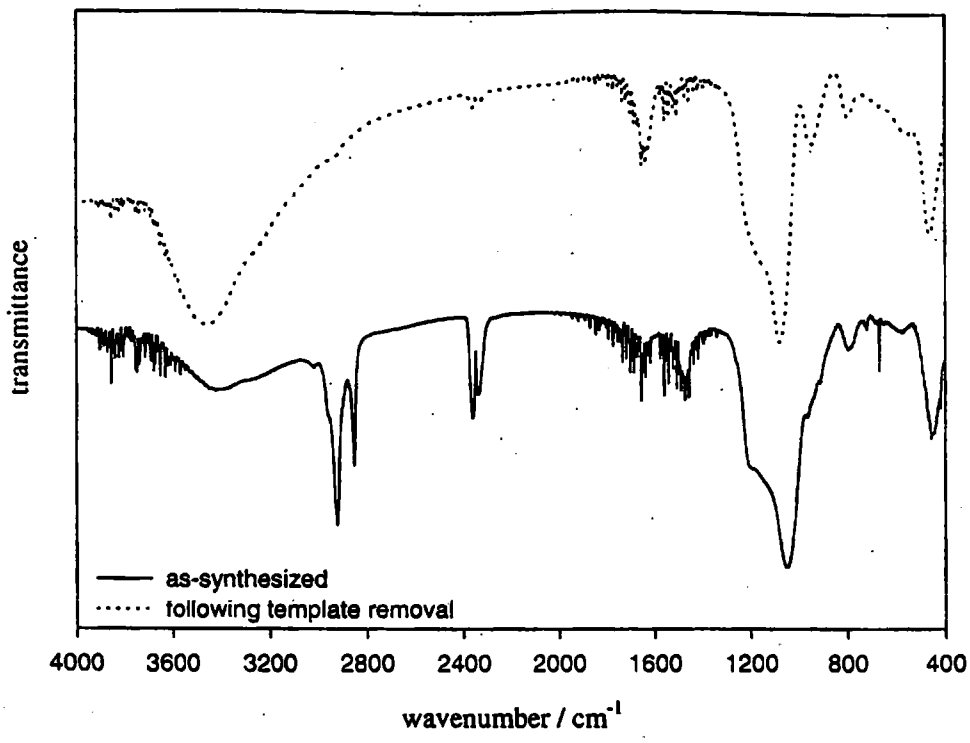

Figure A.14 I.R. Spectra of Aminopropyl-Modified Mesoporous Silica

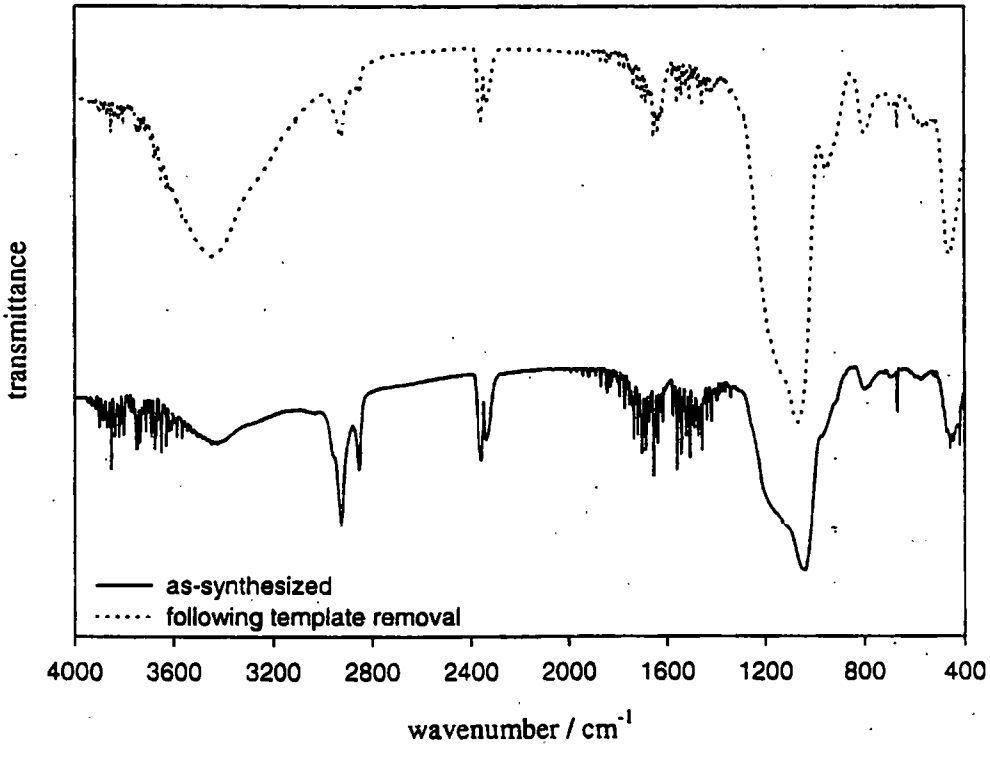

Figure A.15 I.R. Spectra of Mercaptopropyl-Modified Mesoporous Silica

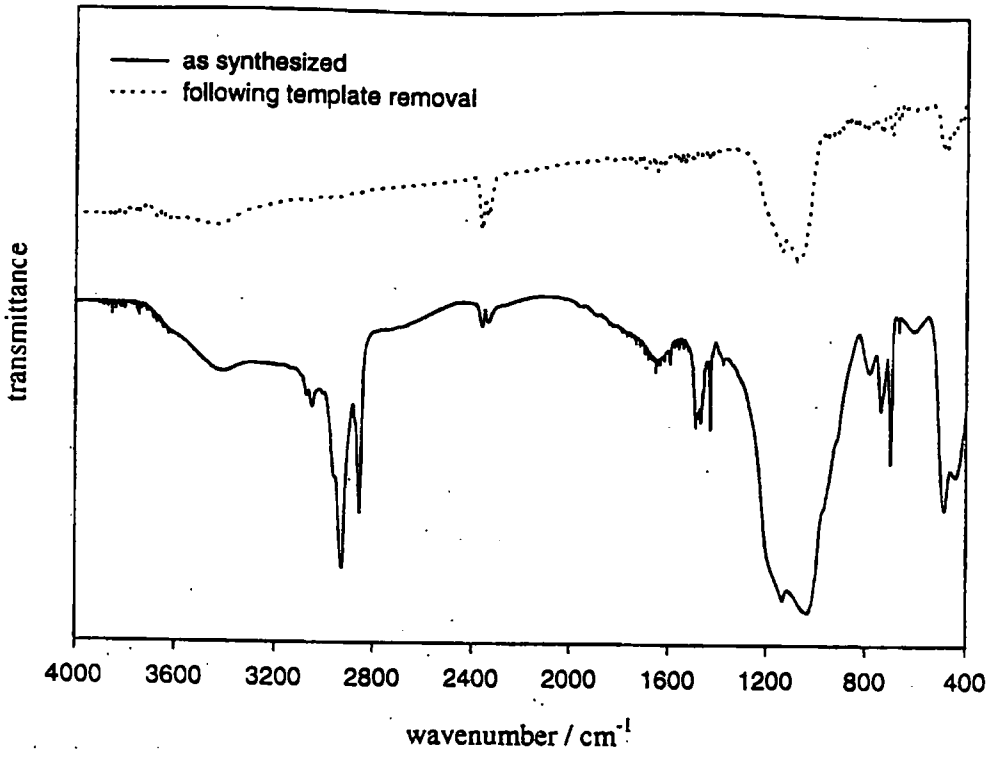

Figure A.16 I.R. Spectra of Tetradecane-Swollen, Phenyl-Modified Mesoporous Silica

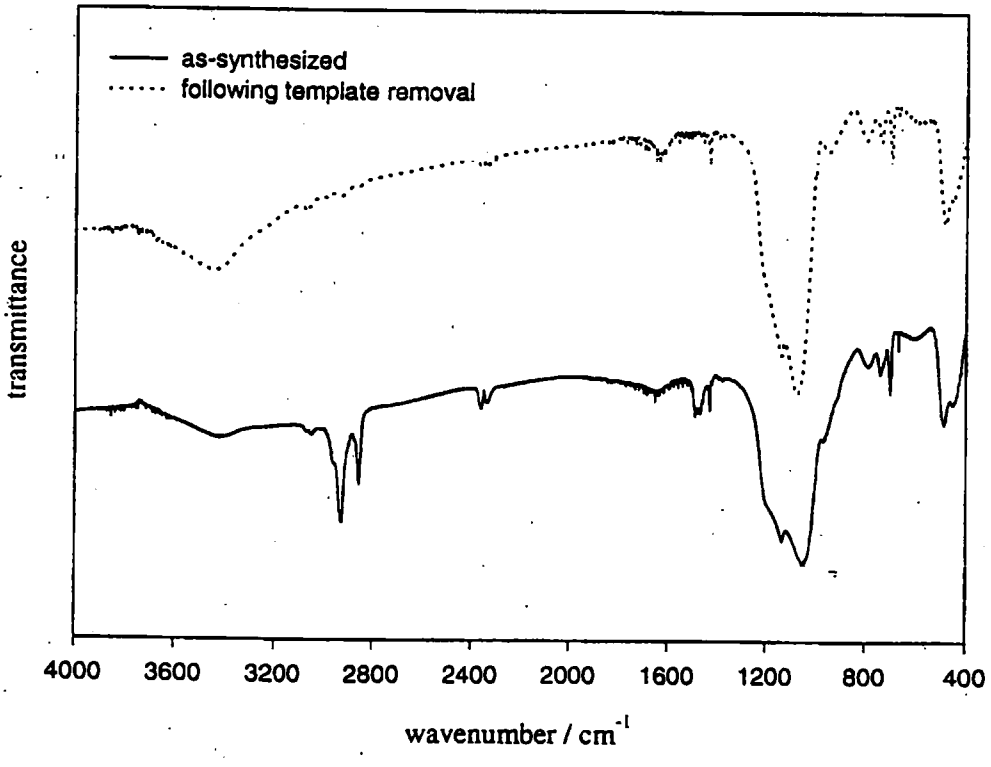

Figure A.17 I.R. Spectra of Unswollen, Phenyl-Modified Mesoporous Silica

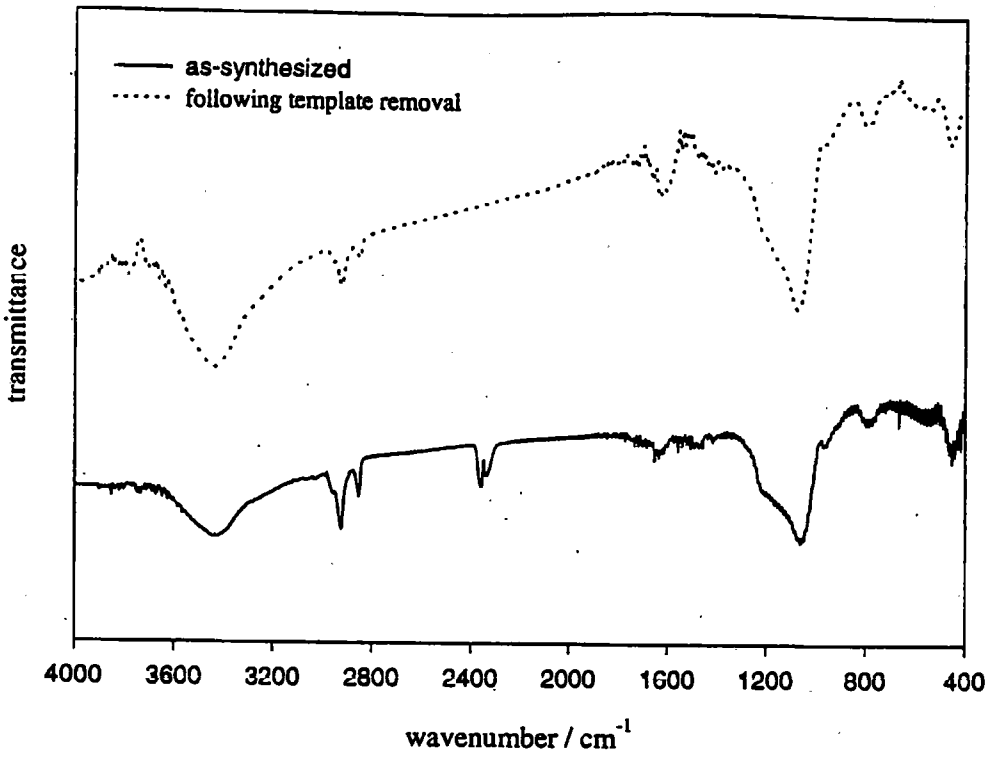

Figure A.18 I.R. Spectra of Vinyl-Modified Mesoporous Silica

APPENDIX A3 - MAS-NMR

A3.1 M41S MATERIALS

A3.1.1 ^{29}Si

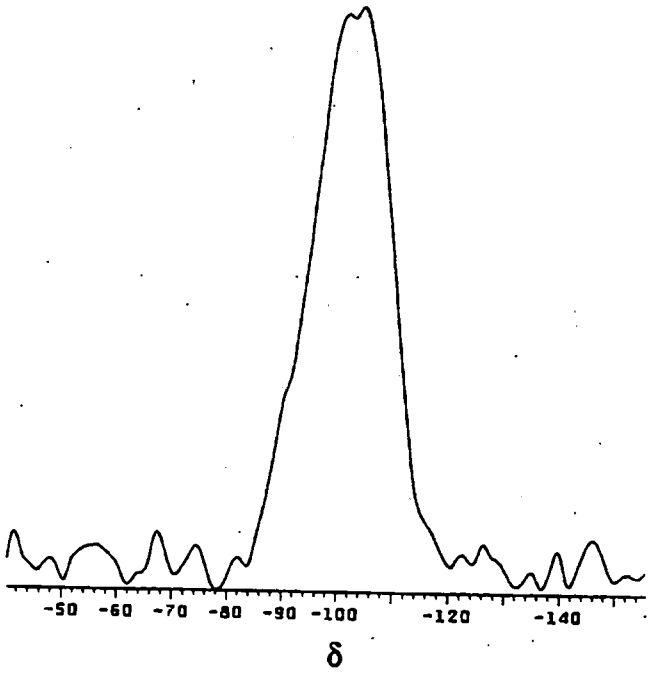

Figure A.19 ^{29}Si MAS-NMR Spectrum of As-Synthesized MCM-41(a)

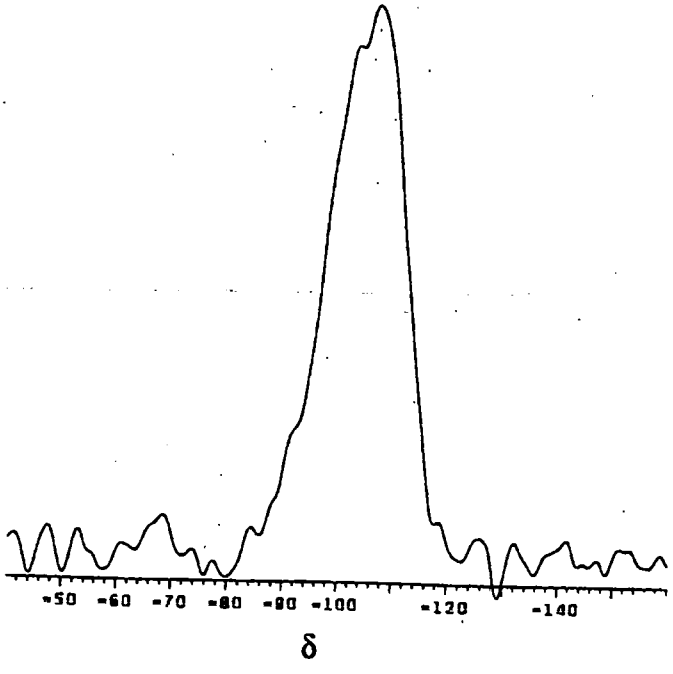

Figure A.20 ^{29}Si MAS-NMR Spectrum of Calcined MCM-41(a)

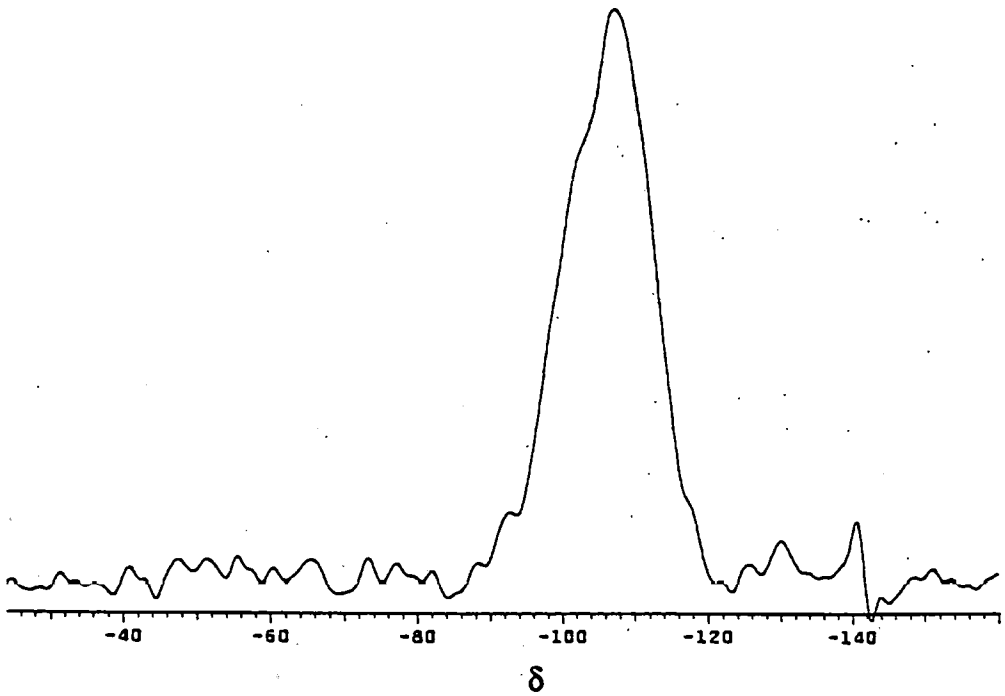

Figure A.21 ^{29}Si MAS-NMR Spectrum of Calcined MCM-41(c).

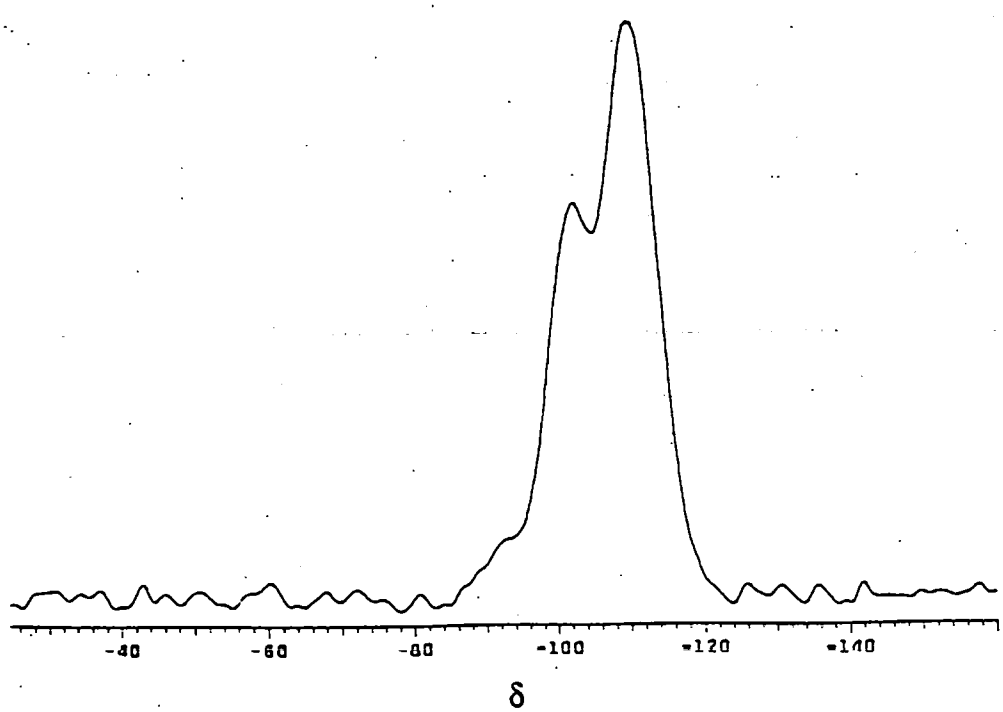

Figure A.22 ^{29}Si MAS-NMR Spectrum of MCM-41(c) Following Water Sorption

A3.1.2 ^{27}Al

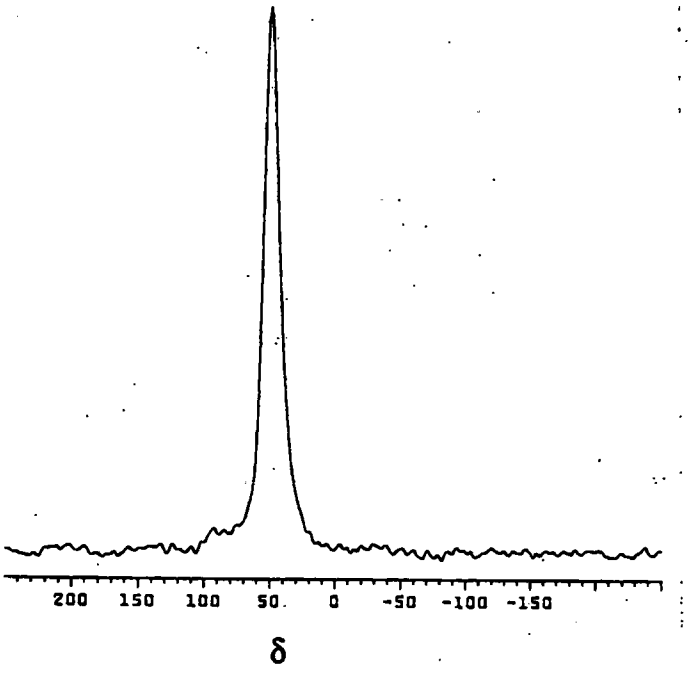

Figure A.23 ^{27}Al MAS-NMR Spectrum of As-Synthesized MCM-41(a).

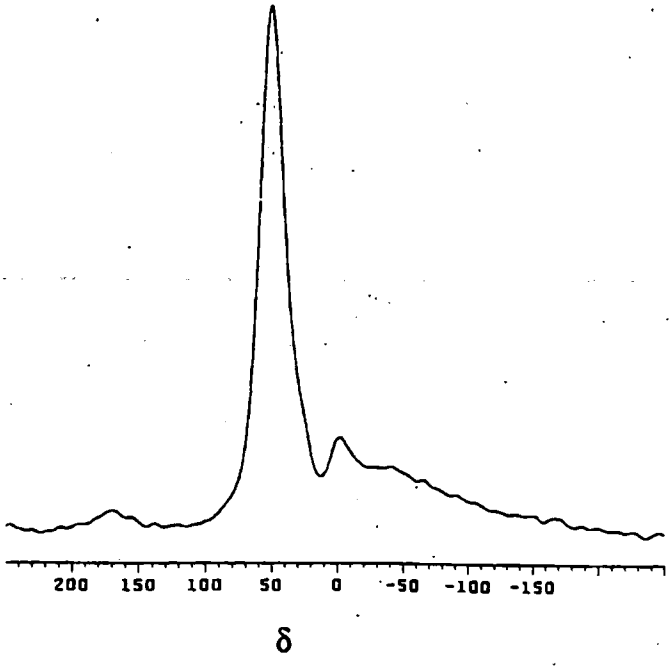

Figure A.24 ^{27}Al MAS-NMR Spectrum of Calcined MCM-41(a).

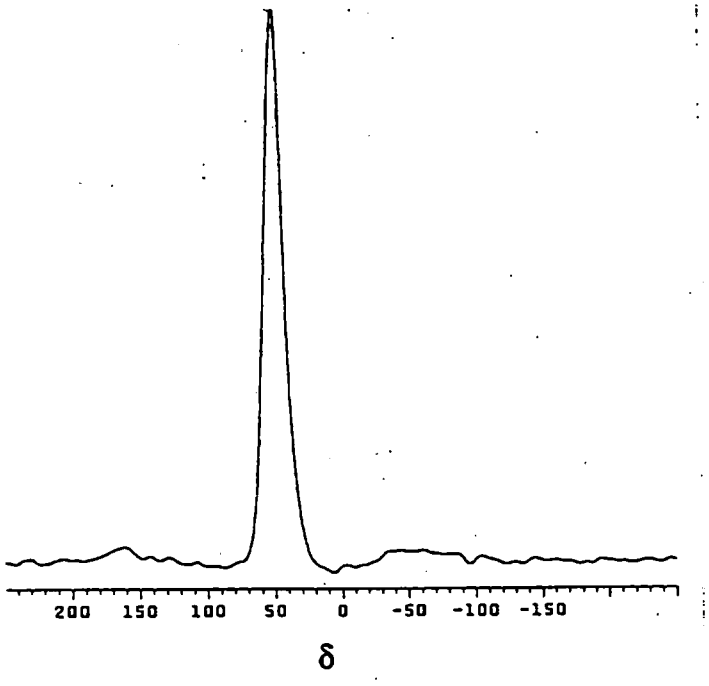

A.25 ^{27}Al MAS-NMR Spectrum of As-Synthesized MCM-41(c).

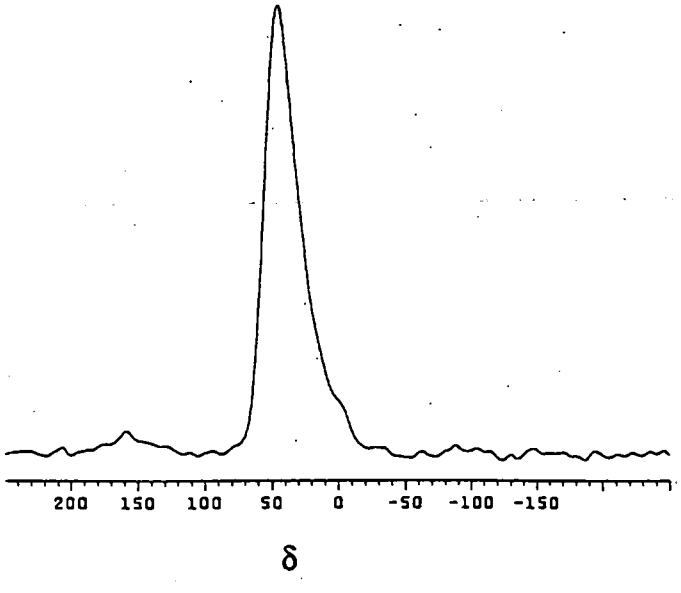

A.26 ^{27}Al MAS-NMR Spectrum of Calcined MCM-41(c).

A3.1.3 ^{13}C

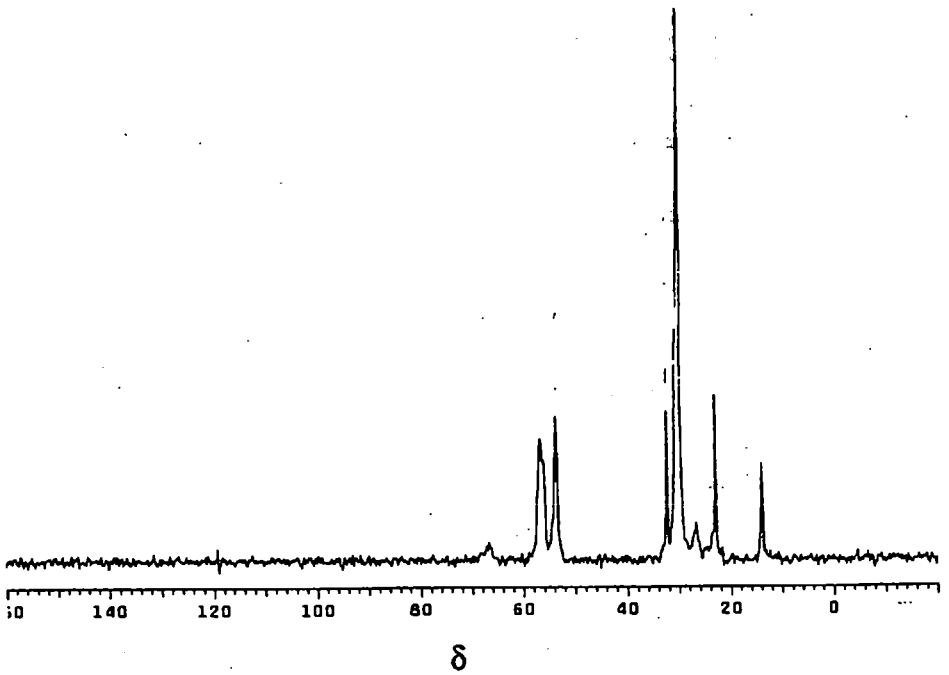

A.27 ^{13}C MAS-NMR Spectrum of As-Synthesized MCM-41(a).

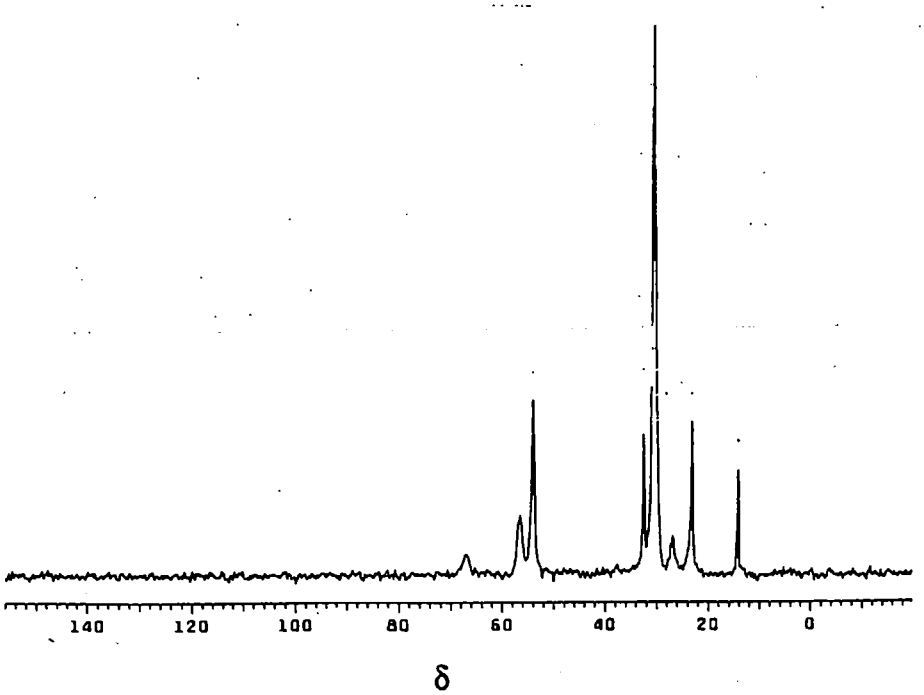

A.28 ^{13}C MAS-NMR Spectrum of As-Synthesized MCM-41(b).

A3.2 Organically-Modified Mesoporous Silica

A3.2.1 ^{29}Si

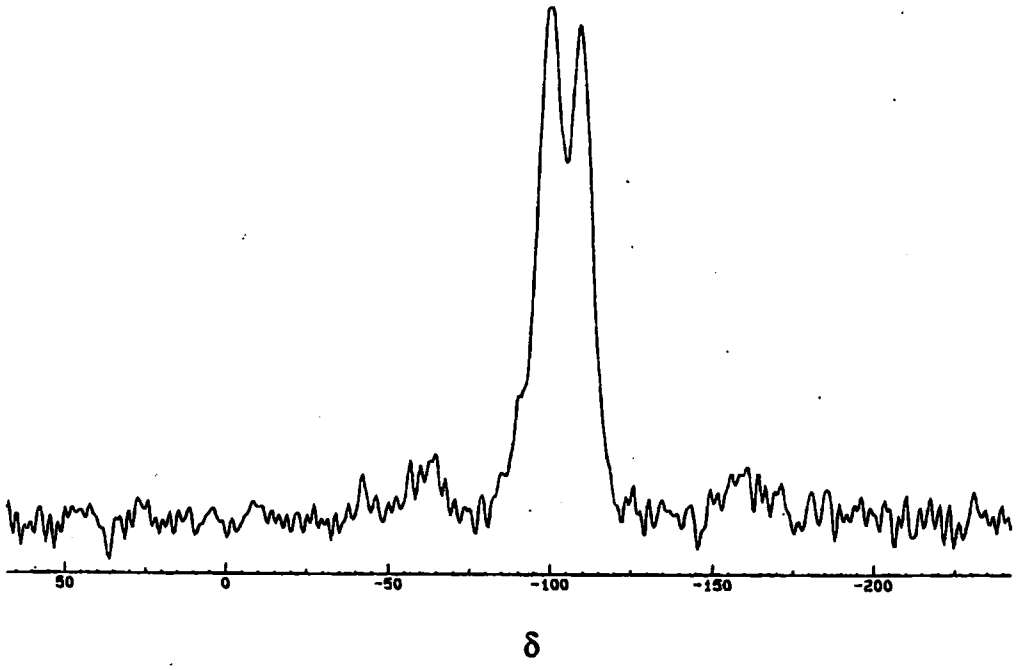

A.29 ^{29}Si MAS-NMR Spectrum of As-Synthesized Aminopropyl-Modified Silica.

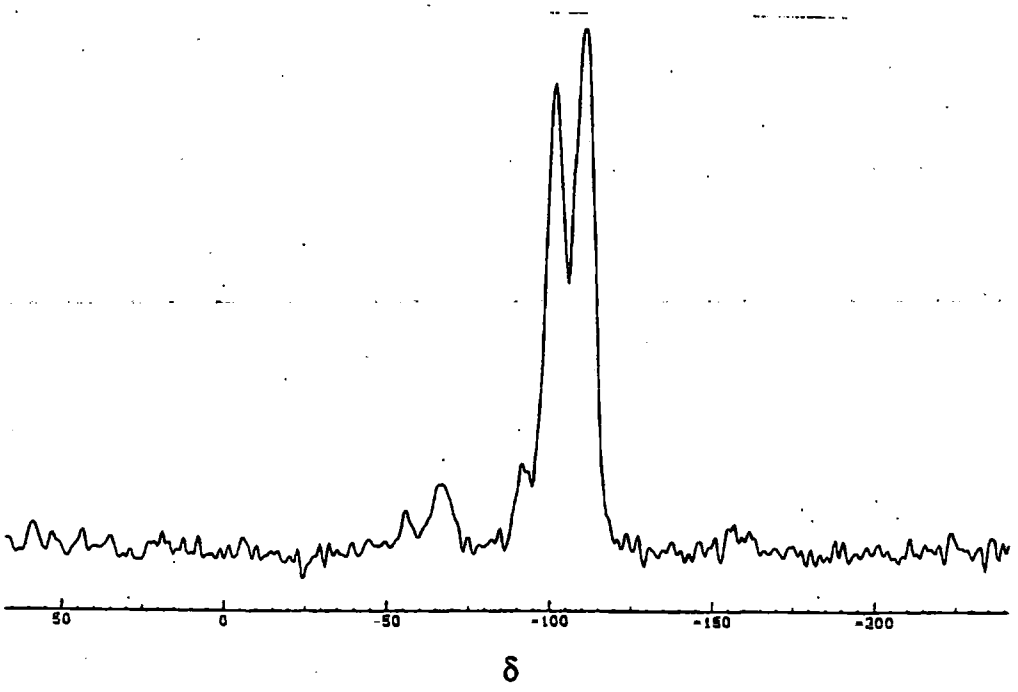

A.30 ^{29}Si MAS-NMR Spectrum of Aminopropyl-Modified Silica Following Template Removal.

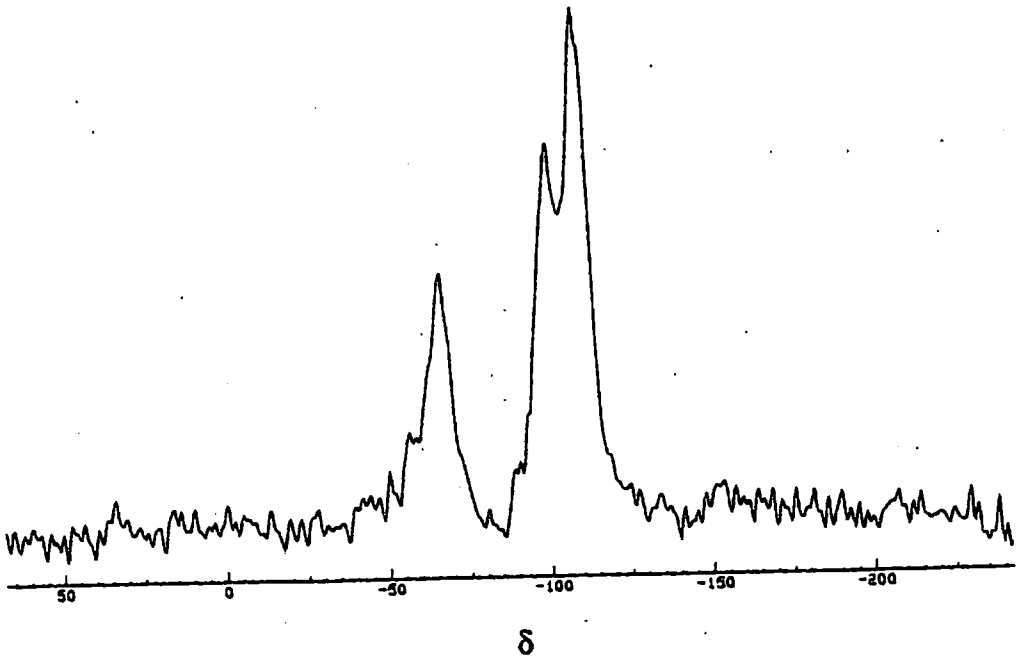

A.31 ^{29}Si MAS-NMR Spectrum of As-Synthesized Mercaptopropyl-Modified Silica.

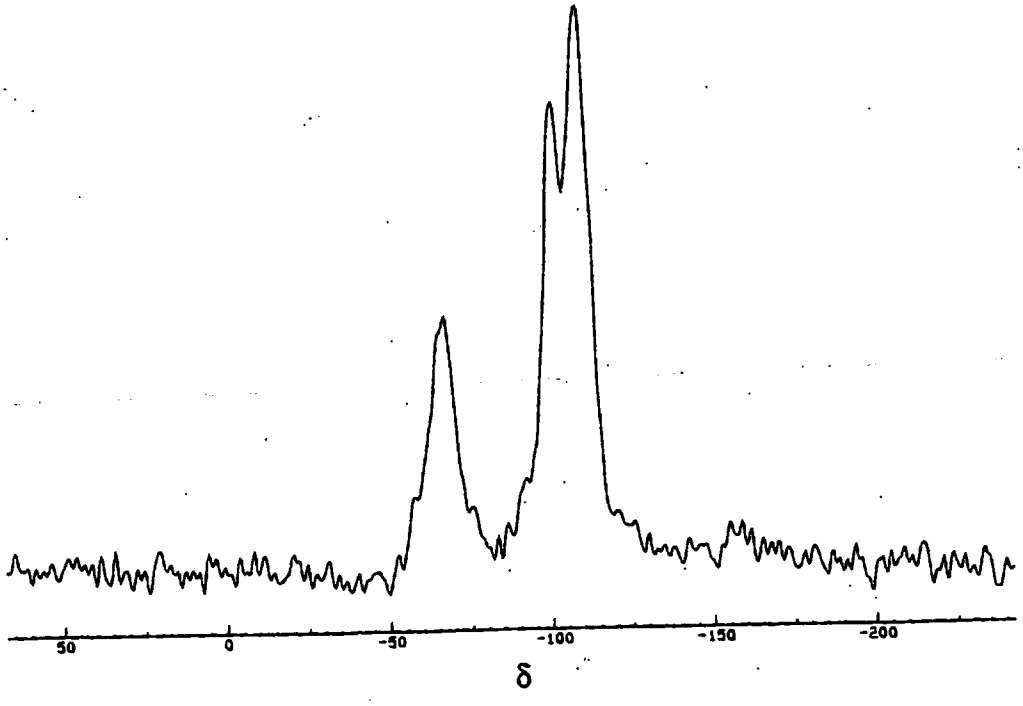

A.32 ^{29}Si MAS-NMR Spectrum of Mercaptopropyl-Modified Silica Following Template Removal.

A3.2.2 ^{13}C

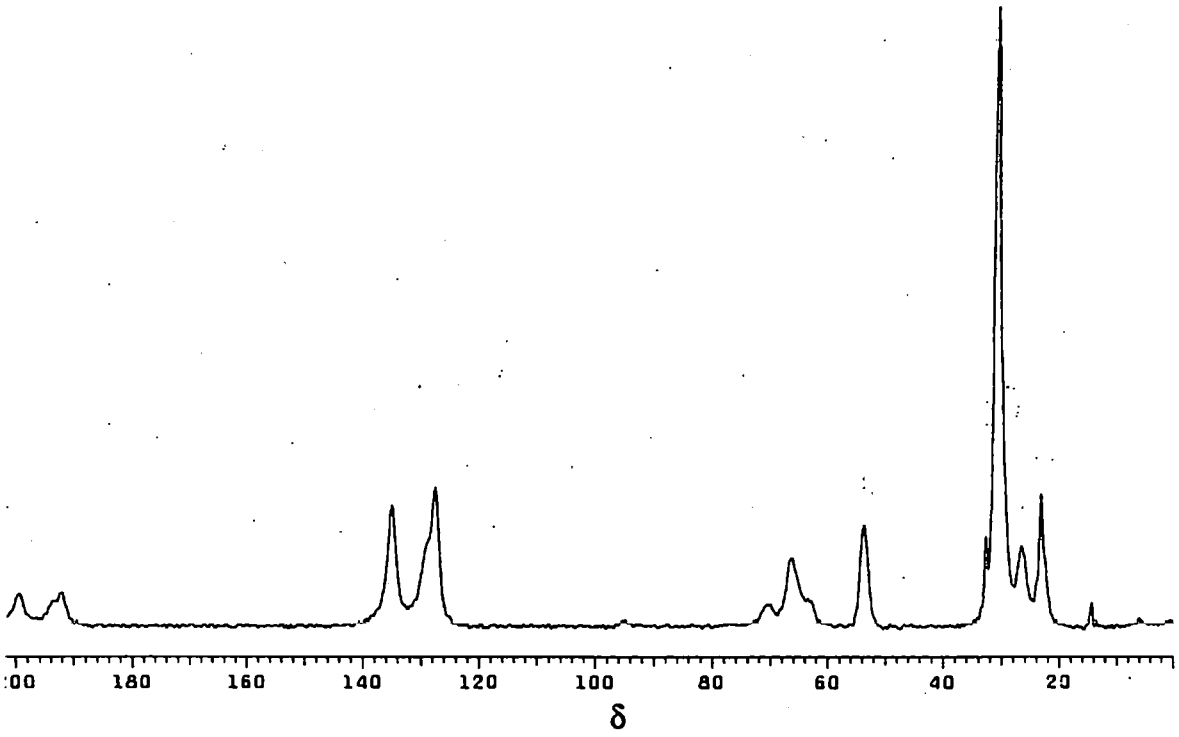

A.33 ^{13}C MAS-NMR Spectrum of As-Synthesized Phenyl-Modified Silica.

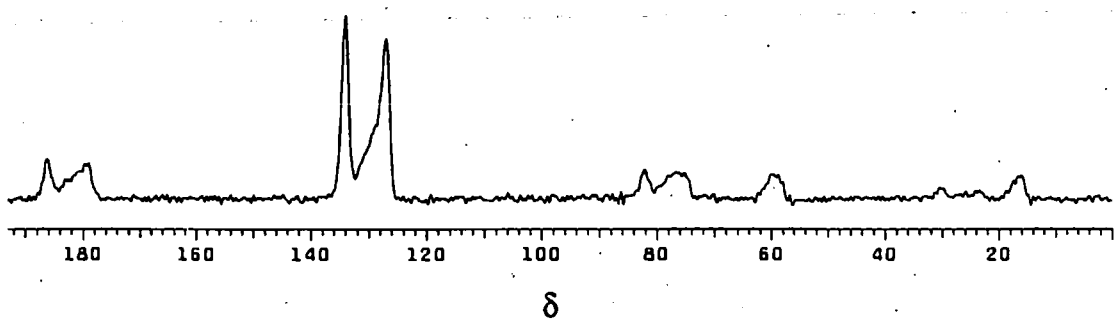

A.34 ^{13}C MAS-NMR Spectrum of Phenyl-Modified Silica Following Template Removal.

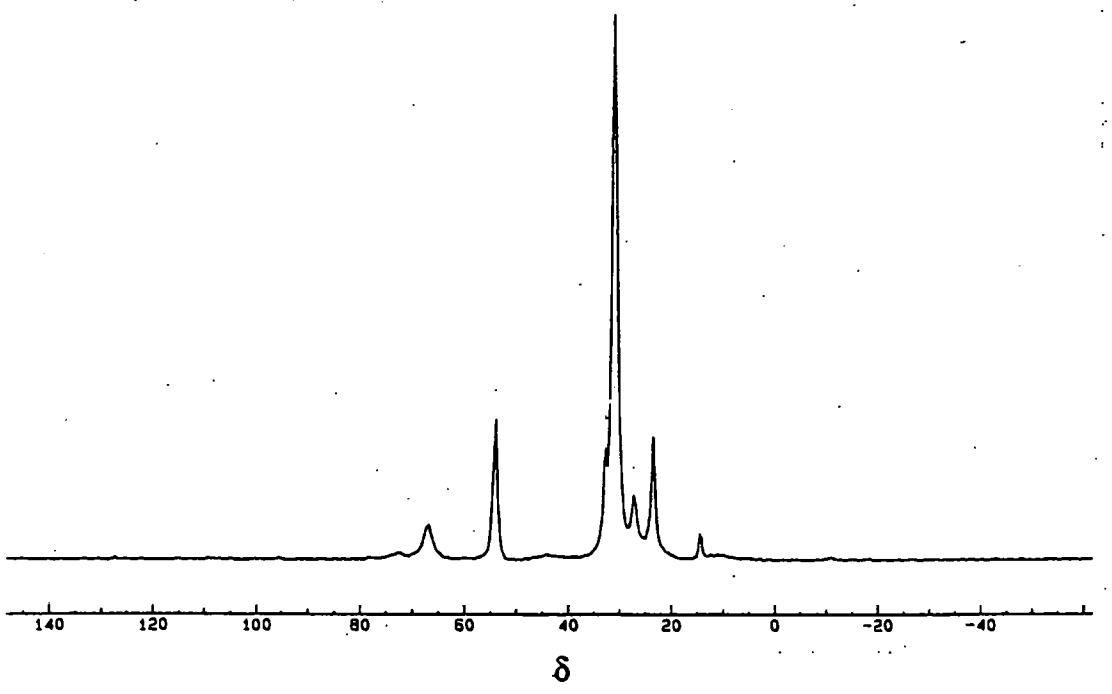

A.35 ^{13}C MAS-NMR Spectrum of As-Synthesized Mercaptopropyl-Modified Silica.

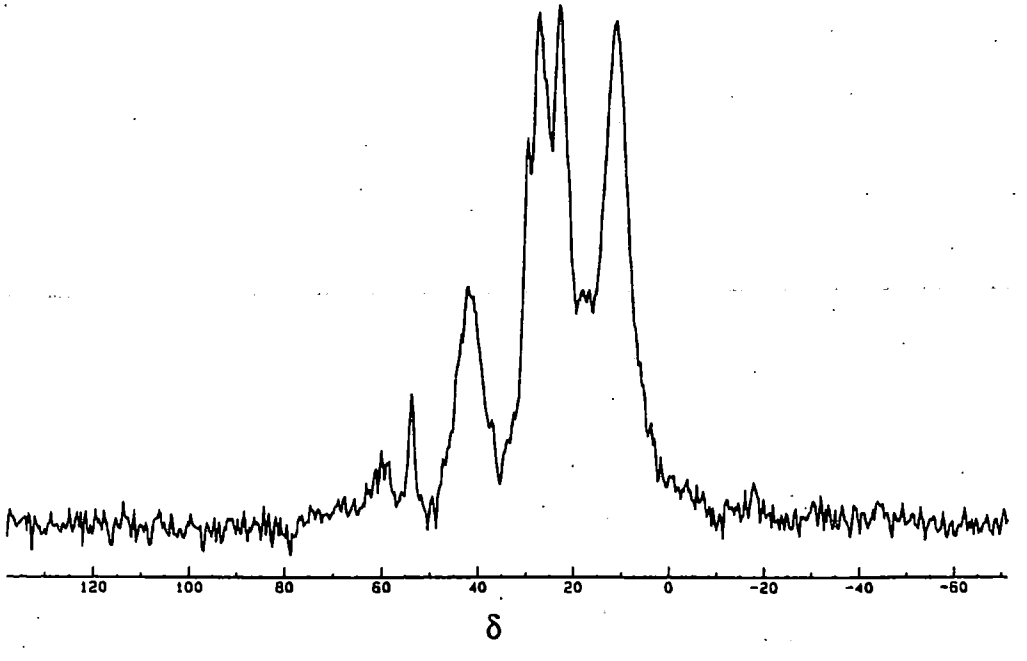

A.36 ^{13}C MAS-NMR Spectrum of Mercaptopropyl-Modified Silica Following Template Removal.

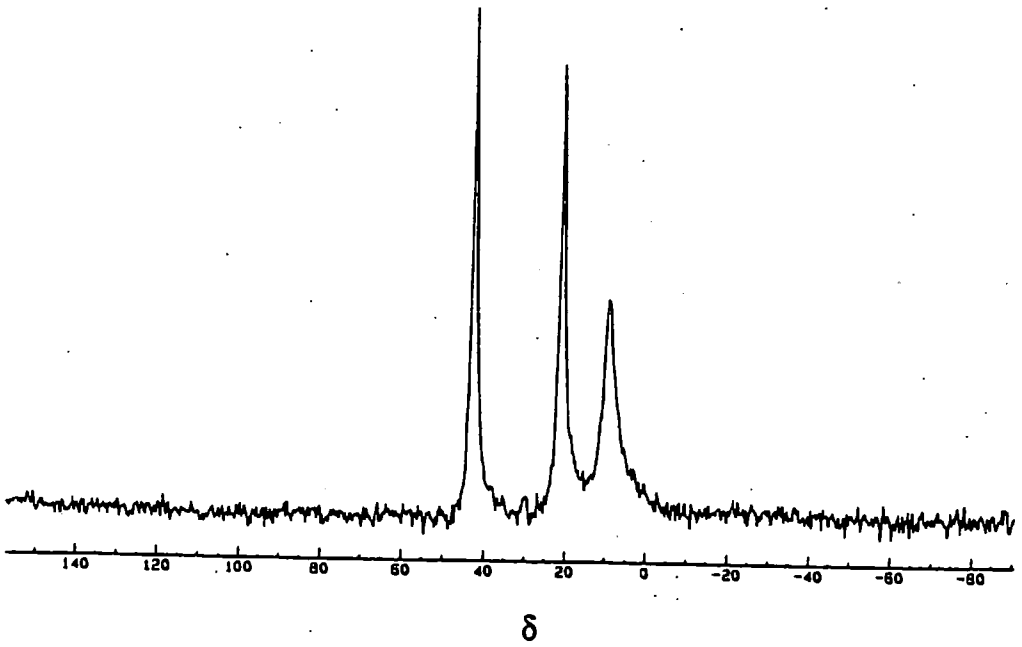

A.37 ^{13}C MAS-NMR Spectrum of Aminopropyl-Modified Silica Following Template Removal.

APPENDIX A4 - SURFACE AREA STUDIES

A4.1 GRAVIMETRIC SPRING CALIBRATION CURVE

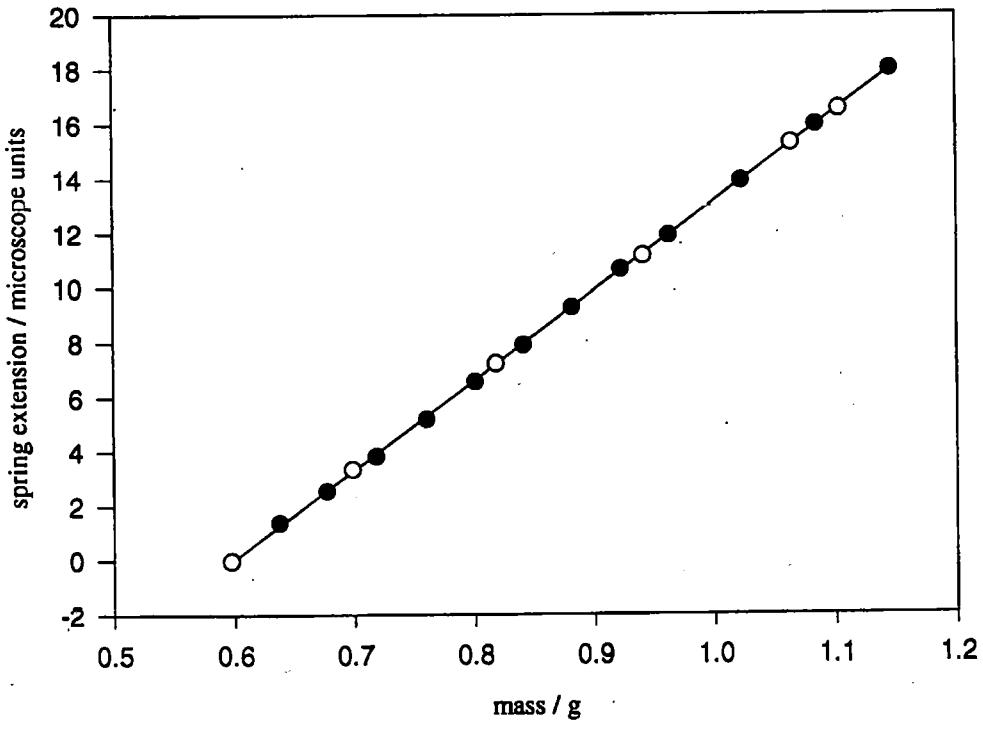

Figure A.38 Gravimetric Spring Calibration at 303 K.

Spring Sensitivity = 32.68 microscope units g^{-1}

A 4.2 N_2 and O_2 BET Plots for M41S-Materials

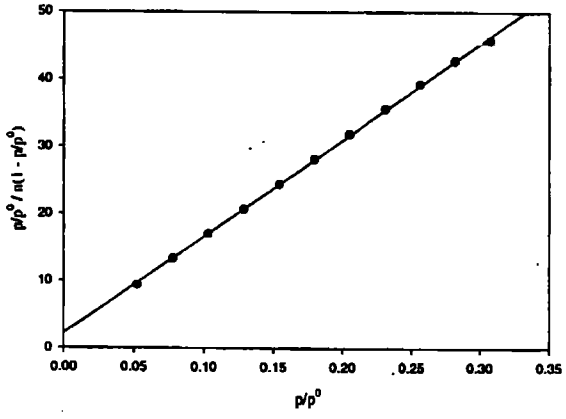

Figure A.39 BET Plot of N_2 sorption at 77 K on MCM-41(a).

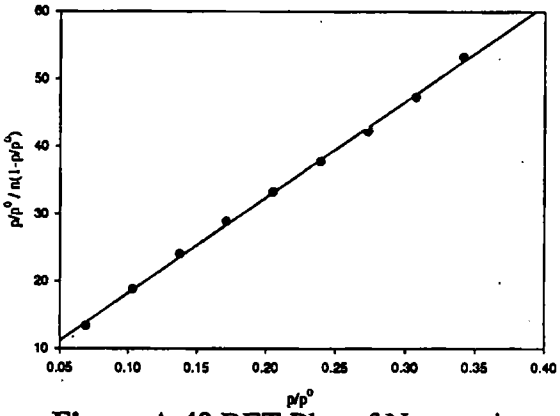

Figure A.40 BET Plot of N_2 sorption at 77 K on MCM-41(b).

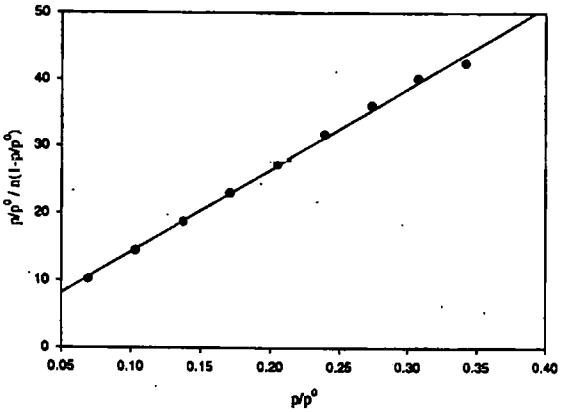

Figure A.41 BET Plot of N_2 sorption at 77 K on MCM-41(c).

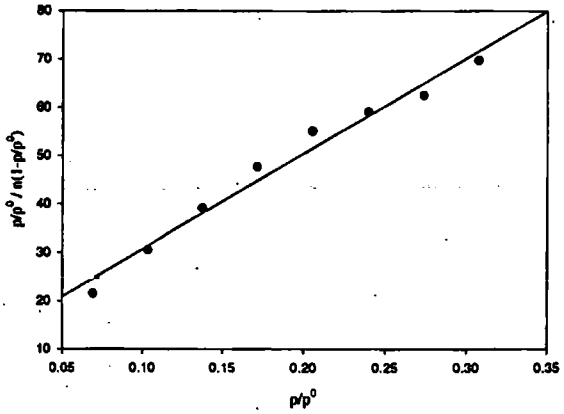

Figure A.42 BET Plot of N_2 sorption at 77 K on MCM-41(d).

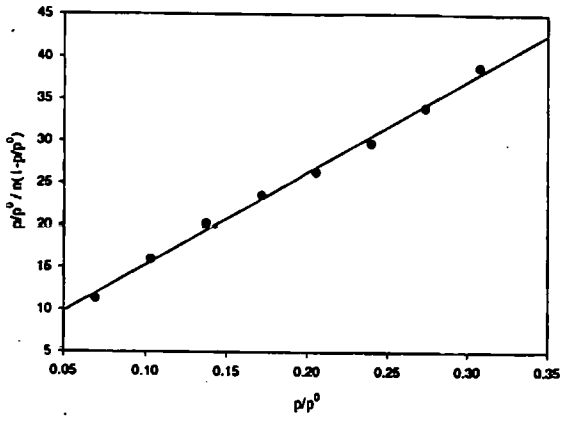

Figure A.43 BET Plot of N_2 sorption at 77 K on SiMCM-41(a).

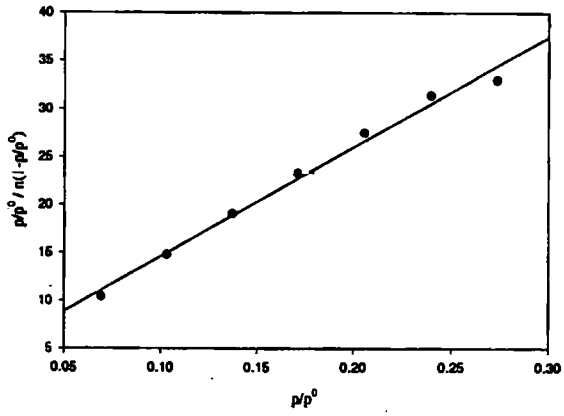

Figure A.44 BET Plot of N_2 sorption at 77 K on SiMCM-41(b).

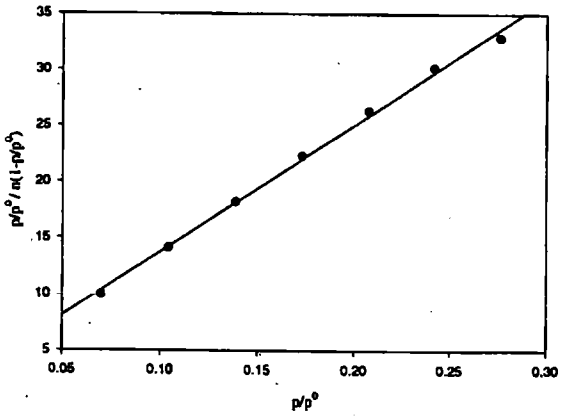

Figure A.45 BET Plot of N_2 sorption at 77 K on FeMCM-41.

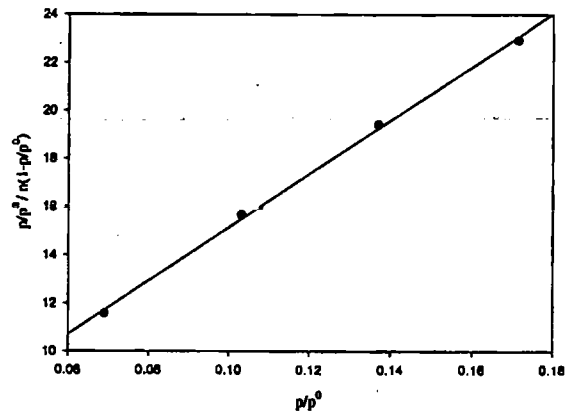

Figure A.46 BET Plot of O_2 sorption at 77 K on SiMCM-41(b).

A4.3 Organically-Modified Mesoporous Silica

A4.3.1 N_2 BET and Langmuir Plots

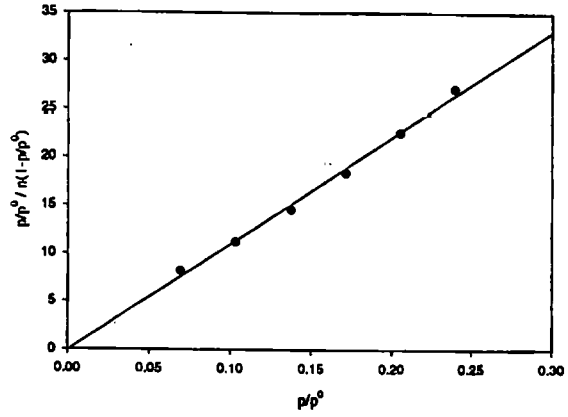

Figure A.47 BET plot of N_2 sorption on PhMCM-41 (Burkett), (n_m = 9 mmol g^{-1}).

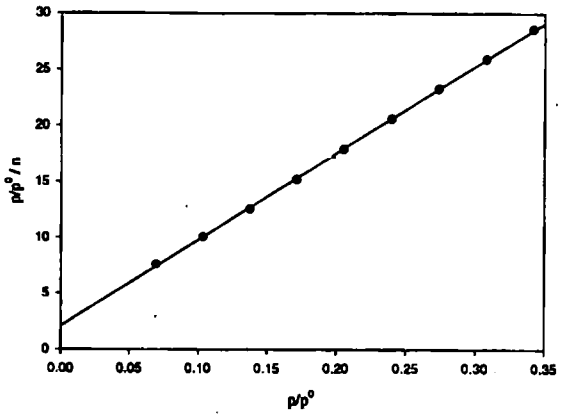

Figure A.48 Langmuir plot of N_2 sorption on PhMCM-41 (Burkett), (n_m = 12.0 mmol g^{-1}).

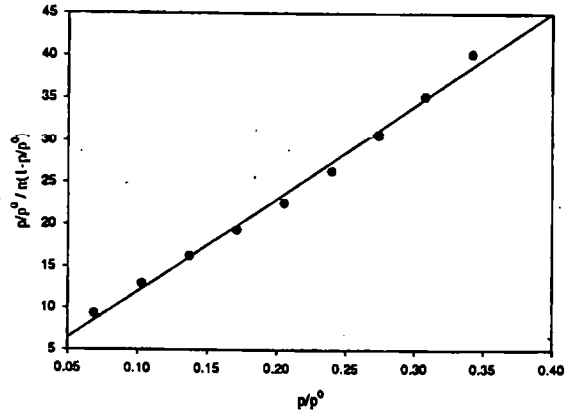

Figure A.49 BET plot of N_2 sorption on unswollen Ph-M.S. (n_m = 8.94 mmol g^{-1}).

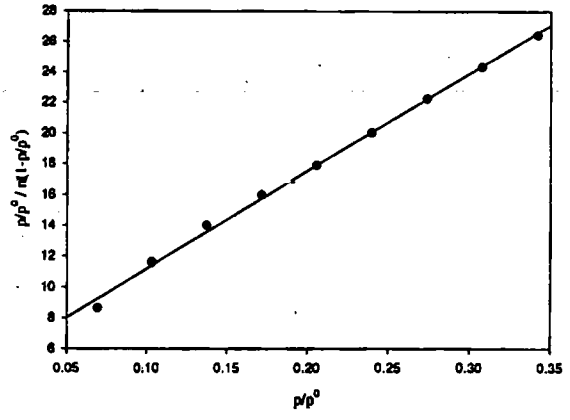

Figure A.50 Langmuir plot of N_2 sorption on unswollen Ph-M.S. (n_m = 14.6 mmol g^{-1}).

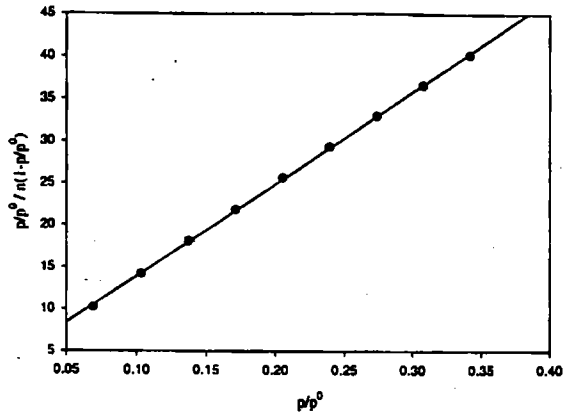

Figure A.51 BET plot of N_2 sorption on MES-swollen Ph-M.S.(n_m = 8.86 mmol g^{-1}).

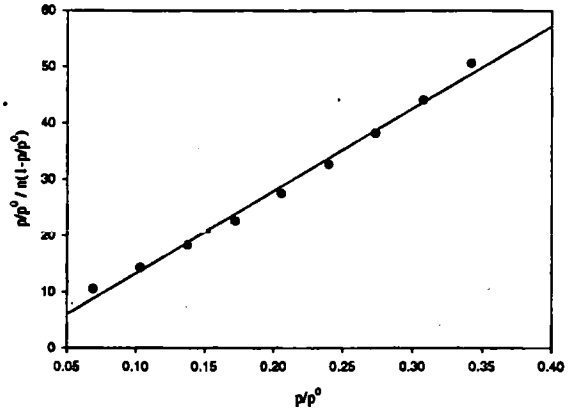

Figure A.52 BET Plot of N2 sorption on TET-swollen Ph-M.S.

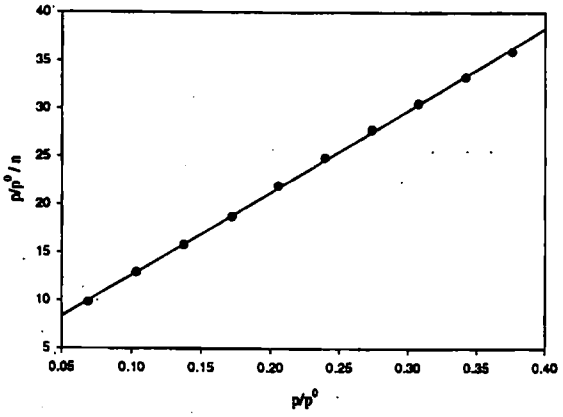

Figure A.53 Langmuir Plot of N_2 Sorption on TET-swollen Ph-M.S.

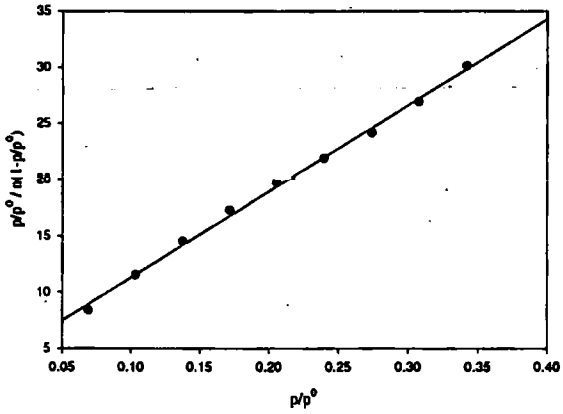

Figure A.54 BET Plot of N_2 Sorption on Vinyl-M.S.

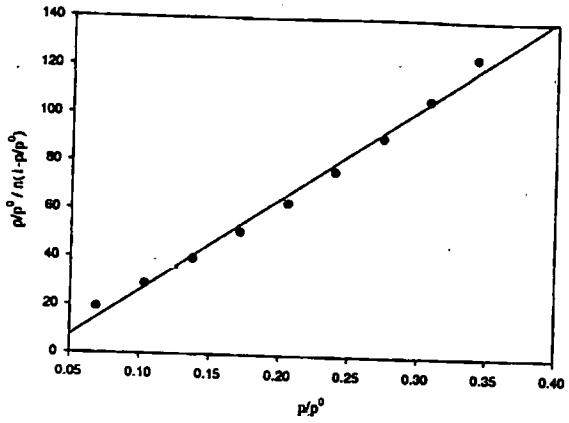

Figure A.55 BET Plot of N_2 Sorption on AP-M.S.

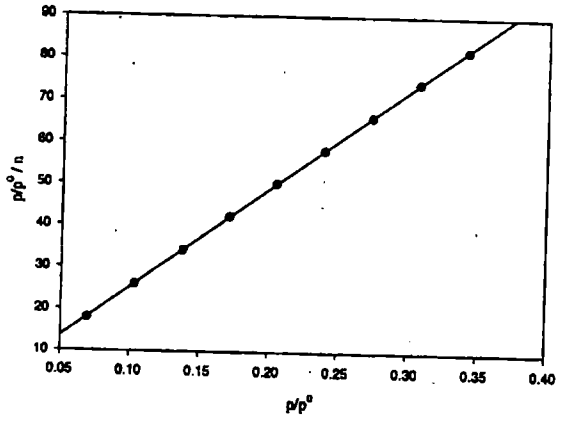

Figure A.56 Langmuir Plot of N_2 Sorption on AP-M.S.

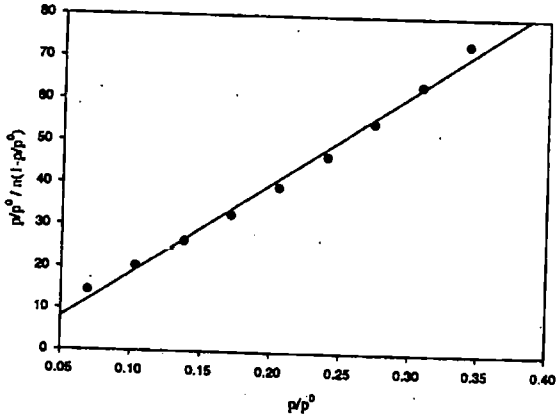

Figure A.57 BET Plot of N_2 on MP-M.S.

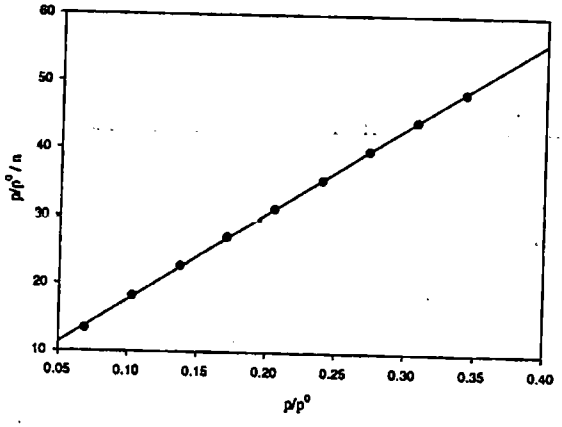

Figure A.58 Langmuir Plot of N_2 Sorption on MP-M.S.

A4.3.1 Benzene and Butanol BET and Langmuir Plots

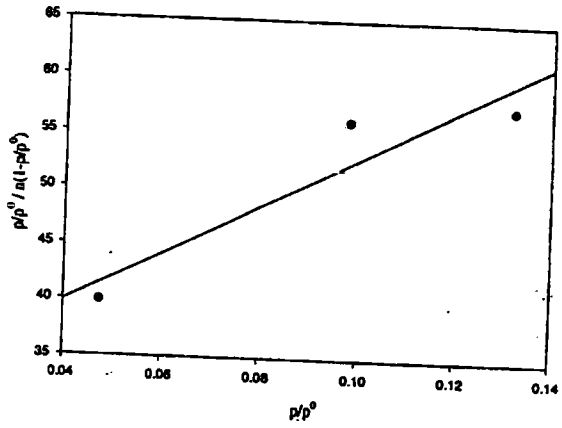

Figure A.59 BET Plot of Benzene Sorption on MES-swollen Ph-M.S.

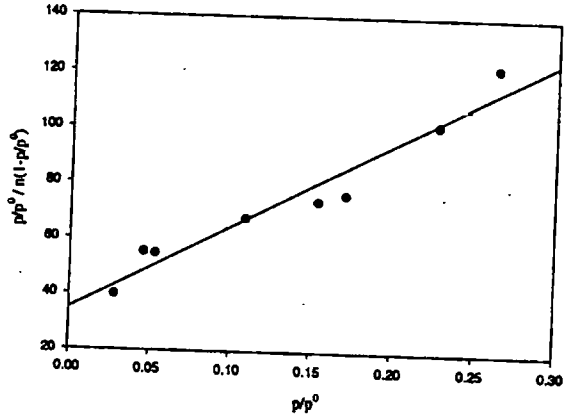

Figure A.60 BET plot of Benzene Sorption on PhMCM-41 (Burkett).

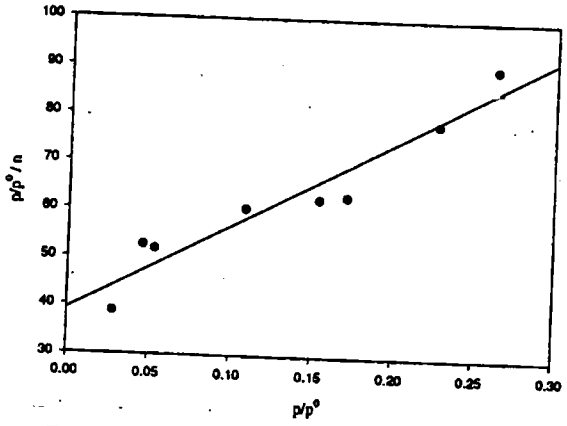

Figure A.61 Langmuir plot of Benzene Sorption on PhMCM-41 (Burkett).

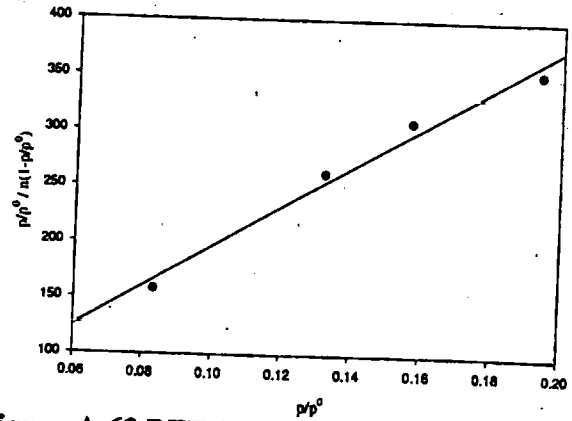

Figure A.62 BET Plot of *n*-BuOH Sorption on PhMCM-41 (Burkett)

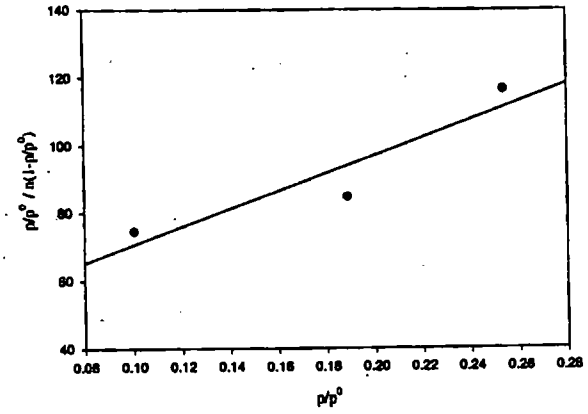

Figure A.63 BET Plot of *t*-BuOH Sorption on PhMCM-41 (Burkett)

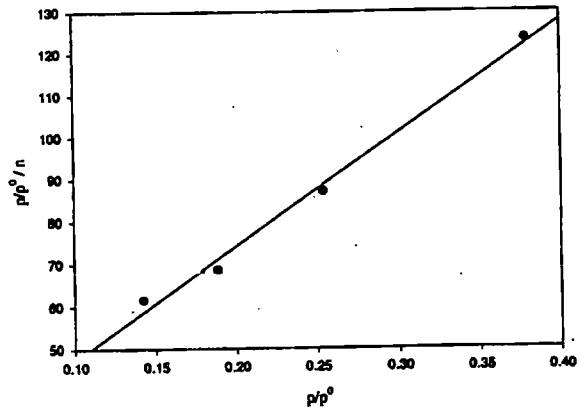

Figure A.64 Langmuir Plot of *t*-BuOH Sorption on PhMCM-41 (Burkett)

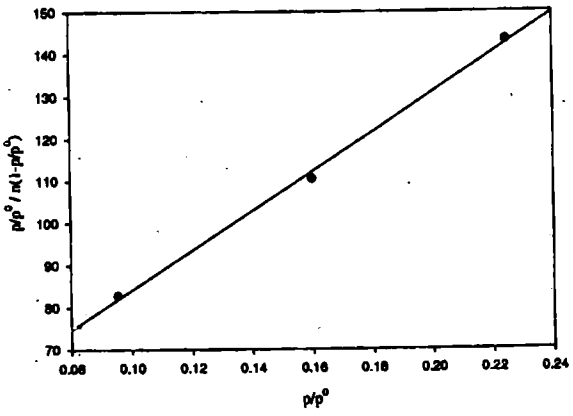

Figure A.65 BET Plot of *n*-BuOH Sorption on MES-swollen Ph-M.S.

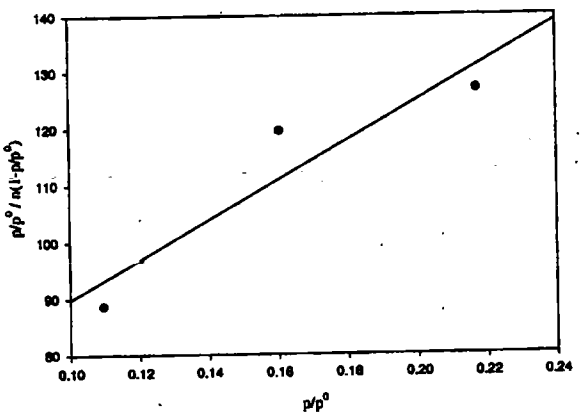

Figure A.66 BET Plot of *t*-BuOH Sorption on MES-swollen Ph-M.S.